Yves Narcisse Nguegan Tchokonte

Real-time identification and monitoring of the voltage stability margin in electric power transmission systems using synchronized phasor measurements

kassel university press

This work has been accepted by the faculty of Electrical Engineering and Computer Science of the University of Kassel as a thesis for acquiring the academic degree of Doktor der Ingenieurwissenschaften (Dr. –Ing.).

Supervisor: Prof. Dr. Albert Claudi
Co-Supervisor: Prof. Dr. Bernd Weidemann

Defence Day 29. Juni 2009

Bibliographic information published by Deutsche Nationalbibliothek
The Deutsche Nationalbibliothek lists this publication in the Deutsche Nationalbibliografie; detailed bibliographic data is available in the Internet at http://dnb.d-nb.de.

Zugl.: Kassel, Univ., Diss. 2009
ISBN print: 978-3-89958-756-2
ISBN online: 978-3-89958-757-9
URN: urn:nbn:de:0002-7573

Printed in Germany

Acknowledgements

This work has been carried out during my employment as a research assistant at the chair for Power Systems and High Voltage Engineering of the University of Kassel in Germany. At this point I would like to express my sincere gratitude to a number of people for the support and the assistance during the realization of this thesis.

Firstly thanks to the almighty and merciful God for the blessings that have been extend to me all my life and during the time at the University of Kassel.

I would like to express my deep thanks and profound regard to the head of the chair: Prof. Dr. Albert Claudi who hired me, became my supervisor and thus gave me the possibility to write this thesis. Thank him I had the opportunity to get better acquainted to the academic world. He majorly contributed to this thesis by giving me the possibility of sole responsible research, by providing me excellent working conditions, and by his priceless advices and encouraging discussions.

I am very thankful to my co-supervisor Prof. Dr. Bernd Weidemann for his constructive comments during the very few discussions we had.

I acknowledge Mr. Holger Kühn from E.ON Netz in Germany, as it was through discussion with him that the main idea of this dissertation was born. Also thank you for the constructive discussions and ideas.

I would like to thank my colleagues at the University of Kassel: Günther Köhler, Dr. Gernot Finis, Mrs. Ursula Henrich, Oliver Schröder, and Oliver Belz for being there when I needed them, for the very good teamwork and for contributing to a pleasant work atmosphere. Special thanks to Oliver Belz, who occupied the neighbour office. He has been listening to all my complaints and thoughts on the matters of this thesis, and has contributed in the span of his possibility with constructive comments although being busy with his own thesis. He has also been my main partner for discussions beyond the scope of the thesis.

I would also like to thank particularly all the students who have worked with me during my time at the University of Kassel. Their ideas have inspired me and their preliminary works were an important condition to complete this work. I would like to name at this point: Christoph Reinbold, Sven Behnke, Timm Eberwein, Aboubakar Ismaila, Thorsten Reimann, Jian Jun Wang, Mohammad Dawood, Andrea Schmitt, Mathias Eisenberg, and Franck Martin.

The thesis would have not been possible to realize in this form without the support of the Danish TSO Energinet DK. For the generously share of data, thoughts and ideas as well as field experience at our meetings I would like to thank: Dr. Per Lund, Carsten Strunge, Dr. Torsten Lund, Hans Abildgaard and particularly Samuel Thomasson. They all pointed out the study direction and I am very thankful to all of them.

At some occasions I had the luck to experience very inspiring discussions with Prof. Dr. Thierry Van Cutsem (University of Liège, Belgium), Prof. Dr. Michael Fette (University of applied sciences, Bielefeld, Germany), Dr. Walter Sattinger (SwissGrid, TSO Switzerland) and with Prof. Dr. István Erlich (University of Duisburg, Germany). I would like to thank them for their patience and for finding time for meetings.

I would like to express my deepest appreciation to my parents, brothers and sisters and to Patrick Pouedogo for their love, support and encouragement throughout all these years.

And definitely I must thank above all my wife Natalia and my both children Eva and Olga for their support, their limitless love and to have arranged themselves so well at home during the time dad was physically seldom present and spiritually often absent.

Kassel, 09.04.2009 Yves Nguegan

Abstract

The changes which appeared during the last decades in the electricity markets led to an increased utilization and a higher loading of the electric transmission grids worldwide. The power transmission systems are nowadays operated on the brink of their technical limits and thus became more vulnerable to instabilities and cascading failures than before.

The increase number of yearly power systems outages worldwide shows that the need of better monitoring concepts and tools fitted to the actual and future situation of power systems became urgent. Such systems will support the transmission system operators by the online assessment of the system state and permit the transition from a reacting system operation to a foresighted system operation. In this context, the use of synchronized phasor measurements is becoming an important tendency for the surveillance of the power systems. They are provided by phasors measurements units (PMUs) considered to be one of the most important measuring devices in the future of power systems. Defining the appropriate PMU system application is a utility problem that still must be studied and optimised. To make sense of the PMUs data, the system operators need tools that will help them infer the meaning of the data and to discern their interrelationships.

In this thesis, the PMUs are turned to useful sources of real-time data. They provided the required information needed by the grid operator on the actual system state and are combined with relevant data of the given system with the aim to early detect impending voltage instability. Furthermore the data are used to define the minimal voltage stability margin i.e. how far a given system operating state is from a state where voltage instability will occur. Thereby, a statement on the actual system operating state is made on the base of the actual active load transfer on each individual transmission line of the grid section considered.

The illustration of the power transfer situation on the lines is made on the base of a new developed mathematical function, in an active power-voltage plane using the so-called PU-characteristics. A progressive calculation of the transfer function during the system operation leads to PU-curves for each new operating point. The assessment of the voltage stability state is carried out by the coeval consideration of predefined criteria, from an optimized stability index determined, for the power transfer stability, and for the stability of the voltage profile at the line receiving end.

The method developed in this work can be used for the monitoring of individual power lines of the power system as well as for the monitoring of transmission zones retaining several transmission lines, whereby it uses the advantage of the synchronization of the measurements from a minimal number of PMUs. The principles of the method build the foundations of the development of a tool for the analysis and the visualization on the voltage stability situation in power transmission systems using simulated or field PMU data sets. The exactness, the robustness and the applicability of the method is verified on a two-bus test-system as well as on the western Danish power system, wherefore a digital model was provided by the Danish transmission system operator Energinet DK.

The optimal positioning of a minimal number of PMUs for the monitoring of the determined transmission zones within the section of the western Danish transmission grid considered, according to the principles of the developed method, is realized by means of an elaborated strategy for PMUs placement.

The monitoring method proposed in this thesis described an innovative and efficient alternative for the online surveillance of the voltage stability in power transmission systems using PMUs data. The work realized shows on the example of an existing power system structure how measurements from distributed PMUs can be combined with relevant transmission lines parameters, and be handled to detect forthcoming voltage stability problems in power systems at early stage.

Kurzfassung

Titel der Arbeit: *„Online Identifikation und Überwachung der Spannungsstabilitätsreserve in elektrischen Übertragungsnetzen unter Verwendung zeitsynchronisierter Zeigermessungen“*

Die aktuellen Veränderungen im Bereich der Elektrizitätswirtschaft führen weltweit zu einer erhöhten Ausnutzung sowie zu einer stärkeren Auslastung der Übertragungsnetze. Durch einen Betrieb dieser Netze nahe an ihren technischen Grenzen steigt damit die Wahrscheinlichkeit des Auftretens von Stabilitätsproblemen. Die weltweit zunehmende Anzahl an Netzausfällen zeigt, dass der Betrieb elektrischer Übertragungssysteme am Rand ihrer technischen Grenzen immer schwieriger zu realisieren ist. Daher nimmt die Notwendigkeit moderner Überwachungskonzepte, methoden sowie-tools, angepasst bzw. anpassbar an die derzeitigen und zukünftigen Betriebsbedingungen, immer weiter zu. Derartige Hilfsmittel können den Netzbetreiber bei der System-Online-Zustandsbewertung unterstützen sowie den Übergang von einer reagierenden Prozessführung zu einer vorausschauenden Prozesslenkung ermöglichen.

In diesem Zusammenhang stellt die Verwendung zeitsynchronisierter Zeigermessungen, die durch sogenannte PMUs (*Engl: Phasor Measurements Units*) erfassbar sind, einen neuen vielversprechenden und zukunftsträchtigen Trend bei der Überwachung von elektrischen Energieversorgungsnetzen dar. Allerdings sehen sich die Betreiber elektrischer Energieversorgungsnetze durch die Entwicklung und Einführung derartiger innovativer Überwachungssysteme mit einer stets wachsenden Datenflut konfrontiert, deren sinnvolle Interpretation unabdingbar ist, um die Sicherheit der Netze weiter zu optimieren. Vor diesem Hintergrund befasst sich die vorliegende Arbeit mit der Entwicklung einer Methode für die Onlineüberwachung der Spannungsstabilität in elektrischen Energieübertragungssystemen.

Als zentraler Punkt dieser Arbeit werden hierzu PMU-Daten als Online-Datenquellen verwendet und mit relevanten Daten des

betreffenden Netzes kombiniert. Das Ziel ist es, im Online-Modus Informationen über den aktuellen Betriebszustandes des Netzes zu erhalten und diese für eine frühzeitige Erkennung von Spannungsinstabilitäten zu nutzen. Darüber hinaus wird mit Hilfe der Daten die minimale Spannungsstabilitätsreserve bestimmt und ermittelt, wie weit ein gegebener Netzzustand von einem spannungsinstabilen Netzzustand entfernt ist. Auf Basis des berechneten aktuellen Wirkleistungstransfers für jede betrachtete Übertragungsleitung kann so eine Aussage über den aktuellen Spannungsstabilitätszustand getroffen werden. Die Darstellung der Transfersituation der betreffenden Leitung erfolgt ausgehend von einer in dieser Arbeit erarbeiteten mathematischen Funktion in der Wirkleistungs-/Spannungs-Ebene mittels sogenannter PU-Charakteristiken. Die dazu notwendige Berechnung der Leitungsflüsse in progressiven Betriebspunkten führt auf PU-Kurven für jeden neuen Betriebszeitpunkt. Die Beurteilung des Spannungsstabilitätszustandes erfolgt anhand der gleichzeitigen Betrachtung vordefinierter, aus einem optimierten Stabilitätsindex ermittelter Kriterien der Transferstabilität sowie der Stabilität des Spannungsprofils am empfangenden Ende einer Übertragungsleitung.

Die in dieser Arbeit entwickelte Methode kann für die Überwachung sowohl einzelner Leitungen eines Netzes als auch ganzer Übertragungszonen mit mehreren Übertragungsleitungen eingesetzt werden. Dabei kommt sie durch Ausnutzung des Vorteils der Synchronisation verschiedener Messungen mit einer verminderten Anzahl von PMUs aus. Ihre Genauigkeit, Robustheit und Anwendbarkeit wurde anhand zweier Test-Systeme verifiziert. Als Testsysteme dienten dabei zum einen ein Zwei-Sammelschienen-System sowie zum anderen das westdänische Versorgungsnetz, dessen digitales Model von dem dänischen Übertragungsnetzbetreiber Energinet DK zu diesem Zweck zur Verfügung gestellt wurde.

Auf Grundlage der erarbeiteten Methode wurde unter Verwendung von simulierten sowie reellen PMU Daten ein Tool zur Analyse und Visualisierung der Spannungsstabilitätssituation in elektrischen Übertragungsnetzen entwickelt. Darüber hinaus wird in der vorliegenden Arbeit eine nach den Prinzipien der entwickelten Methode optimierte Positionierung einer möglichst geringen Anzahl von PMUs zur Überwachung der jeweils definierten Übertragungszonen innerhalb des westdänischen Übertragungsnetzes vorgeschlagen.

Das in dieser Arbeit entwickelte Überwachungsprinzip liefert eine innovative und effektive Möglichkeit für die Überwachung der Spannungsstabilität in Energieübertragungssystemen unter Verwendung von PMUs. Die Methode zeigt am Beispiel einer reell existierenden Netzstruktur, auf welche Weise die Messungen aus verteilten PMUs mit verschiedenen relevanten Netzleitungsparametern kombiniert und bearbeitet werden können, um bevorstehende Spannungsstabilitätsprobleme im Stromnetz frühzeitig zu erkennen.

Table of Contents

Abbreviations and symbols

ΔT_e	Change in electrical torque
K_D	Damping torque coefficient of a synchronous generator
K_S	Synchronizing torque coefficient of a synchronous generator
L_{df}	Self-inductance of direct-axis field
T_D	Damping torque of a synchronous generator
T_S	Synchronizing torque of a synchronous generator
T_m	Tap changer mechanical time delay
X_d	Synchronous Reactance in rotor direct-axis
X_q	Synchronous Reactance in rotor quadrature-axis
r^{max}	Upper tap limit
r^{min}	Lower tap limit
ω_N	Rotor angular velocity
$\Delta\delta$	Rotor angle perturbation of a synchronous generator
AVR	Automatic Voltage Regulator
CHP	combined heat and power
COMTRADE	COMmon format for TRAnsient Data Exchange
CPU	Central processing unit
DG:	Decentralized or Distributed Generation
DSA	Dynamic Stability Assessment
HVDC	High-Voltage Direct Current
IEEE	Institute of Electrical and Electronics Engineers
Kbps	Kilobits per second
kV	Kilovolts
Mbps	Megabits per second
MTU	Master Terminal Unit
MW	Mega-Watts
NORDEL	Organisation for the Nordic Transmission System Operators
PMU	Phasor Measurement Units
RAM	Random access memory
RTU	Remote Terminal Units
SCADA	Supervisory Control and Data Acquisition
SVC	Static Var Compensator

UCTE	union for the co-ordination of transmission of electricity
ULTC	Under-Load Tap Changer
E	Output Voltage of a generator
pu	Per Unit

1 Introduction

An important characteristic of the contemporary technology is the existence of many different technical systems. According to their intended functionality and design, these systems vary in complexity and size. A distinction is made between compact and large technical systems. Typical examples of compact technical systems are: the cell-phone, the automobile and the computer. The complexity grade is increased in large technical systems, principally due to the amount of the structural components. Moreover such systems are spatially extended. To this second category of technical systems belong: the telecommunication networks, the traffic networks, the railroad networks and the electric power systems. A rigorous definition of technical systems will specify them as socio-technical systems; mostly because technical systems are socially structured. For traffic networks for example the social aspects are represented by the legal norms governing the traffic systems, whereas the roads and highways, the automobiles and the traffic lightning can be considered as the technical aspects. Generally seen, the technical systems play an important role in the industrialisation process and in the economic development of a country. They also have a significant impact on the daily social life. Undoubtedly, the technical systems have many beneficial effects but they also create new problems. Some of the situations to be administrated by their daily operation are among others: the assessment of negative external influences, the evaluation of the risks of failures and disaster, the system asset management, the system control, and the coordination problems between the system's structural components. Another characteristic for large technical systems is their constitution through many technical subsystems. These are usually independent in their individual conception and function, but are dynamically interconnected during the whole system operation. For this kind of systems it is particularly true that a constant grow in the system complexity constrains the designated system operator to elaborate new and effective conception and planning methods; furthermore it imposes also the development of more and more robust and sophisticated tools for the optimal representation of the evolution of the systems operational states.

The representation of the states of a technical system is motivated by the purposes of its surveillance and control. These actions are usually taken by a qualified personal in the system monitoring and control centre.

The surveillance of the operation of a technical system is for primordial importance particularly to ensure the system normal modus operandi and integrity. For more efficiency the surveillance of technical systems must be targeted and in (near) real-time modus. By the surveillance of technical systems it should be differentiated between *stability* and *security* issues. The optimal definition of both terms is decisive for the further qualification of the operational states of a given system. The stability analysis evaluates the actual system state. It allows the system operator to assess if a given system constellation will exhibit runaway dynamics (catastrophic failure) or return to an equilibrium (operating point) favourable to the further normal system exploitation in response to perturbation. It also permits to verify whether the conditions for the further save operation of system are respected.

The security analysis combined given system states with worsening scenarios to assess the system condition. The stability analysis is important in the control theory in general and for the control of a given technical system particularly. From a design and operational point of view it could be said that control is applied stability. It is a grave issue because feedback can result in systems that fail catastrophically due to instabilities [36].

The functions required for the monitoring of a technical system and their interactions are principally dictated by the end goal of the monitoring. Generally the system operational condition is analysed on the base of some measurements characterising its state, usually followed by their visualisation and interpretation.

The requirements for the real-time system monitoring can be generalised for all technical systems as follows:

- A suitable representation or modelling of the system to be monitored
- The real-time measurements of variables relevant for the evaluation of the system operational condition
- The real-time analysis of the system condition on the base of the realised measurements and according to the predefined conditions of normal operation.
- A rapid and meaningful representation of the results on the analysis.

To these can be added:

- An alarm raising when dysfunctions or critical operations conditions are recognized
- A listing of recommendations to normalize the system in case of the apparition of operational dysfunctions.
- The archiving of systems past modes (this can be helpful for the detection of typical critical situations)

The real-time aspect of a system monitoring has to be interpreted in light of the processes monitored and the communication capabilities of the monitoring system [11]. The real time monitoring trending is supplied by the continuous stream of one or several measurements in the system condition analysis tool.
According to the monitoring concept the measured data can originate from one or several measuring items. By several measuring items the measurements can be realized at the same location (different variables) or at remote locations (same or different variables). The further processing and analysis can respectively be separated of conjoint. For each system the principal challenge is always to develop an analysis tool to extract a useful knowledge from the realized measurements.
This thesis deals with the particular case of the real-time monitoring of the voltage stability in electric power systems.

1.1 Problem statement and motivation

Electric power is nowadays more than on ordinary commodity; it is an energetic vector of high importance for industrialized societies. Any long interruption of electrical energy supply cripples the business of a majority of activity sectors [1]. The ability of a power system to supply adequate electric service on a nearly continuous basis, with few interruptions over an extended time period is denoted in [2] as its reliability. The reliability and thus the continuous availability of these integrated systems formed by generation, transmission and distribution is a major concern for their operators in all industrialized countries. The reliable operation of a power system includes its technical safety as well as a sufficient transmission capacity. The reliability is a function of the time-average performance of the power system; it can be judged by consideration of the systems behaviour over an appreciable period of time. To be reliable, the power system operation must be stable most of the time. For this reason the planning, operation and control of a power system are to a significant extent governed by stability consideration [3].

The term stability in reference to power systems is defined as the continuance of the intact operation of power systems also following a disturbance [2], [12]. The conditions of intact operation are fixed by the technical operational limits and the physical limits applied to power systems. These limits concern the operation mode of the system and the thresholds fixed for its variables. Stability is a time-varying attribute which can only be evaluated by studying the performance of the power system under a particular set of conditions. The classification of the stability phenomena for power systems is made taking these particularities in account. The important aspects of these phenomena for power systems are elucidated further in this work, with an emphasis done on the voltage stability phenomenon.

1.1.1 Increase of power system failures worldwide

The figure 1.1 made on the base of the table presented in Appendix A shows an important increase of the power systems outages also termed as blackouts during the last decade. The tendency is still growing.

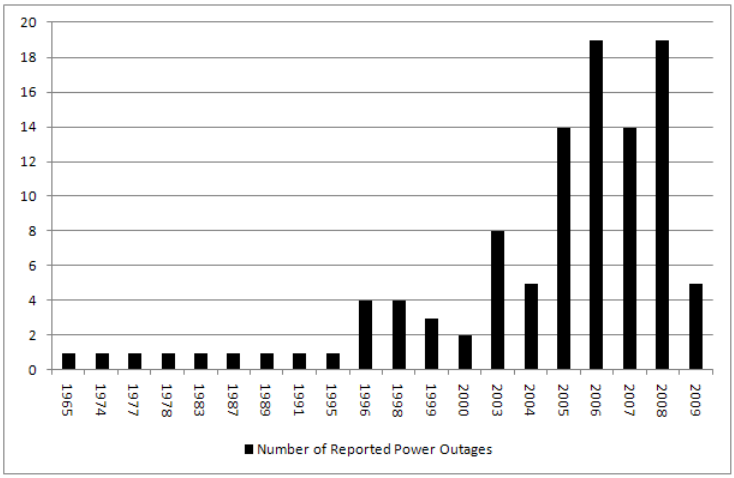

Figure 1.1: Total number of some yearly reported power systems outages worldwide (Until February 2009)

Different causes are listed in the table in appendix A as the initiating events of the power systems outages. Some of them can be termed as unanticipated and unavoidable seen from the side of the system operator. In certain cases the system operator cannot influence the degree of damages induced in the power system by these causes and their respectively corresponding grid events. But, in several cases the scale of the degradation of the power system could have been reduced by: the utilization of the adequate system defence plan and the presence of a sense of urgency of the situation (situational awareness).

Some power system outages originate sometimes from planned situations which are inadequately monitored during their realization. Also in this second case the lack of situational awareness is one of the reasons of the resulting system failures.
The growing tendency observed in the number of yearly power systems outages worldwide is therefore not only provoked by the augmentation of the critical climatic situations but surely also due to the inappropriateness of the existing monitoring of the power system to the actual situation in the electricity market. It became more difficult for the system operators to correctly assess the stability state of the power systems.
The monitoring philosophy of the electric power systems is since the liberalization of the electricity market subjected to strong changes by several factors of influence. These factors include:

- The separation of electric power generation and the grid operation what complicates the system technical optimization of the power plants output,
- the long delays by the upgrading and expansion of the electric grids and the more hardly forecastable energy transits, what lead to an augmentation of the bottlenecks in power systems,
- A constant augmentation of the demand of the electric power, the increase of the interconnections and of the power exchanges between neighbouring power systems, what raised the utilization of the transmission paths in the power systems

All these make the power systems more vulnerable to critical operational situations and to instabilities. Voltage instability is thereby one of the most important problem.

1.1.2 Power system real-time monitoring data sources

The critical nodes in power systems are nowadays mostly monitored using static or quasi-static methods and measurements. These methods are based on the cyclic non synchronized acquisition of root-mean-square measurements from remote terminal units (RTUs) of a SCADA (Supervisory Control and Data Acquisition) system. The traditional SCADA systems give only, if at all, very few information on the power system transients. For power systems which characteristics changes in fraction of seconds, the provision of more precise snapshots including the system transients can be crucial for the maintenance of the system integrity and the limitation of cascading failures in critical situations. The use of the Synchronized phasor measurement technology based on measuring items called Phasor Measurement Units (PMUs) is in this regard a good alternative. PMUs directly measure the phasors of the power system state variables which can be transmitted to the control centre via high-speed reliable communication infrastructures. The dynamic stability assessment based on data sets collected by PMUs is becoming the tendency in the monitoring of power systems. Due to their unique ability to provide synchronized phasor measurements of voltages and currents from widely dispersed locations in an electric power grid, PMUs are nowadays considered to be one of the most important measuring devices in the future of power systems. The PMUs can be used to build wide area measurement and protection systems to complement classic protection and SCADA applications to prevent cascading system outages and voltage instability.

On the other hand the utilization of the PMUs required their optimal positioning in the system and the accordingly handling of their data.

1.2 Objective and contribution

The emergence of innovative monitoring technologies yields a growth in the amount of the operational performance data of the power systems. To make sense of these data, the system operators need tools that will help them to infer the meaning of the measured data and, to discern their interrelationships with other already available system's data. Therefore robust algorithms must be developed to process and extract useful information from the PMUs data sets. As a contribution to the exploitation of the PMUs data sets, this thesis deals with the application of synchronized phasor data for the monitoring of the voltage stability of power systems particularly as influenced by the active power transfer magnitudes throughout their transmission networks[1].

The objective of the thesis is to develop an innovative method for the appropriate handling of the data measured by some distributed PMUs, with the aim to detect as early as possible when the power transmission system is in the process of losing its voltage stability. The method should permit to determine and visualize the voltage stability margin of the system operating points i.e. to define, in real operation time, how far a given operating point is from a point where voltage instability may occur. Furthermore, the practical applicability of the developed method should be demonstrated for an existing power system, wherefore the optimal PMUs placement must be defined. Therefore, a cooperation agreement is signed in the framework of this thesis with the Danish transmission system operator Energinet DK, to guarantee the access to a real power system dynamic model to be used for simulations, as well as to operative PMUs data used for the definition of an appropriate handling of such data in regard to real-time power system monitoring in general and to the application and the tests of the developed monitoring principle particularly.

[1] Influence of the loading of the transmission devices on the voltage stability

1.3 Tools and test systems

All the power system calculations and simulations relative to the tests of the monitoring method are realized with the grid calculation software DIgSILENT[2] "PowerFactory" further simply named PowerFactory®. PowerFactory® is a tool for application in the analysis of electric power systems and their control processes. It disposes of an integrated graphic user interface which includes drawing functions, analysis functions, and documentation functions as well as the important static and dynamic calculation functions in the form of an interactive grid diagram. The calculations functions comprise: the load flow calculation, the short circuit calculations, and the stability calculations. Also the analysis of the harmonics, the protection coordination and the modal analysis belong to the functions of the program. The management of the data necessary for the calculation of the energy supply system components (e.g., transmission line data, generator data) takes place with the help of an extensive data bank. The investigations carried out within the scope of this work are focused on the load flow and on stability calculations.

The advantages of the use of PowerFactory® for this thesis are principally:

- The simulations of the variables of interest can be performed in phasors as they are measured by the PMUs; directly usable data, termed later in this work as simulated phasor data is outputted.
- Variable time step is well adapted for long-term phenomena like voltage instabilities.
- Complete models with both fast transients and long-term dynamic are available.

[2] DIgSILENT = **DIg**ital **SI**mu**L**ation and **E**lectrical **N**e**T**work calculation program

The real voltage stability analysis by the principles and the theory of the method developed for the voltage stability monitoring is done using Matlab® from the Mathworks Inc. For this purpose the available phasors data are imported in Matlab® where they are worked out using the implemented algorithms.
Five test-power systems are used throughout the thesis. In regard to the analyses realised in the framework of this thesis, following utilization of these is made:

- Dynamic models of a *six-bus test-system* and of the *western Danish power system* (DK-VEST) are implemented in PowerFactory® for the simulation and the illustration of some theoretical aspects of the voltage stability in power systems.
- The study of PMUs positioning methods in power systems is made on: the *IEEE 14-bus test system*, the *IEEE 57-bus test system* and on DK-VEST. Thereby only the topological structure of these systems is considered.
- The simulated phasor data utilized by the tests of the developed PMU based voltage stability monitoring method originated from the dynamic simulations of the DK-VEST model and of a *two-bus test system* also implemented in PowerFactory®.

1.3 Outline of the thesis

The thesis started in chapter 2 with a presentation of the limits to be observed by the operation of the power systems. The particularities of the actual operational environment of the power systems are debated. It is followed by an overview of the evolution of cascading failures in power system. A discussion of the difference between the stability and security concepts for power systems is made. The chapter is closed by the classification and distinction of the power system stability phenomena.
As the main subject of this thesis the voltage stability of power systems is separately analyzed in chapter 3. The definition of this problem in the context of the thesis is given, a sub-categorization is proposed, and a study of the mechanisms of voltage instability in power systems is done.

Chapter 4 begins with the presentation of the mathematical background of the power voltage stability phenomenon. The objective followed is the recognition of the occurrence of the voltage instability according to the stability definitions given in chapter 3, and the theoretical definition of the limit of voltage stability. A survey of the methods for the voltage stability analysis is realized as next, and their applicability for online monitoring purposes are discussed. The presentation of the concept of stability monitoring used in this thesis ends this chapter.

Chapter 5 presents an overview of the theory of the synchronized phasors measurement. The general concept of the PMU based monitoring of power system is discussed and the related problems and practical considerations are analyzed. The question of the positioning of the PMUs in power systems is debated on the example of a practical comparison of methods for the optimal PMU placement. Finally a survey of the existing applications of synchronized phasor measurements is done.

The development of an innovative method to assess the voltage stability of electric power transmission paths in real time modus using PMUs data sets is presented in the chapter 6. The method is based on the voltage stability principles discussed throughout the thesis. This chapter includes the brief presentation of the tools developed for PMU data handling and for phasors based voltage stability analysis. The applicability of the method is tested on a small (two-bus) test system and on a large power system represented by the 400 kV transmission system of DK-VEST, for which the PMUs locations are defined for its complete observability.

The Chapter 7 reminds the focus of this thesis and summarized the work done. The chapter is ended by some proposals for future work.

2 Assessment of the power systems state

This chapter presents the power systems physical and theoretical operating limits as the core of further considerations of the assessment of their operating status. Some aspects of the power system's operation in the deregulated environment are presented to show out the reasons why modern power systems became more vulnerable to contingencies. The typical evolution of cascading systems failures is explained. It is followed by the definitions and the separation of the concepts of power security and stability. Finally a classification of the power system stability phenomenon is done and the causes of different types of instabilities are debated.

2.1 Introduction

2.1.1 Power systems as Complex Entities

Power systems are one of the most wide-spread and complex man-made infrastructure systems. The size of a power system is usually evaluated with regard on the number of the nodes used to represent it during its calculation[3] and their operational complexity is particularly due to the multitude of their interdependent constituent's parts. From a functional point of view, the complexity of the power systems technical operation comes principally from:

- The multiplicity of the time scales implicated (from few microseconds for transients phenomena to some minutes for power plants thermal processes)
- The fundamental oscillating character of their electromechanical phenomena
- Their non-linearity (Their behaviour depends on many factors an variables)

[3] Consideration of the power systems digital models.

This situation is worsened by the number of the power systems components and their diversity in the same constituent's categories: e.g.: More loads and many different types of loads or load areas[4], more generation and many different types of generation units.
The operational behaviour of each component is particular and became more complex as more control units are needed for each many different items in the power systems. The control units are used to supervise and if needed to regulate the behaviour of the system components individually but always in regard to their interaction with the rest of the system. Therewith, the entire power system performance is controlled at each operating instant. The principal goal followed is the maintenance of the system in an operating state suitable for the continuous and faultless power delivery. The conditions of normal operating conditions are bounded by the systems variables operating limits.

2.2 Power systems operating limits

Electric power can be stored only in very few cases and must mostly be consumed as it is produced. The normality of the power supply and thus of the power system operation is conditioned by a constant balance between the power generation and the power consumption at the loads. The continuous variations in the demand and supply[5] induce also a constant variation in the variables of the power systems and hence in their operational conditions. As mentioned above, the conditions for a reliable and secure operation of power systems are defined by a set of predefined technical thresholds which must be always observed.

As presented in [14] the technical operational thresholds for power systems can be divided in: *physical* and *system theoretical*. The physical thresholds refer to the limits of the respective systems variables.

[4] Allusion to the types of loads: rural, residential, industrial, commercial etc.
[5] In a system with a large share of distributed generation and renewable energy resources, also supply will vary considerably [13]

They can be summarised by the following equations [14]:

$$\begin{aligned} U_{min} < U_i < U_{max} \\ I_{ij} < I_{max} \\ f_{min} < f < f_{max} \end{aligned} \tag{2.1}$$

Where i and j represent some given nodes (buses) of the system.

The system's voltages, currents and frequency thus have limit values for which the system operation is admissible. The definition of the operating limits is individual for the power system components i.e., each electrical equipment[6] within the power system has its operating limits. The limits defined in (2.1) are also relevant for the power systems buses serving as connection points to the electrical equipment. Other operating limits are constituted by the real and reactive power flows on individual equipment under steady state, short-circuit, and transient conditions as specified by the equipment manufacturer or owner [20]. Examples are the active power limit and the reactive power limit of synchronous generators.

$$\begin{aligned} Q_{min} < |Q_i| < Q_{max} \\ P_{min} < P_i < P_{max} \end{aligned} \tag{2.2}$$

With i representing a given electrical equipment.

Power systems operating limits are based upon operating limits as applicable to its components and can be then understood as:

The maximum or minimum voltage, current, frequency, or real and reactive power flows through a power system that would not violate the applicable physical limits of any equipment comprising the system under all operating conditions.

[6] Electrical Equipment: Every electrical device with terminals that may be connected to other electrical devices

On the other hand the power systems are constantly subject to some variations and perturbations which are susceptible to jeopardize the compliance of their physical limits.

2.2.1 Modification and Perturbation of the Power Systems Operation

The variations in the state of power systems are materialized by the changes of their operating point, what is equivalent to the change of the values of one or more systems variables or operating parameters. They are generated through voluntary switching operations in the system control centre or introduced by not influenceable causes. To the latest belong the contingency situations. These are failure or outage of a system component, such as a generator, transmission line, circuit breaker, disconnector, or other electrical element. A contingency also may include multiple components, which are related by situations leading to simultaneous component outages [20]. Contingencies are triggered by system internal changes or occur due to external influences. To the systems internal changes belong for example: The variations in the power demand (load profile), the isolation failures, the system topology changes for exploitation reasons and the intermittent factor of the generation. As examples of external influences could be considered the grid events leading to the physical outage of a given power system equipment, e.g.: Line outage due to the climatic aggressions (lightning stroke, ice accumulation on a line segment), a tree fall or an accidental plane landing on a transmission line (see figure 2.1).

Some of the power system internal changes such as the load profiles can be forecasted with a relatively good accuracy; see for examples: [15], [16], and [17]. On the other hand many of the grid contingencies are stochastic and unpredicted. In every case an efficient system operation must guaranty that, by occurrence of a contingency or in case of an internal change the resulting new system operating point is also acceptable regarding the pre-defined technical operating constraints.

For a power system subject to state changes, it is important that when the state changes are completed, the system settles to new operating points such that no physical constraints are violated. This implies that, in addition to the next operating conditions being acceptable, the system must survive the transition to these conditions [12].

The system theoretical thresholds are then required to continuously maintain the power systems in a state where the physical constraints are respected. They describe the property of the power systems to reach an operating point where its physical limits are still adequate after a state change. This property builds the base for the definition of the power systems operating security. A following paragraph argues the definition of the term security in relevance to power systems. The exigencies to the power systems security calculations are dictated by the overall situation of the electric power market and the presumed resulting impact on the power systems operation.

The following paragraph presents the actual operating situation for contemporary power systems and points out the new challenges the transmission systems operators are confronted to during the daily system operation.

Figure 2.1: Typical example of unpredicted grid event: A plane landing on a 380 kV transmission line on the 17.08.2008 near Ulm-Kempten in Germany [Source: Spiegel TV]

2.3 Power systems operation in the deregulated context

2.3.1 Operating conditions

There was a time when power systems were developed and operated in regulatory frameworks. During that period of time, the electric utilities were defined as vertically-integrated[7] companies operating under business models involving monopoly and oligopoly franchises. Under a certain regulation, each local electric utility held a government-granted franchise, giving it the exclusive right to provide electric service in a given territory.

[7] Vertically integrated meant they performed all of the functions involved to produce, transport and distribute electric power for a defined region [4]

This situation has changed during the last decades with the advent of a significant deregulation or liberalisation of the electric power markets[8]. This means among other that there is no longer a strict monopoly in electric power business. The functions performed by a single vertical utility are fragmented and shared among a number of separate companies [4]. The power sector is henceforth characterized by an horizontal-integrated structure, where the power transmission is a distinct business activity linking the two other sectors of activity i.e.: the power generation and distribution. The trend towards the liberalization of electric power sector has been undertaken (concomitantly with market reforms in other sectors, such as telecommunications and public transport) in order to increase efficiency and enhance service quality. This resulted in the creation of a competitive environment in this sector to which the electric utilities have to adapt their working rules. An important consequence of the liberalization of the electricity markets is the development of new products and services. The utilities politics is henceforward more customer-orientated[9]. The major differences between the monopolistic and the liberalized electricity market are summarized in figure 2.2 for some given problem areas.

[8] Directives EC 96/92 and CE 2003/54

[9] In a liberalized market, customers turn out to become the even most influential part of the electric utilities' selection environment… business and industrial customers have learned to aggregate their demand and their market power in building purchase co-operations or asking for a master agreement covering for example all national subsidiaries of a firm… Private customers cannot be ignored any longer as they have influence on the decision making and the public image of utilities…[5]

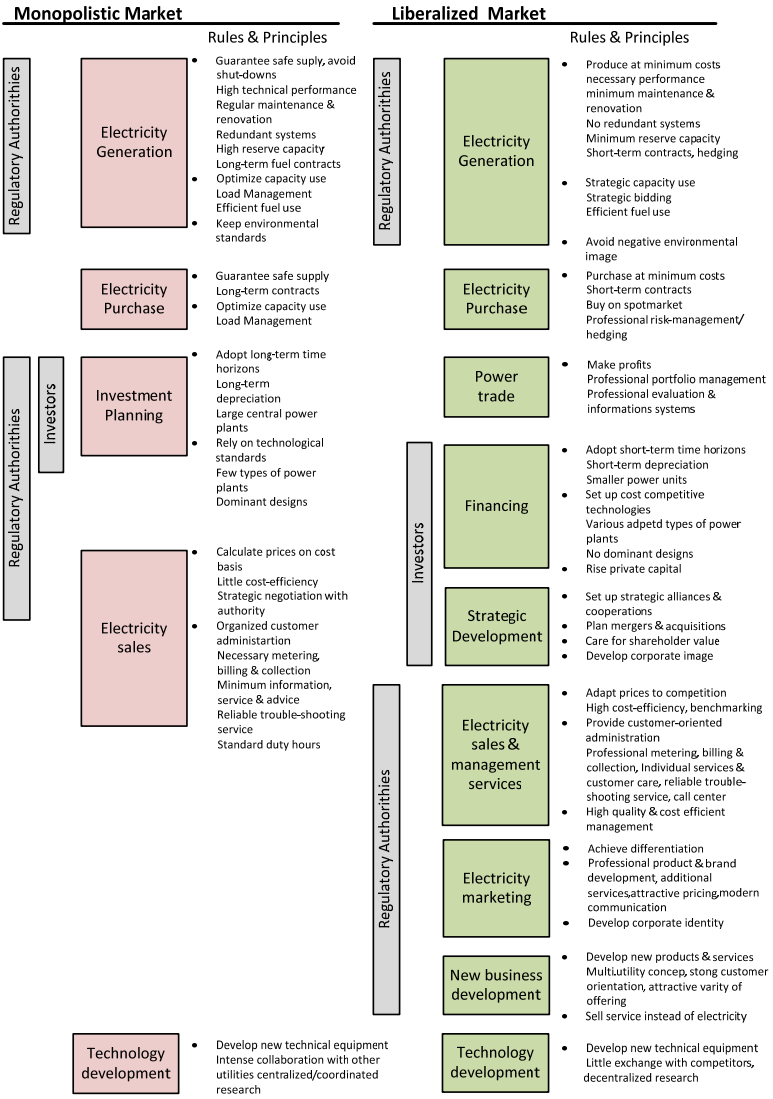

Figure 2.2: Management rules and principles for selected problem areas in electricity supply [5]

The liberalization leads to a rapid multiplication of the actors on the electric power sector. The idea of a competitive and wide-spread electricity market gives the possibility to the consumers to choose their electricity provider on a price-quality-service base, even beyond the limits of their own countries. This leads to interconnections between power systems and to the creation of new loading patterns. Furthermore it yields physical energy flows with considerably increased amplitudes as those for which the power systems networks were conceived at first. This situation is directly linked to the rapidly growth of the electricity demand observed during the last decades in many industrialized countries. In the context of the deregulation, the complications surrounding rising demand for electricity are intensified by the massive integration of decentralized or distributed generation units - connected at all voltage levels- into the existing power systems. The share of such generation units in the electricity production is still increasing in several countries. Some of the advantages presented by distribution units are:

- The power plants are installed relatively near to the customers. That contributes to the reduction of the costs for power transmission and distribution and sometimes of the power losses.
- Locations are easier to find for “small” power plants
- The installation time is reduced by decentralized generation units
- The technology used is more environmental-friendly
- The cogeneration – one of the most used form of decentralized generation- improve the energy efficiency of the installations

With the large scale connection of distributed generation units to the bulk power networks the grid operators are facing new problems:

- The faultless coordination of the decentralized power plants with the bulk power systems[10] and moreover,
- the appearance of the bi-directional energy flows between the respective voltage levels.

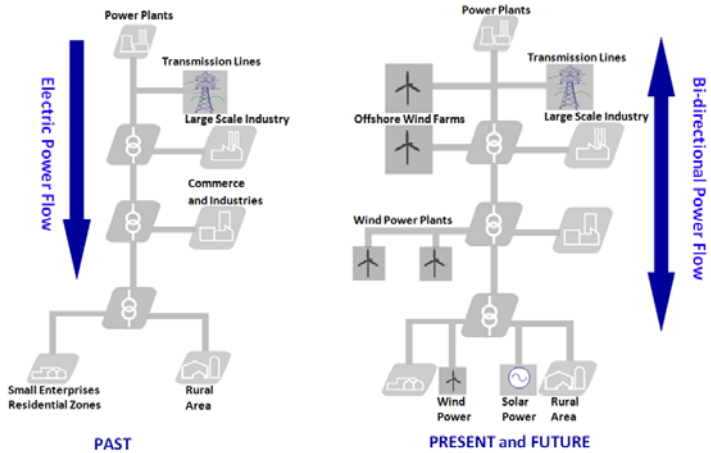

Figure 2.3: Changes in the electric energy supply structure

As a direct consequence to the rising transfers of electrical energy, the utilization of the transmissions systems has increased. Due to the partly highly meshed character of the existing power systems[11] the energy transfer patterns are more complicated and most of the time unpredictable during the system operation.

The effects resulting from the transfer flux on a transmission line within a given system are unpredictable as well and can be even

[10] A typical example is named in [6]: …In western Denmark the penetration of DG units is high compared to the load demand. In some periods the wind power can cover the entire load demand…
To ensure a stable operation, it is necessary to have some regulation options which can include: The lowering of the outputs of other small power plants or the export of the surplus of energy…

[11] this is particularly true for European power grids

extended to the neighbouring systems. As an example: a commercial transaction between North-Germany and South Germany can induce electric fluxes un-identified but important in their amplitudes, on transmission lines in the Benelux, France or Switzerland. These effects are non negligible, because they can contribute to the variations of the amplitude of the transmission systems loading in a bad way.

The consideration of all these facts combined with the health concerns and environmental and costs pressures on transmission systems expansions[12] which have been thereby kept relatively slow, have forced the power systems operators to reduce their operating margins limits. This results in larger stress of the transmissions systems which are operated closer to their loading limits than before. In the case of a transmission system operating near its loadability limits[13] the occurrence of a contingency situation (e.g.: further impending power flows through the outage of a parallel transmission line) can lead to a system abnormal behaviour[14].
The non detection of an abnormal behaviour in sufficient time interval to launch the corrective actions[15] can result in a system failure. A failure at one location of the transmission system can quickly degenerate in cascading failures affecting the behaviour of a larger portion of a given power system. The cascading failure is the usual mechanism for large collapses (blackouts) of electric power transmission systems [18].

[12] A typical example is given in the reference [34] from the year 1994: The state of Florida enacted a moratorium against the building of' new transmission lines until a formal public policy limiting electric and magnetic field levels near transmission lines was passed. This new regulation is estimated to cost Florida utilities an additional $100 million to *$5* billion over the next 30 years. Similar measures have been proposed in other states of the USA…

[13] The conditions of the loadability limits must be properly defined under a specific set of assumptions.

[14] Limit compliance violation

[15] e.g.: Load shedding

Typical examples of power systems collapse causes by cascading failures are:

- the August 1996 blackout in North-western America that disconnected 30,390 MW of power to 7.5 million customers [19] and,
- the August 2003 blackout in North-eastern America that disconnected 61,800 MW of power to an area spanning 8 states and 2 provinces and containing 50 million people [18], [19].

Large power systems collapse is typically caused by complex cascading sequences of rare systems events. A description of a typical collapse mechanism is given in the next section.

2.3.2 Cascading events and system breakdown

As said above, electrical power transmission systems are interconnected networks of large numbers of components that interact in diverse ways. When component operating limits are exceeded protection acts and the component “fails” in the sense of not being available to generate or transmit power. Components can also fail in the sense of misoperation or damage due to aging, fire, weather, poor maintenance or incorrect design or operating settings. In any case, the failure causes a transient and causes the power flow in the component to be redistributed to other components according to circuit laws, and subsequently redistributed according to automatic and manual control actions. The transients and readjustments of the system can be local in effect or can involve remote components, so that a component disconnection or failure can effectively increase the loading of many other components throughout the network. In particular, the propagation of failures is not limited to adjacent network components. The interactions involved are diverse and include deviations in power flows, frequency, and voltage as well as operation or misoperation of protection devices, controls, operator procedures and monitoring and alarm systems. However, all the interactions between component failures tend to be stronger when components are highly loaded.

For example, if a more highly loaded transmission line fails, it produces a larger transient, because there is a larger amount of power to redistribute to other components, and failures in nearby protection devices are more likely [18]. Moreover, if the overall system is more highly loaded, components have smaller margins so they can tolerate smaller increases in load before failure, the system nonlinearities and dynamical couplings increase, and the system operators have fewer options and more stress.

A typical large blackout has an initial disturbance or triggering events followed by a sequence of cascading events. Triggering event separates the period of accumulating multiple "indirect" (not causing directly an emergency situation) factors from the sequence of events that represent the course of emergency and have a direct cause-effect relation with subsequent phases of the system emergency.

At the initial stages the cascading process develops relatively slowly and accelerates in the course of emergency [21]. Each event further weakens and stresses the system and makes subsequent events more likely. Examples of an initial disturbance are short circuits of transmission lines through untrimmed trees, protection device misoperation, and bad weather. A generalized scenario of the development of a cascading failure is schematized on the following figure 2.4 on the base of the analysis of sequences of events at development of system cascading emergencies[16] that have occurred in the past years in power systems of different countries worldwide.

[16] Some real system cascading failures which happened the last years worldwide are fully described in [18, 19, 20, 21]

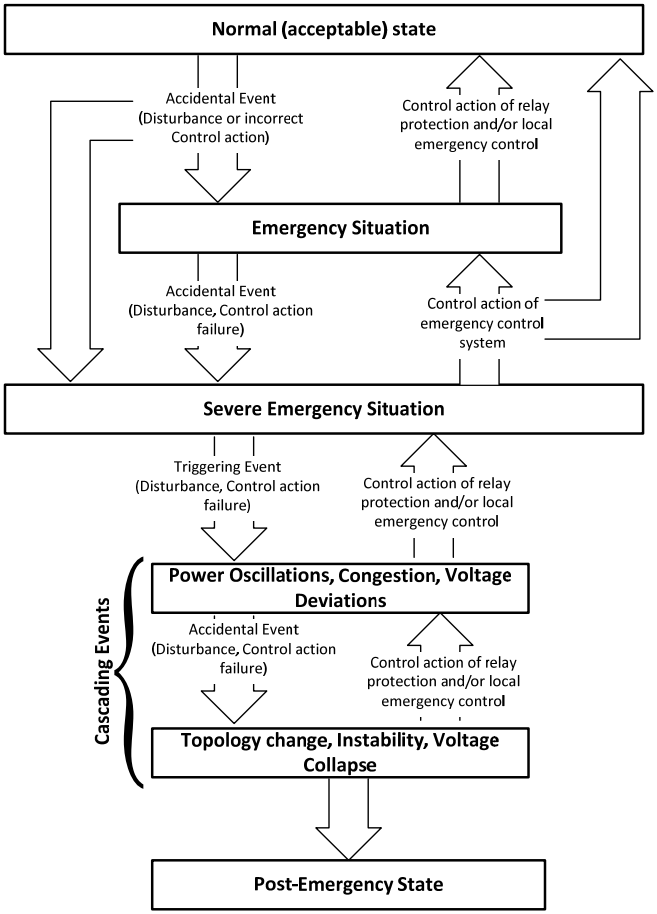

Figure 2.4: Typical scenario of cascading system breakdown

The blackout events and interactions are often rare, unusual, or unanticipated because the likely and anticipated failures are already routinely accounted for in power system design and operation. The complexity of the cascading failure phenomenon is such that it can take months after a large blackout to sift through the records, establish the events occurring and reproduce with computer simulations and hindsight a causal sequence of events.

2.3.3 Power system monitoring to mitigate the violations of operating limits

As stipulated in [7] and [8] the most of the North American blackouts were due to the lack of situational awareness. This assumption can be extended to most of the other large system blackouts which happened throughout the world during the last years. The triggering event of the majority of those systems failures was associated to the overloading of a transmission path. In a deregulated environment, the transmission system operators must be supported by efficient tools for the real-time assessment and the eventually correction of the system state for the safe systems operation near their technical limits. These tools should permit to know at each operating instant if the regnant operating point is safe. In other words they must allow defining how much power can be transferred safely across a transmission system without violating any operating limit. Their functions should be resumed in the real-time quantification of the power transfer amount and the further calculation of the margin to a defined transfer capacity limit of the transmission system. The often occurrence of several transmission systems breakdowns worldwide let suppose that, the performance of the currently available means for system state calculation and visualisation are still limited. Thus the need of innovative tools to monitor the power transmission systems became more urgent than before. An efficient system monitoring will significantly contribute to maintain the system within the defined acceptable operating limits as the daily operating conditions vary.

To reach this goal of a secure operation of power systems, the system theoretical limits defined in 2.2.1 must be always respected. The system theoretical limits include [14]:

- The power system stability[17],
- The power systems outage security[18] and,
- The power systems short-circuit power.

[17] Its classification follows in a further paragraph of this work
[18] e.g.: N-1 criterion (outage of the electrical equipment)

The situational awareness during the power system operation requires the continuous and conjointly surveillance of all these limits. Taking in account the evolution observed during the recent years on the electric power market worldwide the exigencies to the power systems security calculations have also evaluated. The consideration of the power stability has gained a greater importance as before when the power system security assumptions were only limit to the calculation of the systems outage security and short circuit power.
The next section defines the concepts of power system stability and security and elucidates the relationship between them.

2.4 Power system stability

2.4.1 Definition and distinction from power security

As defined in [12] the s*ecurity* of a power system refers to the degree of risk in its ability to survive imminent disturbances (contingencies) without interruption of customer service. According to the same reference, it is related to the robustness of the system to imminent disturbances and, hence, depends on the system operating condition as well as to the contingent probability of disturbances. According to Prabha Kundur [23] power system stability may be defined as the property of a power system that enables it to remain in a state of operating equilibrium under normal operating conditions and to regain an acceptable state of equilibrium after being subjected to a disturbance. A general and formal definition of the power stability is proposed in [12, 24] and sounds as follows:

Power system stability is the ability of an electric power system, for a given initial operating condition, to regain a state of operating equilibrium after being subjected to a physical disturbance, with most system variables bounded so that the integrity of the system is preserved.

Taking in account the association of the power stability to the continuous intact operation of the power system also after a disturbance, a direct and tight relationship is established between the power systems security and stability. The system security is distinguished from the system stability in terms of the resulting impact of a given system event on its operational status. The power system surveillance thus comprises a post-event (static) aspect and a dynamic aspect. The first is to verify that no equipment ratings and systems constraints are violated after the systems changes has occurred. The latest is to check if the systems behaviour is always intact and its constraints are respected during the transition from an operating point to another. For these reasons, the stability analysis of power systems is considered to be an integral component of the system security assessment. The monitoring of the power system stability and security is simultaneous, but the exigencies to the tools for system dynamic stability and security assessment differ.

2.4.1.1 Parenthesis on contingencies screening

The difference between both power systems stability and security concepts comes from the consideration of eventual contingencies. The power system stability assessment is done on the base of data sets assumed to represent a true steady-state operating condition whereas its security assessment is extended by the considerations of some forecasted conditions determined by a set of contingencies. A subsidiary tool for contingencies screening, analysis and ranking is then needed for this purpose[19]. A key decision for the implementation of such tools is the scope of contingencies to be studied. For some reasons, not the least of which is the security state calculation (computation) speed, it is impractical and uneconomical [12] to fully study all possible contingencies. Only a set of credible (pre-assigned) contingencies is usually considered.

[19] Subsidiary tool for contingencies screening, analysis and ranking is then needed. Such a tool will evaluate of the impact of the occurrence of a list of contingencies (e.g.: line outage, generator outage) on the regnant power system condition.

The credible contingencies are selected and ranked on the basis they have a high probability of occurrence and a significantly high degree of severity, given the large number of components comprising the power systems. The selection can be obtained from system operation past experiences or is based on the applicable operating criteria such as N-1 or N-2[20], which must in turn be specified in terms of voltage level and electrical/geographic region (for example, "all N-1 for a given voltage level and above, within the study region") [25].

A typical algorithm reflecting the essence of the contingency screening and ranking purposes is the look-ahead ranking algorithm presented by Hua Li et al. in [22]. The principle of the look-ahead contingency screening and ranking is two-fold:

1. to rapidly screen out, from a large set of credible contingencies on a power system with committed power transactions, the set of insecure contingencies and critical contingencies. Insecure contingencies will result in immediate system collapse while critical contingencies will result in very small load margins with respect to committed power transactions; and
2. to rank the set of severe contingencies according to their impacts on the power systems with committed power transactions.

One physically meaningful impact is the look-ahead load margin of the power system to a define collapse point.

Several algorithms have been developed by other researchers and can be found in the specialized literature. Aside the important computational intensity (particularly in case of very large power systems), a major shortcoming of the contingencies screening is still the completeness of the list of contingencies considered.

In some particular cases there is always a risk that, under certain operating circumstances a "non-credible" contingency appears and lead to a cascading failure of the system.

[20] Under N-2 means the outage of two system's components of the same class or function (2 generators or 2 transmission lines) or the outage of components from separate classes (e.g.: 1 generator and 1 transmission line)

The monitoring theory developed in this thesis is limited to the consideration of true system operating conditions i.e. of the power system stability.
A definition of the power system stability in the context of the thesis follows in a next paragraph.

2.4.2 Power system stability problem

2.4.2.1 Concept of stability for power systems

Stability is a condition of equilibrium between opposing forces. For the power systems the forces in opposition are constituted by the electric power *generation* and *consumption* (load demand). The stability of a power system is hence by its ability to remain in operating equilibrium. By occurrence of a system change or a disturbance the stability depends on the initial operating condition and the nature of the disturbance. Instability results when a system change or the disturbance leads to an imbalance between the forces in opposition. To maintain the stability the system must successfully meet the load demand under a satisfactorily operation within the boundaries of the operating limits at each equipment. A power system is stable if following a system variation (e.g.: Change in the load demand) or a contingency it will reach a new equilibrium state where all the physical limits –defining the system normal state- are available or can eventually be restored by automatic controls or human operators. On the other hand, if the system is unstable, it will result in a run-away or run-down situation characterized by the degradation of the system operation normality; e.g.: progressive decrease in bus voltage. A system is unstable if it is operated at a point where its physical limits are violated or where a normal system operation cannot be restored. Power system stability is a single problem; however it is impractical to deal with it as such. Instability of power systems can take different forms and is influenced by several factors. Analysis of stability problems, including the identification of the essential factors that contribute to instability is facilitated by the classification of stability into appropriate categories [12, 24].

The principles of the power stability categorization are elucidated in the next sub-paragraphs and standard classifications are given.

2.4.2.2 Power system stability classification

The primary purpose of classifying power system stability phenomenon is to aid in its analysis as different techniques are employed to ferret out the underlying causes of the symptoms of a particular disturbance.

The general principles of the classification of the power are defined by Kundur in reference [23]. These principles are further used in [12] to justify the typization of the power system stability. According to these references, the classification of the power system stability is based on the following considerations:

- The physical nature of the resulting instability (related to the main system variable in which instability can be observed).
- The size of the disturbance considered (which influences the method of calculation and prediction of stability).
- The devices, processes, and the time span (that must be taken into consideration in order to assess stability) and
- The most appropriate method of calculation and prediction of stability.

An overall description of the power system stability problem is illustrated by the following figure 2.5. The different categories of power system stability are identified and their classes and subclasses are highlighted.

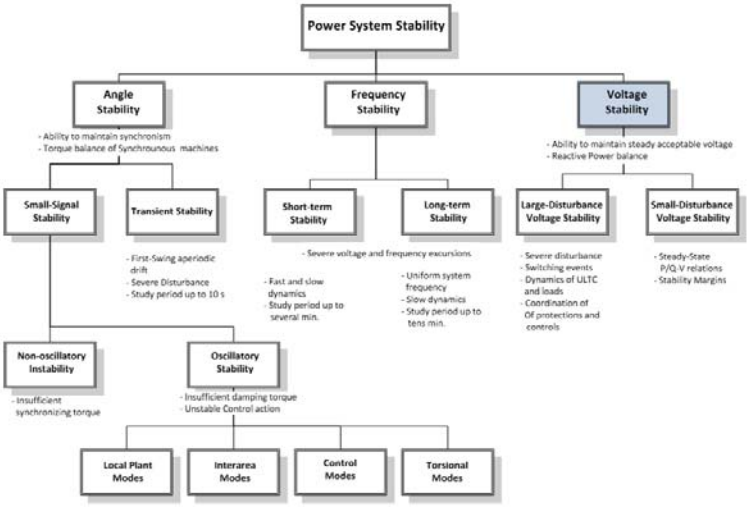

Figure 2.5: Classification of power system stability

A Rotor Angle Stability

As already said above, the total active electrical power fed into the power system by the generators must always be equal to the active power consumed by the loads, this includes also the losses in the system. Under such normal operating conditions that will also mean a similar balance between the loads and the power fed into the generators by the prime movers, e.g. the hydro and steam turbines. The balance observed is associated to the equilibrium between the mechanical torque (generator input) and the electrical torque (generator output). If the system is perturbed, this equilibrium is upset, resulting in acceleration or deceleration of the rotors of the generators. If one generator temporarily runs faster than another, the angular position of its rotor relative to that of the slower machine will advance. The resulting angular difference transfers a part of the load from the slow machine to the fast machine, depending on the theoretically known power angle relationship. This tends to reduce the speed difference and hence the angular separation [26].

Beyond a certain limit an increase in angular separation is accompanied by a decrease in power transfer; this further increases the angular separation and thus leads to instability. The instability occurs in this case in the form of increasing angular swings of some generators leading to their loss of synchronism with other generators. And the *rotor angle stability* is then concerned with the ability of interconnected synchronous machines to remain in synchronism under normal operating conditions and after being subjected to a disturbance.
The change in electrical torque ΔT_e of a synchronous machine following a disturbance can be resolved in two components. Its equation is given in [27]:

$$\Delta T_e = K_S \cdot \Delta\delta + K_D \cdot \Delta\omega = T_S + T_D \tag{2.3}$$

The first component $K_S \cdot \Delta\delta$ is the synchronizing torque T_S which represents the torque change in phase with the rotor angle perturbation $\Delta\delta$. The second component $K_D \cdot \Delta\omega$ is the damping torque T_D and determines the torque change in phase with the speed deviation $\Delta\omega$. K_S and K_D are respectively the synchronizing torque coefficient and the damping torque coefficient.
The existence of both components of torque guarantees the rotor angle stability of each synchronous generator within a power system. The Lack of synchronizing torque results in *non-oscillatory* (aperiodic) *instability* whereas the lack of damping torque results in *oscillatory instability*.

For more convenience in the analysis the rotor angle stability is splitted in two subcategories:

- Small signal stability
- Transient stability

Small signal stability is concerned with the ability of the power system to maintain synchronism under small disturbances. The disturbances are considered to be sufficiently small that linearization of system equations is permissible for purposes of analysis [12, 23]; e.g.: small changes in load.

In today's power systems, small-disturbance rotor angle stability problem is usually only associated with insufficient damping of oscillations[21]. The time frame of interest is on the order of 10 seconds following the disturbance.

The stability modes involved in small signal rotor angle stability are constituted by:

- Local plants modes also called machine-system modes, which involve small parts of the power system and are associated with rotor angle oscillations of a single machine against the rest of the system.
- Interarea modes, associated to the oscillations of a group of generators in one power system area swinging against a group of generators in another area.
- Control modes are local modes resulting from poorly tuned control units.
- Torsional modes are associated with turbine-generator shaft system rotational components. They may be caused by interaction with the excitation control, speed governors, High-Voltage DC (HVDC) controls and series capacitor compensated lines.
-

Transient stability is concerned with the ability of the power system to maintain synchronism when subjected to severe disturbances; these include: the loss of a generating station, loss of a transmission lines carrying bulk power, or the loss of a major load. Instability is in the form of aperiodic drift due to insufficient synchronizing torque, and is referred to as first swing stability. In large power systems, transient instability may not always occur as first swing instability associated with a single mode; it could be as a result of increased peak deviation caused by superposition of several modes of oscillation causing large excursions of rotor angle beyond the first swing.

[21] The non-oscillatory instability problem has been largely eliminated by use of continuously acting generator voltage regulators; however, this problem can still occur when generators operate with constant excitation when subjected to the actions of excitation limiters (field current limiters) [12].

The time frame of interest in transient stability studies is usually limited to 3 to 5 sec following the disturbance. It may extend to 10 sec for very large systems with dominant inter-area swings.

The physical phenomena following the power system disturbances for the case of the rotor angle stability are explained here above. The occurrence of this instability can also seriously damage the generators, what will result in costly overhaul and long downtimes for their repair. The equipment safety thus requires the use of unit protection devices. Trivially said these are of the form of sensors detecting when a generator begins to go out-of-step, as soon as this is the case, the sensors will trip the generators. Since the system is interconnected through transmission lines, the imbalance in the generator electrical output power and mechanical input power is reflected in a change in the flows of power on transmission lines. The attempt to overcome the rotor angle instability can thus create, in certain cases a critical stability situation on the transmission lines of a power system. This is particularly true in the case of the coincidence of the trip of the out of step generator with high power transfers over the transmission lines. This can result in other emergency situations, e.g.: lack of reactive power, transmission lines overloading etc. This is a typical example of the transposition of instability in the power systems.

B Frequency stability

Frequency stability refers to the ability of a power system to maintain steady frequency following a severe system upset resulting in a significant imbalance between generation and load. It depends on the ability to maintain or restore equilibrium between system generation and load, with minimum unintentional loss of load. Instability that may result occurs in the form of sustained frequency swings. A typical cause for frequency instability is the loss of generation; whereupon the system frequency drops.

The primary control then immediately activates (usually in the period of 2 to 30 seconds after the disturbance [28]) the spinning reserve[22] of the units scheduled for this purpose.
The goal is to restore the balance between generation and load. Due to its proportional character the primary control cannot return the frequency to its nominal value and there always will be a certain frequency offset. A Secondary control is activated afterwards (in the period of 30 seconds to 15 minutes [28]) with the purpose of eliminating area control error, restoring system frequency to nominal, and freeing primary reserves. If it is not successfully controlled the frequency instability could lead, beyond a certain limit of the frequency swings to tripping of generating units and/or loads by protection devices. In large interconnected power systems, this type of instability is usually associated with the power systems islanding. Stability in this case is a question of whether or not each island will reach a state of operating equilibrium with minimal unintentional loss of load. It is determined by the overall response of the island as evidenced by its mean frequency. Generally, frequency stability problems are associated with inadequacies in equipment responses, poor coordination of control and protection equipment, or insufficient generation reserve. As stipulated in [12], the characteristic times of the processes and devices that are activated during frequency excursions, will range from fraction of seconds, corresponding to the response of devices such as under-frequency load shedding and generator controls and protections, to several minutes, corresponding to the response of devices such as prime mover energy supply systems and load voltage regulators. Therefore, as identified in figure 2.5, frequency stability may be a short-term phenomenon or a long-term phenomenon.
A detailed summary of the two first power system stability problems as defined on figure 2.5 is given in the preceding paragraphs.

[22] The spinning reserve is the unused generating capacity which can be activated on decision of the system operator. It is provided by increasing the power output of generating devices which are synchronized to the network and able to affect the active power. For most of the generators, this increase in power output is achieved by increasing the torque applied to the turbine's rotor

The third power system stability problem is the voltage stability. Further analyses and the monitoring method proposed in the framework of this thesis are focused only on this last type of power system stability. A discussion on the aspects of the voltage stability, in general and as used in the context of this thesis is made separately and follows in the next chapter.

2.4.2.3 Alternative classification of the power system stability

At this point and as inspired from [29], the voltage stability is placed within the general context of power system stability according to other classification principles. Based upon the time frame and the instability driving force criterion, the following classification of the power system stability is obtained:

Table 2.1: Alternative power system stability classification

Time Scale	Generator-driven	Load-driven
Short-term	Rotor angle stability	Short-term voltage stability
Long-term	Frequency stability	Long-term voltage stability

Also in the case of the voltage stability the short term time frame characterizes electromechanical dynamics lasting for a few seconds. Automatic voltage regulators, excitations systems, turbine and governor dynamics all act in this time frame. On the other hand, in the long term time scale the power system transients last for several minutes. Various systems dynamic component such as: transformers tap changers and generators limiters are present in this time frame.

2.5 Chapter summary

Despite the increased complexity of contemporary power systems and the new challenges introduced by the prevailing electricity market conditions, the operation of power systems is constrained by strict operational limits. An enumeration of these limits is given in this chapter.

The compliance of these limits is presently more difficult than ever before as the power systems are operated closer to them. This makes the system more vulnerable to unanticipated disturbances and to all types of contingencies. Their occurrence can have fatal consequence in form of cascading system failures or blackouts. A typical scenario of such a cascading event is illustrated by the figure 2.4. The surveillance of power systems is thus more important than in the past, to assess their status in accordance to the defined constraints. Thereby it can be differentiated between the concepts of stability and security of power systems. The difference between these two issues is explained in this chapter. Further attention is given to the concept of the power system stability. A classification of the power system stability is given. The general classification principles are elucidated. It is followed by a categorization of the power system stability phenomena. It comprises: the rotor angle stability, the frequency stability and the voltage stability. A particularisation of the two first categories is done in this chapter. An alternative classification considering the time frame and the instability driving force criterion is given further. As the principal subject in this thesis the voltage stability phenomenon is separately studied in the next chapter. Emphasis is made on its definition and practical description.

3 Power system voltage stability

This chapter gives an overview of the voltage stability problem in power systems. The definitions of this problem are given as applied for power systems and in the context of this thesis. Complementary to the categorization given in the previous chapter, a sub-categorization is done based on the times scales of various power system's events. A detailed description of the most important mechanisms of voltage instability completes the chapter. Describing the instability mechanisms, emphasis is put on the contribution of relevant power system components in the voltage instability and the recognition of its occurrence using the notion of the maximal deliverable power.

3.1 Introduction

3.1.1 Definitions

As presented in the previous chapter the power system operation is accompanied by a range of grid switching operations and grid disturbances. By their occurrence the transfer conditions (line flows) throughout the entire power system are modified, the system inter-dependencies are redefined and new values are set for the systems variables. According to the system overall operating limits, the maintenance of an admissible voltage profile is of crucial importance for the further system exploitation, also after a disturbance. This fact leads to the most popular definition of the voltage stability:

Voltage stability is concerned with the ability of a power system to maintain acceptable voltages at all buses in the system under normal condition and after being subjected to a disturbance [23].

Voltage instability results from a progressive fall or rise of voltages of some buses.

The voltage instability phenomenon is thus manifested in the form of uncontrollability of the voltage magnitude at a number of network buses. Possible outcomes of voltage instability are:

- Outage of electrical equipment (loss of load in an area, or tripping of transmission lines and other elements by their protective systems)
- Load increase
- Decrease in the generation
- Limitation in the voltage control devices[23]
- Etc.

A normal system operation is depicted by the power generation following the power demand and a sufficient power supply at the loads all the time. The driving forces for voltage instability are usually the loads. In response to a disturbance, the power consumed by the loads tends to be restored by the action of motor slip adjustment, distribution voltage regulators, tap-changing transformers, and thermostats. Restored loads increase the stress on the high voltage network by increasing the reactive power consumption causing further voltage reduction. A run-down situation causing voltage instability occurs when load dynamics attempt to restore power consumption beyond the capability of the transmission network and the connected generation [12], [29]. Therefore as stipulated in [29]:

Voltage instability stems from the attempt of loads dynamics to restore power consumption beyond the capability of the combined transmission and generation system.

The voltage instability can be loosely associated to a state where the power system does not behave in an expected manner when operating changes influencing its voltage levels occur. An unexpected behaviour of a power system can mean for example that the switching-on of a load causes the power consumed at a system node to decrease[24] [30].

[23] E.g.: Generators hitting their reactive power capability limits

[24] Turning another light on, makes the room gets darker

Any operating point where an unexpected behaviour of the power system is observed in regard to the maintenance of an acceptable voltage level is qualified as *voltage unstable*.

Voltage instability is then the absence of voltage stability; it is generally characterized by the loss of a stable operating point as well as by the deterioration of voltage levels in and/or around an electric centre within a given power system area.

The systems rate of return to a normal voltage level after a disturbance or a fault is called the *voltage recovery*.

Another term usually used in conjunction with power system voltage stability problems is *voltage collapse*. In the context of the power systems operation as seen from a node or an area, the term voltage collapse signifies the impossibility of the further operation at this node or area due to inadequate voltage levels. In the spirit of [12], [31] the voltage collapse is the process by which a relatively fast sequence of events, accompanying voltage instability leads to unacceptably voltage values -in general a non-recoverable situation- in a significant part of the power system. It is the possible[25] result of an unabated worsening of the voltage stability. Voltage collapse which is usually associated with the decay of the voltage magnitude is summarized as: a sudden catastrophic transition to an unacceptably and non-recoverable voltage level triggered by a sequence of instability events.

The power system can thus undergo voltage instability or collapse at one bus or at many buses simultaneously with varying step interval according to the time scale of the events influencing the instability. How fast the transition is done from a voltage stable operating point to a voltage unstable one depends on the systems dynamics involved.

[25] Voltage collapse is not always the final outcome of voltage instability [29]

3.1.2 Time-scales and sub-categorization

Voltage instability and collapse dynamics span a range in time from a fraction of seconds to ten of minutes. A time-scale chart [32] is used to describe the dynamic time response of the main power systems components and control devices and actions playing a role in power systems voltage stability.

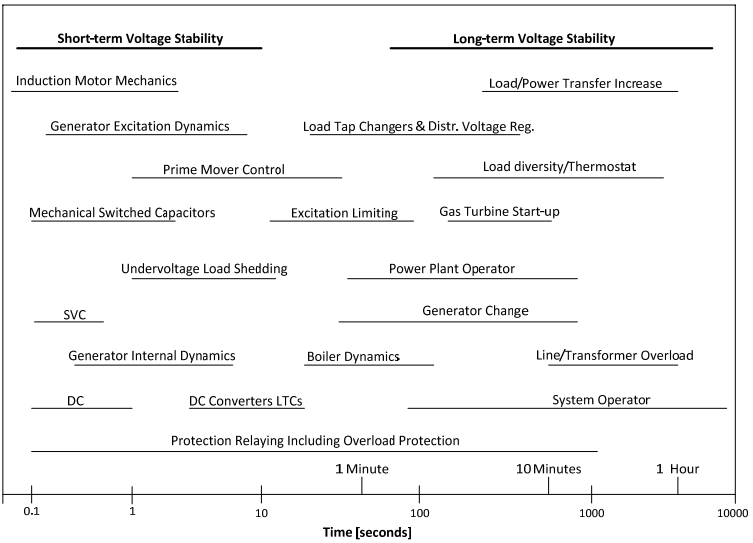

Figure 3.1: Time-Scales of voltage stability dynamics [32], [49]

Many power systems components and control devices play a role in voltage stability. However according to their role in the overall power system operation they will affect the voltage stability more or less significantly by occurrence of a particular disturbance or instability scenario. This issue is discussed in a next paragraph treating the questions of the mechanisms of the voltage instability. Depending on the time frames concerned voltage stability problems voltage stability may be either a short-term or a long-term phenomenon as identified in figure 3.1.

Short-term voltage stability is driven by dynamics of fast acting (recovering) load components such as induction motors, electronically controlled loads, and HVDC converters. They tend to restore power consumption in a very fast time scale after a contingency. The study period of interest is in the order of tenth of seconds. This is similar to the study of rotor angle stability. On the other hand, *long-term voltage stability* involves slower acting equipment such as tap-changing transformers, thermostatically controlled loads, and generator current limiters. The study period of interest is extended to several minutes.

Voltage instability in the long-term time scale can include effects from the short-term time scale; for example, a slow voltage instability taking several minutes may evolve fast and end in a voltage collapse in the short-term time scale.

If the risks through long term voltage instability are well known for power systems, several factors, such as increasing proportion of air conditioning and in general induction motor load, growing penetration of dispersed generation consuming reactive power without voltage control, increased use of various types of electronically controlled loads, and finally introduction of HVDC ties linking weak areas, point out at an increasing risk of voltage instability in the short term the last years. It was even suggested that part of the problems that led to the recent North American blackout of August 2003 might be linked to short-term voltage instability [33].

Power system voltage stability can also be sub-categorized into: *large-disturbance voltage stability* and *small-disturbance voltage stability*. Large disturbance voltage stability refers to the ability of the power system to maintain acceptable nodes voltages following large disturbances such as system faults, loss of generation, or circuit contingencies. The study of large-disturbance voltage stability phenomenon requires the examination of the power system's response over a period of time sufficient to capture the performance and interactions of such devices as motors, underload transformer tap changers, and generator field-current limiters. The study period of interest may extend from a few seconds to tens of minutes.

Small disturbance voltage stability is associated to the capability of the system to maintain acceptable nodes voltages when subjected to small perturbations such as incremental changes in system load. This form of stability is influenced by the characteristics of loads, continuous controls, and discrete controls at a given instant of time. This concept is useful in determining, at any instant, how the system voltages will respond to small system change [12].

3.2 Mechanisms of voltage instability

This paragraph provides an overview into the principal causes of voltage instability in power systems. A brief description of the load, generation and transmission aspects of this instability phenomenon is given. The goal followed is to define a common base appropriate for the recognition of the occurrence voltage instability.

3.2.1 Introduction

In the previous chapter 2 the general collapse mechanism is described as the succession of uncontrolled events jeopardizing the system normal operation or stability; the general conception of the stability for power systems is assimilated to their ability to maintain the balance between the power generation and the load demand. In paragraph 3.1.1 the occurrence of voltage instability is related to a certain malfunction or limitation in the load restoration used to re-establish the pre-disturbance consumption of the load. The term load restoration is also used to characterize the reestablishment of normal (stable) conditions of power system operation i.e.: acceptable voltage magnitudes at the system's nodes, with a sufficient power supply to the loads (consumers).

A classical example of a voltage collapse occurred on July 23, 1987 in Tokyo, Japan [34], [35]. The forecasted temperature was 91°F (32,8°C)[26] and the forecasted power consumption level was 38500 MW. The day turned out to be hotter than expected with temperatures reaching a steamy 102°F (38,9°C). By 1130 a.m., the forecasted load had been adjusted to 40000 MW. At approximately 1:00 p.m., the load power demand increased at a rate of 400 MW/min (setting a record for load power demand increase) and the line voltage began to sag. By 1:20 pm. The line voltage was more than 20% lower than the normal operating voltage. At this point, protective relays shut down parts of the city with loss of power to 2.8 million customers. The adjusted forecast for the load power exceeded Tokyo Electric Power Company's (TEPCO) maximum generation capabilities. To compensate for this high level of demand, TEPCO tried to import power from neighbouring utilities. Despite this action, the system was not able to deliver the required power to the load centre of Tokyo. The mismatch in demand and supply caused the voltage levels to decrease until a widespread system outage occurred.
This is a good example of a highly stressed system. The system stress is characterized by a high level of load power coupled with a large amount of long distance power transmission. The situation in Tokyo was further exacerbated by the record increase in power demand.

As illustrated by the example of the system failure in 3.2.1, three important factors are involved in the power systems voltage stability:

- The load characteristics (power demand)
- The generation capacity
- The transmission capacity

Due to a voltage change at a system node the load (generally represented by its active power component) will change as well. The load recovery depends on its characteristic behaviour. This behaviour impacts on the node's voltage recovery, which is the reestablishment of an acceptable voltage level at the node.

[26] Conversion of Fahrenheit in Celsius = (TFahrenheit - 32) × 5/9

A direct influence on the voltage level itself at a given node is achieved through the so called voltage control devices; e.g.: generators (machine excitation), tap changers, Static Var Compensator SVC[27]. Their principal role is to maintain or keep a normal voltage at the power system's nodes as the system's condition varies. Logically it is critical for the local (at one bus) voltage stability when the devices assigned to its control hit their operational limits. However, due to the highly interconnection level of the power systems a local phenomenon will influence the behaviour of the entire (global) interconnected system, as well as the overall situation of the interconnected system influences the operating circumstances at each individual bus or station. Seen from this position the operation of the voltage controllers can have the inverse effect as the one expected due to the actual unfavourable mode of operation of the interconnected power system. For these reasons, the mechanisms widely believed to be critical in the voltage collapse are those of the load dynamic and of the voltage control devices.
The following subparagraphs explain how the load response and the control mechanisms namely: the tap changing and the machine excitation control can influence the voltage stability of power systems.

3.2.2 Load dynamic response

The load is the part of a power system that remains most difficult to model. This is among others due to following factors [43]:

- The large number of diverse load components.
- The ownership and location of load devices in customer facilities not directly accessible to the electric power system operator.
- The lack of precise information on the composition of the load.
- The lack of accurate system tests for identifying load models.

[27] Static Var Compensator: is an electrical device for providing fast-acting reactive power compensation on high- voltage electric transmission networks

To these can be added the continuing fluctuation in demand but also to the lack of specific knowledge about how the power drawn by the load devices depends on voltage and frequency [39]. The frequency dependence of loads is not used in this work, since in voltage stability incidents the frequency excursions are not of primary concern [29]. The load dynamic response is a key mechanism of power system voltage stability driving the dynamic evolution of voltages. With the rest of the system conditions remaining in charged, if the load at a particular bus is varied, the voltage at the bus will also vary. Voltage at other nodes will also vary as a response to this load change. In other words voltage at a load bus is elastic with respect to power (active and reactive) delivered at that node. Several works and studies have shown the importance of an accurate load representation in the voltage stability analysis [32], [40], [41]. Depending on the type of analysis performed, the load models can be classified into two categories: static load models and dynamic load models.

A load is called static if the power taken by the load is dependent only on voltage and not on time. For example a constant impedance load, lighting load, a constant current load are static loads. The time variation of the load power drawn by such loads is due to the variation of the voltage. One says that the power varies in step with the voltage in such loads. And a static load model characterizes the power consumed by the load as algebraic function of the voltage magnitude. On the other hand, a load is called dynamic if the power drawn by the load is a function of voltage as well as time. For example, consider an induction motor driving a constant torque load. If the voltage changes suddenly, the motor decelerates and the power (both active and reactive) drawn by motor become functions of speed (slip) and hence of time. The power will stabilize at new values corresponding to new value of voltage after sufficient time decided by mechanical time constant of the motor. In some cases, it is possible that these new values correspond to a stalled condition. A dynamic condition can be introduced for a static load when it is combined with the use of tap changer.

The tap changing itself is analysed further in this paragraph, but in the forefront of the study of the influence of the tap changing on the power system nodes voltages we can say that; These tap changers affect (vary) the voltage level only with a certain delay. Thus the load presented to the power system after a voltage variation appear to be time varying due to time varying tap changer actions. The combination of static loads models with tap changers is very often used in the analysis of power system voltage stability for representation of the load-voltage dynamic. A load voltage characteristic or simple load characteristic gives the active and reactive power consumed by the load as a function of voltage as well as of a variable Z introduced in the reference [29] as the load demand by Van Cutsem and Vournas, but which is more exactly defined in [42] as the *load scaling factor*. The load scaling factor is a dimensionless parameter with a constant value, multiplied to the known nominal load power at a system node to obtain the instant required load power or load demand. It can be related to the amount of connected loads from same or different types. The scaling of this parameter is usually used by digital simulations of power systems to launch a change the load connected at a given node for example.

The load demand is distinct from the actually consumed load power. The comprehension of this distinction is primordial to understand the transfer instability mechanism elucidated in a further paragraph on the base of the voltage stability definition.

3.2.2.1 Static load: exponential load

A widely used static load model is the exponential load model. Its load characteristic in a general form and in consideration of the load demand is given by the following equations:

$$P = zP_0 \cdot \left(\frac{U}{U_0}\right)^{\alpha} \tag{3.1a}$$

$$Q = zQ_0 \cdot \left(\frac{U}{U_0}\right)^{\beta} \tag{3.1b}$$

Where z is the demand variable. The subscript 0 indicates an initial operating condition. Thus U_0 is the reference voltage, zP_0 and $zQ_0$are the active and reactive powers consumed under a voltage U equal to U_0. P_0 and Q_0 are known as the nominal load powers in contrast to the consumed load powers P and Q. The coefficients α and β describe the voltage sensitivity of the active and reactive power respectively. These coefficients can be interpreted as follows. Considering a voltage variation ΔU for which the equation (3.1a) can be linearized to:

$$\Delta P = \alpha P_0 \frac{U^{\alpha-1}}{U_0^{\alpha}} \Delta U \tag{3.2}$$

Solving (3.2) for the reference voltage yields for the active power

$$\frac{\Delta P}{P_0} = \alpha \cdot \frac{\Delta U}{U_0} \quad \Leftrightarrow \quad \alpha = \frac{\Delta P/P_0}{\Delta U/U_0} \tag{3.2a}$$

With a similarly result for the reactive power

$$\frac{\Delta Q}{Q_0} = \beta \cdot \frac{\Delta U}{U_0} \quad \Leftrightarrow \quad \beta = \frac{\Delta Q/Q_0}{\Delta U/U_0} \tag{3.2b}$$

Constant impedance load (Z), constant current load (I) and constant power load (P) characteristics are obtained by using the typical values of α = β = 2, 1 and 0 respectively.

Fractional exponents have been attributed to certain load components. These are enumerated in the next table 3.1.

Table 3.1: A sample of fractional load exponents [29], [44]

Load Component	α	β
Incandescent lamps	1.54	---
Room air conditioner	0.50	2.5
Furnace fan	0.08	1.6
Battery charger	2.59	4.06
Electronic compact fluorescent	0.95-1.03	0.31-0.46
Conventional fluorescent	2.07	3.21
Television	2	5.1
Refrigerator	0.77	2.5
Large industrial motors	0.07	0.5
dishwasher	1.8	3.6
Boiler, Oven	2	0

Fractional load exponents can be also defined for defined load classes. Such classification is presented in [43] on the base of load classification and measurements conducted by the South African power system operator ESKOM. The load classification thus depends on the loads types available and the exponents values obtained are particular to the grid considered and would probably differ for other power systems. Nevertheless the work realised by ESKOM serves as a good reference for the process of definition of the load exponents.

Table 3.2: ESKOM Load Classes exponents [43]

ESKOM Load Class	α	β
Residential Class	1.74	2
Commercial Class	0.88	2.31
Rural Class	0.8	1.3
Gold Mining Industry	0.39	0.61
Non Metallic Industry	0.7	0.58
Basic Metallic Industry	1.65	5.10
Other Mining Industry	0.30	0.60
Chemical Industry	0.61	0.37
Other Manufacturing Industry	0.86	1.67

Illustration of the influence of the exponent's values

Let us consider the 60-kV substation ABS2 on DK-VEST[28]. As represented by the figure 3.2, its power factory® single-line illustration shows four elements directly connected to this bus. The interconnection with the bulk power system is through the transformer (tap-changer) ABS3-ABS2. The three rest elements are: a static load (l_ABS2), a synchronous (s_ABS2Q) generator and an asynchronous (a_ABS2W) generator.

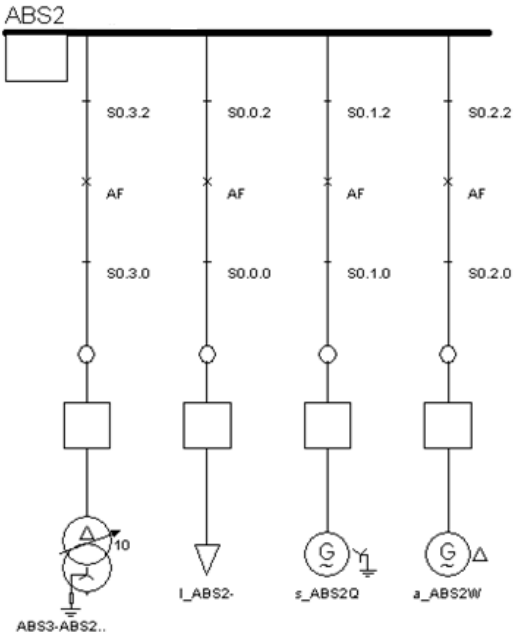

Figure 3.2: Load bus ABS2 on DK-VEST

[28] DK-VEST: Is the denomination given to the model of the western Danish power system used in this work. A general description of this power system is made further in this work, also its single line diagram is presented (see chapter 5, 5.2.6.6). A dynamic model of this power system representing a snapshot of its operating condition on 01.01.2007 at 23:59, implemented in PowerFactory® was available in the framework of this thesis for grid calculations and simulations purposes.

Relevant for the simulation at this moment of the work is only the static load. It is modelled as an exponential load using the equations 3.1a and 3.1b. A dynamic behaviour is introduced as mentioned in the further paragraph by the effect of the tap changer. The effects of the taps adjust as well as the consideration of generators reactive power limits are disabled for simplicity during this simulation. The initial values of the load model variables are given in the table 3:

Table 3.3: Initial values of the exponential load variables at ABS2

P_0, [MW]	Q_0, [Mvar]	U_0, [pu]	z	α	β
67	16.75	1	1	0.8	1.8

The influence of the exponent values on the load bus voltage is shown by the variation of their constant values and the succinct step variation (load demand scale is equal to 1) of the load factor z, to simulate an augmentation of the load demand at this bus. For each new value of step variation of z a load flow calculation is done and the resulting load bus active power-voltage point is represented. This procedure is done for each constant set of the load exponents until the non-convergence of the load flow calculation algorithm is reached. The resulting curves are each the succession of the calculated active power-voltage points for each exponents sets. The curves obtained for the initial exponent's values (see table 3.3) and for some other load exponents freely chosen in tables 3.1 and 3.2 are compared in figure 3.3.

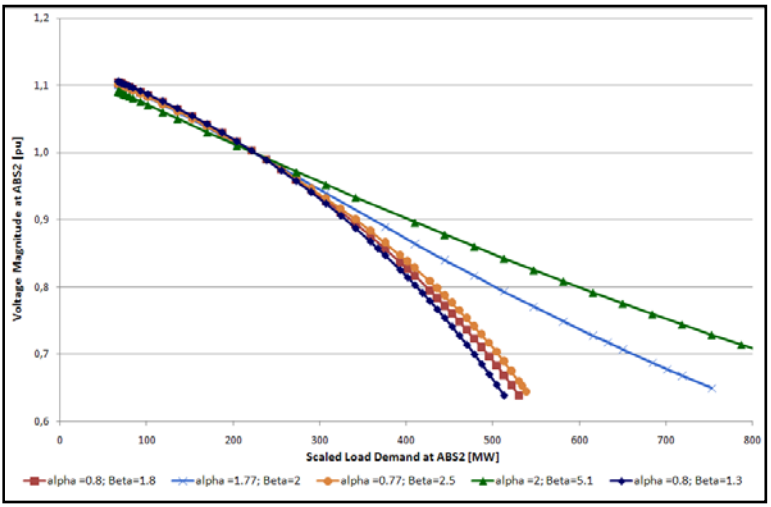

Figure 3.3: Active power-voltage curves at ABS2 for different load exponents sets

As a result of the simulation the maximum possible load demand to be connected at ABS2 as constrained by the convergence of the load flow algorithm for a given overall system state is obtained. It is materialised by the value of z at the latest calculated point for each curve:

Load Exponents (α,β)	(0.8,1.8) Initial Condition	(1.77,2)	(0.77,2.5)	(2 , 5.1)	(0.8,1.3)
Maximum Load Demand z	7.911	11.238	8.038	12.263	7.654

Leaving by side the discussion on the resulting voltage levels and the eligibility of the non convergence of the load flow as of the system state's assessment criteria (this will be done later in this thesis) it can be concluded that, although the same demand scale step variation remains the same in all cases the behaviour of the bus voltage is different for each load exponents sets. A point to point comparison is even not possible in some cases, because the load flow calculation have more solutions in some simulations than others.

Apart from underlining the influence of the exponential load exponents on the voltage behaviour according to the load demand, which can change several times on a time (hourly), daily or seasonal basis at a given bus, this simulation shows once more the importance of the right definition or approximation of the load exponents when modelling exponential loads.

3.2.2.2 Generic dynamic load model (aggregated load)

The definition of load classes is intended to gather individual load elements of the types of function in common groups. The term load itself can have several meaning in the power system engineering such as [45]:

a) A device connected to a power system that consumes power.
b) The total power (active and/or reactive) consumed by all devices connected to a power system.
c) A portion of the system that is not explicitly represented in a system model but rather is treated as if it were a single power-consuming device connected to a bus in the system model.
d) The power output of a generator or generating plant.

The set of all such devices connected at a given bus constitutes the *bus load*. While it might be possible to identify the voltage response characteristics of a large variety of individual equipment of which power load is comprised, it is not practical or realistic to model a bus load by individual equipment models.

The aggregation of loads is the solution. The load is an aggregation of various down-stream loads each with a dynamic attribute [46].

In this context, the aggregated load for transmission system analysis includes not only the connected power consumption devices, but also some of the following devices [45]:

- Substation step-down transformers including the tap changer
- Sub-transmission and distribution feeders
- Voltage regulators
- Shunt capacitor banks, and
- various reactive power compensation devices

And the load dynamic response is a reflection of the collective effects of all downstream components ranging from the transformers (tap changers) to individual household loads. The time span for a load to recover to steady-state is normally in the range of several seconds to minutes, depending on the load composition [24].

The numerical representation of the aggregated load for voltage stability analysis involves several aspects that are not captured by static exponential load models. These factors include dynamics due to voltage sensitive loads, thermostatically controlled loads, voltage regulating device behaviour, nonlinearities in voltage characteristics at low voltages due to motor stalling and tripping, discharge lighting, and others.

To represent the active part of an aggregate load, the non-linear dynamic load model with exponential recovery proposed in [40], [47], and [50] is used in this work. This model is based on field measurements executed in the southern part of Sweden [50] and published in [47] and [49]. The mathematical equations describing the load model are:

$$T_{pr}\frac{dP_r}{dt} + P_r = N_P(U) \qquad (3.3a)$$

$$N_P(U) = P_s(U) - P_t(U) \qquad (3.3b)$$

Where, P_r is an internal state variable modelling the load recovery dynamics or active power recovery.

The response of the load can be divided into a transient characteristic $P_t(U)$, right after the disturbance, and a steady-state characteristic $P_s(U)$. U is the per unit magnitude of the voltage

imposed on the load. T_{pr} is the load recovery time constant. $P_t(U)$ and $P_s(U)$ are given by the equations:

$$P_t = P_0(U)^{\alpha_t} \qquad (3.3c)$$

$$P_s = P_0(U)^{\alpha_s} \qquad (3.3d)$$

With P_0 the rated power consumption of the aggregated load at the rated voltage U_0. These are the pre-disturbance values of the active power and the bus voltage respectively. α_s and α_t are the steady state and transient active – load voltage exponents.
A similar first-order differential system model can be deduced for the load reactive power consumption in the same way except that the steady state and transient voltage exponents in this case would be denoted by β_s and β_t
The total active load demand is found as:

$$P_d(U) = P_r + P_t(U) \qquad (3.3.e)$$

Figure 3.4 shows qualitatively the meaning of equations (3.3a) and (3.3b) when an ideal voltage step change is applied.

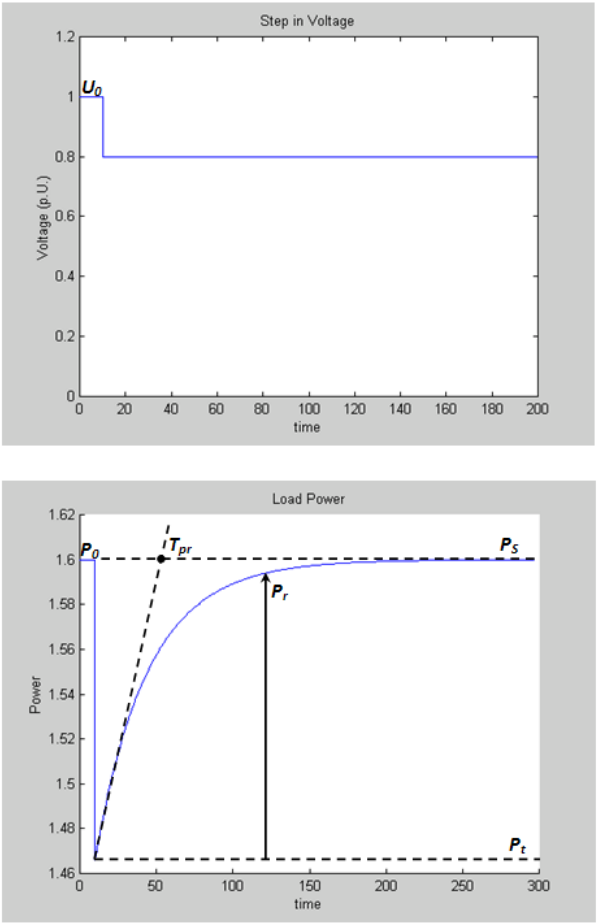

Figure 3.4: Aggregate (active) load typical response to a step-voltage change

The load behaviour is thus characterized by a time constant and transient and steady state load-voltage dependence parameters. Following the drop, demand power will recover to a steady-state value with time-constant T_{pr}.

The recovery of the active power originates from the behaviour of available control devices [50]. α_s or the steady state load-voltage dependence quantifies how much load has been restored after the recovery; a value equal to 0 means a fully restored load, while a different value indicates partly restored load. Furthermore, the steady state voltage dependency α_s may present negative values.

The stationary level reached by the load after the recovery is then higher than the expected one, resulting in an overshooting in the load. The transient load-voltage dependence α_t describes how the load behaves at the disturbance moment. If α_t is equal to 0, the load behaves as a constant power, if it is equal to 1 the load behaves as a constant current, and if it is equal to 2 as constant impedance [40].

Practical voltage recovery by occurrence of a disturbance

As a matter of fact, slow voltage recovery phenomena can have secondary effects such effects such as operation of protective relays (e.g.: under-voltage tripping), electric load disruption, motor stalling etc. This can be due to the voltage level staying under a certain level during a certain period of time. A situation of voltage recovery following a disturbance on ABS2 (see figure 3.2) on DK-VEST[29] is depicted in figure 3.5. A three-phase short circuit was introduced at 0,1 second and cleared after 0,2 seconds of a 0,8 seconds total simulation time. The load exponents are those of the initial condition and in opposite to the simulation in figure 3.3, the effects of the tap-changer and the reactive power limits of the connected generators are activated in this case. The resulting voltage magnitude and active power at ABS2 are then represented.

[29] Denomination used for the western Danish power system. A dynamic model of this power system implemented in PowerFactory® was available for simulation purposes in this thesis. More details on this power system and its structure are given in chapter 5

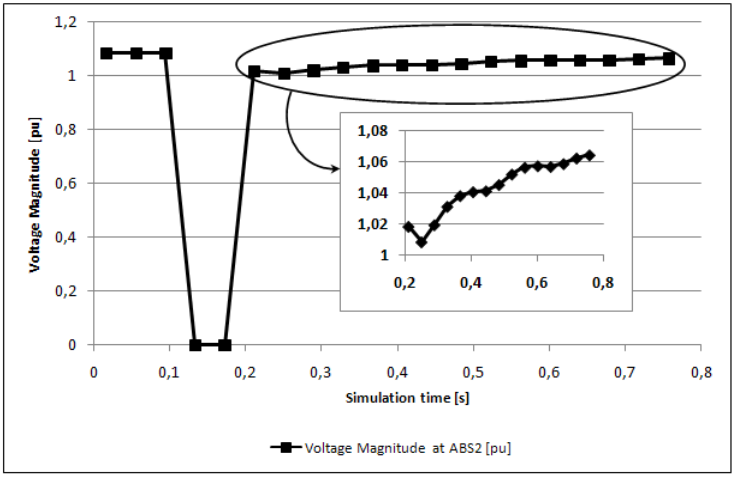

Figure 3.5: Voltage magnitude by occurrence of three phase short circuit at ABS2

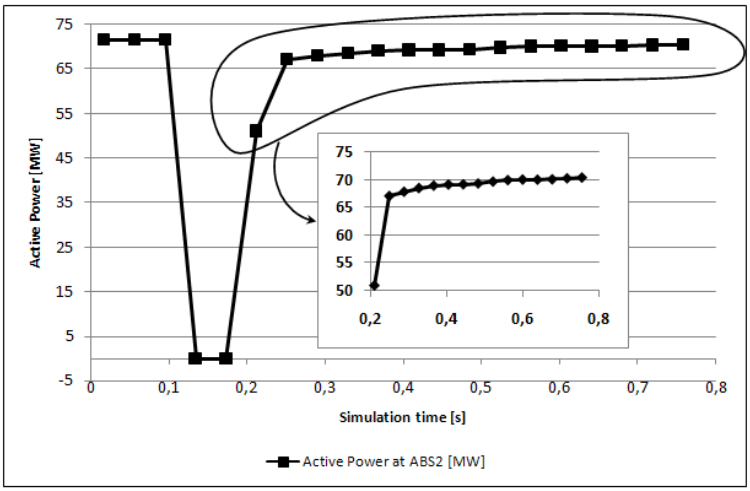

Figure 3.6: Active power by occurrence of a three-phase short-circuit at ABS2

As seen on figure 3.5, when the fault clears, the voltage recovers quickly to another level and slowly builds up to the normal voltage. The period of slow recovery is mostly affected by the load dynamics.

The voltage recovery is delayed by the load dynamics. At the same time, according to the duration of the process, the slow voltage recovery may trigger the operation of protective devices and/or create operational situations jeopardizing the system stability such as the disconnection of electrical equipment. As an example, due to the voltage recovery during the simulation of a tree-phase short circuit at ABS2 the synchronous generator s_ABS2Q went out of step and was disconnected at 0,737 seconds of the simulation time. The figure 3.7b shows the opened circuit breaker at the end of the simulation as illustrated by PowerFactory®.

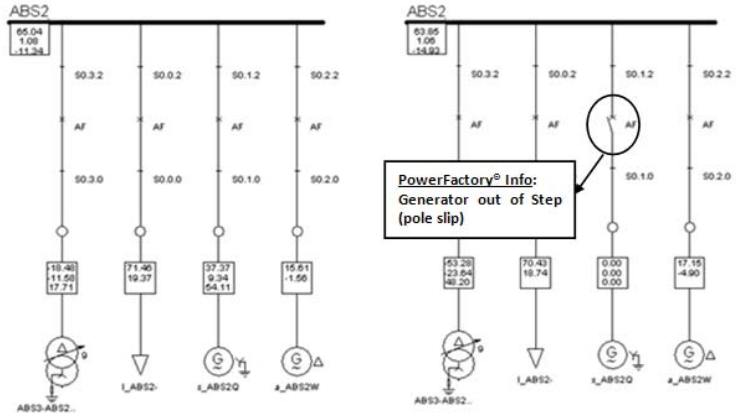

a) Before Simulation **b) End of Simulation**

Figure 3.7: Topology at ABS2 before and at the end of the simulation of a three-phase short circuit event

Generally seen, the load recovery phenomena can extend on a time span from tenth of seconds to tenth of minutes [44]. They correspond to the tendency of the load to regain the consumption they had prior to a given disturbance. It is a matter of an intrinsic load behaviour or of the regulation effects.

Due to the load recovery dynamics, a power system, which survives a transient event, may experience potential long-term voltage instability as its loads tend to recover and restore acceptable operating conditions.

3.2.3 Load restoration through adjustable transformer tap changing

Typically a transformer has two sides: the primary side which is connected to the power source via the transmission system, and the secondary serving the load. According to the first transformer law, the voltages on the two sides of a transformer are proportional to the turn's ratios of their windings, i.e.:

$$\frac{U'}{U} = r \tag{3.4}$$

When load levels and/or load voltages changes frequently, it is common and sometimes necessary to adjust the transformers tap ratio to follow the changes in power system conditions and hence maintain the load voltage within a desired level. A transformer tap is a connection point along a transformer winding that allows a certain number of turns to be selected. The tap selection is made via a tap changer mechanism.

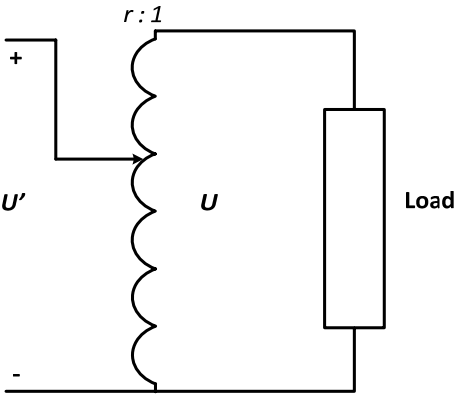

Figure 3.8: Schematic Diagram of a tap changer [39]

By this mean, a transformer with a variable windings ratio is produced, enabling voltage regulation of the output. A tap changer is thus a device fitted to power transformers for regulation of the output voltage to required levels. Obviously it is impractical to change the transformers turns ratios while they are de-energized or unloaded. On load tap changers (OLTC) or simply load tap changers (LTC) are devices which allow adjusting the turn's ratio of the transformer without interrupting the power flow in the apparatus.
In practice, the turn's ratio takes on a finite number of positions and each tap changing is a discrete event. Two adjacent tap positions result in a voltage change. The time required to move from one tap position to another depends largely on the tap changer design, and may vary from a few seconds to several minutes. A minimum of 5 seconds is given in [29] and the time required for the tap changer to complete one tap movement is called its mechanical time delay denoted by T_m.
One important constraint in the LTC operation is that the variable tap ratio has a limited regulation range (i.e.: maximal tap position).
The tap-changing mechanism is usually motor-driven and can be controlled manually or automatically. In the automatic mode, the output voltage of the transformer is compared to a reference voltage and a raise/lower signal is sent to the tap changer motor when the output voltage falls outside a specified band, called a *dead band* [51]. Typical values of the lower limit (r^{min}) of the dead band are from 0,85-0,9 pu and for the upper limit (r^{max}) 1,10-1,15 pu. The dead band must be larger than the voltage between taps (tap increment); otherwise, it will ''hunt'' endlessly and burn up the tap changer. However, the dead band must also not be too wide, because the purpose of voltage regulation will be defeated. Ordinarily, the dead band is set to a voltage between two and three tap increments. The tap increment is typically in the range of 0.5% - 1.5% of the nominal secondary voltage.

The two usual models for tap-changing dynamic are:

A. Discrete Model: Hereby the tap changing is activated after a given time delay if the load voltage U falls beyond a given voltage range and the transformer ratio is changed by one tap step instantaneously. The size of each tap change is defined as Δr. t_k with $k = 0, 1, 2, \ldots$, is the discrete operating time instants is given by the recursive equation:

$$t_{k+1} = t_k + \Delta T_k \tag{3.5}$$

Thereby t_k is not an independent variable and ΔT_k is not necessarily constant because it depends upon the device characteristics and voltage error. The integer advances from k to $k+1$ when the time elapsed since $t_k$becomes equal to ΔT_k. The calculation of ΔT_k is possible through [29]:

$$\Delta T_k = T_d \frac{d}{|U_2 - U_2^0|} + T_f + T_m \tag{3.5a}$$

With U_2 : the controlled voltage, U_2^0: the reference voltage, d: the half dead band, T_d: the maximum time delay of the inverse-time characteristic. This time is usually chosen large enough for selectivity purposes. T_f the fixed time delay, T_m is defined above.
The tap changing at a time $t_k$follows the logic:

$$r_{k+1} = \begin{cases} r_k + \Delta r & if\ U_2 > U_2^0 + d\ \ and\ r_k < r^{max} \\ r_k - \Delta r & if\ U_2 < U_2^0 - d\ \ and\ r_k > r^{min} \\ r_k & otherwise \end{cases} \tag{3.5b}$$

The LTC is activated and the counter k is set to zero at each time t_0 the load voltage increases outside of the dead band limits.

$k = 0$ if $|U_2(t_0^+) - U_2^0| > d + \varepsilon$
and

$|U_2(t_0^-) - U_2^0| \leq d + \varepsilon$

Using the optional hysteresis term ε the effective dead band is larger for the first tap movement and the LTC becomes more reluctant to initiate a sequence of tap changes [29].

B. Continuous model:
The continuous LTC model assumes a continuously changing tap. All the range of the tap positions between r^{min} and r^{max} are taken in account. The continuous dynamic LTC model is usually modelled as integral controller and is given by the following differential equation:

$$\frac{dr}{dt} = \frac{U_2 - U_2^0}{T_c} \qquad (3.5c)$$

The time constant $T_c > 0$ is derived in [29] as:

$$T_c = \frac{T_d d}{\Delta r} \qquad (3.5d)$$

and is used to model the delay constant.

3.2.3.1 Simulation of the LTC's effect on load voltage profile

To illustrate the effect of a LTC the following six-bus test system was modelled (in PowerFactory®).

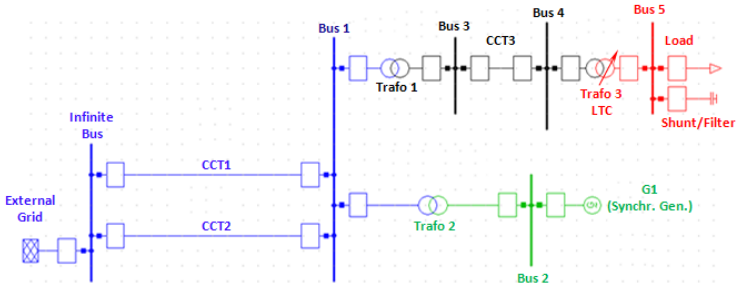

Figure 3.9: Six-bus test-system

The listing of the complete equipment data is given in appendix B. The following description of the system is just limited to some key data for understanding the simulation conditions.

Five different voltage levels are here represented: 400 kV (blue), 150 kV (black), 60 kV (red) and 24 kV (green). The load is connected at 60 kV at bus 5. This bus is termed as the load bus. The Generator is connected at 24 kV at bus 2. An external grid equivalent is connected at the infinite bus. The buses 4 and 5 are interconnected by a transformer (Trafo 3) with implemented tap changing function.

The discrete model is chosen for the LTC in the six-bus test system and has the following settings:

Table 3.4: Tap changing settings of the LTC in the six-bus test system

LTC Settings	Settings Values
Tap Increment	Adjusted at 0,5% and at 1,5%
Tap position	Neutral 10, Min: 1 Max: 21
Controlled Node	Low Voltage (Bus 5)
Control Mode	Voltage (Phase: positive Sequence)
Voltage Set Point	1 pu
Lower voltage bound (r^{min})	0,97 pu
Upper voltage bound (r^{max})	1,1 pu
Controller Time Constant (T_d)	15 s

The load is modelled as an exponential load using the equations 3.1a and 3.1b. Its initial variables values are given by the following table 3.5:

Table 3.5: Load model settings in the six-bus test system

P_0, [MW]	Q_0, [Mvar]	U_0, [pu]	z	α	β
50	24,2161	1	1	0.8	1.8

The dynamic load behaviour is introduced by the LTC, which reaction is launched by a variation of the voltage level at bus 5. Two dynamic simulations of a load change at bus 5 (long term voltage stability) permitted to vary the load bus voltage. Both simulations differ only by the value of the tap increment used; respectively: 0,5 % and 1,5%. Thereby, the load is increased[30] each 30 seconds beginning from the tenth of a total simulation time of 1400 seconds (23 minutes: 10 seconds).
The voltage time characteristics obtained at bus 5 are presented in figures 3.10 and 3.11.

[30] The scaling factor is increased by 2% of the initial value until the 1090 s, then by 20% from the 1120 s, and finally by 30% from the 1210 s of the total simulation time.

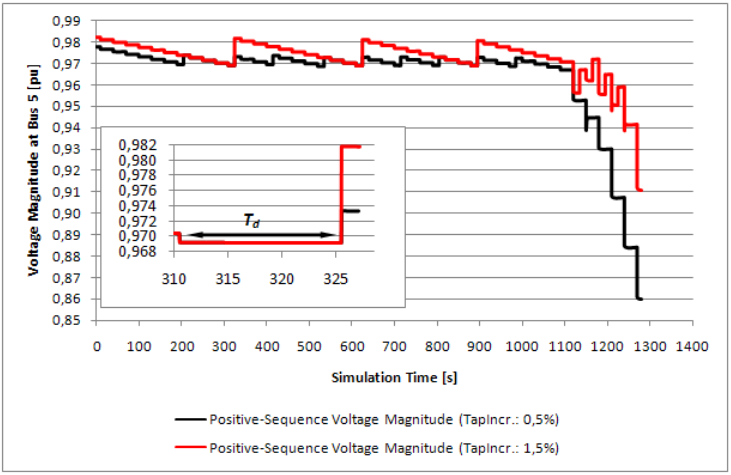

Figure 3.10: Voltage response at bus 5 of the six-bus test system for different tap increments values

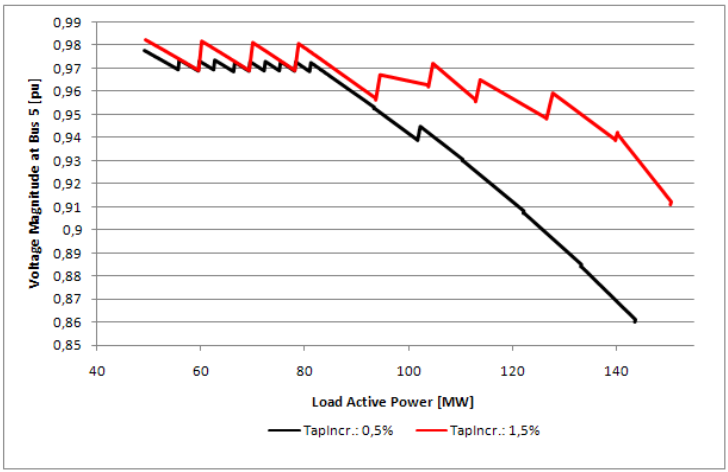

Figure 3.11: Load active power-Voltage characteristic at bus 5 of the six bus test system for different tap increments values

The load increase logically results in a decline of the bus voltage. Under the value of the lower voltage bound and after the defined time constant T_d the voltage is increased by the the action of the LTC.
At the beginning of the simulation the tap position is neutral. In the case simulated here a greater tap increment restore the load at a higher level and thus permit a longer stable operation of the system materialized by fewer LTC triggering. But in both cases, after reaching the maximal tap position, the load restoration is not possible anymore and a monotonic decay of the node voltage cannot be avoided. The maximal tap position is reached at 985 seconds and 1240 seconds of the total simulation time for the a tap increment equal to 0,5 % and 1,5% respectively. In absence of other restorative steps, voltage instability will occur and in a worse scenario this instability can mark the beginning of cascading system failures.
The limitation coming from the load restoration devices, due to their design or to their parameterization device have an important impact on the voltage stability. When they hit their operating limits and particularly in case of persistence of the contingency, the voltage stability at their connecting node is jeopardized. It is then recommendable that the system operator has information on the actual operating state of such equipment.
As it can be seen on figures 3.10 and 3.11, the LTC regulation range affects the voltage profile stability. The occurrence of the voltage instability in this case matches its first definition as given in paragraph 3.1.1 for the power system voltages in general. In the same paragraph another voltage instability definition is given and concerns the run down situation resulting from the action of loads dynamics –to which the LTC can be included- beyond the system's restorative capability. This matter is treated in the next paragraph for the LTC.

3.2.3.2 Reverse action of the LTC associated to voltage collapse

The analysis of the reverse effect of the action of the LTC in this work is done qualitatively according to some general mathematical principles, with reference to the available literature. Thereby, a detailed and practical proof of the theory developed is foregone.

Since the LTC action presumed a heavy loading at the controlled node or generally a heavy loading of the power system it is sensible to know whether the tap changing at a node is still appropriate to the system overall situation. A pertinent aspect of an unstable tap changing operation associated to the voltage collapse mechanism has been investigated in [52] and [53] on the base of a simple power system with a tap changer:

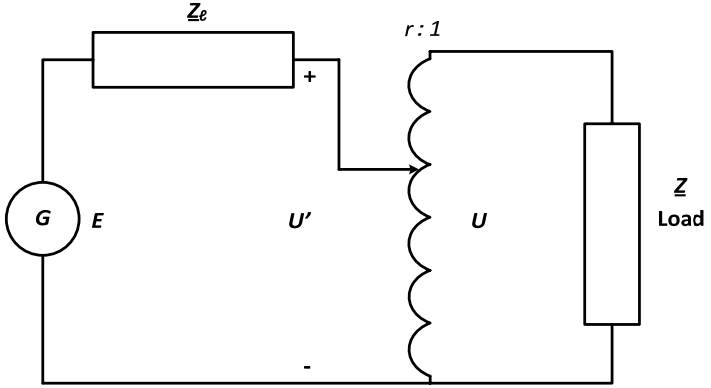

Figure 3.12: two-node power system with a tap changer

Apart from the tap changer, this simple system structure comprises a load modelled as an impedance[31] $\underline{Z} = Z\angle\theta$, a generator modelled a constant voltage source i.e. its output voltage E is always maintain at a constant level of E_0, and a transmission line represented its impedance.$\underline{Z_\ell} = Z\angle\theta_\ell$.

[31] The validity of the representation of the load through an impedance is discussed further in this work

Summarized from the references and outgoing from the structure on figure 3.12, the voltage magnitude on the load side is described as function of the tap ratio r by the equation:

$$U(r) = \frac{rE_0Z}{\sqrt{r^4Z_\ell^2 + 2r^2ZZ_\ell \cdot cos(\theta_\ell - \theta) + Z^2}} \tag{3.6}$$

Resulting from the equation (3.6) and for a set of variables randomly chosen, a typical curve of the load voltage magnitude–tap ratio characteristic is shown on figure 3.13.

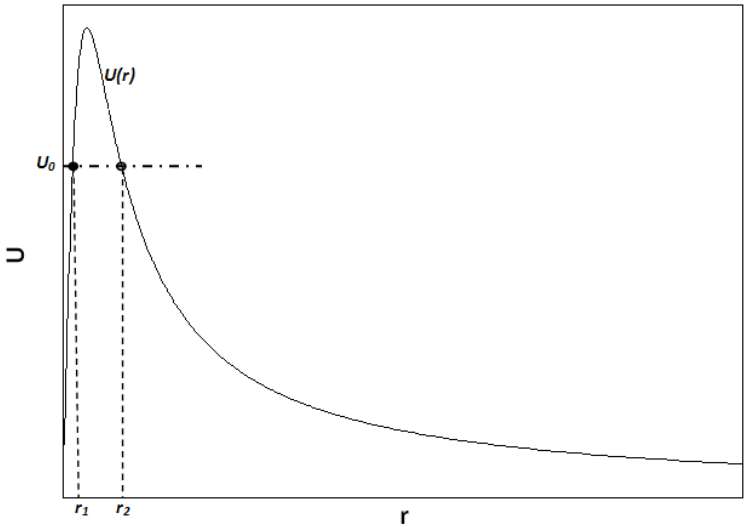

Figure 3.13: Typical load voltage magnitude-tap ratio characteristic

This curve is obtained for each new value of the load voltage and the resulting fixed tap-ratio during a power system operation. For a reference voltage value U_0 there are at most two intersection points r_1 and r_2 with the characteristic curve. They represent the equilibrium points of the system. The intersection r_1 is the only stable equilibrium. The tap changing operation is normal at this point and an increase of the tap ration results as expected in a voltage increase.

But, after a certain maximum value of r the action of the tap changer is reversed. The further increase of r leads to a decaying voltage. If realized in this region, the tap changing operation will contribute to the voltage instability, and must be blocked for system safety.
This short analysis provides some insight in the tap changing phenomena as a possible mechanism of voltage instability. In certain circumstances of power system operation the tap changing is undesirable and contributes to voltage collapse.

3.2.4 Reactive power limitation in generation capability

The power generation capacity of the power system is of crucial importance to maintaining the system voltage stability. The total power generation capacity of the power system is composed by the active power generation and the reactive power generation, each with a given purpose in the electric power supply. Sufficient active power generation capacity is scheduled to cover the load demand and to withstand possible contingencies through proper power system operation planning. Reactive power generation, however, is more difficult to schedule as the load reactive power demand is (locally) conditioned by the system voltage profiles. Normally the reactive power demand increases as the system voltage decreases. The increase in reactive power consumption can be critical for the maintenance of the voltage stability if it is not balanced with the reactive production. As an example induction motors loads used in residential AC units "stall" following a system fault causing a momentary voltage drop. Stalling means that they will greatly increase their consumption of reactive power (by a factor of 4 or more) virtually instantaneously (i.e., within milliseconds). If the system cannot respond with increased reactive power production through adequate reactive power resources, the voltage at the point of connection will decline to a point of collapse and a cascading effect could ensue.

Reactive power is produced by generators or compensation devices, such as capacitors. The produced reactive power is consumed not only by induction motors but also to a lesser extent by transmission and distribution lines. Also a fault on the lines will launch voltages decline within the power system. Voltage stability is threatened when a disturbance increases the reactive power demand beyond the sustainable capacity of the available reactive power resources. As a matter of fact, in almost all voltage instability incidents, at least one crucial generator is operating at its maximum reactive power generation capacity. The Voltage stability is thus closely coupled with the system reactive power generation capability and the study of the limitations of the reactive power generation equipment is very important for the analysis of the voltage stability problem.

Synchronous generators are the primary source of active and reactive power and to a great extent are responsible for the voltage support across the power system. The operation of a synchronous generator is characterized by three variables the active power P, the reactive power Q and the terminal voltage U. As it can be easily imagine there are some limitations on the values taken by P, Q and U. These limits are dictated by an admissible function of the generator. These limits are summarized in terms of PQ relationships under constant U which take on the form of the generator capability curves. An example of such curves is given in the next figure 3.14 for an unsaturated round rotor synchronous generator.

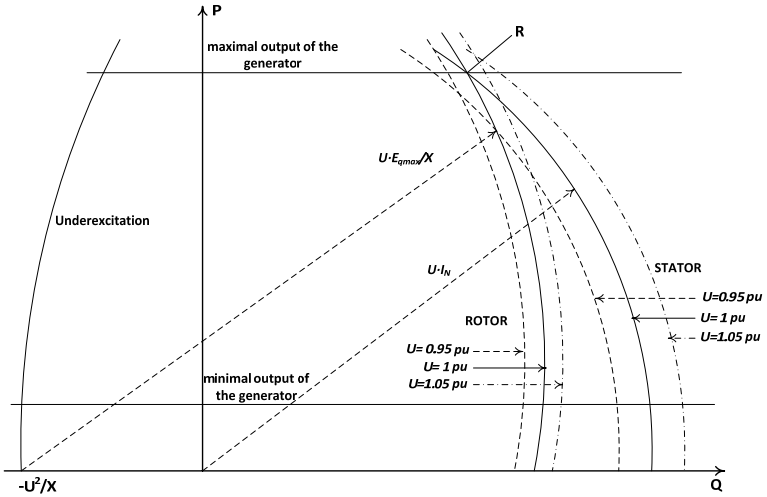

Figure 3.14: Capability curves for an unsaturated round-rotor machine

For the unsaturated round-rotor machine considered the synchronous reactances are equal to:

$$X_d = X_q = X \tag{3.7a}$$

Under constant U, the armature limit corresponds to the operation points for which the stator current is equal to the nominal current I_N. In per unit one has:

$$S^2 = P^2 + Q^2 = U^2 \cdot I_N^2 \tag{3.7b}$$

With a constant U this equation is a circle centred at the origin, with a radius $U \cdot I_N$. The rotor limit also called field current limit [23] corresponds to operating points for which the field or excitation current I_f is equal to the maximum permissible value during the machine operation due to thermal restrictions. Its characteristic curve is established here neglecting the stator resistance.

Let I_{fmax} be the maximal value of the filed current. Its relation to the maximal output voltage of the generator is given by the equation:

$$E_{qmax} = \frac{\omega_N \cdot L_{df} \cdot I_{fmax}}{\sqrt{3}} \qquad (3.7c)$$

The corresponding active and reactive powers are found as:

$$P = \frac{E_{qmax} \cdot U}{X} \cdot sin\varphi$$
$$Q = \frac{E_{qmax} \cdot U}{X} \cdot cos\varphi - \frac{U^2}{X} \qquad (3.7d)$$

The angle φ in (3.7d) is the internal angle of the machine. It represents the angle between the rotor current in the quadrature axis and, the magnitude of the phase voltages.
The elimination of φ gives:

$$\left(\frac{U \cdot E_{qmax}}{X}\right)^2 = \left(Q + \frac{U^2}{X}\right) + P^2 \qquad (3.7e)$$

Which corresponds to a circle with centre at $\left(P = 0, Q = -{U^2}/{X}\right)$ and a radius of ${UE_{qmax}}/{X}$. The resulting curves are then represented on figure 3.14 together with the limit of the maximal output of the generator, the minimal generation of the generator[32] and the underexcitation limiter operation. The underexcitation limit marks the maximal reactive power the generator can absorb without losing synchronism. The curves are presented for an ideal situation. In practice they will probably look different.
The point R is the intersection of the rotor and stator limits under rated voltage and thus corresponds to operation at rated power.
Important is to mention the effect of the terminal voltage as shown by the capability curves.
For a given active power, a larger terminal voltage yields to an augmentation of the reactive limits. This is illustrated by a larger stator limit and a slightly larger rotor limit in the case presented.

[32] In thermal power plants the necessity to generate a certain minimal is linked with the maintenance of the combustion stability.

The terminal voltage support from the generator is triggered when the power output is within the capacity limit of a generator. The terminal voltage of the generator is then regulated by its automatic voltage regulator (AVR) with the goal to maintain it constant.
A schematic description of a typical AVR also called excitation control system is given in [44].

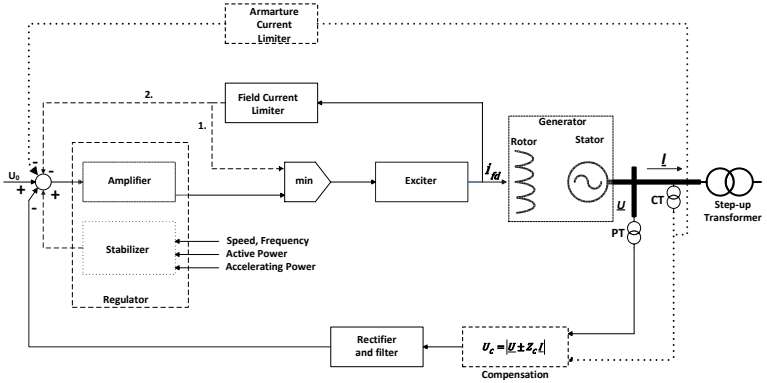

Figure 3.15: Design principle representation of an excitation control system

The generator terminal voltage U is measured through the potential (voltage) transformer PT, then rectified an filtered so as to produce a DC signal U_C proportional to the RMS value of the AC voltage. The voltage regulator compares the signal U_C to the reference U_0, it then amplifies the difference $U_0 - U_C$ and brings it into a form suitable for the control of exciter. The general principle of the regulator is to raise the generator excitation voltage in response to a decrease in U_C or an increase in U_0, and conversely. The regulator can be provided with a power system stabilizer providing additional damping torque through excitation control if required.

Also possible to be acting at the summation point of the regulator is the regulator compensation; which aimed at meeting dynamic performance and accuracy specifications, in particular counteracting too large exciter time constant. This compensation can use the generator field current i_{fd} or the exciter field current. Using the minus sign by the compensation, a signal proportional to the voltage at some point beyond the generator terminal is obtained and the excitation system regulates the voltage at this point closer to the transmission system. The plus sign is used to regulate the voltage at a fictitious point “within” the generator [44], [29]. The excitation control system is provided with several limiting circuits. The role of underexcitation limiter is explained above. The armature current limiter prevents excessive current in the armature winding. Overexcitation limiters (OXL), maximum excitation limiters and field current limiters are all names for the limiting devices that protect synchronous machine field windings from overheating. The limiting action provided by these devices must offer proper protection while simultaneously allowing maximum field forcing for power system stability purposes [54]. The OXL and to some extend the armature current limiters are the ones primarily related to the voltage instability phenomena.

3.2.4.1 Response of a voltage regulated machine to a disturbance

To simplify the analysis let us consider once more a machine with a round rotor $\left(X_d = X_q = X\right)$. An equivalent circuit of the synchronous machine is the following:

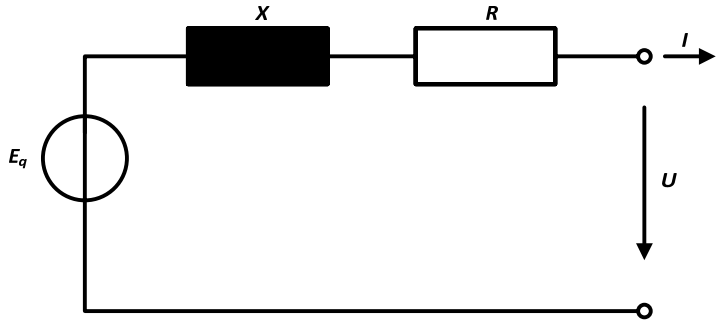

Figure 3.16: Equivalent circuit of a synchronous machine in steady state [55]

Seen from the terminal, the generator pole wheel voltage of the generator is then calculated as:

$$E_q = \vec{U} + \overrightarrow{RI} + \overrightarrow{jXI} \qquad (3.7f)$$

The terminal voltage U is supposed constant and the phasor diagram given by the equation (3.7f) when R is neglected is:

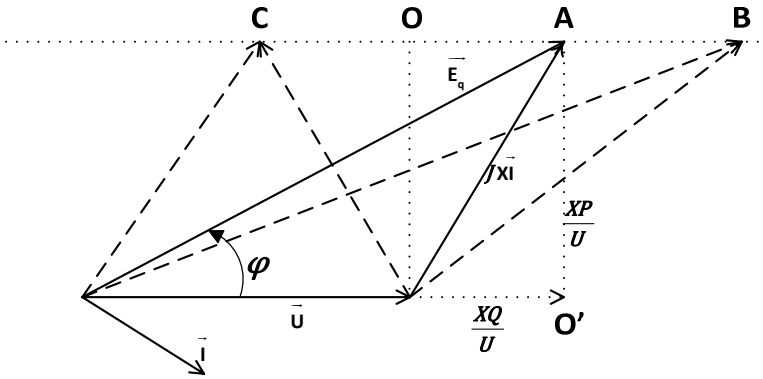

Figure 3.17: phasor diagrams of voltage regulated machine with round rotor and constant terminal voltage (R =0)

In the diagram in figure 3.17 the projection of $\overrightarrow{jXI}$ on the axis of U is:

$$XI_Q = \frac{XQ}{U}$$

And perpendicularly to this axis

$$XI_P = \frac{XP}{U}$$

The active power supply is supposed constant. This is true in absence of speed regulation or by absence of frequency variation. Due to the constancy of P and U the phasor $\overrightarrow{jXI}$ can move only on a parallel to $\vec{U}$.

Lets us consider the QU characteristic of the bulk system as seen from the machine terminal nodes approximated by the sloped straight line numbered 1 on the following figure 3.18:

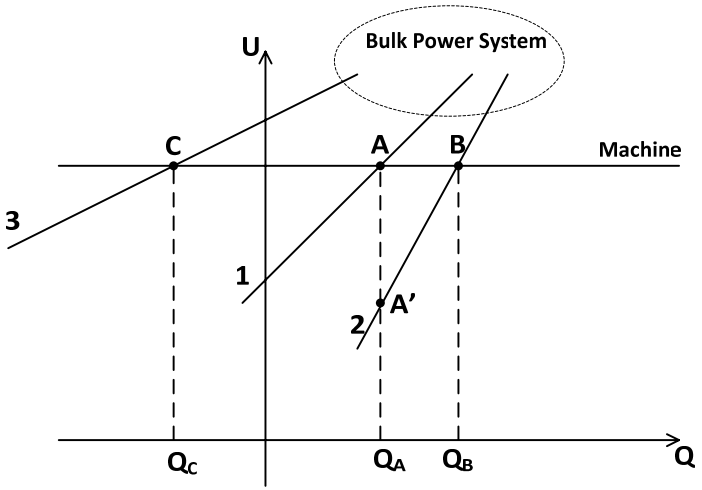

Figure 3.18: QU Characteristics under disturbances

With the assumptions done above the corresponding machine QU characteristic is horizontal. In practice this horizontal characteristic is over and under-limited by the maximum producible reactive power of the machine. In the following we suppose that these limits are not reached.

The operation point of the system is represented by the intersection between the characteristics of the machine and of the bulk system. This corresponds to the point A in figure 3.18.

Let us suppose that a first disturbance which occurs on the power system which modifies its characteristic from 1 into 2. If the machine produces a constant reactive power Q_A, the new operating point will be A' and the terminal voltage will decrease. The voltage being regulated, the final resulting operating point will be B. The maintenance of the voltage level requires the machine to produce more reactive power, ($Q_B > Q_A$). On the other hand a second disturbance which modifies the characteristic 1 into 3 will provoke the raising of the voltage by a constant reactive power. In presence of the voltage regulation the new operating point will be C, where the machine produces less reactive power ($Q_C < Q_A$).

The phasor diagrams corresponding to the operating points B and C are represented on the figure 3.17. Under the effect of the first disturbance the endpoint of the vector $\overrightarrow{E_q}$ moves rightwards. The Magnitude E_q of the output voltage and hence the field current increase through the action of the regulator. This situation is inversed for the second disturbance. The point "O" corresponds to a zero value of the reactive power. Right to "O" the system is overexcited, left to "O" it is underexcited.

As the voltage collapse is usually associated to the terminal voltage decay, the main stream of the literature only considered the action of the OXL to influence the voltage stability. In reality the system underexcitation can also influence the voltage stability in a certain sense. In both cases the capability of the synchronous generator to furnish the reactive needed to maintain the terminal voltage. If following, to a disturbance the reactive power demand on generators exceed their field current and/or the armature limits, this denotes a limitation in the reactive capability of the machine; the voltage regulation will not be triggered and the terminal voltage is not longer maintained constant. This situation is partly forwarded by the action of the OXL. After the excitation system field current limit is reached (due to a large reactive power output of the generator) the generator field current is automatically fixed by its OXL to the maximum permissible value.

With the constant field current, the point of constant voltage is pulled back behind the synchronous reactance instead of at the generator terminal and, therefore, the generator loses its capability to maintain its terminal voltage constant. This mechanism equivalently increases the network reactance significantly, further aggravating the voltage collapse condition [23].

3.2.5 Consequence of the power transfer on power lines and limitation of their capability

The variations in the system's condition i.e. in the voltage levels are principally due to the (stochastic) variations of the power transfers in accordance to the load demand. The system goes unstable because it is operated at its loading limits or in an undesirable mode. Any change of the power system operation, due to instability vectors as: load increase, generator outage, line outage, short-circuit redefines the transfer conditions i.e. the mode of operation in the whole interconnected system automatically. Mathematically seen, the differential equations describing the system inter-dependencies[33] are recalculated and new load flow solutions are found at the system's steady state.

The interconnection between the power systems components is carried out by the overhead power lines and the power cables.

[33] See Chapter 4

These can be gathered under the general term *power lines*. According to their utilization purpose the power lines can be classified into [56]:

- Distribution power lines: used by power transmission over short distances usually under several tens of kilometres and in some rare exception until some hundreds of kilometres and more. The maximal voltage level is around 220 kV.
- Backbone transmission lines: For power transmission over several hundreds of kilometres distances with possible voltages levels until 500 kV.
- Transmission tie lines: for the connection between separate neighbouring power systems. The power transmission distance in this case, can reach more than thousands of kilometres with a voltage level over 1000 kV.

The general transfer mode of the system can be evaluated only on the base of the power lines transfer.
Two basic requirements to the power line transfer, just as for the power supply in general are: its reliability and the quality of the resulting voltage profile. These two issues are as elucidated later directly related to the voltage instability phenomenon.

As already said, a major factor contributing to voltage instability are the voltage variations that occurs when electric power (active and reactive) flows through the transmission network. Hence the line power transfer impacts on the system voltage profiles and is thus directly linked to the voltage regulation. The voltage deviations resulting from the power transfer must always be confined within the system voltage operating limits. The reliability of the power line transfer is endangered when the maximum deliverable power is reached. In the sense of the words used here, the point of maximum deliverable power is the point marking the start of an abnormal transfer behaviour, i.e. of the transfer instability.

The electrical distance between the transmission line impedance and the impedance of the transferred power sink (load impedance) dictates the maximum power that can be transported through a given power line. The condition of the maximum deliverable power for power systems application is derived in [29]. According to this reference:

Under a constant power factor, the maximum power is delivered when the load impedance becomes equal in magnitude to the transmission impedance.

3.2.5.1 Illustration of the maximal deliverable power

The maximal deliverable power can be derived from load flow equations obtained from the following simple structure [29], [57] in figure 3.19.

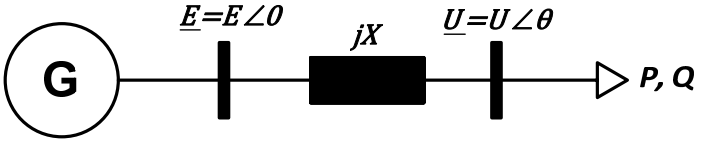

Figure 3.19: Circuit representation for the illustration of the maximal deliverable power of a power line

The voltage source is ideal with a constant voltage supply $\underline{E}$ for the load through a transmission line represented uniquely by its reactance. The load voltage is represented by its magnitude and phase angle.

The voltage on the load side is obtained by:

$$\underline{U} = \underline{E} - jX\underline{I}$$

The apparent power consumed by the load is:

$$S = P + jQ = \underline{U} \cdot \underline{I^*} = U \cdot \frac{\underline{E^*} - \underline{U^*}}{-jX} =$$

$$= \frac{j}{X}(E \cdot Ucos\theta + jE \cdot Usin\theta - U^2) \qquad (3.8)$$

The active and reactive powers consumed by the load are deduced from (3.8).

$$P = -\frac{EU}{X} sin\theta \tag{3.8a}$$

$$Q = -\frac{U^2}{X} + \frac{EU}{X} cos\theta \tag{3.8b}$$

The equations (3.8a) and (3.8b) are the load flow equations of the lossless system. Combining these equations and eliminating θ to determine for which values of (P, Q) there is a solution, one gets equation 3.9.

$$U^4 + U^2(2QX - E^2) + X^2(P^2 + Q^2) = 0 \tag{3.9}$$

This is a second-order equation with respect to U^2. The condition to have at least one solution is:

$$(2QX - E^2)^2 - 4X^2(P^2 + Q^2) \geq 0 \tag{3.9a}$$

Which is equivalent to

$$-P^2 - \frac{E^2}{X} Q + \left(\frac{E^2}{2X}\right)^2 \geq 0 \tag{3.9b}$$

Assuming that the inequality is always true, the two solutions of (3.9) are given by:

$$U = \sqrt{\frac{E^2}{2} - QX \pm X\sqrt{\frac{E^4}{4} - X^2P^2 - XE^2Q}} \tag{3.10}$$

A further transformation of the equation (3.10) is

$$U = \sqrt{E^2\left(\frac{1}{2} - \frac{QX}{E^2} \pm X\sqrt{\frac{1}{4} - \left(\frac{XP}{E^2}\right)^2 - \frac{XQ}{E^2}}\right)}$$

Equal to

$$\frac{U}{E} = \sqrt{\frac{1}{2} - \frac{QX}{E^2} \pm X\sqrt{\frac{1}{4} - \left(\frac{XP}{E^2}\right)^2 - \frac{XQ}{E^2}}} \qquad (3.10a)$$

By substitution of the short-circuit power at the load side, $S_{SC} = {E^2}/{X}$ the representation of the equation (3.10a) defines a three dimensional surface as shown in figure 3.20. The resulting curves illustrate the relationship between load voltage and the transferred active and reactive power. They thus represent the transfer situation on a power line as it is influenced by all the grid components. It visualizes the set of operating points (on the surface) that the combined generation systems and a given transmission system can sustain according to a certain system loading. These operating points are termed as feasible. Each curve inclination corresponds to a constant value of a power factor Φ and vice versa. The relationship $Q = P \cdot tan\Phi$ is true for all feasible operating points. The figure 3.20 is realized with freely chosen different values of Φ.

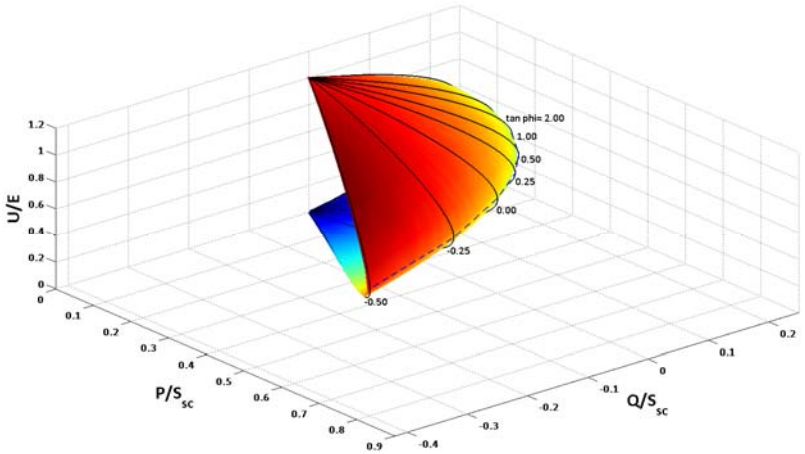

Figure 3.20: Voltage as a function of load active and reactive powers [57]

A projection of the diagram on the "PU" plane shows in figure 3.21 the shape of the PU characteristic of the power transfer. Mathematically seen the function in (3.9) have the form of two half parabolas; An upper half parabola built for the "+" in front of the internal square root in (3.10a) and a lower half parabola resulting from the solution with the "-" sign. The voltage is in general higher on the upper part of the curve. The extreme points of each the curves, linked up by the dashed line on the figure 3.21 mark the point where the equation (3.9) has only one solution. The behaviour of the curvatures changes each after these points. This extreme point is known in the Mathematics as the *vertex* of the parabola. This denomination will be also used in this work. As it will be seen later the vertex point is assumed to be the critical point beginning from which the voltage stability is jeopardized. The vertex coordinates are values of active power and voltage $(x_{vertex}, y_{vertex}) = (P_{vertex}, U_{vertex})$ at the load side which must be calculated to define the maximal deliverable active power of the power line.

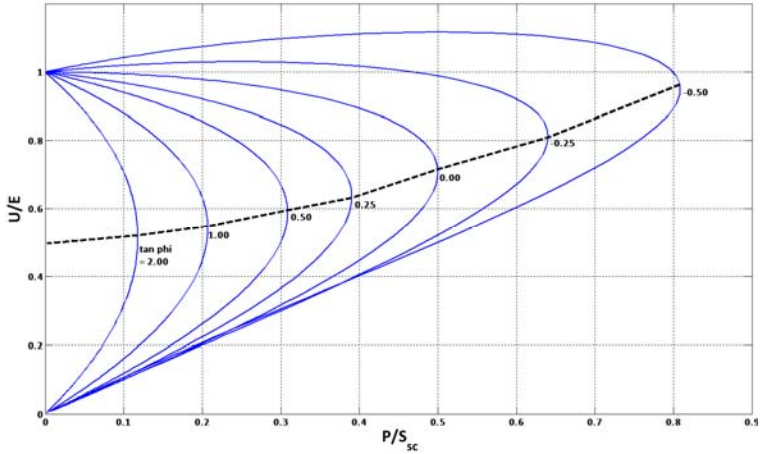

Figure 3.21: Active load voltage characteristics for constant load factors

Regarding the PU curves in figure 3.21 it can preliminary be observed that as the load is more and more compensated ($tan\Phi$ is smaller) the vertex is greater. However the corresponding voltage at which the vertex occurs also increases.

This situation can be quite confusing assuming that, if the voltage stability begins at the vertex it would mean that the instability occurs in certain cases at the voltages close to normal operation values[34]. Furthermore the two voltages are very close to each other (the PU curves are narrower) so that further analysis is needed to defined which of the solutions is acceptable for the given operation mode. By negative values of $tan\Phi$ (overcompensated loads), when more active power is consumed, more reactive power is produced by the load. This is characterized by a portion of the upper half parabola along which the voltage increases with the load power.

Theoretical and practical Voltage Instability and stability margins

The condition of the voltage stability in the form of the stability of the electric power transfer mode on the transmission line and the voltage profile at the load side results and can be analyzed on the PU curve. Using this curve, the characteristic obtained covers the complete region of operation mode of a transmission line. Namely the curve characteristic for a given transmission line always begins at its no-load (open-circuit) operation point and ends at the short-circuit operation point. Thereby the current value at the load side end is increased from a (near) zero value at the no-load point to greater value towards the line short-circuit point [58].

[34] The normal voltage operation values will be given later in this thesis.

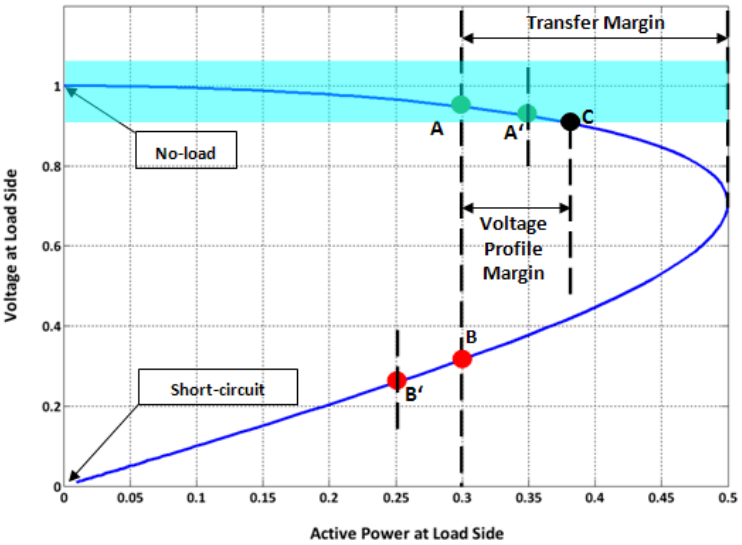

Figure 3.22: PU Characteristic for explanation of voltage stability limits

In the figure 3.22 is a PU curve corresponding to $tan\Phi = 0$. Let us consider for this constant load factor the effect of the load active power increase. The dotted line shows that for each value of the ransferred power there are two possible operating points A and B. The point A represents a higher voltage value associated to a lower current. At the point B the voltage value is lower as in A and is associated to a higher current. A load increase by constant load factor is accompanied by an increase of the load admittance [57] and is coeval to a displacement of the actual operating point.

Outgoing from Point A, an increase in the load admittance (respectively decrease of the load impedance) leads to a reduction in the voltage with simultaneous increase of the active power transferred. As a result the load consumption moves from A to A'. This is the expected mode of operation of a power system. The operation of the combined load and transmission system on the upper half parabola of the PU curve is thus stable.

At point B on the lower half parabola however, a load increase leads to the reduction of both the voltage and the active power at the load side. The point B' on figure 3.22 corresponds to the operating point reached in this second eventuality. If the load is purely static, a further system operation at B may be possible but not viable due to the low voltage and high current. This is however a matter of viability, not of stability.

By assuming the action of some load controllers or some inherent mechanisms implemented in the power systems to sustain the load demand to achieve a specified power consumption the operating point B becomes unstable through the inverse influence generated by such control equipments. This behaviour was elucidated in the previous paragraphs. For this reason the operation of the combined load and transmission system on the lower half parabola of the PU curve is undesirable and unstable.

The PU characteristic is separated in a stable and unstable branch. The stable branch starts at the no-load point and end at the vertex point. An operating point situated on this branch is assumed as stable. From the vertex point afield the system operation is unstable. The stability of the transfer mode on a transmission line is a voltage issue. The stability margin of the transfer modus ($Transfer\ Margin$) is easily defined as the absolute difference between the values of the active power at the vertex point (P_{vertex}).and at the operating set point (P_{actual}).

$$Transfer\ Margin = |P_{vertex} - P_{actual}| \tag{3.11}$$

According to the requirement of the maintenance of permissible voltage levels at each time of and in all condition of the system operation, as formulated in the first definition of the voltage instability above, the evaluation of both transfer and voltage profile instability issues at the load bus is simultaneously possible combining of the PU curve with a defined voltage profile stability band (shaded area on the figure 3.22). This band is formed by the upper and lower limits of voltage values for the normal (stable) system operation.

Their values are chosen at 1.1 and 0.9 respectively for this thesis. Whereby, the lower limit is given by [56] as the usually maximal permissible decrease of the voltage level in contingency situation at the power systems substations. The upper limit correspond also the usual upper limit of the dead band of the LTCs. These limits values can be freely varied to obtain a stricter (narrower band) or less strict (larger band) voltage profile stability requirement.
The margin of the voltage profile stability is calculated considering the first intersection of the PU-curve with the stability band. In the case of the figure 3.22 at this is the point C (P_C).
Considering the point A as the actual operation point, for the case presented in the figure 3.22 and from a practical point of view the voltage profile instability occurs before the transfer instability. It is calculated as

$$Voltage\ Profile\ Margin = P_C - P_{actual} \tag{3.12}$$

It is then meaningful to consider the minimal margin value as the real voltage stability margin.

3.3 Chapter summary

Aside from contingencies like line tripping, load increase or generator outages, voltage instability in power systems originates from the delayed voltage recovery after a disturbance induced by the response of their load components after system's voltage changes and a lack of power reactive reserve by the generators. The voltage regulating equipments (e.g.: LTCs, SVCs or OXLs) contributes to voltage instability by respectively ceasing the voltage regulation reaching their physical limitations imposed by their design and implementation; or having an adverse effect to the one expected if its action is triggered at an operating point unfavourable to its regular function. Indeed, the system's voltage variations and the load transfer between the power system's nodes are interdependent. The power transfer between the systems nodes is: constrained by the impedance of the transmission power line, stochastic and automatically redefined by each system change.

Mathematically seen and as already said above, by each system change the differential equations describing the system inter-dependencies are recalculated and new load flow solutions are found for the system's steady state. The system is voltage unstable when the new operating solutions are found beyond the physical and theoretical voltage limits of normal operation. The latest is equivalent to an unfavourable operating mode for the action of the voltage sustaining equipment. Voltage stability impacts on the ability of the power systems to fulfil their assignment to supply the consumers (loads) at any instant with sufficient power as demanded. The maximal possible (active) power transfer between the system's nodes or stations with respect of the voltage stability conditions can be illustrated by the power lines PU-curves at constant load power factors. These curves indicate the voltage stability stiffness of the system with respect to active power load variations. Combining the PU-curves with a load terminal voltage profile stability band permits the evaluation of the minimal voltage stability margin. In view of the practical assessment of the voltage stability the challenge is to accurately characterize the transfer mode of the power lines in accordance with the total system loading at each operating instant.

This task is particularly important for the backbone and tie transmission lines for which a physical connection to the loads usually does not exist. Furthermore the right calculation of the values of the active load at the operating set point and at the resulting vertex point is needed for the exact determination of the stability margins.

4 Voltage stability analysis

The mathematical concept of the voltage stability based of the bifurcation theory is provided in this chapter. The Saddle-Node (SN) bifurcation is associated to the voltage instability phenomena. Its occurrence conjointly marks the starting point of the voltage instability and the limit of voltage stability according to the second definition of the voltage stability given in chapter 3. As next an overview of the actual important trends in the voltage stability analysis is proposed. Several methods of voltage stability assessment using different various stability indices are described. An evaluation of the applicability of each method is briefly done. Finally the concept of the real time voltage stability monitoring used in this work is presented.

4.1 Mathematical concept

In the previous chapters power systems were presented highly nonlinear dynamical entities, operating in a constantly changing environment where loads, generators outputs and key operating parameters change continually. The qualitative change in the behaviour of any nonlinear dynamical system due to the change of one or more parameters is caused by the so called bifurcations. Bifurcation is a French word that has been introduced into nonlinear dynamics by Poincare. It is used to indicate a qualitative change in the dynamics of a system, such as the number and type of solutions under the variation of one or more parameters on which the system in question depends. Many of the ideas and calculations resulting from the bifurcation theory can be used or adapted for engineering purposes.

Bifurcations can be divided into two classes [60] [61] depending on the behaviour of the system dynamic manifolds and equilibrium points:

- Local bifurcations, which can be analyzed through changes in the local stability properties of equilibrium points, periodic orbits or other invariant sets as parameters cross through critical thresholds and
- Global bifurcations often occur when lager invariant sets of the system collide with each other or with system's operating points. Such bifurcations cannot be detected purely by a stability analysis of fixed operating points.

In bifurcation problems, it is useful to consider a space formed by using the state variables and the control parameters, called the state control space. In this space, locations at which bifurcations occur are called bifurcation points [37], [38]. Sometimes variations of any parameter in the system may result in complicated behaviour which gives rise to system instability. Therefore the study of the bifurcations (especially catastrophic bifurcations) is often used as the mathematical background for the description of all types of power systems instabilities. Bifurcation theory assumes that system parameters vary slowly and predicts how the system typically becomes unstable.

The main idea is to study the system at the threshold of instability. Regardless of the size or complexity of the system model, there are only a few ways in which it can typically become unstable and the bifurcation theory mathematically describes these ways.

4.1.1 Local bifurcations and instability conditions

Many physical problems yield mathematical descriptions that are a mixture of ordinary differential equations ODE's and algebraic equations. Power systems and electric circuits fall into this category [59]. For the purpose of the bifurcation study, the dynamic behaviour of a power system is described by a set of nonlinear differential and algebraic equations DAE's represented by the equations (4.1a, b):

$$\dot{x} = f(x, y, \lambda, p) \quad (4.1a)$$
$$0 = g(x, y, \lambda, p) \quad (4.1b)$$

Where $x \in R^n$ is a vector of state variables that represents the state variables of generators, loads and other system controllers; $y \in R^m$ is a vector of steady state algebraic variables that result from neglecting fast dynamics such as some load phasor voltage magnitudes and angles; $\lambda \in R^\ell$ is a set of uncontrollable parameters such as active and reactive power load variations; and $p \in R^k$ is a set of controllable parameters such as tap changer settings, or the set points of other systems controllers such as: AVR and SVC.

$f: R^n \times R^m \times R^\ell \times R^k \to R^n$ corresponds to the nonlinear vector field directly associated with the state variable x; the vector $y \in R^m$ represents the set of algebraic variables defined by the nonlinear function $g: R^n \times R^m \times R^\ell \times R^k \to R^m$ which typically corresponds to load bus voltages and angles, depending on the load models used.

The bifurcations associated to power systems stability problems are local bifurcations. They are studied through the eigenvalues of the linearization around an operating point (equilibrium points) of the DAE's used to model the system [62], [63]. Local bifurcation analysis of power systems identify qualitative changes in system equilibrium points of ODE's system of such as number of equilibrium points and their stability features as the parameters are subject to vary slowly, and these bifurcation concepts can be easily extended to DAE's systems [64].

The equations (4.1a) and (4.1b) can be summarized as:

$$\begin{bmatrix}\dot{x}\\0\end{bmatrix} = \begin{bmatrix}f(x,y,\lambda,p)\\g(x,y,\lambda,p)\end{bmatrix} = F(z,\lambda,p) \qquad (4.1c)$$

With $F = (f,g)$ and $z = (x,y)$.

The stability feature of an equilibrium point and the associated local bifurcations is determined by the eigenvalues of the total system Jacobian matrix if $D_y g\,(x,y,\lambda,p)$ is non singular along system trajectories of interest. The behaviour of the system (4.1c) along these trajectories is thereby determined by the local ODE reduction:

$$\dot{x} = f(x, y^{-1}(x,\lambda,p),\lambda,p) \qquad (4.1d)$$

The expression $y = y^{-1}(x,\lambda,p)$ comes from applying the *Implicit Function Theorem*[35] to the algebraic constraints in (4.1b) [63], [65]; and $D_y g\,(x,y,\lambda,p)$ is the Jacobian of the algebraic constraints in (4.1b) and denotes the matrix of partial derivatives of the components of g with respect to instantaneous variables y.

The system Jacobian matrix or system state matrix is determined as [64], [67]:

$$A = D_x f|_0 - D_y f\big|_0 D_x g|_0^{-1} D_x g|_0 \qquad (4.2)$$

Standard bifurcation theory deals with the study of the stability of ODE systems as they move from equilibrium point to equilibrium point as the parameter λ slowly changes. The detection and typization of the local bifurcations is done by monitoring the eigenvalues of the system Jacobian A given in (4.2).

[35] The Implicit Function Theorem permits the extension of a large number of results from linear algebra in the non linear space providing thereby local solutions. This theorem will not be explained in details in this work. By interest the lector can refer to [66] and [68] for more information.

The following local bifurcations are related to power systems:

- Node Focus: These types of bifurcations appear by a complex conjugate pair of eigenvalues merging into one real eigenvalue or vice versa, as λ changes. This type of bifurcation does not seriously impact on the system stability but seems to be precursor to other types of bifurcations [63].
- Limit Induced: These bifurcations correspond to equilibrium points where system limits are reached as λ changes. The corresponding eigenvalues undergo instantaneous changes that may affect the system stability [63], [67].
- Singularity Induced: This type appears if due to singularity of the Jacobian of the algebraic constraints. It corresponds to equilibrium points where an eigenvalues of the system Jacobian A changes from $\pm\infty$ to $\pm\infty$.
- Hopf Bifurcations: In this case, two complex conjugate eigenvalues of *A* cross the imaginary axis as λ changes. This results in limit cycles that may lead to oscillatory instabilities in power systems.
- Saddle-Node SN: When the Jacobian of the system state matrix A has one zero eigenvalue with unique nonzero eigenvectors, the equilibrium point $(x_0, y_0, \lambda_0, p_0)$ is typically referred to as SN point. In power systems, this bifurcation point is associated with voltage stability problem due to the local merger (disappearing) of equilibrium points as λ changes.

4.1.2 Saddle-node bifurcation

The Saddle-Node bifurcation may be locally described by the following simple example in figure 4.1[36]. This figure illustrates the bifurcation curve of single variable system [69], represented by the ODE:

$$\dot{x} = \lambda - x^2 \tag{4.3}$$

According to the instability condition defined above, the bifurcation diagram in figure 4.1 consists of a stable region represented by the solid line and an unstable region illustrated by the dashed line. Both regions are formed by the different equilibrium points found for (4.3) as λ changes. λ is named the bifurcation parameter. Of particular Interest is the equilibrium point located at the origin where the unstable and stable equilibrium points merge. This point is referred to as a saddle node bifurcation.

The Saddle-Node bifurcation is characterized by two equilibrium points which variations form the parabola in figure 4.1. This parabola exists for $\lambda \geq 0$. For $\lambda > 0$ two equilibrium points may be found: $+\sqrt{\lambda}$ which is the stable equilibrium point, and $-\sqrt{\lambda}$, the unstable equilibrium. For $\lambda = 0$ only one solution exists. That is the bifurcation point.

At the bifurcation point the system has one zero eigenvalue of $D_x S|_0$. Where S is the function given by the right hand side of (4.3) and D_x is the derivative of this function with respect to x.

[36] It does exist several practical software tools for the study of differential equations and calculation of bifurcations: e.g. Content®, MATCONT®,AUTO 2000®, UWPFlow®, etc. The bifurcation diagram in figure 4.1 is realized with MATCONT®.

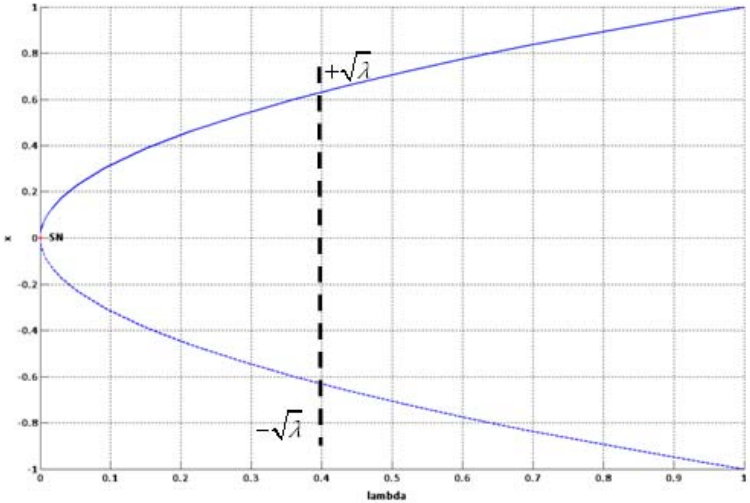

Figure 4.1: Bifurcation diagram of the equation (4.3); stable equilibrium points are found on the solid line of the curve and unstable equilibriums points are on the dashed line of the curve as the bifurcation parameter varies. The stable and unstable regions are separates by the SN point

Saddle-Node bifurcations are therefore local bifurcations, occurring where the equilibrium points coalesce and then locally vanish for further values of the bifurcation parameter [65]. This behaviour is similar to the one observed for the PU characteristic described in chapter 3 and Saddle-node bifurcations are dynamic instabilities of differential equation models that have been associated with voltage collapse problems in power systems. They play an important role in the comprehension of the voltage instability phenomenon. The conditions needed for detecting these types of bifurcations using power flow equations for a dynamic model of AC/DC systems, represented by differential equations and algebraic constraints are presented by Cañizares in [70].

4.2 Overview of the methods of voltage stability analysis

4.2.1 Introduction

It exists several methods for the analysis of power systems stability. They can be divided in *static* and *dynamic* analysis methods.
Static analysis methods permit the evaluation of the system's stability state with help of load flow equations. They utilize a snapshot of the system at a point in the time domain trajectory and give an indication of the system stability at this specific operating point. Traditional methods of voltage stability investigation have relied on static analysis methods. This consideration is practically viable by the characterization of the voltage collapse as a process being primarily considered as a small signal phenomenon. Some of the static methods further assess the proximity to unstable operation at the operating point considered. On the other hand Dynamic analysis methods embrace the theory that voltage stability is a dynamic phenomenon. Through dynamics simulations in time domain the power system's incidents possible to induce voltage instability can be chronologically represented; Furthermore, the dynamics of the system's control devices, the switching operations, the action of the compensation and the protection devices can be considered so that a more practical and accurate definition of the "real" stability limits is possible.

An enhancement of static analysis methods is possible by using a system snapshot of the system conditions comprising all stability relevant dynamics time frames (see figure 3.1) as input for the evaluation of the system condition. The combination of such data with a powerful static stability analysis method is a good solution to the problem of the online monitoring of voltage stability analysis.

After the general mathematical characterisation of the voltage instability used to complete its practical mechanisms presented in chapter 3; an overview of some static voltage stability analysis approaches presented in the literature follows in the next subparagraphs. A description of the ins and outs of the methods is made. Following the main idea of this thesis a short discussion is done on the applicability of the methods for the purposes of the real time voltage stability monitoring.

Indeed, to prevent critical circumstances in power systems, an anticipatory system operation should be always preferred to a reactive one. For this reason the stability margin remains the best instability indicator. The voltage stability margin was presented in the previous chapter as the difference between the operation and the voltage instability points based on a key system parameter e.g.: line power flow. The final goal followed by the voltage stability analysis of power systems must be the characterization of its stability margins. The steps to be put back are hereby the margins computation and their quantitative determination. This requires the detection of the instability point itself and the assessment of its distance from the actual operating point. An important feature required for the methods used for stability assessment in general is thus the ability to calculate the stability margins.

4.2.2 Contingency analysis

Hereby, the system response is analyzed (for a given operating condition) for large disturbances that may lead to voltage instability and collapse. The system is considered stable if it can withstand each of a set of credible incidents referred to as contingencies. In case of the long-term voltage stability analysis, the credible contingencies considered are usually the outages of transmission and generation facilities (N-1 criterion). The sequence of events leading to such outages does not really matter. Multiple contingencies (e.g.: N-2) may also be considered. For short-term voltage stability, the system response to short-circuits is investigated in addition to outages.

A contingency screening tool (see paragraph 2.4.1.1) is needed for this method. In common practice the possible operator actions, being deemed too slow are not considered and solely the system ability to survive the credible contingencies is assessed taking in account the solely eventual action of post contingency controls that do not prevent load power restoration. Complementary to this, the adequacy of stronger controls is checked against more severe (i.e., less probable) disturbances [71]. In a view of the real time monitoring of the voltage stability following drawbacks can be denoted for this method:

- The grid calculations done usually use static methods. These methods run with a rough system model, describing the dynamic of the power system with low accuracy. For instance, they cannot account for post contingency controls that depend on the system time evolution [71]
- As already alluded in the chapter 2.4.1.1 limiting stability (or security) monitoring of a power system only to a number of credible contingencies exposed to risk of appearance of non credible contingencies susceptible to lead to a voltage collapse.
- Complicated interpretability of the calculation results and the difficult visualization of the stability margin.
- Most often, the post contingency stability status of the power system model at operating point is approximated by numerical methods using the standard load flow equations (usually the Newton–Raphson algorithm). Their divergence is then used as criterion of instability. Among other problems this approach suffers from the following shortcomings:
    1) The divergence may result may result from purely numerical problems that are not related to a physical instability.
    2) In truly unstable cases the system operator is left without information regarding the nature and the location of the problem
    3) It gives no information about the stability margins.

While contingency analysis focuses on a particular operating point, it may be also desirable to determine how far a system can move away from this operating point and still remain in a stable state. This type of analysis involves large but smooth deviations of given system parameters from an initial value into a direction worsening the system stability state. One says the system is stressed and the inducing parameter is simply referred as the system stress. Such parameter is typically the load increase and/or generation rescheduling (e.g. within the context of a transaction) which stresses the system by increasing power transfer over the power lines, throughout the interconnected system and/or by drawing on reactive power reserves. The system *loadability limit*[37] thus corresponds to the maximal value the stress parameter can take until the voltage instability occurs. The determination of loadability limits has prompted much interest for bifurcation analysis of power systems. The stress parameter is then the bifurcation parameters and the definition of the loadability limits, in case of the voltage stability is associable to the detection of the available Saddle-Node bifurcation points.

4.2.3 Detection of bifurcations

The singularity of the Jacobian of the system equations is one the probable reason of the divergence of the conventional methods for solving system equations like the Newton-Raphson algorithm [62]. This makes the definition of the bifurcation point difficult, faulty or even impossible in some cases. The bifurcation point must be a possible operation state of the system. Continuation methods overcome the difficulties of the successive load flow calculation and allow tracing the complete voltage profile by automatically changing the value of the bifurcation parameter without worrying about singularities of the system equations. It is then possible to define the position of the bifurcation point, i.e. the stability limits on the trajectory defined by the system state variable λ responsible of the stress.

[37] In practice the voltage loadability limit will then be equal to the minimal of the voltage stability limits defined in chapter 3

4.2.3.1 Continuation method strategy

The strategy used by the continuation is illustrated in the next figure.

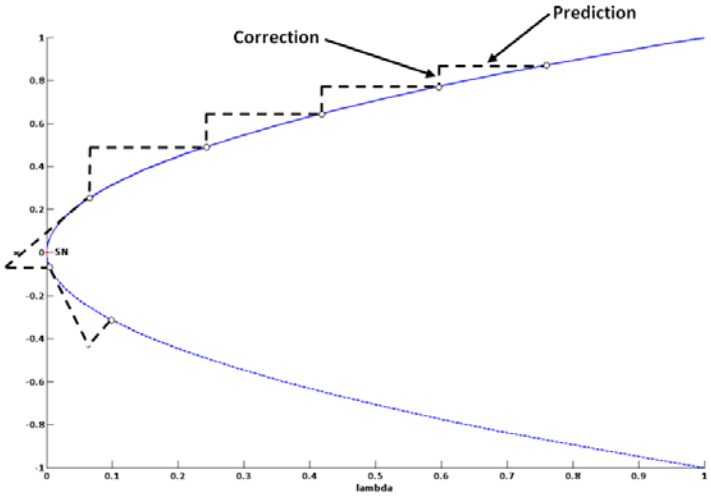

Figure 4.2: Illustration of the prediction-correction principle by the continuation method

The continuation power flow is an iterative process which outgoing from a known initial operating situation (x_j, λ_j) consist in the calculation of a new situation (x_{j+1}, λ_{j+1}) with $\lambda_j > \lambda_{j+1}$.

One iteration is divided into two phases: The prediction and the correction. The predictor-corrector scheme is employed to find a solution path of a set of power flow equations that have been reformulated to include a bifurcation (load) parameter. As shown in figure 4.2, it starts from a known solution and uses a tangent predictor to estimate a subsequent solution corresponding to a different value of the bifurcation parameter. A complete step to obtain the new operating point is illustrated by the figure 4.3.

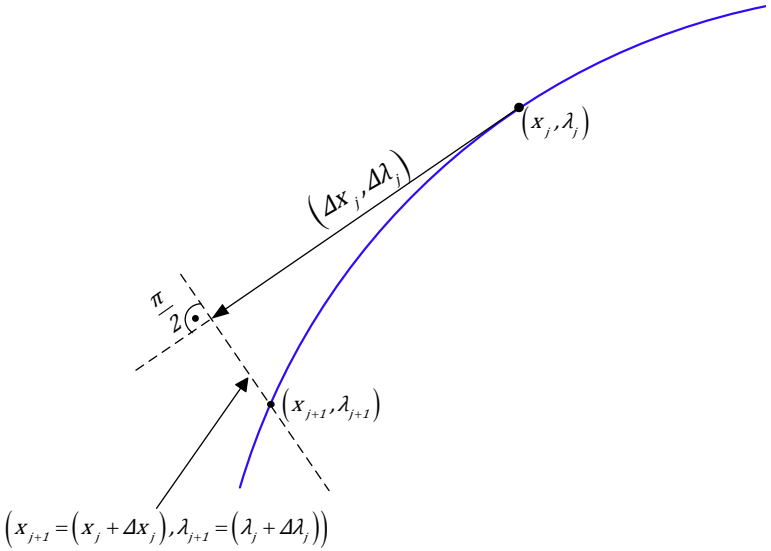

Figure 4.3: Prediction-correction step

The direction vector Δx_1 and the parameter step $\Delta\lambda_1$ result from the normalization of the tangent vector. Details on their formulation and a full description of the prediction-correction techniques can be taken from [72], [73].

$$\Delta x_1 = \Delta\lambda_1 \cdot \left.\frac{dx}{d\lambda}\right|_1 \qquad (4.4a)$$

$$\Delta\lambda_1 = \frac{k}{\left|\left.\frac{dx}{d\lambda}\right|_1\right|} \qquad (4.4b)$$

With $k \in R^+$, a constant that controls the size of the predictor step.

4.2.3.2 The Direct method

Another method for the detection of the bifurcations named the direct method or Point of Collapse PoC by its authors has been proposed in [74] and adapted by [76] where tests on AC/DC systems are reported. A direct calculation of the Jacobian permits to define the stability limit which is attained by its singularity. The bifurcation point is thus characterized by the system Jacobian, having a single and unique zero eigenvalue, with non-zero left and right eigenvectors.

The bifurcation analysis gives useful information about the behaviour of the power systems during instability. Also the points where the instability occurs can be found. In regard to the applicability of this method for the real-time monitoring of the voltage stability many shortcomings can be pointed out:

4.2.3.3 Shortcomings of the bifurcation analysis

- The bifurcation analysis is a purely mathematical method. It requires the complete description of the system with differential equations resulting from the load flow equations and an intelligent definition of the systems state variables and of a bifurcation parameter. These actions can be termed as the system mathematical modelling. The system mathematic modelling, as a first step to the bifurcation analysis of modern power systems (which are: very large, highly meshed, interconnected, and comprise a lot of different equipment) is a very complicated task which can be solved (if even possible) only neglecting a lot of systems dynamics relevant for the voltage stability considerations. In [73] Cañizares pointed out one such problem associated to the continuation method, which is: the possible elimination of variables associated to system controls with limits, particularly bus voltages with large reactive power support.

These voltages change slowly or do not change at all, until voltage control is lost when minimum or maximum limits are reached. Furthermore, depending on the system variations produced by the bifurcation parameter, an area that initially is not considered critical due to small changes on the associated system variables could become critical when close to bifurcation. Hence, variables that are eliminated in early stages of the continuation process might become later a source for significant computational errors.

- Another problem related to development of the system equations is the consideration the variations of the behaviour of some power system's components. A simple example is the modelling of the behaviour of an HVDC system. This must fit the actual mode of operation of the HVDC system i.e. must be in accordance with the energy flow direction. For each direction a new system of equations is needed. For real-time purposes much effort must be done to make the model equations adaptive to the system changes.
- The prediction-correction scheme required the assumption of a changing direction of bifurcation parameter. Such assumptions, as well as the judicious choice of the bifurcation parameters are easier to do for a standardized behaviour of the power systems. But in many cases the grid behaviour is not standardized so that such information is not readily available.
- The calculation speed is slow and the computational burden is high for large power systems.

A solution to reduce the amount of the initial model equations and thus the computational burden is to represent parts of the system by some form of a reduced order equivalent model. This process is called a dynamic reduction of the system or system dynamic equivalencing.

General principles of the dynamic reduction of large power systems

The study of the power systems stability in general requires their exact modelling and the digital time-domain resolution (simulation) of huge amount of nonlinear DAE's describing their behaviour at each time of their operation. Principally due to the large size and complexity of modern interconnected electric power systems the computation time and the analysis effort to interpret the results and translate them into operating guidelines or planning recommendations can be very large. Mostly, the study of the power systems stability is limited by the capacity of the computer programs used to solve the system's equations[38]. The optimal power systems dynamic equivalencing could provide significant benefits for such analysis tasks.

A good definition of the dynamic equivalencing is given in [77]. As specified in this reference: dynamic equivalencing consists: of reducing the complexity of the system model, e.g., by reducing modelling detail and eliminating buses and generators, while accurately retaining the important characteristics of the system. Many methods and algorithms for the power systems dynamic reduction have been proposed since the late 1960's. Some of them are described in [77], [78], [79], and [80].

[38] The following information is given in [77]... Power system stability programs allow utilities to model 12000 or more buses and several thousand generating units…This information is by interest to let be confirmed by a power system software analysis developing company.

The work of Yucra-Lino in [81] proposed new dynamic equivalencing concepts, where the linear and non-linear characteristics and behaviour of the power systems are considered together. After the definition of the part of the power system to be reduced, which is usually termed as the "external area", in opposition to the "internal area" which remains unreduced; the following general procedure is applied to obtain a grid equivalent:

1 The coherency identification:

At this step coherent generators are identified and grouped together. The methods for the coherency definition are based on the principles of the weak links between the generators or in a more classical method on the rotor angles differences resulting from the simulation of a specified fault[39]. An alternative to these methods is proposed in [81] namely:

1a) *the identity recognition:*

The difference between the two theories is that the first one consists principally in the evaluation of the phase identity of the rotor angle to identify similar machines in terms of coherency, whereas the second additionally evaluates the amplitude of the rotor angle to defined together oscillating machines.

2 The Generator aggregation:

After a group of coherent generators is identified, the generators in it are aggregated and reduced to one or a few equivalent generators. In a classical aggregation form, the generators in a coherent group are represented by an equivalent classical generator model. In its simplest form, the equivalent inertia is the sum of the inertia of all generators in the group, and the equivalent transient reactance is obtained by paralleling the transient reactances of all generators in the group [77].

[39]The tolerance coefficient which specifies the maximum number of degrees of swing by which the rotor angles of two generators may deviate from one another and still be coherent is usually equal to 5-10 electrical degrees

Different principles are used for the equivalencing of the generators controllers. They consist among other others in:

a) Splitting of coherent generator group in subgroups with similar controllers [82].
b) A controller with the best similarities to all controllers in the coherent group is chosen. The parameters fitting is realized by simulating disturbances in the frequency range [83].
c) A suitable fact is to choose the optimal equivalent controller using the controller of the largest subgroup. This optimal equivalent controller is used for the equivalent of the whole group [81].
d) Another alternative is to select the controller of the greatest generator of the coherent group to build a standard controller [81]

The majority of the generator aggregation algorithms presented in the main stream of the relevant literature are developed and tested only for synchronous generators. No papers treating the case of induction machines (usually used to model wind power plants for example) were found.

3 Network Reduction

Finally the equivalent generators are inserted into the system and the generators in the associated coherent groups are removed. The network is modified to maintain the balanced steady state power flow conditions. The power system network is then further reduced by elimination of the needless nodes and the creation of new transmission lines. An adaptive reduction technique which can be used for this purpose is described in [84]. This automatically determines the buses to be eliminated such that maximum advantage is taken of network sparsity.

Considering the structure of modern power systems, the reduction of the size of the system to model mathematically is strictly advisable prior to applying the bifurcation analysis for stability monitoring purposes in real time modus. The reduced systems must be dynamically totally equivalent to the original to avoid a faulty assessment of the stability. Here above, a detour is done to describe a typical dynamic reduction procedure of the of power systems.

Nevertheless the use of the dynamic equivalencing procedure in stability studies is linked with a certain dilemma. On one hand it is almost indispensable regarding the size of the power systems, but on the other hand it could lead to a lot of possible inaccuracies.
Thereby important behaviour of the power systems components in particular operating situations can be neglected (e.g.: two generators termed as coherent can in real operating situations behave completely different as supposed) and the topology of the network is changed. The step 3, surely redefines new connecting points for the transmission lines and therefore altered the stochasticity of the power flows observed in the real power systems. No theory is available yet for the aggregation of induction machines (generators) which are an important component of contemporary power systems. The ideas of dynamic equivalencing are interesting, but still need to be further worked out to be applicable to power systems.

That being said, it can be concluded that, even if it can legitimately refer to the bifurcation theory to describe the mathematical foundations of the instability problems of the power systems, the use of the bifurcation analysis for the online monitoring of the stability of power systems, particularly the voltage stability is still problematic when applied to large power systems. The method is computationally intensive and much preparatory work (system reduction) must be done to ease its application. The preparatory work will simplify the development of the systems equation but can also lead to false stability assessment due to the inappropriate system modelling.

4.2.4 Direct measurement of a reduced state vector

Another method computing the minimum singular value of the system Jacobian as power system voltage stability index is proposed by Bergovic and Phadke in [85]. The method presented determines coherent clusters of load buses in a power system based on an arbitrary criterion function. The system clustering is based on the assumption that system phasors measured at coherent buses changes in a coherent fashion when the system loading changes and moves towards voltage instability. The coherency algorithm is described in the framework of graph theory and the analysis is completed with defined coherency criteria. Thereby, the power system is modelled by generator swing dynamics and power flow equations on load buses. The Jacobian of the system is a matrix containing all the system phase angles and voltage magnitudes. The proximity of the system state to voltage instability is assessed by tracking the minimum singular value of the system Jacobian in real-time. An enhancement in comparison to the iterative (indirect) calculation of the state vectors (operating point) from power flow measurements (e.g.: in the bifurcation analysis) is here the direct measurement of the system state vector. A measurement system installed, acquires only the relevant system state vectors constituted by the generators and load buses voltage phases angles and magnitudes at regular time intervals. By this way, the system Jacobian could be recalculated at the rate of measurement updates. The problems associated with such measurements are mainly due to the difficulties in synchronization of a measurement system distributed over a wide geographic area. The synchronization problem is successfully resolved by the availability of the Global Positioning System (GPS) satellite synchronization signals[40].
The *Singular Value Decomposition* (SVD)[41] of the Jacobian produces the proximity indication of the system state to instability.

[40] The theory of synchronized phasors measurements and its advantages is detailed in a further chapter

[41] The detailed explanation of the SVD technique is beyond the scope of this work, by interest it can be referred to specialized literature.

This method presents some advantages due principally to the faster assessment, induced by the direct measurement of a reduced state vector. In view of the real time monitoring of the voltage stability there are still some limitations concerning the computational efficiency of this method. The time won by at the measurement stage can be loose at the calculation stage principally constituted by the SVD, which is an iterative process. Also some questions arise on the interpretability of the results and on the validity of the defined coherency criteria for different operating situations.
Generally for the methods based on the detection of bifurcations (study of the eigenvalues of the Jacobian) is that they are focused on the unstable mode of operation of the power systems. The aspect of the instability represented by the magnitudes of the system's voltages is thereby almost forgotten.

4.2.5 Q-U Modal Analysis

The modal analysis technique involves also the computation of eigenvalues and the associated eigenvectors of a power system state Jacobian matrix. But in this case the condition of instability is different. This method is proposed as follows in [89], [90] and [91], and uses a reduced Jacobian matrix to examine the interdependency between the incremental change in bus voltage magnitude and the incremental change in bus power injection. Thereby the active power at the operating points is considered constant. The linearized steady state system power voltage equations are given by:

$$\begin{bmatrix}\Delta P\\ \Delta Q\end{bmatrix} = \begin{bmatrix}J_{P\theta} & J_{PU}\\ J_{Q\theta} & J_{QU}\end{bmatrix} \cdot \begin{bmatrix}\Delta\theta\\ \Delta U\end{bmatrix} \tag{4.5}$$

Where,
ΔP = incremental change in bus active power, ΔQ = incremental change in bus reactive power, $\Delta\theta$ = incremental in bus voltage angle, ΔU = incremental change in bus voltage magnitude.
To express the relation between ΔQ and ΔU for a small change in real power, $\Delta P = 0$ is assumed.

This leads to:

$$\Delta Q = \left(J_{QU} - J_{Q\theta}J_{P\theta}^{-1}J_{PU}\right)\Delta U \qquad (4.5a)$$

The expression in the brackets in (4.5a) represents the reduced Jacobian matrix of the system. It relates the bus voltage magnitude and reactive power injection.

Let assume

$$J_R = \left(J_{QU} - J_{Q\theta}J_{P\theta}^{-1}J_{PU}\right) = \xi \cdot \Lambda \cdot \eta \qquad (4.5b)$$

With: ξ: the right eigenvector matrix of J_R; η: the left eigenvector matrix of J_R and Λ: the diagonal eigenvalues matrix of J_R.
Using the equations (4.5a) and (4.5b) the incremental changes in reactive power and voltage are related by:

$\Delta U = \Delta Q \cdot J_R^{-1} = \Delta Q \cdot \ \xi \cdot \Lambda^{-1}\ \eta$ or

$$\Delta U = \sum_i \frac{\xi_i \eta_i}{\lambda_i} \Delta Q \qquad (4.5c)$$

λ_i is the ith eigenvalue, ξ_i is the ith right eigenvector of J_R and η_i is the ith left eigenvector of J_R.
λ_i, ξ_i and η_i define the ith mode of the system.

The ith modal reactive power variation is:
$\Delta Q_{mi} = k_i \xi_i$ with k_i a normalization factor such that $k_i^2 \sum_i \xi_{ji}^2$=1 with ξ_{ji} the jth element of ξ_i
The ith modal voltage variation can therefore be written as:

$$\Delta V_{mi} = \frac{1}{\lambda_i} \Delta Q_{mi} \qquad (4.5d)$$

From the equation (4.5d), the stability of a mode i with respect to reactive power changes is defined by the modal eigenvalues λ_i. Large values of λ_i suggest small changes in the modal voltage for reactive power changes. As the system is stressed, the value of λ_i becomes smaller and the modal voltage becomes weaker. By λ_i equal to zero the corresponding modal voltage collapses since it undergoes infinite changes for reactive power changes [91]. A system is therefore stable defined as voltage stable if all the eigenvalues of J_R are positive. By positive eigenvalues the variations of the modal voltage and the modal reactive power are along the same variations. By negative eigenvalues their variations are opposite [89]. This phenomenon serves as background to the stability assessment using QU curves shortly presented in the sub-paragraph 4.2.7 of this chapter.

The modal analysis can be “pushed” until the definition of the participation factors showing which grid components contribute the most to the instability by their more increased reactive power consumption. Used by this way, the eigenvalues analysis provides a relative measure of the system to voltage stability analysis. The results are numeric. They can be used to quantify the stability margin. To be effective, for practical real-time implementation the modal analysis must be combined with graphical QU-characteristics.

4.2.6 Application of Artificial Neural Networks ANNs

The use of ANNs has won an increased interest for power systems applications during the last years. Their applications are diverse and also include the monitoring of the voltage stability. Among all kinds of ANNs, the most widely used are multi-layer feed-forward neural networks [86], [87], [88].

These networks can be trained with a powerful and computationally efficient method called error back-propagation. A description of the general structure of such ANN's can be seen in [87]. The procedure of the voltage stability monitoring always comprises the steps of:

- *Choice of the ANNs training mode:* this first step is done offline. The two modes of ANNs training used are the sequential and random presentation of training patterns. The first mode calls for generating the training data according to pre-specified scenarios (e.g.: load increasing patterns or other possible contingency patterns until the predefined voltage stability limits are reached [86]) and they are presented to the ANNs for training in that same order. In random presentation a pre-specified number of training patterns are generated randomly within specified loading ranges and are presented to the ANNs in a random order.
- *Selection of the voltage stability features:* Also this second step is made offline. The selected features must characterize properly the voltage stability situation of the power systems for a variety of power systems operating conditions. The features selected serve as input for the ANNs. They can be some system variables correlating with the system voltage and thus influencing it [86] or stability indices formulated to give a "statement" on the system voltage situation (L-index for [87], and sensitivity analysis in[88]).

- *Training the ANN:* Also done offline. The ANN is trained to recognize the signs of voltage instability, using the selected features.
- *Stability assessment:* This is the only step realized online. On the base of the preparatory work done on the first two steps, the stability status of each operating points is assess and eventually the margin is directly calculated from the trained ANN.

The application of ANNs, considerably reduces the computational burden of the stability assessment. A wise selection of the stability features can permit the calculation of the stability margins. However the contingency selection for which the neural networks are trained must be optimal. The appearance of an "unknown" operating case, or a case of large number of inputs by relatively smaller number of training examples, may result in poor ANNs performance.

4.2.7 PU and QU Curves

The PU curves are the most used method of predicting voltage instability. They are used to determine the loading margin of a power system. The PU curve for a bus can be obtained by increasing the total load at the bus or area and performing successive power flow calculations, whilst maintaining a constant power factor. In these cases The PU Curve is in reality just the connection of the successive calculated (normal load flow calculation) or predicted (continuation load flow) operating points, for a given power factor. Examples of such curves are the figures 3.3 and 4.1. The voltage at a given bus is plotted as a function of the total active power load, until the critical loading point is reached. The margin between the critical point and the actual operating point is used as voltage stability criterion.

The critical point in figure 3.3 is the point of divergence of the load flow algorithm. The power system analysis software used stops the load flow calculation at this point. The drawback of the consideration of the load divergence to qualify the maximal instability point is pointed out in the sub-paragraph 4.2.2. The maximal point in the figure 4.1 is obtained using a continuation software. The critical point is the SN bifurcation point. The active power is equivalent to the bifurcation parameter "*lambda*". The shortcomings of using this method to define the critical point are those of the bifurcation analysis. A good and more realistic solution to the representation of the of the PU curves is the use of the equation of the power transfer between a power source and a power sink. This is demonstrated by the calculation of the maximal deliverable power in the subparagraph 3.2.5.1. A PU characteristic is directly obtained as the resulting curve of the *U(P)* function. The vertex point is the critical stability point. The curves are represented for each new power factor and thus contain information about the corresponding reactive power. The instability mechanisms described by the bifurcation theory can be retrieved by analyzing the position of the potential operating points (solutions of the transfer equations) on the branches of the curves.

QU curves are used to indicate the sensitivity and variation of bus voltages with respect to reactive power injections and absorptions, according to the principles described in the modal analysis in 4.2.5. The QU curves at a test bus are generated by placing a variable reactive power source with infinite limits at the bus. Successive power flows are performed for different scheduled values of bus voltage, and the required reactive power injection is measured. The reactive power margin is the MVar distance from the operating point to the bottom of the QU curve. The QU curve can be used as an index for voltage instability. The point where dQ/dV is zero is the point of voltage stability limit.

QU curves can also be found as a projection of the curves on figure 3.20 on the “QU” plane.

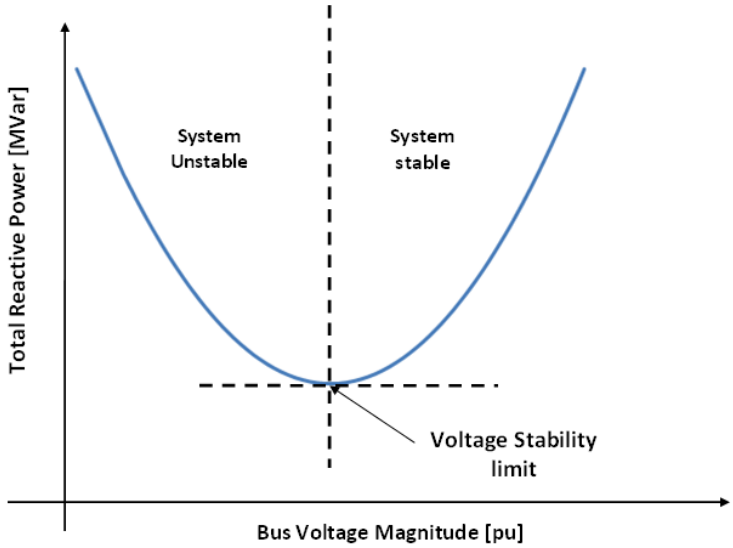

Figure 4.4: Typical theoretical QU Curve

As for PU curves, continuation power-flow programs can be used for QU curves to obtain solutions below the bifurcation point, but this is not usually necessary [91].

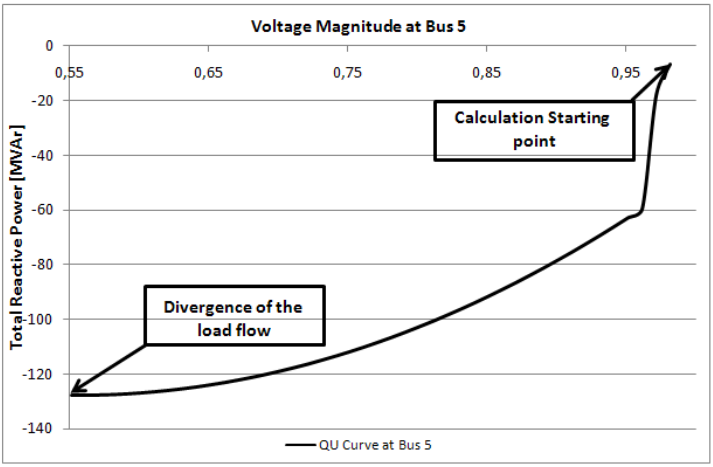

Figure 4.5: Practical QU curve at the load bus 5 of the six-bus system in chapter 3, realized in PowerFactory®

The figure 4.5 shows a calculation of a QU-Curve as done in practice. As described above: The script used attaches a fictitious generator at bus 5 and calculate the load flows from a voltage set point until the load flow does not converge any longer. The point of the load flow divergence marks the reactive power limit of the power system. As seen on figure 4.5. The limit corresponds to a very low voltage. In such a case, according to the first voltage stability definition the real limit of stability is much higher than the one found by the program.

4.2.8 L-index

The L-index is proposed by Kessel und Glavitsch in [93] as an indicator of impeding voltage stability. Starting from the subsequent analysis of a power line equivalent model, the authors developed a voltage stability index based on the solution of the power flow equations. The L index is a quantitative measure for the estimation of the distance of the actual state of the system to the stability limit. The L index describes the stability of the complete system using the expression:

$$L = \underset{j \in \alpha_L}{MAX}\{L_j\} = \underset{j \in \alpha_L}{MAX} \cdot \left| 1 - \frac{\sum_{i \in \alpha_G} \underline{F}_{ji} \cdot \underline{U}_i}{\underline{U}_j} \right| \tag{4.6}$$

Whereby α_L is the set of loads nodes and α_G is the set of generator nodes. L_j is a local indicator that determinates the busbars from where collapse may originate. The L index varies in a range between 0 (no load) and 1 (voltage collapse). The stability limit is reached for $L_j = 1$. This index has been further optimized by Huang and Nair [94] to track the dynamic voltage collapse as it progresses. The authors used the L index to provide meaningful voltage instability information during dynamic disturbances in the system. They reformulate the local indicator L_j from [93] in terms of the power as:

$$L_j = \left| \frac{S_{j+}^*}{\left(Y_{jj}^+ \cdot U_j^2\right)} \right| \tag{4.7}$$

Whereby,
S_{j+}^* is the complex conjugate injected power at bus j.
Y_{jj}^+ is the transformed admittance given by the equation $Y_{jj}^+ = \frac{1}{Z_{jj}}$
U_j is the complex voltage at bus j
The complex conjugate injected power consists of two parts:
$S_{j+} = S_j + S_j^{corr}$

The complex power term component S_j^{corr} represents the contributions of the other loads in the system to the index evaluated at the node j. and is found as:

$$S_j^{corr} = \left(\sum_{\substack{i \in Loads \\ i \neq j}} \frac{Z_{ji}^*}{Z_{jj}^*} \cdot \frac{S_i}{U_i} \right) \cdot U_j \qquad (4.7a)$$

In equation (4.7a) Z_{ji} and $Z_{jj}$are respectively the off-diagonal[42] entries and the main diagonal elements of the system impedance matrix. The complex voltage U_j is affected by the bus power S_j and the term S_j^{corr}.

The value of L_j is also here decisive for the stability assessment. For a stable situation the condition $L_j \leq 1$ must be fulfilled all the time at each node j.

An important information missed in this method is the quantification of the distance to instability.

[42] The *off-diagonal* entries are those not on the main diagonal

4.2.9 Power transfer stability index based on the system Thevenin equivalent

A Power transfer stability index is proposed in [95]. The index uses the ideas developed in [96] and [97]. The stability indices presented consider the Thevenin equivalent of the power system connected to a load bus where an apparent load is connected. Figure 4.6 exemplarily shows the concept used.

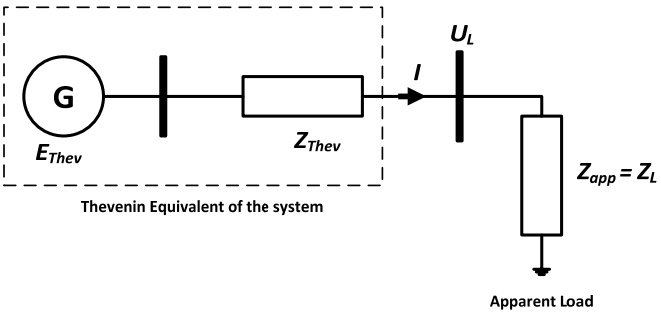

Figure 4.6: System Thevenin equivalent and local bus

The current drawn by the load is given by:

$$\underline{I} = \frac{\underline{E}_{Thev}}{\underline{Z}_{Thev} + \underline{Z}_L} \tag{4.8}$$

The load apparent is written as,

$$\underline{S}_L = \underline{Z}_L \underline{I}\underline{I}^* = \underline{Z}_L \left|\underline{I}\right|^2 \tag{4.9}$$

Substituting (4.8) in (4.9) one gets

$$\underline{S}_L = \underline{Z}_L \cdot \left| \frac{\underline{E}_{Thev}}{\underline{Z}_{Thev} + \underline{Z}_L} \right|^2 \tag{4.9a}$$

Assuming that $\underline{Z_L} = Z_L \angle \alpha$ and $\underline{Z_{Thev}} = Z_{Thev} \angle \beta$ the equation (4.9a) is rewritten as:

$$\underline{S_L} = Z_L \angle \alpha \cdot \left| \frac{\underline{E_{Thev}}}{Z_{Thev} \angle \beta + Z_L \angle \alpha} \right|^2 \qquad (4.9b)$$

α is the phase angle of the load impedance and β is the phase angle of the Thevenin impedance.
The magnitude of the load apparent power in (4.9b) can be expressed as,

$$S_L = \frac{E_{Thev}^2}{|Z_L \angle \alpha + Z_{Thev} \angle \beta|^2} \cdot |Z_L| \qquad (4.9c)$$

Further transformation of the equation in (4.9c) leads to,

$$S_L = \frac{E_{Thev}^2 Z_L}{Z_{Thev}^2 + Z_L^2 + 2 Z_{Thev} Z_L cos(\beta - \alpha)} \qquad (4.9d)$$

The maximum of the load apparent power is found after nullification of the differentiation of the equation (4.9d) with the respect to the load impedance and the substitution $Z_L = Z_{Thev}$.

$$S_{Lmax} = \frac{E_{Thev}^2}{2 Z_{Thev}\big(1 + 2cos(\beta - \alpha)\big)} \qquad (4.10)$$

The maximum load apparent power given by equation (4.10) is also considered as the maximum loadability limit which depends on the Thevenin Parameters varying with system operating conditions. The difference $S_{Lmax} - S_L$ defines the power margin. The maximal power transfer is found when this margin will be equal to 0. This occurs if $\left|\underline{Z_L}\right| = \left|\underline{Z_{thev}}\right|$. The impedance equality obtained here fortifies the theory of the condition of maximal deliverable power given in the paragraph 3.2.5 of this work in accordance with [29]. A stability index can be defined using the impedances or the fact that the ratio S_L to S_{Lmax} must be less than 1 for stability.

In other words instability occurs when

$$\frac{S_L}{S_{Lmax}} = 1 \tag{4.11}$$

Putting equations (4.9d) and (4.10) into (4.11) and after simplification an alternative index is found as:

$$\frac{2S_L Z_{Thev}\big(1 + cos(\beta - \alpha)\big)}{E_{Thev}^2} \tag{4.12}$$

The values of 4.11a will fall between 0 and 1. The value of 1 is the voltage stability limit.
The work of Bergovic et al in [98] also results in the formulation the transferred stability power margin in dependency of the Thevenin impedance. Mathematically the power margin defined in [98] is given by the equation:

$$\Delta S_L = Z_L I^2 - Z_{Thev} I^2 \tag{4.13}$$

A general problem by these methods is the estimation of the Thevenin impedance as seen from a load bus in real power systems. The work of Leif Warland in [97] expands the method presented in [96] to achieve a better estimation of the system's Thevenin equivalent.

4.2.10 Line stability index

Moghavemmi and Omar [99] derived a line stability index based on the power transmission concept in a single line, in which discriminant of the voltage quadratic equation is set to be greater or equal than zero to achieve stability. If the discriminant is small than zero, the roots will be imaginary, which means that cause instability in the system. The index is developed on the base of a simple structure of a single line within a power system as shown in the figure 4.7.

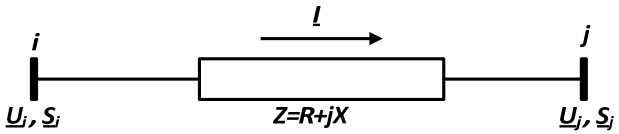

Figure 4.7: Representation of a transmission line

The line stability index is formulated as [99],

$$L_{mn} = \frac{4XQ_j}{\left(U_i sin(\theta - \delta)\right)^2} \tag{4.14}$$

Where θ is the line impedance angle and δ is the angle difference between the lines ends. The stability between each two bus bars of the interconnected system can thus be evaluated. Index values close to 1 mean the system is closer to its instability between those two bus bars points.

The quantification of the voltage stability margin between the system busbars can surely add more value to this index.

4.3 Chapter summary

A mathematical background to the voltage instability phenomenon in power systems is given in this chapter using the bifurcation theory. The occurrence of the so-called Saddle-Node bifurcation point is related to the beginning of the power system voltage instability. This point also mathematically defines the limit of the system voltage stability. This bifurcation point can be found by continuing the load flow of the power system, changing one representative parameter (e.g.: the system load) until it occurs. For this purpose the power system's is modelled by a set of DAE's describing its dynamic behaviour. The bifurcation points are possible operating points of power systems. Behind these points, further system operation is unstable. The detection of the bifurcation points is presented as one possible method of voltage stability assessment, whereby only the saddle-node bifurcation point is interesting. The development of the system mathematical model is thereby a difficult task which is advisable to realise for a reduced dynamic equivalent of the power system under study.

The principles and the shortcomings of the dynamic equivalencing are given in this chapter. Other trends in the voltage stability assessment are the use of: The non convergence of the load flow algorithm by simulation of different possible contingencies, the degeneracy of the load flow Jacobian matrix, its minimum singular value, and its condition number as indices of power system small disturbance voltage stability. Some methods based on these principles are presented here above. The modal analysis of the power system utilises the sign of the eigenvalues of the Jacobian matrix as stability index. Using artificial neural networks, typical stable power system behaviour can be trained. This trained network model can be used to make instability predictions from other input data sets. Problematic is thereby the constriction to the cases trained, taking in account that instability can result from a large variety of disturbances. Nevertheless the judicious choice of the relevant training parameters (e.g.: Voltage magnitudes) can be a good solution to the prediction of voltage instability. The PU and QU curves are the most popular methods for the voltage stability analysis. They respectively mark the maximal transfer limits of active and reactive powers at a given node bus. In view of the real time voltage stability monitoring the PU curves realized as the resulting function of the maximal deliverable power is a good solution to represent the impending instability. Further indices used the equality of the system Thevenin impedance with the impedance of the load bus and the nullification of the discriminant of the voltage quadratic equation at the load bus for recognition of the instability.

Outlook

An overview of the important trends and methods for the voltage stability evaluation in power systems is furnished in the paragraphs above. As indicated, the stability indices presented are all used for the computation of the voltage stability limit of power systems and are almost all based on steady-state principles.

In this thesis static analysis methods will be combined to relevant system constant data and to dynamic system data for the assessment of the power system voltage stability in real-time modus. The dynamic data used must provide a picture of the transient system condition as seen from different nodes of a defined observed area.

A comprehensive stability analysis is then performed using the received data sets as inputs. This analysis must take place in (near) real time, and with sufficient speed to give the system operator the time to react to impending instability. It can thus make an optimal use of its system ensuring thereby the maintenance of normal operating conditions. The approach used for the dynamic voltage stability monitoring is explained in the next chapter.

5 Guiding principles of the real-time voltage stability monitoring

The concept of the real-time voltage stability assessment (VSA) to be implemented in this thesis is presented in this chapter. The individual functions fulfilled by each component of the VSA are described and the interactions are highlighted. The concept developed is adapted from the principles of the dynamic security assessment of power systems described in [25]. The monitoring functions described in this reference are re-tailored to fit the needs of the dynamic voltage stability monitoring.

In view of the monitoring of the system's transients, the synchronized phasors measurements are introduced as a considerable enhancement to the RTU's data usually used in daily operation of power systems. As such data will be further used in this work; some important theoretical aspects of the synchronized phasors measurements in power system are presented. The phasor calculation algorithm is explained and a short insight in the phasor measurement device is given. A typical layers structure of a PMU based monitoring system is illustrated. It is followed by a discussion of some practical considerations of the PMU technology. Emphasis by the discussion is made: on identified problems related to the real time applications of the PMU data, on the theory relative to the PMUs positioning in power systems and on various applications of PMU data. Hence, the general principles of some usual placement techniques are discussed. The results of their utilization on two test systems are compared. On the basis of the comparison results the defined best algorithm was used to calculate the PMU placement on a real power system namely the western Danish grid (DK VEST). Finally a survey, although by no exhaustive means gives a glimpse of some existing system operational applications of synchronized phasor measurements.

5.1 The Real-Time voltage stability monitoring concept

5.1.1 Components of the Real-time Voltage Stability Monitoring

In the context of this thesis, the stability assessment of a power system is resumed into three principal steps:

- **The system state measurement**: To provide a delivery of consistent loads flow results based on real-time measurements of relevant systems variables, reflecting its actual operating condition at each measured instant.
- **The voltage stability analysis or evaluation**: To determine whether the actual system operating conditions are acceptable from a point of view of the predefined stability conditions.
- **The voltage stability margin calculation**: To assist the operator in the task of maintaining the system in a sufficiently stable operating state and when needed to bring the system from a near unstable state to a more stable one.

The chronology of the system stability assessment process is illustrated by the figure 5.1. The situation around two successive operating instants T_0 and T_1 is described.

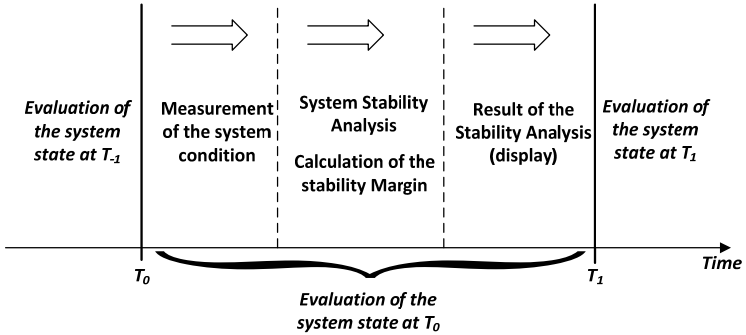

Figure 5.1: Chronology of the system stability assessment

The system dynamic data used as input for the stability assessment are collected at the instant time T_0 by the measuring instruments placed at defined system's nodes. All the next steps are done on the base of these dynamic (*not hypothesized*) data. The capture of the consistency of the system's state change between T_0 and T_1 is only possible at the time instant T_1. The stability analysis, the margin calculation and the presentation of the analysis are complex tasks which must be completed in a time interval appropriate to the systems dynamics, for a robust stability assessment.

The flow chart in figure 5.2 shows the key components for the stability assessment and the interactions between these. The structure is realised to fulfil the conditions of the real-time stability monitoring in the framework of this thesis. In general, the differences between distinct conceptual designs for the online stability assessment result majorly from the functions required. Also the inputs and interrelationships between the functions can differ in separate cases.

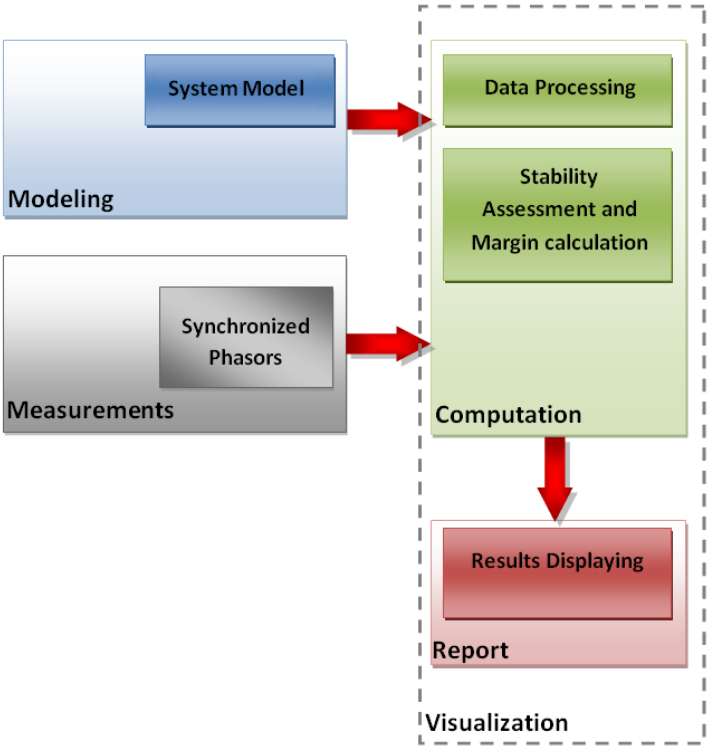

Figure 5.2: Conceptual implementation of the real-time Voltage Stability Assessment (VSA)

A short description of each component in figure 5.2 follows.

A Modelling

The first component of the voltage stability assessment (VSA) in figure 5.2 is represented by the modelling of the system to be monitored. The system to be monitored is also called the monitoring object. An optimal model representation of the physical structure of the monitoring object gives knowledge about the relevant data[43] to describe its behaviour. For electrical equipment in power systems, an equivalent circuit representation based on the electrical properties of the monitoring object alleviates the characterization of its dynamic response to the changes in the bulk system. The characterization of the physical interrelationships is usually materialized through mathematical equations which are then used for further considerations.

The monitoring object chosen in this work is represented by a unique transmission device (power line) or a set of several, but individually considered transmission devices gathered in a transmission zone[44].

B Measurements

A snapshot of the system condition is provided periodically. It consists of data sets formed by relevant system's state measurements which build the primary data sources for the VSA.

The traditional Power system's state monitoring approach is based on the Supervisory Control and Data Acquisition (SCADA) system. The typical SCADA structure comprises: a central host (Master Terminal Unit, MTU), field data gathering and control units or Remote Terminal Units (RTUs), a communication system and a software application to control the RTUs. SCADA systems are designed to capture and deliver the power system performance in 5 to 20 second intervals. A steady-state snapshot of the transmission system gives an overview of topology, power flows, voltage profiles and power-frequency controller operation. The information displayed covers the complete national operation area and eventually partial sections of the neighbouring systems [9], [10].

[43] These data can be then read out from the system technical specification

[44] This expression is defined further in this thesis

But as SCADA systems capture only steady state operation they prevent the monitoring of fast transient phenomena. Other shortages of the RTUs-SCADA measurements are their low sampling density and their asynchronous character[45]. Based on SCADA data, real time operation of power systems became increasingly problematic because it is inappropriate to the conditions actually faced by power systems operators.

With the advent of the Phasor Measurement Units (PMU's), fast transients can be tracked at high sampling rates. This allows the monitoring of transient phenomena in the power systems [100]. Furthermore, the completion of the Global Positioning System (GPS) of satellites provides the component needed for the synchronization of several PMU's distributed throughout interconnected power systems. The GPS time synchronization enables the accurate time tag of each recorded data sample at each PMU location to better than 100 nanoseconds accuracy.

At the present time, the PMUs dynamic performance under transient conditions still should be specified and verified by their users to meet their application needs. However, the PMUs dynamic data sets usually consist of the magnitudes and angles of the system's nodes voltages and currents, supplemented by the system's frequency. These measurements are termed as synchronized phasors measurements or synchrophasors. It is now assumed that the applications of synchronized measurements for power grids will provide the real time operating staff with previously unavailable yet greatly needed tools to avoid grid instabilities, and to monitor generator's response to abnormal excursions in system frequency. Due to the possibility of the synchronization of the measurements from remote locations, the PMU is now in the spotlight as the key technology for the Wide Area Monitoring Systems (WAMS).

[45] For a right or exact assessment of the system operating state it is more useful that all field measurements from different RTUs have the same timestamp. In other case they are asynchronous. By asynchronous measurements the risk that measurements from remote RTUs locations delivered at the MTU at the same time described two different system states. That can false the assessment of the system condition.

These systems are used to monitor wide area power information from distributed locations within a given power system or covering neighbouring power systems. The PMU based WAMS are nowadays still used as supplement to the SCADA systems. The method of the phasors sampling is presented in the next chapter also the general principle of the Wide Area Monitoring (WAM) is illustrated.
In this thesis, synchronized phasors are combined with relevant transmission line model data to build up the input data of the VSA. Thereby the system frequency is not considered.

C Computation

Recently, technology capabilities of both generating and collecting data have been increasing rapidly. The dramatic cost decrease of mass storage devices makes it possible to store huge amounts (terabytes – 10^{12} bytes) of data efficiently. Also the power system field is presently facing an explosive growth of data [101]. Aside the centralized field data archives and data from simulations, an important contribution to this comes from the emergence of innovative monitoring and control systems such as the PMUs. In order to gain any advantage of all these data, it is assumed that system operators need robust algorithms and tools that will help them infer the meaning of the data and to discern their interrelationships.
The typical process (in figure 5.3) of extracting useful knowledge from stored data sets can be generally described using the Data Mining (DM) approach. Data mining, which is also referred to as knowledge discovery in databases, is the process of extracting implicit, previously unknown and potentially useful information (such as: constraints or regularities) from data in databases and using it [101], [102].

The mining process of the input data takes place at this stage of the VSA. Once the input data is defined this process falls as illustrated in figure 4.10 in the following steps [101], [103]:

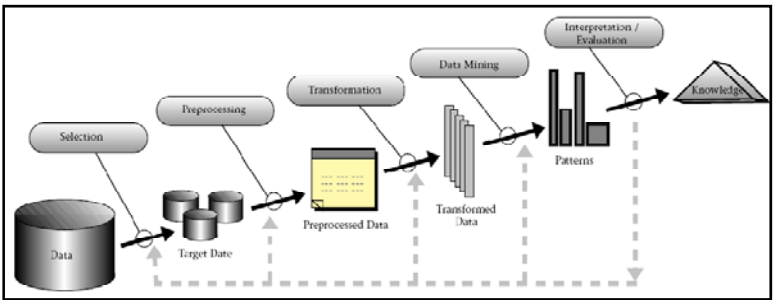

Figure 5.3: An overview of the steps that compose the DM process [103].

- ***Data selection***: The step consists of choosing the goal and the tools of the data mining process identifying the data to be mined then choosing appropriate input attributes and output information to represent the task.
- ***Data preprocessing and data transformation:*** Preprocessing and transformation operations include organising data in desired ways converting one type of data to another (e.g. from symbolic to numerical) defining new attributes, reducing, the dimensionality of the data, removing noise and outliers, normalizing if appropriate deciding strategies for handling missing data.
- ***Data mining***: the transformed data is subsequently mined using one or more techniques to extract patterns of interest.
- ***Result interpretation and validation:*** For understanding the meaning of the synthesized knowledge and its range of validity the data mining application tests its robustness using established estimation methods and unseen data from the data base.

- ***Incorporation of the discovered knowledge***: This consists of presenting the results to the decision maker who may check/resolve potential conflicts with previously believed or extracted knowledge and apply the new discovered patterns.

These steps described with exact accuracy the computation process to be realized in this thesis, to intelligently and automatically transform the processed data from distributed PMU's into useful information and knowledge on the voltage stability margin of power systems. This process must take place in real time modus.
For more effective voltage stability monitoring the computation process must be combined to an interactive visualisation tool.

D Report

"A picture is worth a thousand words" is a saying that refers to the idea that complex problems can be described with just a single still image, or that an image may be more influential than a substantial amount of text. It also aptly characterizes the goal of visualization where large amounts of data must be absorbed quickly [60]. The first step of the visualization is the data computation described earlier. It is followed by a report of the results to display the results of the voltage stability analysis.
The report function in figure 5.2 packs the information generated by the computation process of the measurements and the calculations into a single computer-generated image enabling the viewer to interpret the sense of the data more rapidly and more accurately. The computer image will be generated for each measured data sets. Following the advice given in [104] the computation and the report processes are made in the same software environment.

5.2 Synchronized phasors and measurements units

5.2.1 Phasor definition

A phasor is a complex number used to represent sinusoidal functions of time. The basic definition of the phasor representation of a sinusoid is illustrated in figure 5.4. Assume a single frequency constant sinusoid is observed starting at time t=0 as shown in the figure. The sinusoid can be represented by a complex number called 'Phasor' which has a magnitude equal to the root-mean-square (rms) value of the sinusoid, and whose angle is equal to the angle between the peak of the sinusoid and the t=0 axis.

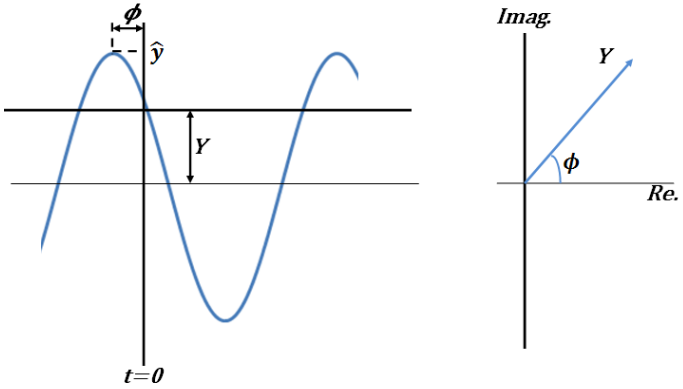

Figure 5.4: Phasor Representation

The sinusoidal quantity in figure 5.4 is of the form

$$y(t) = \hat{y} \cdot \cos(\omega t + \phi) \qquad (5.1)$$

Where,

$\hat{y}$ is the magnitude of the sinusoidal waveform

$\omega = 2\pi f$ is the signal angular frequency, depending on the instantaneous frequency f.

ϕ is the angular starting point for the waveform or phase angle. It is arbitrary and depends upon the choice of the axis t=0

The resulting phasor is calculated as:

$$Y = \frac{\hat{y}}{\sqrt{2}} e^{j\phi} = \frac{\hat{y}}{\sqrt{2}} (\cos\phi + \mathrm{j}\sin\phi) \qquad (5.1a)$$

A phasor represents a single frequency sinusoid (pure wave) and is theoretically not directly applicable for transient purposes where the wave form is often corrupted with other signals of different frequencies. It is then necessary to extract a single frequency component of the signal and then represent it by a phasor. The Fourier transformation, most commonly the Discrete Fourier Transformation DFT [107] is often used for the extraction of the single frequency component of interest. An illustration of the estimation of phasors from sample data is shown in figure 5.5. The sampling clocks are usually kept at a constant frequency even though the input signal frequency may vary by a small amount around its nominal value [105].

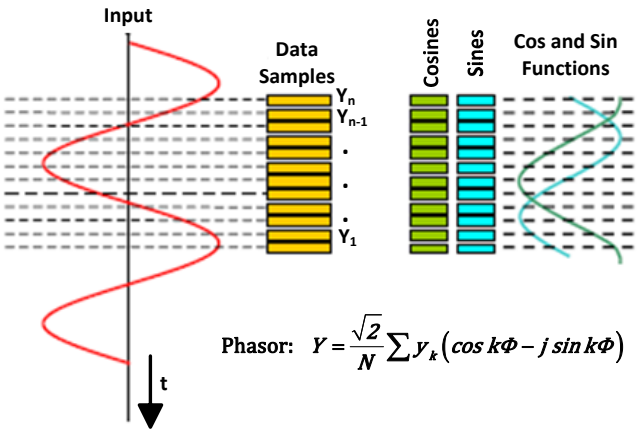

Figure 5.5: Illustration of the estimation of phasors from data samples using Discrete Fourier Transformation

In practical cases the phasor definition is made only under consideration of a portion of time span over which the signal is assumed constant and for which the phasor is represented. This time span can be called a data window or a finite window.

5.2.2 Phasors calculation and update

Outgoing from the previous paragraph, it is obvious that the idea of a phasor can be used in transient conditions by considering the decomposition of the waveform in its fundamental frequency components observed over a finite window. For real time purposes the phasors calculation must be a continuous process. It is then necessary to consider algorithms which will update the phasor estimate as newer data samples are acquired. Applicable processes for updating of phasors are presented in [106], [107]. These can be summarized as follows:

In case of an N samples y_k, obtained from the signal $y(t)$ over a period of the waveform:

$$Y = \frac{1}{\sqrt{2}}\frac{2}{N}\sum_{k=1}^{N}\left(y_k \cdot e^{-jk\frac{2\pi}{N}}\right) \tag{5.2}$$

or,

$$Y = \frac{1}{\sqrt{2}}\frac{2}{N}\left\{\sum_{k=1}^{N} y_k \cdot \cos\left(\frac{k2\pi}{N}\right) - j\sum_{k=1}^{N} y_k \cdot \sin\left(\frac{k2\pi}{N}\right)\right\} \tag{5.2a}$$

Using θ for the sampling angle $2\pi/N$, it follows

$$Y = \frac{1}{\sqrt{2}}\frac{2}{N}\{Y_c - jY_s\} \tag{5.2b}$$

Whereby

$$Y_c = \sum_{k=1}^{N} y_k \cdot \cos(k\theta)$$

And

$$Y_s = \sum_{k=1}^{N} y_k \cdot \sin(k\theta)$$

The data window begins at the instant when the first sample is obtained. The sample set is given by:

$$y_k = \hat{y} \cdot \cos(k\theta + \phi) \tag{5.2c}$$

Putting the equation (5.2c) in (5.2) leads to,

$$Y = \frac{1}{\sqrt{2}}\frac{2}{N}\sum_{k=1}^{N}\left(\hat{y} \cdot \cos(k\theta + \phi) \cdot e^{-jk\theta}\right) \tag{5.2d}$$

or,

$$Y = \frac{\hat{y}}{\sqrt{2}}e^{j\phi} \tag{5.2e}$$

which is the familiar equation of the phasor as given by the equation (5.1a).

The instant at which the first data sample is obtained defines the orientation of the phasor in the complex plane. The reference axis for the phasor is specified by the first sample in the data window.

The algorithm for the phasor computation is defined from the equation (5.2b). A recursive algorithm form is more advisable for real-time measurements. Such an algorithm continually actualizes the data stream including the actual sample, so that the older samples are not considered. For two adjacent sample sets: $y_k\{k = 1, 2, \dots, N\}$ and $y'_k\{k = 2, 3, \dots, N+1\}$ and their corresponding phasors:

$$Y^1 = \frac{1}{\sqrt{2}}\frac{2}{N}\sum_{k=1}^{N}\left(y_k \cdot e^{-jk\theta}\right) \tag{5.3}$$

$$Y^{2'} = \frac{1}{\sqrt{2}}\frac{2}{N}\sum_{k=1}^{N}\left(y_{k+1} \cdot e^{-jk\theta}\right) \tag{5.4}$$

The equation (5.4) can be transformed to develop a recursive phasor calculation.

$$Y^2 = Y^{2'} \cdot e^{-j\theta} = Y^1 + \frac{1}{\sqrt{2}}\frac{2}{N}(y_{N+1} - y_1) \cdot e^{-j\theta} \tag{5.5}$$

The angle of the phasor $Y^{2'}$ is greater the angle of the phasor Y^1 by the sampling angle θ. The phasor Y^2 has the same angle as the phasor Y^1.

When the input signal is a constant sinusoid, the phasor calculated from equation (5.5) is a constant complex number. The recursive transformation of a phasor Y corresponding to the data $y_k\{k = r, r+1, r+2, \dots, N+r-1\}$ into Y^{r+1} can be generalized as:

$$Y^{r+1} = Y^r \cdot e^{-j\theta} = Y^r + \frac{1}{\sqrt{2}}\frac{2}{N}(y_{N+r} - y_r) \cdot e^{-j\theta} \tag{5.6}$$

5.2.3 The phasor measurement unit

The concept of using phasors to describe power system operating quantities dates back to 1893 and a Charles Proteus Steinmetz's paper [149] on mathematical techniques for analyzing AC networks. More recently, Steinmetz's technique of phasor calculation has evolved into the calculation of real time phasor measurements [108]. As already been said in the previous chapter the measuring device used for this purpose is the Phasor Measurement Unit (PMU). At present there are about 24 commercial manufacturers[46] of PMUs worldwide. The PMUs manufactured by different manufacturers differs in many aspects so that it is difficult to discuss the PMU hardware configuration in an universally applicable way. A generic PMU architecture which captures the essence of its principal components is given in [107].

[46] Some of them are: ABB, Siemens, Schweitzer Engineering Laboratories, Inc. (SEL), Macrodyne, Inc., General Electric, Areva, and Beijing Sifang Automation Co. Ltd.

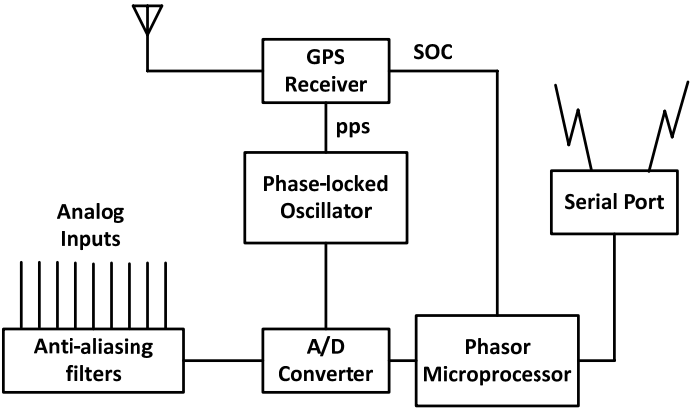

Figure 5.6: Functional block diagram of the elements in a PMU. The general structure, except the GPS receiver is similar to many power system relays and digital fault recorders

The analog inputs are currents and voltages obtained from the secondary windings of the currents and voltage transformers. Thereby, all three phase currents and voltages are used so that positive-sequence measurement can be carried out[47]. The current and voltage signals are converted so that they fit the requirements of the analog-to-digital converters (generally 16-bit converters). The application functions using PMU data are usually interested in signals with frequencies very close to the nominal power frequency. For this reason, the sampling rate of the sampling process dictates the frequency response of the anti-aliasing[48] filters.

[47] Positive sequence measurements provide the most direct access to the state of the power system at any given instant [107]

[48] The term aliasing refers to the distortion that occurs when a continuous time signal has frequencies larger than half of the sampling rate. The process of aliasing describes the phenomenon in which components of the signal at high frequencies are mistaken for components at lower frequencies [http://www.cage.curtin.edu.au/mechanical/info/vibrations/tut3.htm]

These are filters used before a signal sampler, to restrict the bandwidth of a signal to approximately satisfy the *Nyquist sampling theorem* stating that: "*to avoid aliasing occurring in the sampling of a signal the sampling rate should be greater than or equal to twice the highest frequency present in the signal*".
The GPS one pulse per signal (pps) is used in a phase locked loop to create the sampling clock pulses, which are then used for sampling the analog signals. Phasors of currents and voltage are computed by the microprocessor using recursive algorithms. The calculated phasors are combined to form positive sequence measurements, and are time-tagged with the timing information provided by the clock and the Second of Century (SOC) count provided by the GPS receiver.
In addition to positive sequences voltages and currents the PMUs can be also customized to measure local frequency, the rate of change of frequency, the harmonics, the negative and zero sequence quantities as well as individual voltages and currents.
A picture of the PMU used in the framework of this thesis is presented in figure 6.3.

The PMUs are found in the measurements layer of an overall data acquisition and utilisation system stated earlier in this work as Wide Area Monitoring System WAMS.

5.2.4 PMU based WAMS implementation

5.2.4.1 General concept

The PMUs are installed in power systems substations. The selection of substations (PMUs location) where they are placed is decided by the systems operators and usually depends upon the systems monitoring needs, or the use to be made of the measurements they provide. Many theoretical approaches were developed by researchers for the optimal placement of the PMUs. A study of these approaches is briefly done later in this work.

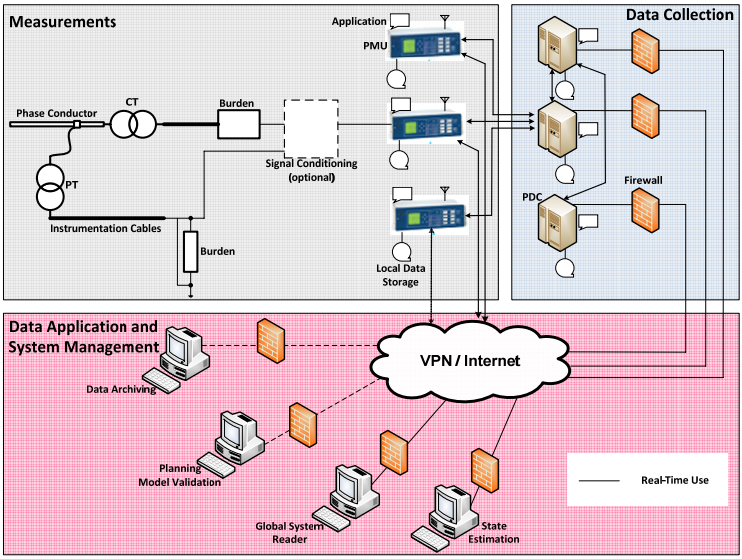

Figure 5.7: PMU based WAMS instrumentation setup

The measured phasor data is used at remote locations from the PMUs installations. The principal application idea of synchronized phasor data is the coeval utilization of data from several distributed PMUs. The simplest and most effective solution to analyze the data at the same time is to concentrate it at one place. This is done in the Phasor Data Concentrator (PDC) or simply Data Concentrator.

Thus, to make a full benefit of the synchronized phasors a complex architecture involving The PMUs, the PDCs and the communication links for the data transfer must exist. A possible layout of this architecture is shown in figure 5.7. This figure presents the basic components of the WAMS as it may appear in a present application.

The PMUs are located in power system substations and provide required measurements of all monitored buses and feeders. The measurements can be stored in local data storage devices, and be assessed in the system data management for post-mortem or diagnostic purposes (planning, model validation). The local storage is necessarily limited, and the stored data belonging to an interesting power system event can be flagged for permanent storage (data archiving) so that it is not overwritten when the local data storage capacity is exhausted. The phasor data is also available for real time steady stream as soon as the measurements are made. However, there may be some local application tasks which require PMU data. The use of a PDC can be dispensable in such cases and the PMU may be made locally directly available for such tasks.
The typical function of the PDCs in the data collection layer in figure 5.7 is to gather data from several PMUs, reject bad data, align the timestamps and create a coherent record of simultaneously recorded data from a wider part of the power system. There are local storage facilities in the PDCs as well as applications functions which need the PMU data available at the PDC [107]. An hierarchical level of the PDCs in figure 5.7 can be viewed as being regional in their data-gathering capability. On a system-wide scale, another level of PDCs with enhanced gathering capability must be eventually contemplated. This is named a Super Data Concentrator in [107] with the same function as the other PDCs.

Some of the communication links are shown in figure 5.7 to be bi-directional. Indeed most of the data flow is from the PMU to the PDC or to system management, or in one direction between the PDCs. But in some cases there are some tasks which require communication capability in the reverse direction e.g.: equipment configuration.

5.2.4.2 Standards

There are two IEEE standards which are relevant to the applications of synchronized phasor measurements. The first one is a general transient data recording file format standard called COMTRADE. This standard is described in IEEE standard C37.111 [109]. COMTRADE is developed by the Power System Relaying Committee. It is intended for use by digital computer based devices which generate or collect transient data from electric power systems. The standard should facilitate the exchange of the transient data for the purpose of simulation, testing, validation or archival storage. In this standard, a common format for data files and exchange medium used for the interchange of various types of fault, test, or simulation data for electrical power systems is defined. Sources of transient data are described, and the case of diskettes as an exchange medium is recommended. Issues of sampling rates, filters, and sample rate conversions for transient data being exchanged are discussed. Files for data exchange are specified. COMTRADE can be used to transfer locally recorded values from a PMU over to the central data storage. The second is the standard applicable to the PMU technology voted as IEEE C37.118: Standard for Synchrophasors for Power Systems or simply: SYNCHROPHASOR [110].

The SYNCHROPHASOR standard was motivated by the wish of PMU users to have interoperability of PMUs made by different manufacturers. This standard is based upon the COMTRADE standard, and was also formulated by experts in the Power System Relaying Committee of IEEE Power Engineering Society [106]. This standard defines synchronized phasor measurements used in power system applications. It addresses the definition of a synchronized phasor, time synchronization, application of timestamps, method to verify measurement compliance with the standard, and message formats for communication with a PMU. In this context, a PMU can be a stand-alone physical unit or a functional unit within other physical units. This standard does not specify limits to measurement response time, accuracy under transient conditions, hardware, software, or a method for computing phasors.

It should be noted that a PMUs may be communicating to the PDC or directly with the VPN/Internet infrastructure via a standard protocol. But, there is also the possibility that a PMU may communicate with a PDC particularly via a proprietary protocol. This last approach is not recommended.

5.2.5 Some limiting factors to the real-time application of synchronized phasor data

5.2.5.1 Communication delays

5.2.5.1.1 Communication options

Communication facilities are essential for applications requiring phasor data at the remote system's control centre. Communication links used by PMU based WAMS include both wired and wireless options.

The *wired communications options* include the following:

- ***Telephone lines***: Leased telephone circuits is still the first communication medium of utilities communications. These offer date rates of up about 56 kbps (analogue) Due to the need of isolation circuits in substations this speed drops around 9,6 kbps. The main advantage of the use of telephone lines is that they are easy to set up and they are economical.
- ***Microwave links***: Point to point microwave links are also being used by utilities to a great extent. Microwave links provide a better option as compared to leased telephone lines, since they are easy to set up and are highly reliable. Digital microwave links are set to replace analogue links in the near future. Digital microwave links fall into two categories: frequency bands less than 10 GHz and frequency bands greater than 10 GHz. Microwaves links continue to be used in many current applications. The main disadvantages of using microwave links are signal fading and multipath propagation.

To serve the needs of the utilities, high-speed data rate capability and noise immunity of digital microwave links can be preferred over analogue microwave links [111].

- ***Power line Carrier***. This technique can be considered for use in WAMS offering data rates in the range of 4 Mbps via the electricity supply grid. Power line technology uses the medium and low voltage electric supply grid for transmission of data and voice. It can be used for both WAMS communication requirements and substation networking [112].
- ***Fibre-optic cables***: These are the communication media of choice nowadays. These media offer an increased channel capacity ranging from 50 million to 1 billion bits per second. A part of this bandwidth can be utilized for usage in WAMS. Aside the high data transfer rates another advantage of using fibre-optics is its immunity to electromagnetic and atmospheric interference. The high initial investment can be seen as a disadvantage for using them.

The principal *wireless communication option* includes the satellite technology. The reference [113] presents and investigates the Low-earth orbiting satellites (LEO; typically 500 – 1500 km above the Earth's surface) as a possible way for the communication of power systems measurements. The use of this technology is principally linked with high costs and narrow bandwidth.

Aside the measure of the data rate (channel capacity) the other significant aspect of data transfer in any communication task is the communication latency. Which is defined as: the time lag between the time at which the data is created and when it is available for the desired application [106]. Although the data volume create by the PMUs is important, it remains quite modest so that channel capacity is rarely the limiting factor in most applications. Most important is the communication delay or latency. Considering the PMUs data as the input for monitoring application this aspect is for crucial importance particularly for real-time applications.

This time can be added to the computation time of algorithm used for the assessment of the system state to find the computational burden of a method of analysis. The estimation of the communication delay is an important aspect of WAMS, since large amount of communication delays lead to slower assessment of the system's stability state.

5.2.5.1.2 Communication delay: causes and calculation

Delays due the use of PMUs and a given communication link are primarily due to the following reasons [114]

- **Transformers delays** coming from the potential transformer (PT) and the current transformer (CT).
- **Finite Window Size of the DFT**: This is the number of samples required to compute the phasors using DFT.
- **Processing time** required in converting data for PT and CT into phasors.
- **Multiplexing and transitions**: Transitions between the communication link and the data processing equipment leads to delays that are caused at the instances when data is retrieved or emitted by the communication link.
- **Communication Link used**: The type of communication link and the physical distance involved in transmitting the PMU output to the central processing unit can add to the delay.
- **PDCs** also have a maximum wait-time (typically of 1-4 seconds), to allow for all the PMU data to come in before aggregated data is outputted by the PDC. If the data from all the PMUs reach the PDC within this wait-time, it outputs the aggregated data right away. However, in the extreme case that the data from one of the PMUs is indefinitely delayed, the PDC will then wait up to its pre-defined wait-time (i.e., 1-4 seconds) before it outputs the data. Hence, the PDC can also introduce an additional delay equal to its wait-time if one of the PMU channels stops transmitting data to the PDC.

In such circumstances, if there are additional PDCs downstream in the point-to-point phasor network architecture (such as the Super PDC), then they too will introduce a secondary delay equal to their wait-time [115].

The communication delay can be generally expressed as [114]:

$$\tau = \tau_f + \tau_p + \frac{L}{R} + \theta \tag{5.7}$$

Where τ is the total link delay, τ_f is the fixed delay associated with the transformers, DFT processing, data concentration and multiplexing, τ_p is the link propagation delay, L is the amount of data transmitted, R is the data rate of the link, and θ is the associated random delay jitter.
For a typical PMU with 10-12 phasors, a fixed delay associated with processing, concentrating, multiplexing, and transformers independently of the communication, is estimated to 75 ms [115]. The delay calculation associated to various communication links is summarized by the following table 5.1.

Table 5.1: Delay calculations associated with various communication links [114], [115]

Communication link	Associated delay-one way (milliseconds)
Fibre-optic cables	≈ 100-150
Digital microwave links	≈100-150
Power line	≈150-350
Telephone lines	≈200-300
Satellite	≈500-700

The propagation delay is dependent on the medium and thus is a function of both the medium and the physical distance separating the individual components of WAMS. It assumed that media like fibre-optics, power lines, and telephone lines, on an average, have a propagation delay of around 125 ms. In the case of LEO satellites, the propagation delay could be as high as 200 ms, because of the distance involved and gateways that connect terrestrial networks to the satellite. Additional delay is caused by the amount of data that has to be transported across the medium.
A practical way to determine the communication delay is the use of the ping command[49].

5.2.5.2 Unavailability and asynchronism of PMU data

The monitoring process can be badly affected due to failure or malfunction of one of the constituents of the WAMS. Such issues may lead to the non calculation of phasors at the concerned PMU locations or to the absence of some PMU data sets. The synchronization of the measurements follows the purpose of the consideration of data sets with the same timestamp for further analysis and application. A divergence in the timestamps of two separated PMUs to be considered together during the stability analysis can be termed as the asynchronism of the PMU data. This will certainly lead to false results. Such deficiencies in the PMU data must be detected and trapped by the algorithms used for their analysis.

[49] By connectivity problems the ping command can be used to check the destination IP address you want to reach and record the results. The ping command displays whether the destination responded and how long it took to receive a reply. If there is an error in the delivery to the destination, the ping command displays an error message [http://technet.microsoft.com/en-us/library/cc737478.aspx].This method can be useful also for connectivity testing.

5.2.6 Minimal PMUs placement

In practice, the usual first step in placing the PMUs is the identification of candidate locations. In an actual power system, there may be certain buses that are strategically important, such as a bus connected to a heavily loaded or economically important area, or a bus anticipated to be a future expansion point. In such a case, PMUs may be placed at the preferred buses. The rest of the system can be monitored by placing some additional PMUs at the other buses. This strategy of solving the question of the PMUs placement (the first step particularly) relies on the engineer's experience and knowledge of the power system.

On the other hand, one of the most important application routines of real time modelling of power system in general is state estimation (SE). SE processes a set of measurements to estimate the state of a power system. Thereby the required analogue data and circuit breakers statuses are provided by SCADA Systems. Switching device statuses are used by topology processor to determine network connectivity. Therefore SE uses analogue measurements, network topology data, network parameters, some pseudomeasurements to produce a best estimation of state variables: voltage magnitudes and phase angles. In the conventional SE, measurement set contains voltage magnitudes, active and reactive power flows, active and reactive power injections. The cases, in which current magnitudes belong to this set, are also considered. Utilization of Phasor Measurement Units (PMU) outputs as inputs for SE would expand the measurement set for SE with voltage and current phase angles.

It is assumed that a set of PMUs primarily placed in a given power system to enhance the SE process can be also used for a variety of other applications. The condition of SE solvability is the considered power system to be observable. The observability of a power system depends on the number of measurement data. Location of measuring devices in a power network is also essential.

The difficulty by the PMUs placement is to define the optimal locations for the complete observability of an entire power system or a region of it. Moreover, it can be concluded from the previous paragraphs that a PMUs network must be supported by important communication infrastructure of sufficient speed to match the required fast streaming of phasor measurements. It is also obvious that power systems are not totally equipped with matching communication. As such, any potential move to deploy PMUs must recognize this limitation. It is a possibility that the benefits brought forth by PMUs could justify the installation of their matching communication infrastructure. However, it must be recognized that deployment of PMUs in every substation is a major economic undertaking[50].

For this reason many alternative and theoretical placement techniques developed in the main PMU research stream consider partial PMU placement. The objective is thereby to monitor a complete power system with the minimal number of measuring devices. An important consideration by the development of these techniques of PMUs placement is the alignment of given power system's nodes to a certain number PMUs according to defined installation constraints and data application purposes. Most of the techniques are usually designed for SE purposes, but as stated earlier the PMUs set configuration thus obtained is usable for other applications (e.g.: Voltage stability monitoring) if it delivers all the measurements needed from the power system region to be monitored.

The PMUs placement techniques are usually used once and offline and can be well utilized as a possible theoretical reference by the final decision making of the PMUs locations in practice.

[50] Reference is taken from the prices per measuring devices (relay with phasor measurement capability) actually proposed by Schweitzer Engineering Laboratories, Inc on its website varying from 1300 € (SEL-734) to almost 10000 € (fully optioned SEL-(421).

The minimal PMU placement is often termed as the Optimal PMUs Placement (OPP) [116] [117]. The reference [117] gives a mathematical expression of the OPP problem. The OPP deals with the question: What should be the minimum number of PMUs to be placed in the network, so that it is possible to extract all needed data for a given application? Seen in this context OPP is a combinatorial problem i.e.: from a total set of K system's substations (or buses), N must be equipped with PMUs. N can be any number between 1 and K, which means that the number of combinations is given by:

$$Number\ of\ combinations = \sum_{i=1}^{K} \binom{K}{i} = \sum_{i=1}^{K} \left(\frac{K!}{(K-i)! \cdot i!} \right) \quad (5.8)$$

This is a large number even for small systems. The IEEE test system[51] in figure 5.8 with 14 buses has approximately 16000 possible combinations.

[51] System data in appendix C

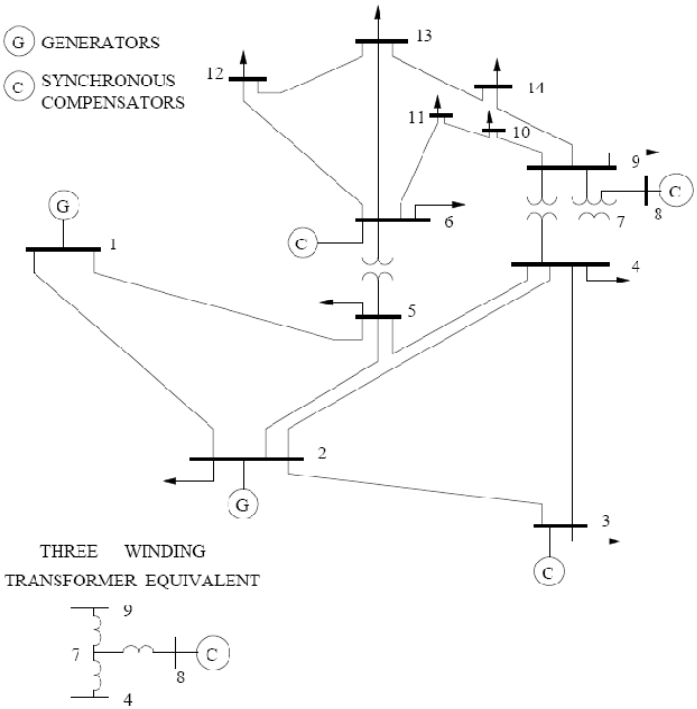

Figure 5.8: Single line representation of the IEEE 14-bus Test System [118]

Many real systems have over a hundred buses, which makes it impossible to try all combinations for the best solution, so the minimal solution must be found in a different way.

One type of solution methods used to solve this kind of problems is iterative search algorithms. Examples of such methods are: Tabu Search, Simulated Annealing and Genetic Algorithms. Common for all of them is that none can guarantee to find the global minimum, but they usually find a solution close to the minimum [117]. The OPP calculation is always subjected to a number of constraints. The most popular constraint is the system *full topological observability.*

Which means that the needed data from the network can be either directly measured or it can be indirectly calculated. Another usual constraint is the *redundancy*; this means that the system is able to handle a specified number of malfunctioning PMUs without violating any of the other constraints. This option is not considered in this work. Finally, the o*bservability of topology* constraint is something different from topological observability despite the similar names. Briefly it means that it is possible to detect the topology status of the network. This topology can be changed if for example the power lines become disconnected due to contingencies. This last constraint is also not used in this thesis but can be useful if the measured data should be used for topology detection purpose.

5.2.6.1 System state definition

The state of a system is usually expressed, in the control theory, as the minimum information needed to fully observe the system. A system is observed when it is possible to extract any information anywhere in time from it, so the state must both express the static and dynamic behaviour of the system. For the stability study of power systems the meaning of the word is different. The state is understood, as the minimum information needed to calculate all static variables. The information about the dynamical evolution of the system is neglected. The state variables are defined from the mathematical set of equations describing the system.

The sets of equation describing the relationship between the system's voltages and currents can be obtained using the π-equivalent representation of each system's transmission lines connecting the whole network together and the first Kirchhoff's law.

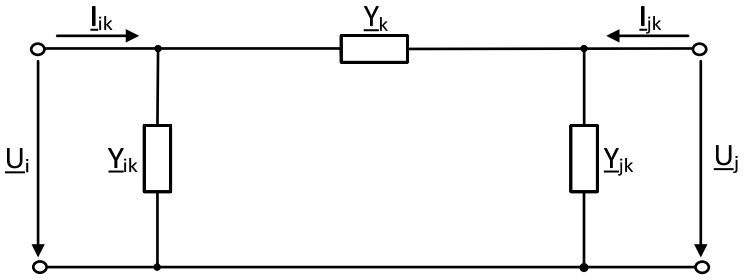

Figure 5.9: π-equivalent circuit of a transmission line

The figure 5.9 describes a transmission line k between the buses i and j. The variable Y represents the admittance and appears thrice in the circuit equivalent in Figure 5.9.$\underline{Y}_{ik}$ and $\underline{Y}_{jk}$ arise from the capacitor properties of an overhead line. $\underline{Y}_k$ is the admittance of the line itself.

Two equations are set-up from the π-equivalent for each line. Thereby the currents $\underline{I}_{ik}$and $\underline{I}_{jk}$ are not identical

$$\begin{cases} \underline{I}_{ik} = \left(\underline{Y}_k + \underline{Y}_{ik}\right) \cdot U_i - \underline{Y}_k \cdot U_j \\ \underline{I}_{jk} = -\underline{Y}_k \cdot U_i + \left(\underline{Y}_k + \underline{Y}_{jk}\right) \cdot U_j \end{cases} \tag{5.9}$$

Assuming the admittance as known, (5.9) comprises two equations with four unknowns. The currents flowing through the transformers can be formulated in the similar way but with other constants than the admittances. The current-flows from the buses are dependent on the voltages. This gives two equations for each line or transformer in the network.

Additional equations are formed using the special properties of zero injection buses. All the buses from this type have no external current flows so that the sum of all currents flowing into these buses must equal zero.

The first Kirchhoff's law is then applied at each system's node:

$$\sum_{k} \underline{I}_k = 0 \tag{5.10}$$

With $k = 1,2,3 \ldots$ the number of the node connections.
Using for example the topology of the following IEEE 14-bus test system in figure 5.8, with one zero injection bus at bus 7, a total of 41 equations and 54 variables are obtained from the equations (5.9) and (5.10).

The 54 unknown variables are composed by: 40 unknown currents resulting from the 40 equations of the 20 lines available (2 unknown currents per line), and 14 unknown voltages by 14 nodes.
An equation system needs at least as many equations as unknown variables for a unique solution to exist, so the system can be made observable by measuring some of the unknown variables. Taking this statement in account, the minimum number of needed measurement points is 54 – 41 = 13 measurements points.

This number of measurements points can differ by the practical calculation of the OPP, since the measurements cannot be chosen arbitrarily in the network but should be chosen at as few buses or substations as possible.

In the next subparagraphs some methods of OPP calculation are studied.

5.2.6.2 Jansson's method

The Jansson's method of OPP calculation is described in [117]. The OPP constraint is the full topological observability. The steps needed in this method to find the minimum number of measurement points are the following:

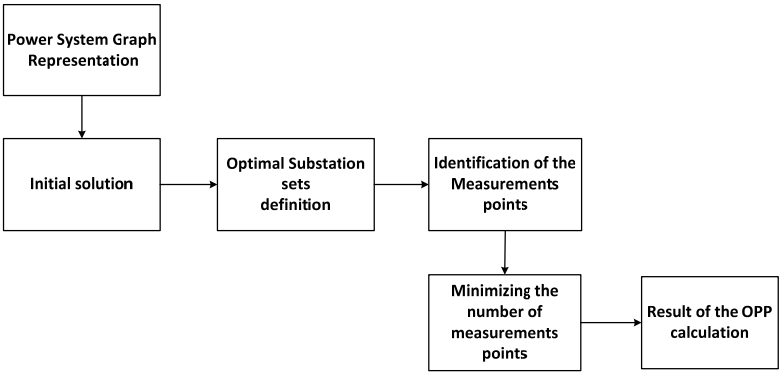

Figure 5.10: Schematic illustration of the Jansson's OPP calculation method

The Jansson's method is an algorithmic solution to the OPP problem. It is subdivided in six principal steps. These steps partly contains some auxiliary steps, however these are not necessary for the general understanding of the method.

Graph representation

There is no difference in how some of the components are treated in the observability analysis. Both lines and transformers can be handled as one type of connection, since both items give rise to the same type of equations. Generator, load or shunt information is no longer necessary when all the zero injection buses in the network have been identified. For this reason by solving the OPP problem a graph representation is preferred to the usual single line diagram [117]. A graph representation of the 14-bus system is exemplarily shown in the next figure 5.11.

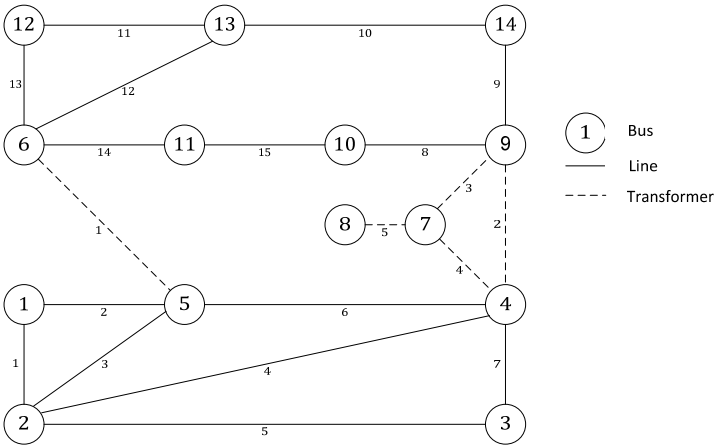

Figure 5.11: Graph representation of the IEEE 14-bus test system

The graph in figure 5.11 contains the system's nodes and edges. Each bus is represented by a node and each line or transformer is represented by an edge.

At this first step of the OPP calculation the graph representation of the system is converted into the Power System Application Data Dictionary (PSADD) format[52] for further consideration. This data format contains all the relevant information about the system elements and topology. It eases a rendition of the system in a calculation environment (e.g.: Matlab®).

[52] Description given in [120]

In PSADD Format the 14 bus test system is defined as:

Table 5.2: IEEE 14 Bus-test system in PSADD Format

Bus		Line			Load		Xformer				Machine			Shunt	
Nr	*Name*	Nr	*FromBus*	*ToBus*	Nr	*BusRef*	Nr	*PrimBus*	*SecBus*	*Type*	Nr	*BusRef*	*Type*	Nr	*BusRef*
1	Bus_01	1	1	2	1	2	1	4	7	FIXED	1	1	Gen	1	
2	Bus_02	2	1	5	2	5	2	4	9	FIXED	2	2	Gen	2	
3	Bus_03	3	2	5	3	12	3	7	9	FIXED	3	3	Mot	3	
4	Bus_04	4	2	4	4	13	4	7	8	FIXED	4	6	Mot	4	
5	Bus_05	5	2	3	5	11	5	5	6	FIXED	5	8	Mot	5	
6	Bus_06	6	4	5	6	14	6				6			6	
7	Bus_07	7	3	4	7	10	7				7			7	
8	Bus_08	8	9	10	8	9	8				8			8	
9	Bus_09	9	9	14	9	4	9				9			9	
10	Bus_10	10	13	14	10	3	10				10			10	
11	Bus_11	11	12	13	11	6	11				11			11	
12	Bus_12	12	6	13	12		12				12			12	
13	Bus_13	13	6	12	13		13				13			13	
14	Bus_14	14	6	11	14		14				14			14	
15		15	10	11	15		15				15			15	

The table 5.2 is principally easy understood. However a precision is needed to be made for the transformers (Xformer). The denomination “FIXED” stands for transformer without a tap changing function.

Initial solution

A good initial solution is “close” to the global minimum in some sense, which makes the search trajectory much shorter. But the algorithm cannot be too complicated, since it will take too much time finding the solution. A trade-off has to be done between time and quality. The algorithm used by Jansson to find an initial solution is the same as in [116]. It is a graph theoretic procedure. A reasonable starting point (initial solution) can be provided by a graph theoretic search which identifies a placement set that makes the system observable [116]. Such a search comprises the following steps:

1. Place a PMU on the node with the highest number of incident edges in the unobservable region. In the first cycle, the unobservable region is the entire power system or the chosen entire region of the power system. The unobservable region is scaled down as the PMUs locations are defined.
2. Determine the observability of the total system topology (according to the PMUs locations found)
3. Repeat from 1 if not full observability.

The second step is very important for this method and will be explained here under with some more details.

Observability calculation

It has previously been described how the single line diagram can be converted to a graph over the substations. Let us introduced the following simple structure of three in series connected buses:

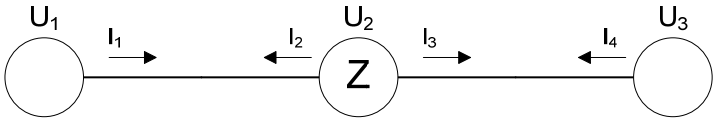

Figure 5.12: graph representation of three in series connected buses, where the middle bus is zero injection.

Each variable in figure 5.12 corresponds to a measuring point (7 measuring points are totalized in figure 5.12: 3 voltages and 4 currents) with each an identification number. Using these identification number and with the help of the equations (5.9) and (5.10) a set of systems equations can be formulated. The result is shown in (5.11), where the first four rows are derived from (5.9) and the fifth row from (5.10).

$$\begin{bmatrix} 1 & 1 & 0 & 1 & 0 & 0 & 0 \\ 1 & 1 & 0 & 0 & 1 & 0 & 0 \\ 0 & 1 & 1 & 0 & 0 & 1 & 0 \\ 0 & 1 & 1 & 0 & 0 & 0 & 1 \\ 0 & 0 & 0 & 0 & 1 & 1 & 0 \end{bmatrix} \cdot \begin{bmatrix} U_1 \\ U_2 \\ U_3 \\ I_1 \\ I_2 \\ I_3 \\ I_4 \end{bmatrix} = \begin{bmatrix} 0 \\ 0 \\ 0 \\ 0 \\ 0 \end{bmatrix} \tag{5.11}$$

The following algorithm detects the dependencies between the system variables:

1. Identify all measurement variables being directly measured by a PMU.
2. Replace all values with zeroes in columns corresponding to variables found in step 1.
3. Find all equations with only one unknown variable, and mark these variables as known (i.e. zero out the columns).
4. Repeat from 3 until no more variables are found in step 3.
5. The system is observable if only zeros are left in equation (5.11).

A variable is considered known when its column in the matrix is replaced with zeroes. The equations are formulated dimensionless, because only the information “known” or “unknown” is relevant.

Finding the optimal substation sets

After the initial solution is found, an optimal solution is determined. As said before this process can be mathematically very intensive for large systems, such that iterative calculation methods must be used. The method used by Jansson is the Tabu Search.

Tabu search

Tabu Search is a flexible method which can be used to solve difficult optimization problems. It was originally presented by Fred Glover in 1986 and is presented in a more actual form in [121] where more details can be taken on this method. Tabu search has been used when solving combinatorial problems like scheduling and routing problems but it is also possible to minimize continuous-valued functions if some sort of discrete coding is used. It is a search method that from a given start point tries to reach the global minimum of a function and it has proven successful in doing so when solving a broad range of problems [117, 120].

The background idea behind Tabu Search is to enhance the efficiency of the search by considering not only the actual neighbourhood of a solution but also the previous trajectory of the search. The search is done through the search space without returning to points already visited. A memory is used to keep track of which points that have been visited during the last steps and any move to these points is declared taboo and thus is forbidden. The simplest form of a Tabu list (also named Tabu memory) memorizes the past solutions and bans them for the next search steps. By this way the solution search procedure will not go in circles or eternally wind up in local optima since those points eventually will end up in the Tabu list. The procedure is iterative and each point is chosen as the best possible point currently not in the Tabu memory, in the neighbourhood of a previous point.
The characteristics of Tabu search that distinguish it from other methods can be summarized as follows:

- It is a deterministic method. The method will always generate the same results if it is restarted with the same parameters. One advantage is that parameters can be tuned to the problem more easily compared to the case where the method uses random properties.
- The search is done on a local level. The next solution is always chosen in a neighbourhood of a previous solution, which forces the search to follow a path instead of jumping around. A disadvantage with this method is that the search can get stuck in unfruitful areas for a long time. Restarting the algorithm at another point usually solves that problem, but then an indicator is needed which tells when it's time for the restart.
- Tabu Search uses a memory as previously mentioned. It helps the method to avoid bad areas it has previously visited. The memory can also give indications of where good solutions might be found (by identifying common features of good solutions).

More definitions have to be made before Tabu Search works properly; the notion of a neighbourhood is one example. A large neighbourhood makes each iteration take long time to complete, but the quality of the iterations might be higher. A smaller neighbourhood might "miss" good search directions, so also here some sort of balance is needed. A stopping condition must also be defined in order to stop the algorithm. The goal is to find out whether the minimal solution has been found or not, when a feasible solution is spotted. Jansson [117] advises therefore the use of a counter to terminate the Tabu search algorithm. The counter counts up as long as infeasible solutions are found, and is cancelled when a new feasible solution is found. The algorithm is cancelled when the counter reaches a threshold value. This method gives also a good indication of when the optimal solution is reached. The algorithm continues until there are few undiscovered feasible solutions left in the current search area and then quits. The drawback of using this method is that it is impossible to estimate the execution time, since the counter is cancelled during the execution.

An algorithm for Tabu Search can now be formulated as:

1. Find an initial solution.
2. Find a neighbourhood.
3. Make the best possible move into the neighbourhood that is not restricted by the Tabu list. (In the In the OPP problem a move can be defined as: *Add PMU* or *Remove PMU*)
4. Update Tabu list.
5. If the new point is a good solution, add to solution list.
6. Check if stopping criterion is fulfilled. If not, repeat from 2.

Minimization of the measuring points

The Optimization is not achieved with the use of the Tabu Search. The previous step considered only the system observability and defined all the system's lines connected to the buses as observed. It can now happen that a line is doubly observed e.g.: if two adjacent buses are equipped each with a PMU. The question at this step is how to reduce the measurement points when solving equation (5.11). The solution is to minimize the number of PMUs used and to disconnect or adjust some measuring points.

Thereby some points are more advantageous as the others. Two steps are needed to do this, first the available measurement points must be identified, and secondly some of those will be removed or adjusted. Two important concepts are measurement points and measurement channels. A measurement point is a point in the network, which is being actively measured by a PMU. A measurement channel is defined, as a number of input channels on a PMU needed to measure a measurement point. It means that a PMU with four measurement channels will theoretically have twenty-five physical input channels[53].
The next Figure 5.13 clarifies the process of minimization of the measuring points.

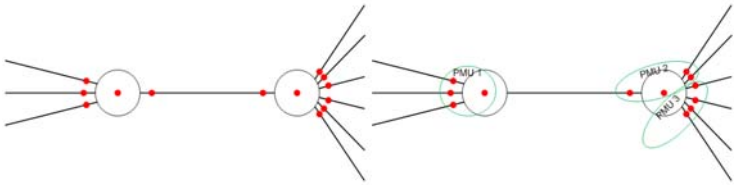

Figure 5.13: Illustration of the minimization of the measuring points

The red points symbolized the measurements points at each system's node. On the left picture in figure 5.13 it can be seen that the bus to the left has 5 measurement points. Theoretically two PMUs (each with 4 measurement channels) are needed to observe this bus. Similarly two PMUs are needed for the measurements at the eight measurements points on the right bus. One measurement point can be removed from the line between them without doing the system unobservable. The total number of PMUs will decrease to three if one measurement point is removed from the left bus, compared to if it is removed from the right bus.
Measurement points are removed according to how many measurement points each substation has and how many channels the PMUs have.

[53] (24+1): 24 inputs for the phase voltage and currents +1 for the power frequency, For the PMU placement only the voltage and current inputs are relevant.

The algorithm is as follows:

1. Calculate n_m for all substations, where n_m = number of measurement points in the substation.
2. Calculate $n_{odd} = (n_m - 1) mod\ c$[54] for all substations, where *c* is the number of measurement channels on each PMU. n_{odd} shows how many measurement points that must be removed in order to reduce the number of PMUs with one.
3. Examine the substations and see if any measurement points can be removed, start with the one with lowest value of n_{odd}.

Result of the OPP calculation

The result of the OPP calculation according to Jansson has the following format:

Table 5.3: Output Format of the OPP Calculation according to Jansson

Number	DeviceRef	Location	PMU Number	Type	AssignDevice

[54] Given two numbers, a (the dividend) and n (the divisor), a modulo n (abbreviated as a mod n) is the remainder, on division of a by n [60].

An explanation of the table contents is the following:

Number:	Consecutive numbering
DeviceRef: PSADD file)	Monitoring object (numeration as in the
Location: monitored	Substation from where the object is
PMU Number: measurement point	Affiliation of a specified PMU to a
Type:	Variable measured VM: Voltage Magnitude VA: Voltage Angle AM: Current Magnitude AA: Current Angle
AssignDevice:	Type of Monitoring Object BS: Bus LN: Line TR: Transformer

5.2.6.3 Altman's method

Another OPP method is presented in [122]. Thereby the goal of the OPP is the system full observability. The full observability refers to a system where all the buses are either directly observed or calculated. A directly observable bus is one where a PMU is located and the voltage magnitude and angle are measured. A calculated bus is observable by other PMUs, but does not have any PMU installed. The observability rules used by Altman are accurately described by the following assumptions (It should be referred to [122] for more details):

1. All buses neighbouring a bus with a PMU are observable themselves
2. If a bus without injection is unobserved and all but one of its connecting buses is observed, then the unobserved bus becomes observed.
3. If all the buses neighbouring a bus without injection are observable, then that bus is also observable.

The strategy of the OPP method from Altman addresses three important topics: system preparation, placement algorithm, and installation scheduling.

System preparation

At this step the single line model of the power system is transformed in a so call placement model. According to [122] the single line models often contain buses and branches that can be neglected or reduced for the OPP calculation. For example, multiple transformers in a substation would represent many buses and branches in the single line model. However, a substation should be considered as a single bus when considering overall system observability, rather than placing PMUs on neighbouring transformers. Outgoing form such principles the author developed some reduction rules to obtain a placement model for which the computation intensity is also diminished.

Typical examples for the system model reduction as presented by Altman are the following:

Transformers Reduction:

As stated above, each side of a transformer could be considered as a separate bus. However, the impedance and distance separating the primary and secondary side are very small. If one knows the variables values at one side of a transformer, then the values the other side can be calculated via the turns ratio and impedance. Since transformers can be treated as a single bus, one of the busses should be deleted. Generally, high voltage systems transfer more energy and are more important. Therefore, the transformer low voltage bus is deleted and the branches connected to him are directly attached to the high voltage bus. According to this principle a three-winding transformer will be represented as a single bus (the one with the highest voltage) connected to all the branches or injection connected to any of the three transformer's sides.

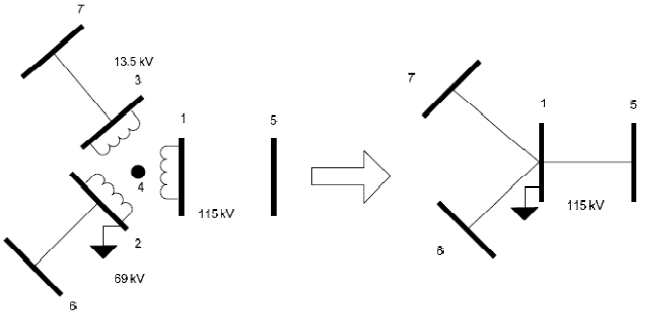

Figure 5.14: Illustration of a three-phase transformer reduction [122]

Generators and Loads:

Multiple generators and loads connected to one bus are all summed up as one injection at the bus. Even a substation with multiple generators eventually placed at different voltage levels (each with its own generation unit connected to an internal bus), should be considered as single bus with a unique injection. There the Low Voltage Side (LVS) is reduced and the injection is connected to the High Voltage Side (HVS) of the substation.

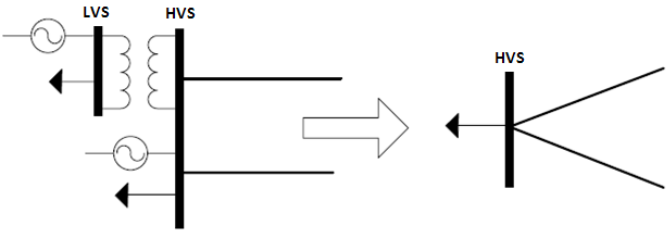

Figure 5.15: Illustration of a substation reduction

Direct Current (DC) lines:

Altman based the reduction principle here on the fact that there is no need to measure the direct current or constant voltage at the terminals of a DC transmission line. Only the buses that act as the interface of DC terminals to the rest of the Alternating Current (AC) system are just as important as any other AC bus for the definition of the system observability. Thus the AC terminal at each end of the DC line should be considered. The DC line itself is not considered and the energy travelling through the line is characterized by an injection on both buses.

Figure 5.16: Illustration of a DC line reduction [122]

Immeasurable buses

The reference [122] also describes certain situations were a bus does have a potential impact on the system monitoring capabilities, but a PMU cannot be placed there due to the some physical or instrument restrictions. For example, there may be a transmission line that is tapped without a substation. If this is the case, the transmission line is removed from the branch list and an injection is added to each bus at the ends of the line as shown on figure 5.14.

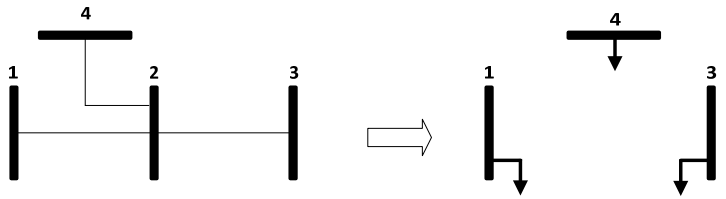

Figure 5.17: Reduction of tapped bus

Further reduction methodologies presented in [122] concern among others: the switched shunts, series capacitors, and isolated buses (zero injection). The cases treated always result from the topological aspects of the power system considered.

It should be mentioned that the reduction process is started from an initial case with the system represented in the IEEE common data format. This format was developed in the 1960's and 70's to create a standard input format for system information on tapes when running power flow programs. The complete format description can be found in [123]. The initial system data described in this format serves as input to the reduction process. This process is coded following the reduction rules presented above to obtain a simplified placement model of the system.

Developing the placement model from the IEEE common format can have some significant limitations. For example, as presented in [123], the IEEE format does not have an explicit way to list DC line data. DC line information should be treated separately from the IEEE model. This data has to be inserted into the placement model directly. Furthermore only buses' net generation and load MW and MVAR are listed.

Generating units or loads that are turned off are overlooked. This could lead to an incomplete injection list and potentially buses being erroneously deleted from the placement model. Either data about “off” machines and loads must be provided to the model developer separately, or the data file has to be taken from the system when all generators and loads are either producing or absorbing real or reactive power. Because of these limitations, the IEEE common data format may not be the best source of system data.

Placement algorithm

After the system simplification, an OPP algorithm is applied in the next step to the placement model obtained. Compared to the used of the Tabu Search in the Jansson’s method the optimization algorithm used by Altman is the so called: *Randomized Greedy algorithm*.

As described in [124] Greedy algorithms (just like Tabu Search) are iterative methods used to find the optimal solution of an optimization problem. Since they make decisions based on what looks like the best choice at the moment, they are not as far-sighted as dynamic programming and other more sophisticated optimization algorithms. Greedy algorithms do not always yield optimal solutions, but for many problems they do.

Summarized from [122] and [124] the general principle of a greedy algorithm is briefly described below.

Given a set of S elements, a greedy algorithm will choose one element at a time based on a greedy choice property until an end criterion is met. The elements in S could be locations, scheduled activities, paths, or items. Each element can be chosen only once and is given a value for its greedy choice property; the so called “greedy value”. At each stage, the element with the greatest greedy value will be chosen and removed from the set of candidate elements. After each stage, the remaining element values will be updated.

This process continues choosing a candidate element one at a time until the end criterion is met. Because of the non-uniform structure of electric transmission systems, most of the proposed placement algorithms are based on incrementally increasing the placement set, rather than pattern recognition. For this reason, Altman termed the Greedy method as very applicable for the PMU placement problem. The goal is to incrementally add a single PMU until the set achieves full observability (end criterion). Every bus is given a value for the greedy choice property. At each stage, the decision where to place a PMU is based on which bus has the greatest value. In the Altman's method application, the greedy choice property is a measure of how many buses can be observed with the placement of a single PMU. Thus, the most apparent greedy choice property would be the number of unobserved buses $H_i$each bus is connected to, (including itself). Simply said, at each stage, the next PMU should be placed on the bus with the most linked unobservable buses. After each placement, the observed status and greedy value of each bus should be recalculated.
A weight function can be assigned to each bus and be a component of the greedy choice property as shown in the next equation:

$$G_{i=}w_i \cdot H_i \tag{5.12}$$

The steps the Greedy Placement Algorithms as applied to a power system graph topology are therefore summarized into:

1 Create the n by n incidence matrix A from the information in the bus and branch vectors. This and the list of buses with injection fully represent the system in the placement model.

$$A_{k,m} = \begin{cases} 1\ if & k = m \\ 1\ if & k\ and\ m\ connected \\ 0\ if & otherwise \end{cases}$$

2 Find the bus with the greatest greedy value. In this algorithm, the unobserved bus with injection and the greatest amount of linked unobserved buses is the bus with the greatest value. If there are multiple buses with the same value, then choose from those buses randomly.

3 Update the PMU set and the set of observable buses. This is easily accomplished using the equation $A_i = F_i \cdot x_i$ from Ali Abur [125], whereby,

$$x_i = \begin{cases} 1 \; if & a\ PMU\ is\ connected\ to\ bus\ i \\ 0 & otherwise \end{cases}$$

$$F_i = \begin{cases} 1 \; if & the\ bus\ is\ observable \\ 0 & otherwise \end{cases}$$

4 Update F in accordance with the observability rules

5 Repeat from step 2, for each successive PMU placement until full observability is reached ($F_i = 1$ for all buses i)

The algorithm in [122] however presents a major deviation from the straight-forward approach listed here above, i.e.: a degree of randomness. Altman justified the randomization of the algorithm with an empirical demonstration on the IEEE 14 bus test system showing that the number of PMUs can be further minimized. The randomized Greedy algorithm uses as starting point not only the bus with the highest greedy value but study the OPP results for three other candidates (buses) chosen randomly. After the first PMU placement all the following PMU placements are decided by according to the greedy value. The solution with the less number of PMUs is chosen as the optimal solution.
The Randomized Greedy Algorithm is described in figure 5.18:

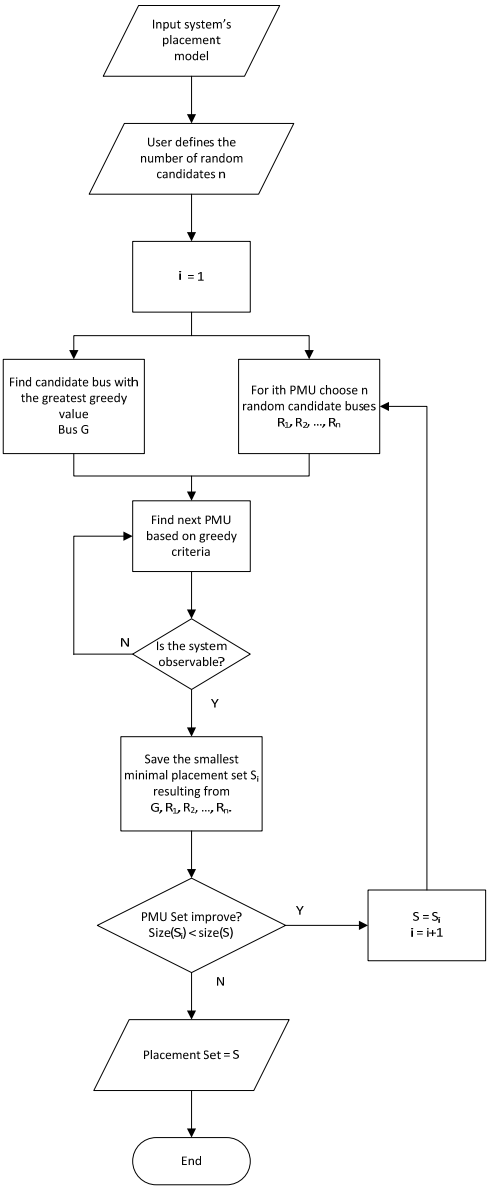

Figure 5.18: Randomized Greed Algorithm: Flow chart [122]

5.2.6.4 OPP features of a power system calculation tool

Seven usual methods or algorithms for PMU placement are implemented in the Power System Analysis Toolbox (PSAT®). PSAT® is a Matlab® toolbox for electric power system analysis and simulation. It is the only power system analysis toolbox available which permit a direct calculation of the OPP using several algorithms. More information on the data format[55] used as input for the calculations, by the program and on the program properties and features can be taken in [126] and [127]. From the seven OPP methods described in [126] two were randomly chosen for further study in this thesis. The end purpose followed remaining a comparison of the OPP results obtained using the chosen algorithms with those from Tabu Search and the Randomized Greedy algorithms.

5.2.6.4.1 Bisecting search method

It should be referred to [116] for the complete description of this method. In this work this description is limited to the illustration of the flow chart of it. This is presented in figure 5.16.

[55] PSAT is able to recognize and convert (using various filters) a variety of data formats commonly used in power system research.

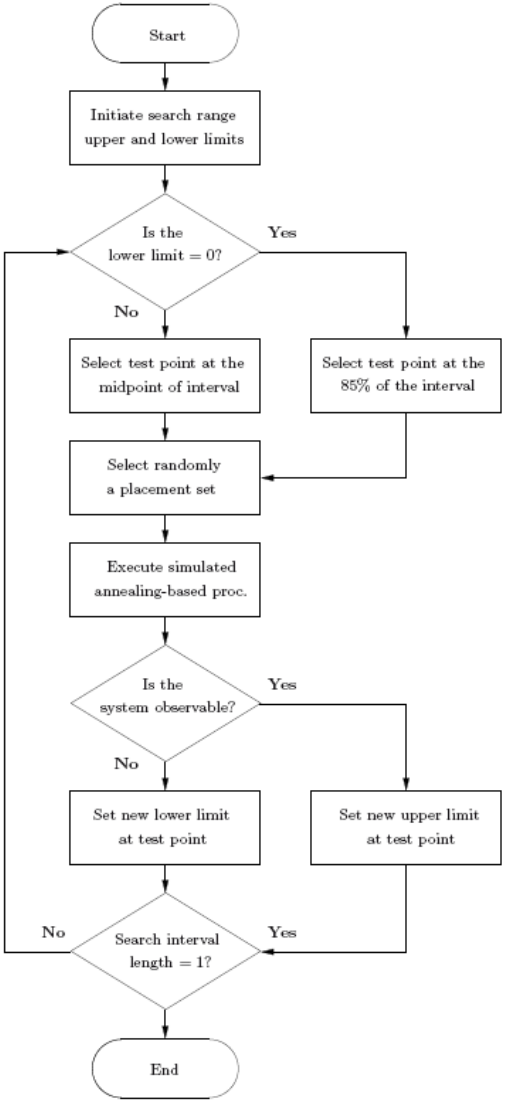

Figure 5.19: Flow chart of the Bisecting Search [127]

5.2.6.4.2 Recursive security N algorithm

The algorithm procedure is described in [128] and can be subdivided in three main steps.

1. **Generation of N minimum spanning trees**: the next figure 5.20 depicts the flow chart of the minimum spanning tree generation algorithm. The algorithm is performed N times (N being the number of buses), using as starting bus each bus of the network.

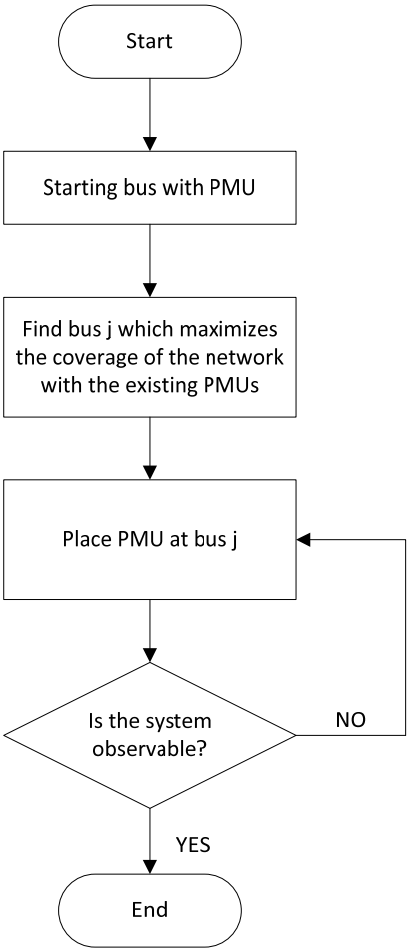

Figure 5.20: First step of the Recursive Security N algorithm

The placement principle used at the first step resembles to the one described by Reynaldo Nuqui in the references [129] and [130]. The method described in these references uses spanning trees to define on which buses PMUs were placed. Spanning trees connect every bus without making any loops. Once a spanning tree is created, the algorithm "walks" along the tree placing a PMU on every third bus to ensure full observability. Because of vast number of possible spanning trees, a large number of spanning trees and placements must be produced to have confidence in a "minimal" placement set.

2. **Search of alternative patterns**: The PMU sets obtained with the step (1) are reprocessed as follows: one at a time, each PMU of each set is replaced at the buses connected with the node where a PMU was originally set, PMU placements which lead to a complete observability are retained.

3. **Reducing PMU number in case of pure transit nodes**[56]: In this step it is verified if the network remains observable taking out one PMU at a time from each set. If the network does not present pure transit nodes, the procedure ends at step (2).

[56] Pure transit nodes are zero injection buses

5.2.6.5 Application of OPP methods to test systems

5.2.6.5.1 Application to the IEEE-14-bus system

The results of the OPP calculation by the different algorithms described above, for the IEEE 14-bus system topology presented in figure 5.8, are now given. A Matlab code was available for the realization of the Jansson's method. The results of the OPP calculation obtained by the Altman's method are taken from [122]. PSAT® was used for the OPP calculation by the bisecting search method and the recursive security N algorithm respectively.

Jansson's Method

Referred to the structure of the table 5.3 described earlier the results of the OPP calculation based on the Tabu search and a further minimization of the measuring points is the following:

Table 5.4: Results of the OPP calculation for the IEEE 14 test –system under full observability constraint using the Jansson's method

Number	DeviceRef	Location	PMU_Number	Type	Assign Device
1	2	2	1	VM	BS
2	2	2	1	VA	BS
3	4	2	1	AM	LN
4	4	2	1	AA	LN
5	5	2	1	AM	LN
6	5	2	1	AA	LN
7	1	2	1	AM	LN
8	1	2	1	AA	LN
9	6	6	2	VM	BS
10	6	6	2	VA	BS
11	12	6	2	AM	LN
12	12	6	2	AA	LN
13	13	6	2	AM	LN
14	13	6	2	AA	LN
15	14	6	2	AM	LN
16	14	6	2	AA	LN
17	5	6	3	AM	TR
18	5	6	3	AA	TR
19	9	9	4	VM	BS
20	9	9	4	VA	BS
21	8	9	4	AM	LN
22	8	9	4	AA	LN
23	9	9	4	AM	LN
24	9	9	4	AA	LN
25	3	9	4	AM	TR
26	3	9	4	AA	TR

It can be seen on table 5.4 that the Jansson's method advises a total number of 4 PMUs placed at the buses 2, 6 and 9 for the complete system observability. To the monitoring objects belong further system components namely some the systems lines and transformers from where the measurements of some defined variables are required to ensure the total system observability. All the monitored objects are red marked on the graph representation on figure 5.21.

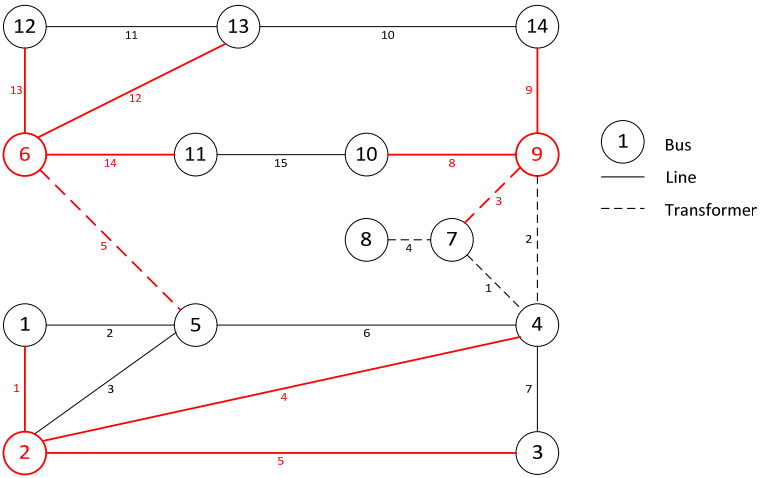

Figure 5.21 Graph representation of the OPP calculation for the IEEE 14 bus test-system according to Jansson's method

Altman's Method

According to principles described in 5.2.6.3 following results are given in [122] for the OPP calculation of the 14 bus system:

Table 5.5: Results of the OPP calculation using the Randomized Greedy Algorithm for the IEEE 14 bus test-system [122]

Placement order	Greedy candidate	Random candidate 1	Random candidate 2	Random candidate 3
1st 2nd 3rd 4th 5th	4 [2 3 4 5 7 8 9] 13 [6 12 13 14] 10 [10 11] 1 [1]	8 [7 8] 2 [1 2 3 4 9] 6 [6 11 12 13] 10 [10] 14 [14]	2 [1 2 3 4 5] 6 [6 11 12 13] 9 [7 8 9 10 14]	10 [9 10 11] 4 [2 3 4 5 7 8] 13 [6 12 13 14] 1 [1]

Table 5.5 presents the results if 3 random buses, 8, 2 and 10 are used as the first placement instead of the greedy candidate. After each first placement, the subsequent placements are made based on the Greedy Method.

The other buses that become observed due to a placement are listed in the square brackets next to the placement bus. As table 5.5 shows, combining the random first placement, Bus 2 (shaded region), with the 2nd and 3rd placements based on greedy values produced the smallest placement set for the IEEE 14 bus test-system.

The number of PMUs required is three. But taking in account the condition of the current measurements and by the absence of this precision in [122] this number is enhanced to 6. This supposes that the observation is done with PMUs with four measurements channels and that all edges impeding to the directly measured buses are observed.
A graph representation clarifies the obtained results.

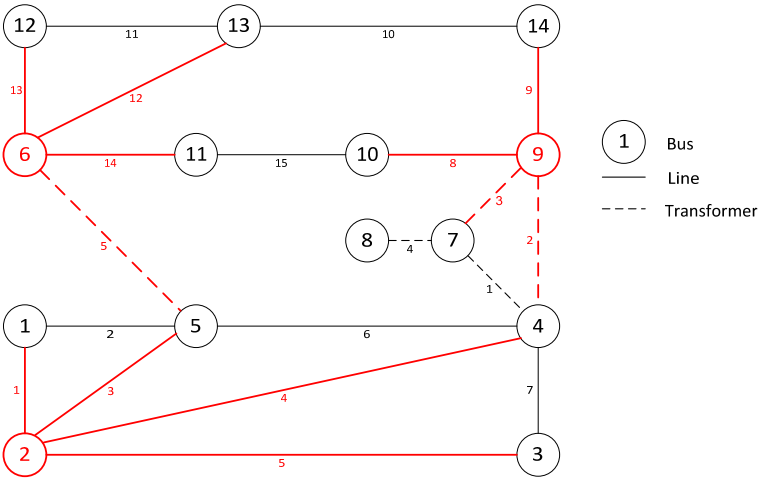

Figure 5.22: Graph representation of the extended Altman's OPP calculation for the IEEE 14 bus test-system

Bisecting search Method and *Recursive Security N algorithm*
These calculations were realized with PSAT®. An abridgement of the screenshots of the PSAT® calculations results with the respective methods is shown in Figure 5.20:

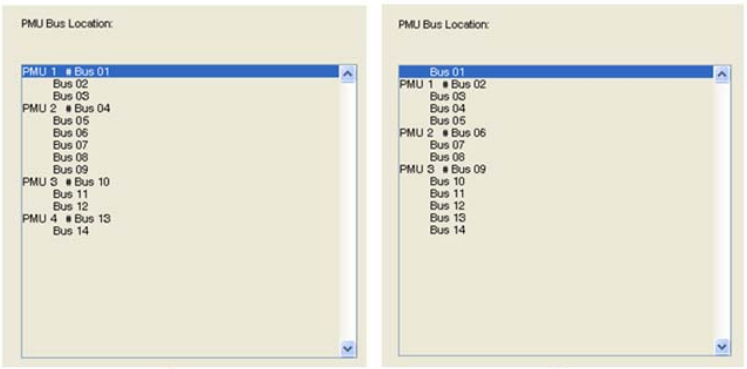

Figure 5.23: Screenshot abridgments of PSAT OPP calculation result using the bisecting search method (A) and the Recursive N algorithm (B) for the IEEE 14-bus test system.

The results shown in figure 5.23 take only the voltage measurements in account. Considering as previously the currents measurements and the number of channels of the PMUs fixed at 4, the final number of PMUs required for the total observability of the system is increased from the number given out by PSAT® to 5 for the bisecting search method and to 6 for the recursive N algorithm.
The obtained results are summarized and directly compared in the next table 5.6. The duration of the OPP calculation for each method is additionally included.

Table 5.6: Summary and comparison of OPP calculation Results for the IEEE 14 Bus Test System

Method	Directly Monitored buses	Total Numbers of PMUs	Duration of the calculation [s]
Jansson's Method	2, 6, 9	4	0,88
Altman's Method	2, 6, 9	6	0,50
Bisecting Search Method	1, 4, 10, 13	5	4,30
Recursive Security N Algorithm	2, 6, 9	6	12,98

As shown in table 5.6, even by the weakly meshed power system the results of the OPP calculation by some usual methods differ. Using the constraints defined in this work 28 - 42% of the buses must be equipped with PMUs.

5.2.6.5.2 Application to the IEEE 57-bus test system

The IEEE 57 Bus test system represents a portion of the American Electric Power System (in the Midwestern US) as it was in the early 1960's. A single line diagram of this system is given in [122]. The equivalent graph representation is shown in figure 5.24. As the reference [122] also gives an OPP solution for this system, a placement calculation was performed with each the other methods for direct comparison. The detailed results of the calculations are presented in appendix D.

The calculations general conditions are the same as by the 14 bus test system before. A summary and comparison of the obtained results are shown in table 5.7.

Table 5.7: Summary and comparison of OPP calculation Results for the IEEE 57 Bus Test System

Method	Directly Monitored buses	Total Numbers of PMUs	Duration of the calculation [s]
Jansson's Method	1, 4, 9, 20, 25, 29, 32, 47, 50, 53, 56	12	88,81
Altman's Method	1, 6, 13, 19, 25, 29, 32, 38, 51, 54, 56	15	5,00
Bisecting Search Method	1, 9, 15, 18, 23, 29, 30, 32, 47, 50, 53, 56	16	19002,19
Recursive Security N Algorithm	1, 4, 9, 20, 25, 29, 32, 44, 47, 51, 54, 56	15	51,81

Similarly to the study of the 14 bus test-system the OPP calculation results for the 57 bus test system differ considerably from method to method. For the complete observability of the IEEE 57 Bus test system by the defined constraints 21 - 26% of the buses must be equipped with PMUs. It took almost five hours time to PSAT® to give a result with the bisecting search method. However, the computation intensity (i.e. the difference in the calculation duration) of the different methods is not a relevant criterion for the OPP; because, as stated earlier this procedure is done offline and once for a given topology. Decisive is the total number of PMUs defined. The smaller PMU number is in both test cases obtained by the Jansson's method with the Tabu search as optimization algorithm. Moreover the result points out which type of measurement are made by the placed PMUs. On this base the Jansson's method were chosen for the OPP calculation of a real power system: the already mentioned western Danish grid or simply DK-VEST.

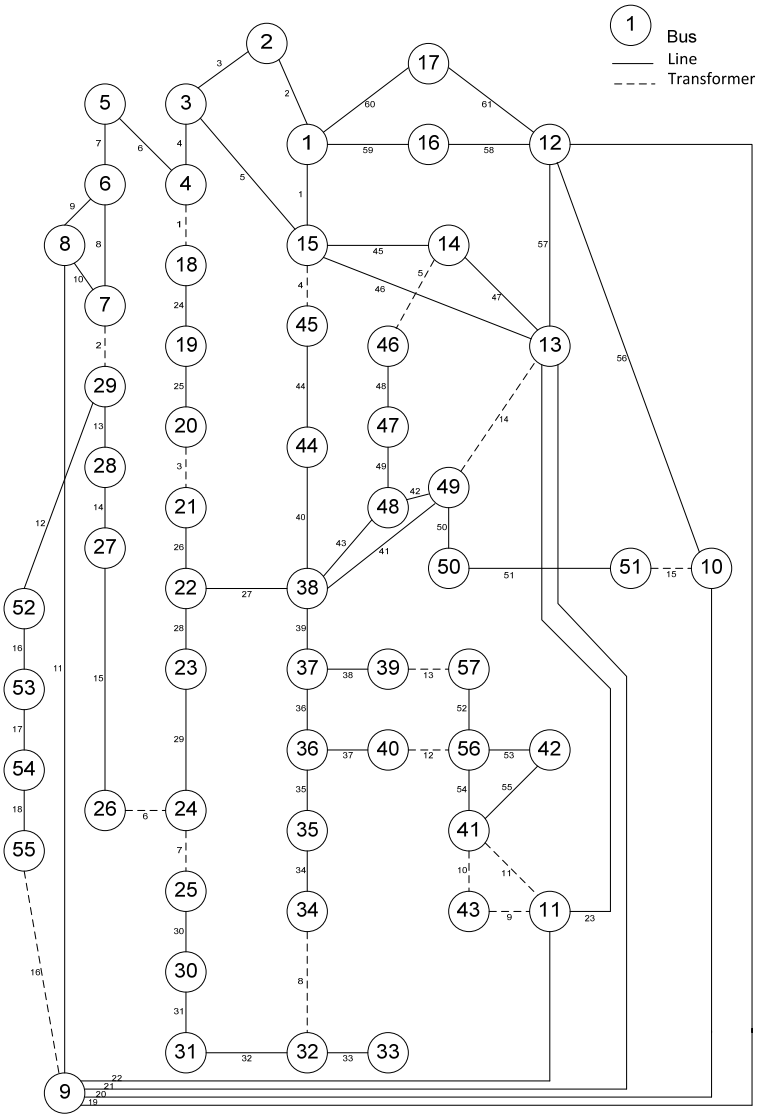

Figure 5.24: Graph representation of the IEEE 57 bus-test system

5.2.6.6 Application of the Jansson's method to DK-Vest

5.2.6.6.1 DK-Vest

A map of DK-Vest is shown on figure 5.25. The transmission system in Western Denmark consists of a meshed 400 kV and 150 kV grid. To the south, it is connected to the UCTE synchronous area via 400 kV, 220 kV and 150 kV AC lines to Germany. To the north, it is connected to the Nordel synchronous area via HVDC links to Norway (1000 MW) and Sweden (600 MW).

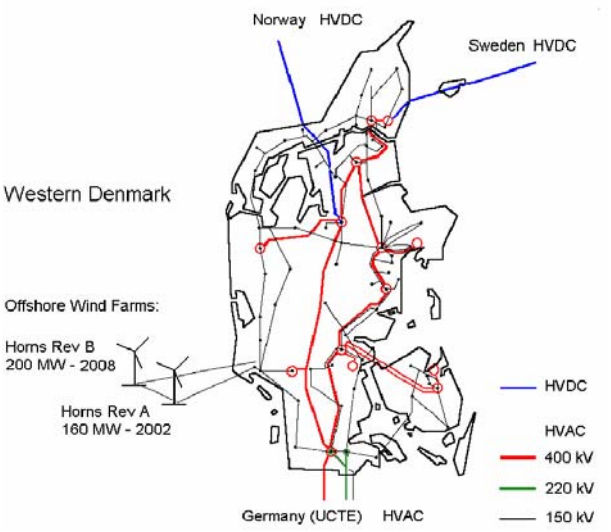

Figure 5.25: Map of DK-Vest [131]

The primary power plants are thermal units, fired by coal or gas. A significant part of today's installed capacity in the Danish system are decentralized units, such as wind turbines and combined heat and power (CHP) units, mostly connected to the distribution grid. This combination results in a change of the classical hierarchical load flow structure.

Former passive networks have become active networks due to the changed load flow direction (see bidirectional power flow, figure 2.2), especially on windy days. In the Western system the offshore wind farm Horns Rev A (HRA) with a rated power of 160 MW is connected to the 150 kV transmission systems. The grid connection of the second offshore wind farm, Horns Rev B (HRB), with a rated power of 210 MW is announced for the end of the year 2009 [131],[132].

As stated in chapter 3, a dynamic model of this power system is used for simulation in this thesis. The dynamic model is developed on the base of the snapshot of the operational status of the power system as taken by the SCADA system on 01.01.2007 at 23:59. For the given instant of operational time all the system status relevant variables values and topology are saved for this purpose. The dynamic model is then implemented in an electric grid calculation environment (i.e.: PowerFactory®) and is used as the base case for the analyses in this work.
A single line diagram of the base case structure of DK-VEST used in this thesis is shown in figure 5.26.
Due to the fact that HRB is presently not grid connected only HRA is considered in the representation and by the system dynamic modelling.
A total system summary of the system model equipment used is made in table 5.8

Table 5.8: DK-VEST: Total System Summary

Number of Substations	280	**Number of Terminals**	52	**Number of Asynchr. generators**	55
Number of 2-W Transformers	230	**Number of Transmission Lines**	150	**Number of 3-W Transformers**	0
Numbers of loads	64	**Number of Synchr. Generators**	141	**Number of shunts**	18

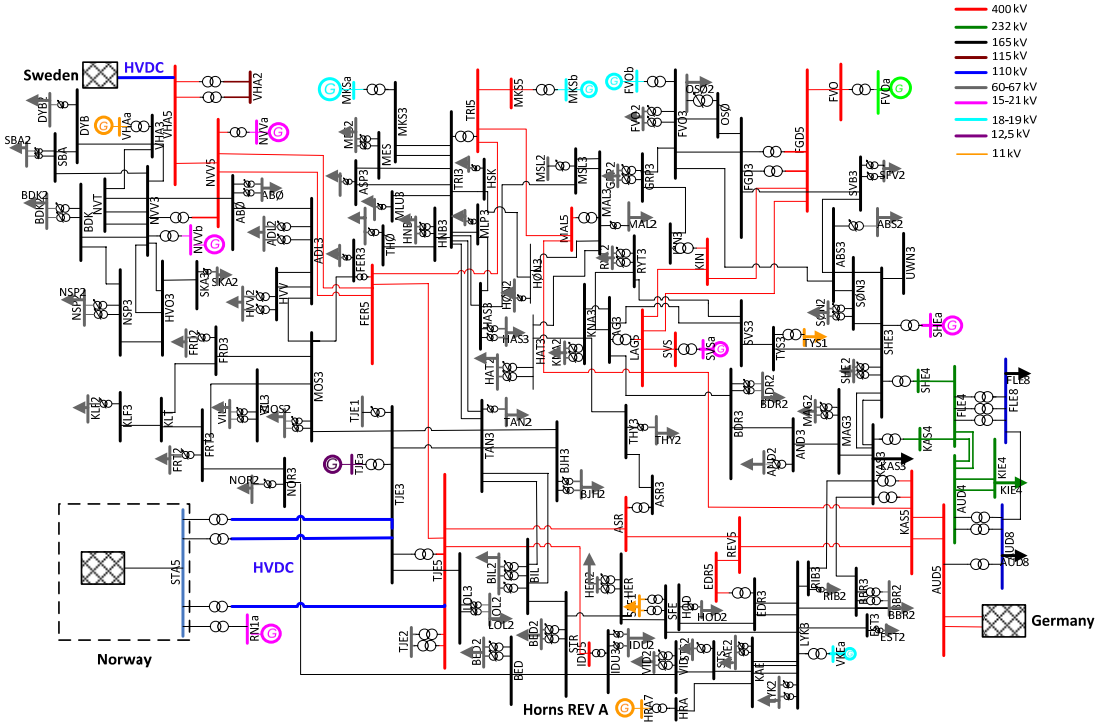

Figure 5.26: Single line Diagram of the complete DK-VEST Structure

5.2.6.6.2 OPP Calculation for DK-Vest

The method of Jansson is used to define the potential and minimal PMUs location in DK-VEST. Eventual availability of any PMUs is neglected (Starting point: PMU Number = 0).

Firstly the OPP is calculated only for a topological structure reduced to the 400 kV level plus the next directly connected buses symbolizing the injections in the transmission level[57]. This option is valuable in case of a PMUs deployment only for the observability of all the DK-VEST 400 kV Buses (and lines).

400 kV+1

After reduction DK-Vest takes the form presented in figure 5.27

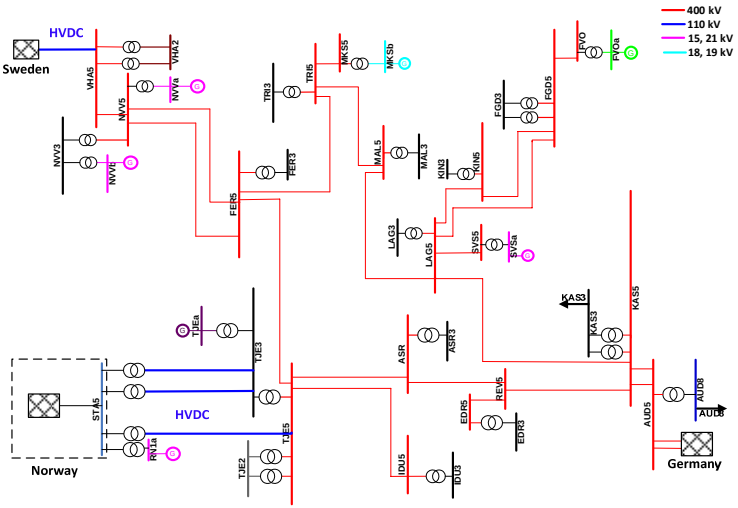

Figure 5.27: Single line diagram of the DK-VEST 400 kV+1

[57] The resulting reduced structure is termed 400 kV + 1

Applying the Jansson's OPP calculation method to this topology gives the following result:

Table 5.6: Results of the OPP calculation for DK-VEST: 400 kV+1 under full observability constraint using the Jansson's method

Number	DeviceRef	Location	PMU_Number	Type	Assign Device
1	3	3	1	VM	BS
2	3	3	1	VA	BS
3	1	3	1	AM	TR
4	1	3	1	AA	TR
5	13	13	2	VM	BS
6	13	13	2	VA	BS
7	16	13	2	AM	LN
8	16	13	2	AA	LN
9	25	13	2	AM	LN
10	25	13	2	AA	LN
11	20	20	3	VM	BS
12	20	20	3	VA	BS
13	14	20	3	AM	LN
14	14	20	3	AA	LN
15	27	20	3	AM	TR
16	27	20	3	AA	TR
17	34	34	4	VM	BS
18	34	34	4	VA	BS
19	15	34	4	AM	TR
20	15	34	4	AA	TR
21	37	37	5	VM	BS
22	37	37	5	VA	BS
23	11	37	5	AM	LN
24	11	37	5	AA	LN
25	8	37	5	AM	TR
26	8	37	5	AA	TR
27	9	37	5	AM	TR
28	9	37	5	AA	TR
29	12	37	6	AM	TR
30	12	37	6	AA	TR
31	10	37	6	AM	LN
32	10	37	6	AA	LN
33	42	42	7	VM	BS
34	42	42	7	VA	BS
35	44	44	8	VM	BS
36	44	44	8	VA	BS
37	23	44	8	AM	LN
38	23	44	8	AA	LN

As it can be seen from table 5.9, the OPP calculation by Jansson defines that a total of 8 PMUs (with two PMUs at bus 37: TJE5) are required for the complete observability of 400 kV+1. More details about the resulting PMUs placement and the monitored objects are given in appendix E, by the PSADD table and the graph representation for the structure in figure 5.27.

DK-VEST

The OPP calculation for the entire DK-VEST topology in figure 5.26 finds a total number of 92 PMUs. However it should be noted that this result is only possible to be obtained without the minimization step of the algorithm. With this option included an infinite loop took place in the calculation so that after 25 hours calculation time no final result could be obtained.

A PSADD file for the total DK-VEST structure is also given in the appendix E.

Table 5.10: Result of the OPP calculation by Jansson for DK-VEST

Method	Directly Monitored buses	Total Number of PMUs	Duration of the calculation [s]
Jansson's Method	4, 13, 21, 23, 29, 40, 48, 49, 50, 59, 66, 68, 75, 83, 86, 90, 99, 105, 108, 110, 120, 128, 131, 173, 176, 203, 210, 212, 219, 220, 224, 226, 232, 233, 235, 243, 245, 253, 254, 256, 266, 267, 274, 276, 279	92	1884,1

5.2.6.7 Discussion on the PMUs placement

As one can see, many efforts have been shared in the previous subparagraphs on the OPP problem. The thematic of the PMUs placement has gained great importance in the PMU research the last years so that it cannot be neglected when studying the aspects of the PMU technology in general.

Rather than to provide an overview of the existing OPP methods, the objective of the previous discussion was to present the main philosophy of what can be called the algorithmic methods of PMU placement on the base of the practical test of some chosen methods. Much more methods for OPP calculation are available in the literature. The references [133], [134] and [135] for example present some recent tendencies in solving this question. OPP methods generally result on 20 - 40% of the total buses of the power system to be equipped with PMUs for full system observability. The algorithms used can consider a list of various constraints coded for a purposeful PMU placement. This surely makes such methods attractive in economical and practical point of views. But in regard of the practical implementation of the results obtained, problematic are still the verification and the practical assessment of the methods. Obtaining a final result is the indicator of the correct termination of the implemented algorithm.

On the other hand it is just the sign of the functional correctness of the input-output behaviour of the algorithm. If the robustness of the algorithm is a decisive criterion for the choice of the calculation method, the optimal specification and codification of the input is the key to the applicability of the results produced. It is nevertheless advisable to verify if these results satisfy the practical monitoring expectations all the time. That will mean for example to verify, according to the results obtained which variables can be calculated from the direct measurements. That being said it can be concluded that the use of such algorithmic OPP calculation methods is useful but their solutions must not be considered as the ultimate PMU placement, but as a possible base for further analysis of the PMUs placement.

The final PMU positioning must be always motivated and effected in view of the monitoring needs of the power system considered and the intended utilization of the measured data. In this regard the following course of actions is elaborated for the practical definition of the PMUs location in electric power grids:

Action 1: Definition of the principal (critical) monitoring objects. In addition or prior to this, the monitoring objective, criteria, and principles must be defined. Also the monitoring algorithm is developed at this step.

Action 2: Find already installed PMUs (if already available) and evaluate their observability horizon in accordance to the defined monitoring conditions. If the entire system i.e.: all the monitoring objects can be observed than the PMU optimal set is found. If reverse go to action 3. In case if none PMUs are available, a PMU can be placed at a node recognized as critical or monitoring relevant and serves as starting point for the positioning of further PMUs.

Action 3: Place a further PMU in a strategic and favourable position in the unobserved region so that the synchronization with the already available PMUs permits the measurement of more unknowns as possible. Repeat this action until all monitoring objects are observed.

5.2.7 Overview of PMU based system operation applications

The expression: “PMU based system operation applications”, is used to qualify those applications which are not embedded in the PMU itself, but are located on computers at the system operations centre or other network locations. These applications utilize synchrophasors to address specific system local or wide issues. The following give a brief description of some present applications.

1) Line Parameter Calculation

Transmission line impedance lumped parameters can be calculated using a PMU at each terminal to measure the voltage and current synchrophasors. Thereby a π-equivalent model of the transmission line is considered.

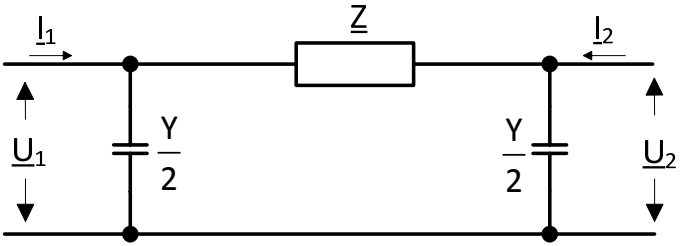

Figure 5.28: Transmission line equivalent model for the calculation of the line parameters

The measurement of the terminal voltages $\underline{U_1}$ and $\underline{U_2}$ and currents $\underline{I_1}$ and $\underline{I_2}$ will allow the computation of the line parameters Z and Y. The reference [136] gives the formulas for the determination of these parameters when the transmission line is operating in steady state:

$$Y = \frac{2\left(\underline{I_1} + \underline{I_2}\right)}{\underline{U_1} + \underline{U_2}} \quad ; \quad Z = \frac{\underline{U_1}^2 - \underline{U_2}^2}{\underline{U_2} \cdot \underline{I_1} - \underline{U_1} \cdot \underline{I_2}}$$

Making the measurements for various load and ambient temperature can permit to account the variability of the line model parameters to them.

This application is a typical example for the utilization of the PMUs for model validation and optimization.

2) State estimation

The state estimation is one of the most popular PMU applications. As said earlier it is the process that defines the state of the power system. More details on the techniques used for the state estimation can be taken from [107]. It is assumed that, providing accurate time voltage and current synchrophasors the PMUs can considerably improve the accuracy and the solution time of the state estimation calculation. However important conditions thereby are the correct location and the sufficient number of the PMUs; Whereby OPP calculations described in previous sections can be helpful.

3) Out-of-step detection

As the out of step or power swing detection more than before requires receiving data at higher rates than the power systems frequency with a near zero latency at the system control centre, many new algorithms using synchrophasors to detect and predict out-of-step conditions are becoming available. The development of such an algorithm based on the principle of the *equal area criterion* is presented in [137].

4) Phase angle difference monitoring

This option takes in account that the flow of power between two nodes varies approximately with the sine of the angle between the two nodes (see equation (3.8a)). This angle is found as the difference between the nodes voltage phase angles. The voltage phase angles at the two nodes are measured by two distinct PMUs and the difference calculated. A critical situation is recognized if this difference exceeds a fixed threshold. The phase angle difference monitoring can be useful for the monitoring of the energy transfer on a power line or during power system restoration. During this second case, system operators often encounter an excessive standing phase angle (SPA) difference across a breaker, which connects two adjacent stations. Closing a circuit breaker on a large difference can shock the power system, cause severe equipment damage, and possibly a recurrence of the system outage [138]. Maximum limits SPA must be imposed upon network loop closure, during the transmission system restoration process. These limits reduce the risk of damage in generation and transmission equipment.

The PMUs are well suited for on-line monitoring of angles, and thus can be helpful for the operator during a power restoration.

5) Power System Damping

Typical example of this application is taken from the reference [139]. Phasor measurement signals are used as only input to a wide-area power system stabilizer (PSS) to increase inter-area mode damping of the Icelandic power system. Using modal analysis and time simulations of a detailed model, it is shown that frequency difference as PSS input gives a damping improvement that is robust to drastic change in system topology. Field data from PMUs indicate high signal quality and that frequency difference is a realistic PSS input.

6) Line Thermal Monitoring

It is recognized that a transmission line may be routed through several different environments where temperature and wind velocity conditions will be different. In this application it is proposed, however, that an average conductor temperature calculation based on real time assessment of measured and design parameters of the transmission line will provide a reasonable and economic method to evaluate the transmission line's loadability. The line impedance parameters are computed based on conductor size and spacing. The resistance with values at 25°C and 50°C generally provided by the manufacturer serve as a basis for the average temperature calculation.

For a more exact temperature calculation it is surely advisable to take in account all the meteorological variables that influence the thermal state of the conductor. These are: the speed and direction of the wind, the ambient temperature and the solar radiation. A method of calculating the current-temperature relationship of bare overhead conductors considering all these parameters is defined in [140].

7) Voltage Stability

Many practical applications combine some of the voltage stability analysis methods presented in chapter 4 with PMU data for the assessment of the voltage stability status of power systems. PMU data based methods combined with the evaluation of the Thevenin equivalent (see 4.2.9) are exemplarily used in [96], [141], and [142] for voltage instability prediction.

A method proposed by Gong in [143] defines a stability index for load buses in power systems using synchronized phasors measurements. Benjamin Genêt uses a minimal number of PMUs measuring the complex voltage at each bus of a power system to calculate its stability index according to the method described in [144]. Larsson et al. [145] defined a method for the calculation of the voltage stability on transmission corridors. As stipulated in this reference, phasors measurements at either end of the transmission corridor are used, to construct a reduced equivalent of the network then used for analytical stability assessment. The result of the stability is displayed using a dynamically updated PU-curve and numerical stability margins. This method also is also based on the estimation of a Thevenin equivalent of the network at a chosen single bus. The current through a single line feeding that bus is used to estimate an equivalent Thevenin equivalent of a possibly complex network and the generation at the remote end. This method is not applicable to meshed power grids.

8) Other Applications

Other applications utilizing synchrophasors data include:

- Post-Disturbance Analysis
- Fault location in transmission lines [146]
- Frequency tracking and instability
- Small signal stability
- Etc…

6 Real time monitoring of the power transfer and of the voltage profile stability

6.1 Introduction

In this chapter an innovative method to assess the voltage stability of electric power transmission paths in real time modus is developed. The notions of the *stability of the transfer modus* of a transmission line and of the *stability of the voltage profile* at a given system bus, directly related to the voltage stability phenomena built the backbone of the proposed monitoring method. These are described earlier in the chapter 3 of this work on the base of the figure 3.22.

The first notion is linked in this work to the PU characteristic of a transmission line and its connected bus in the positive direction of the of the power flow. This PU-characteristic is further considered as the operation curve for a given transmission line. Resulting from the mathematical modelling of the power flow of the transmission line, this characteristic is parabolic (two half-parabolas) in shape and thus shows a maximum according to some defined values of voltage and active power. The vertex of the parabola represents the stability limit of active power delivery. Having crossed this maximum the power delivery becomes unstable and by steady increase of the power generation at one end of the line, the power received at the other line end is reduced instead of increased. From this maximal point the further system operation is unstable. For this reason the distance between the actual operating point and the vertex must be monitored.

On the other hand the voltage profile at all system's buses must always be maintained at a level appropriate to the electric power transmission and distribution.

Due to the incessant dynamics in power systems the system voltage profiles continuously vary at various points. As stated earlier, any change, in any grid equipment, at any grid operation moment will have an impact on the overall voltage situation of the power system and therefore at each bus respectively. The loads were presented as the driving force of the variations within the power system, thus they are assumed to be the principal voltage instability leading factor. One can easily pull the loading of the transmission lines - principally at the highest voltage level- and the demand in electric power together. This is also indirectly regulated by the instant electric power market conditions. The voltage instability in this second case is directly connected to the voltage level at the substations (buses) at the boundaries of each transmission line. The acceptable voltage operation levels are determined by the transmission system operator according to the exigencies of the available system equipment. The upper and lower acceptable voltage levels at a bus in regard to a stable grid operation define the bus voltage profile limit.

The transfer operating mode of each monitored transmission line is formulated in a PU characteristic depending on the load factor. This permits the exact definition of the stability limits of the operating mode for the transmission lines based on the voltage criterion. The combination of the PU characteristic with a defined voltage profile stability band permits the conjoint determination of the transfer and voltage profile stability margins defined in the equations (3.11) and (3.12). The voltage stability margins are directly evaluated on a PU mode without need to specify any loading scenario.
The method can use synchronized phasor measurement data from a single PMU for the voltage stability monitoring of one transmission line or from a set of PMUs to ensure the voltage stability monitoring of a defined transmission zone retaining several transmission lines. In both cases, the PMU data is combined with system relevant parameters to build the input of the stability analysis. During the assessment of the stability status on transmission zones each individual line within the zone is analysed separately.

The applicability of the method is tested on a two-bus test system and on the 400 kV transmission system of DK-VEST. The analyses use simulated phasor data from PowerFactory® as well as real field data from the PMU data archives from the PMUs installed in western Denmark.
A description of the PMUs installations in DK-VEST and of the available communication setup is made to explain the origin of the field PMU data employed. This chapter also includes a brief description of two tools developed in the framework of the thesis for the presentation of field PMU data and for the phasor based analysis of the voltage stability.

6.2 PMU data sets

Two types of PMU data sets are used in this thesis. The first type is *simulated phasor data sets*. These are directly outputted by PowerFactory® as the results of grid calculations and dynamic simulations. The second type is *field phasor data sets*. These are real phasors data sets installed at three 400 kV substations of the western Danish power system DK-VEST described in chapter 5.

6.2.1 PMUs installations in DK-VEST

The actual PMUs positioning in DK-VEST is presented on the next figure 6.1.

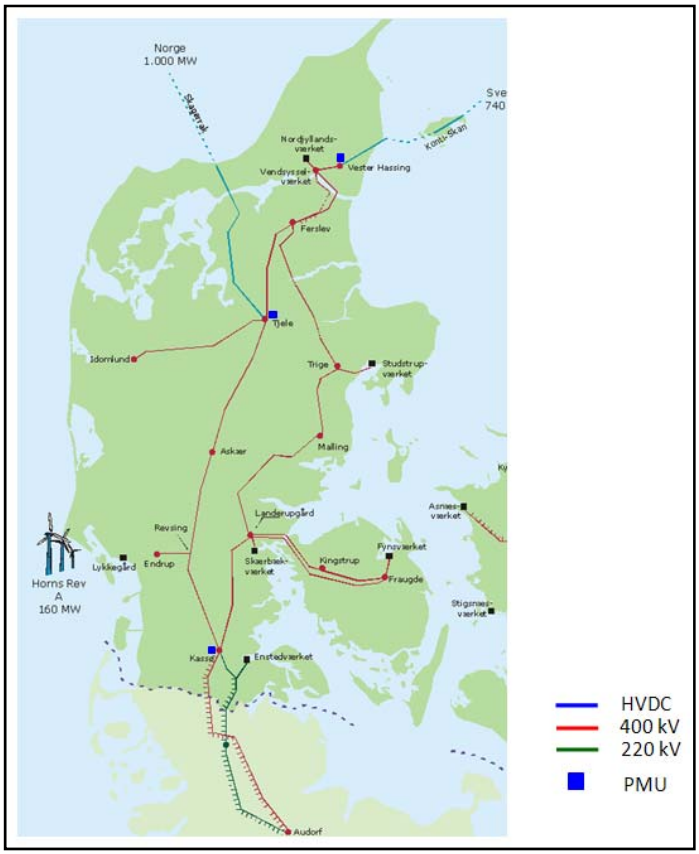

Figure 6.1: Actual PMUs positioning in DK-VEST

Three PMUs are respectively available at the substation in: Kassø (KAS5), Tjele (TJE5), and Vester Hassing (VHA5). All three PMUs monitor the transfer on three lines situated at the borders of DK-VEST, proximately to the connections points with the three neighbouring power systems of: Germany, Norway and Sweden. Seen on an abridgement of the single line representation of DK-VEST, representing the topology of its 400 kV level, with the direct connections to the neighbouring Swedish power system and to the next lower voltage levels the PMU installations look like shown in the figure 6.2.

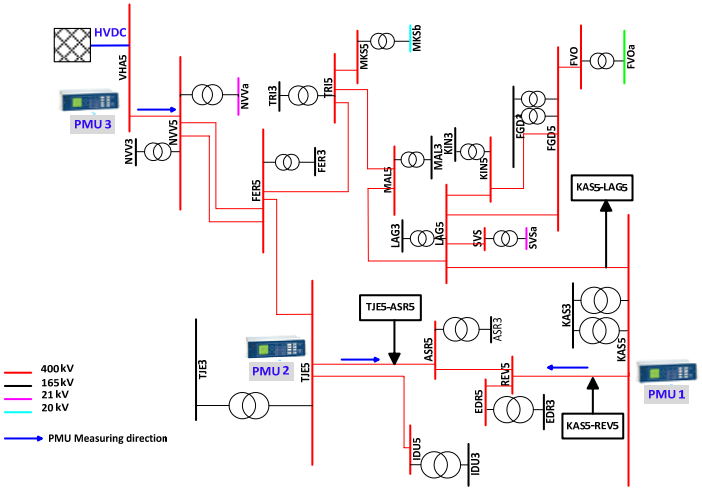

Figure 6.2: Abridgement of the DK-VEST power transmission system

The monitoring objects and the measuring direction of the available PMUs are shown in figure 6.2. A picture of the installation of the PMU 2 at Tjele (TJE5) is shown in figure 6.3.

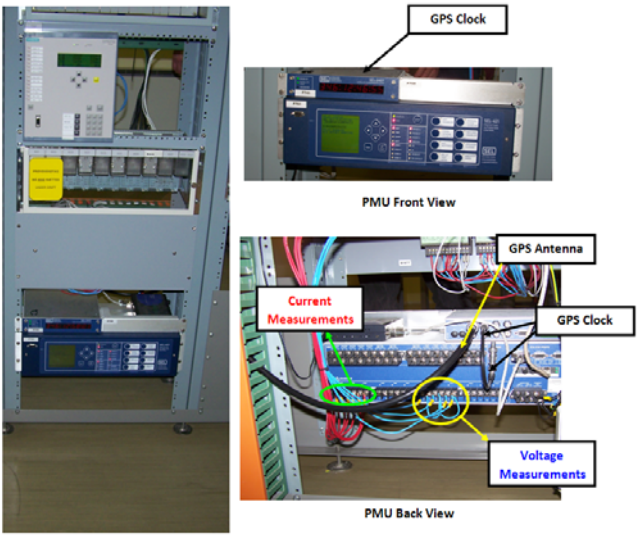

Figure 6.3: PMU installation at Tjele (TJE5). The PMU from type SEL-421 is installed in a 19-inch rack.

The PMUs used, are all of type SEL-421[58] from Schweitzer Engineering Laboratories, Inc. The data measured by the PMUS at the three substations are transferred and gathered using the following communication setup.

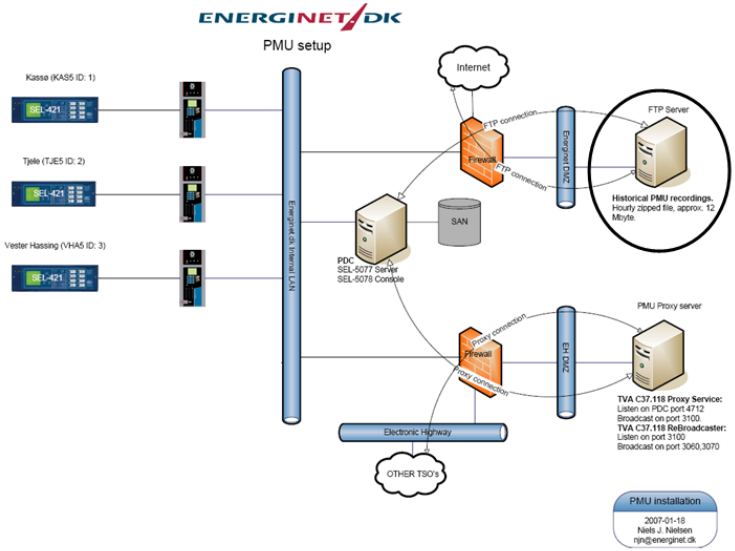

Figure 6.4: PMU Communication Setup [source: Energinet.dk : Danish TSO]

Historical PMU measurements measured at the three PMU-locations are periodically gathered on a File Transfer Protocol (FTP)-server (circled in the figure 6.4). They can be collected from there for further analysis purposes.

[58]The functional capabilities and features of the SEL-421 are given in the relay data sheet available at: http://www.selinc.com/

The PMU data sets are hourly zipped files containing tables with the comma separated values (csv) data of:

- the measurements timestamps
- the complex phase currents and voltages
- the complex positive sequence current and voltage and their resulting positive sequence magnitudes
- the power system frequency (measured at each PMU location)
- the status of the PMU measurement. This additive column is included so that bad data could be filtered out. For example the value “00 00” in the status column is the attribute of a successful measurement.

As said in chapter 4 the consideration of the positive sequence is sufficient for the power system analyses and monitoring.
The data are measured with a sampling rate of 8 kHz and are stored in the csv-table each 40 ms. An unzipped hourly file has approximately a size of 32 Mbytes. If complete, the csv-table is constituted by a total number of 35 columns and 90000 rows.

6.2.2 Offline phasor data presentation and handling

Although the PMU data are intended to be used for online purposes, the development of the voltage stability monitoring method is done on an offline base. An analysis of the recurrent and specific problems as well as the detection of the faults and eventually inaccuracies in the data sets can also be made on this base. An offline tool developed in the framework of this thesis permits the presentation of the field PMUs data sets in a very convenient way for their further analysis. At this instant of the work only the signals of one PMU is processed by comprehensive functions included in the tool.

This tool is developed in Matlab® and its main functions are:

- Selection of the input sources. Here the PMU and the signals to be represented are selected.
- Concatenation of several csv data tables for the consideration of data for several consecutive hours
- Determination of the data quality: The principal quality criteria are the number of missing timestamps and zero-values[59] in the data sets considered. The program also calculate the total missing time so that the user can decide to use the chosen data sets or to chose "better one" in case of a lot of missing data for example
- Calculation of the desired derived signals. Here the resulting active and reactive power are principally calculated using the following formulas:

$$P = U \cdot I \cdot cos(\theta - \Phi) \quad (6.1)$$
$$Q = U \cdot I \cdot sin(\theta - \Phi) \quad (6.2)$$

Whereby,
U is the Voltage magnitude in the positive sequence, I is the current magnitude in the positive sequence, θ is the voltage angle in the positive sequence, and Φ is the current angle in the positive sequence.

The active power will have a positive value when flowing in the measuring direction of the PMUs shown in figure 6.2, otherwise it is negative.

- Direct plotting of the variables time characteristics. The plotting window can hold several plots

[59] The csv tables present sometimes zero values for certain variables. Their appearance can be explained by deficiencies in the measurement process or in the communications links.

The next figure 6.5 exemplarily shows a screenshot of the representation of the calculated active power transferred from the substation ASR5 to substation TJE5 (see figure 6.2), as it is measured by PMU 2 on the 02nd of February, 2007 from 13 pm until 14:59 pm. The plots of the voltage and current phasors representation measured by the PMU 1 at KAS5 for this same day and time interval is shown in figure 6.6.

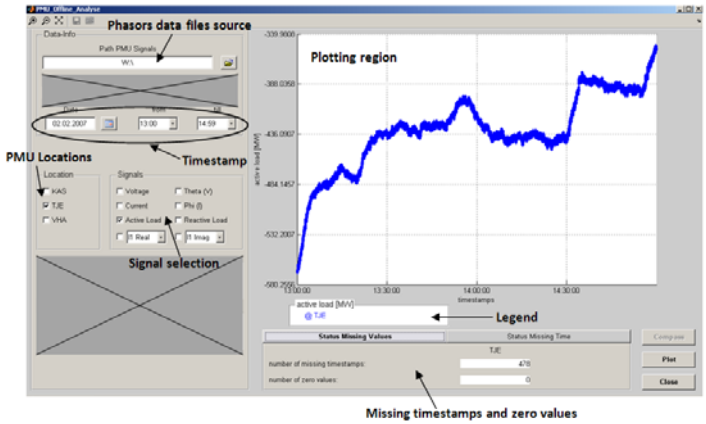

Figure 6.5: Screenshot of the phasor data offline presentation's tool with a description of the user interface

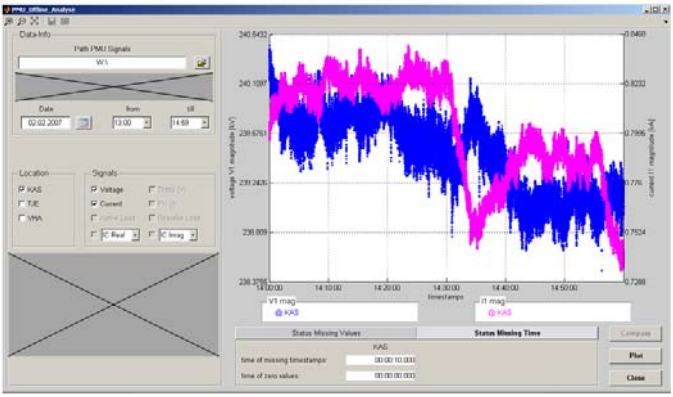

Figure 6.6: Representation of voltage and current phasors at one PMU location

The yet inactivated functions are masked on the figures 6.5 and 6.6. The actual version of this tool is enough to visualize the raw PMU data and to assess the quality of the data measured at each location principally in regard of their completeness. It can also be used for representation of the system behaviour as "seen" by the PMUs for the post mortem analysis of the grid events. The tool must be enhanced and optimized with additional functions for more exhaustive offline analyses.

The problems detected with the help of this tool in the PMU data can be relevant for online purposes and thus must be taken in account by the development of an online tool for the evaluation of the system stability using PMU data sets. A concrete example is the consideration of the missing timestamps. A principal advantage of the use of PMUs is the possibility of their synchronization. It is thus meaningful to compare only phasor data with the same timestamps. By simultaneous use of data from two or more PMUs for stability assessment for example it should be continually verified that all the data considered for the calculation have the same timestamp otherwise the stability evaluation will not be exact. The last sentence of the paragraph 5.4.2 raises this problem.
The voltage stability analysis tool: *AHT-Vstab*[60], developed in the framework of this thesis includes a function for the comparison of the timestamps of two simultaneously used PMUs for the monitoring of a defined transmission zone. Also this tool is developed in Matlab®. A description of AHT–Vstab follows in paragraph 6.10.

[60] AHT: *Anlagen und Hochspannungstechnik*, German name of the Institute for power systems and High-Voltage Engineering of the University of Kassel in Germany.

6.3 General conditions of the development of the monitoring method

As seen in figure 6.2, three PMUs have been already installed on DK-VEST. These have fixed measurement attributes and are placed proximately to the connections points between DK-VEST and the neighbouring power systems. The actual positioning of these three PMUs can be justified by the evolution of the amount of the physical exchanges between DK-VEST and the power systems in Norway (NOR), Sweden (SWE) and Germany (GER) during the last years.

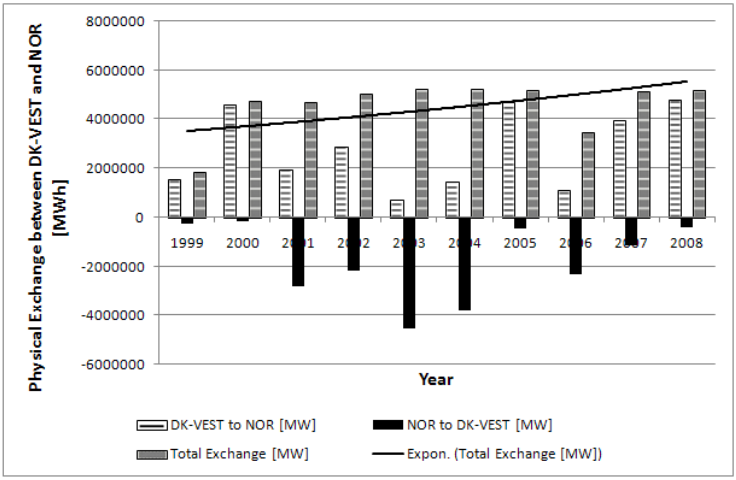

Figure 6.7: Physical Exchange between Western Denmark and Norway from 01.07.99 until 29.12.2008 [Source: Energinet.dk]

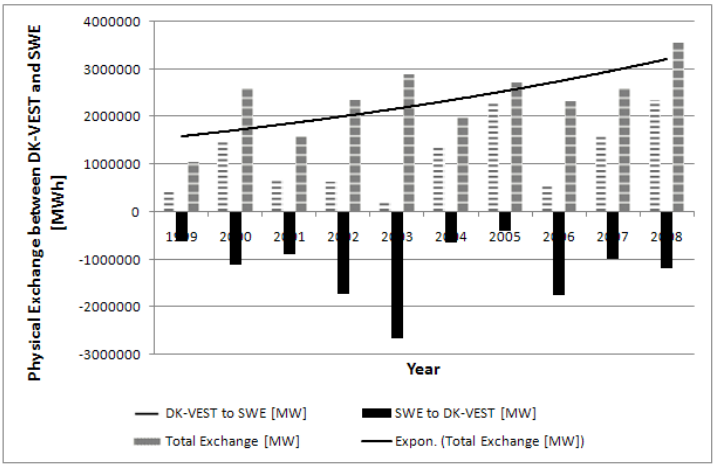

Figure 6.8: Physical Exchange between Western Denmark and Sweden from 01.07.99 until 29.12.2008 [Source: Energinet.dk]

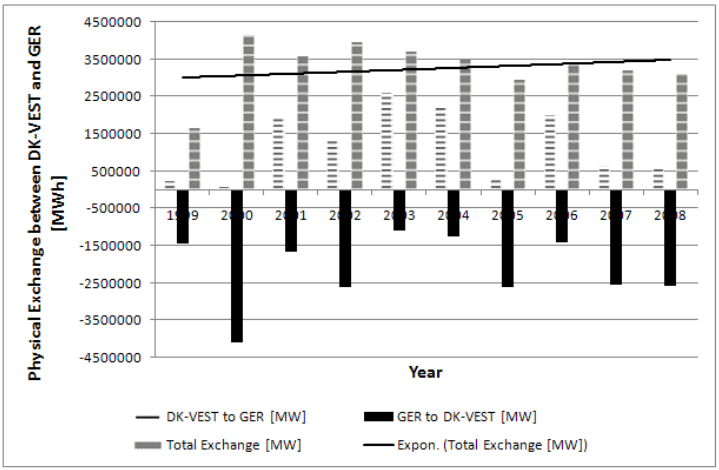

Figure 6.9: Physical Exchange between Western Denmark and Germany from 01.07.99 until 29.12.2008 [Source: Energinet.dk]

The figures 6.7, 6.8 and 6.9 show a clearly augmentation of the total power exchanges between DK-VEST and its neighbouring power systems beginning from the year 2000. The represented trend lines point to an increase tendency also for the coming years. This is surely motivated by the actual electricity market conditions. A direct consequence of this situation is the increased utilization of the transmission lines in DK-VEST in general, and at the transmission level particularly. The transmission lines are hence more exposed to congestion and stability problems. The energy transfer on the transmission lines must be monitored with the goal to recognize the imminence of such problems early enough in order to avoid them. The PMUs actually installed in DK-VEST can be well used for this purpose under the assumption that their data are efficiently and targeted handled. Another question to be solved regards the horizon of observability of the installed PMUs and hence their capability to monitor the rest of the transmission lines. It is obvious that for this purpose more PMUs will be needed. The OPP calculation made for this system on the previous chapter already sustained this idea. The real question to be answered is where should further PMUs be placed?

The stability monitoring concept developed in this work combines transmission lines parameters data with dynamic phasors measurements to determine how far an actual operation point (active power transfer) of a transmission line is from a point where voltage instability will occur. The voltage stability constraints are based on the transfer and voltage profile stability notions discussed at the beginning of this chapter. The representation of calculation results are visualized using an innovative PU characteristic. The progressive calculation of the transferred active power for each measured operating point of the transmission line permits the representation of different PU characteristics for the corresponding timestamps, and in accordance of the changes in the line transfer i.e. the changes in the power system.

Another factor determining the power transmission capability of power lines are the thermal limits. This constraint is not considered for this method.

The method will be verified on the example of the topology of the 400 kV level of DK-VEST as it is presented in figure 6.2. However the method developed is applicable to any other power transmission grid topology. The proposed monitoring method will be adapted to the actual PMUs positioning in DK-VEST, and the locations of further PMUs, for the complete "observability" of all transmission paths in figure 6.2 will be defined.

6.4 Calculation of transmission line transfer capacity limit

6.4.1 Transmission line equivalent circuit

For purposes of analysis involving interconnection with other elements of the power system it is more convenient to use equivalents circuits which represent the performance of the lines as seen from their terminals [23]. Further calculations for the transmission lines are thus realized in this work on the base of their nominal π-equivalent circuit. This equivalent circuit represents sufficiently well and with a very good accuracy the properties of real transmission lines [147] and is usually used for modelling the transmission lines in stability studies. This line equivalent circuit is implemented in the grid calculation tool used for digital simulations within this work; differently from the representation in figure 5.6 in the previous chapter, the line series resistance R and series inductance L for the total length of the line are each hereby represented as lumped parameters.

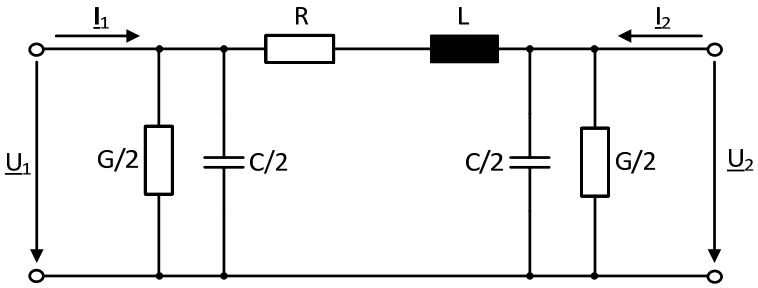

Figure 6.10: π- equivalent circuit of a transmission line with lumped parameters

The equivalent circuit terminals are qualified as the active power source (index 1) and the active power sink (index 2) respectively. This denomination depends on the instant power flow direction and thus can be interchanged several times during the daily operation of a given transmission line. The active power is transferred from the source terminal to the sink terminal.

In a next step the general equations of the transferred active power to and the voltage at the line sink terminal are developed.

6.4.2 Calculation of the current, voltage and active power at the line sink terminal

Knowing the complex voltage and current values at one end of the transmission line it is possible to calculate the corresponding values at its other end [147], [148]. The calculation required the knowledge of the line parameters: R, L, G, and C too.

The π-equivalent circuit in figure 6.10 is extended by the introduction of $\underline{I}_m$and $\underline{U}_m$:

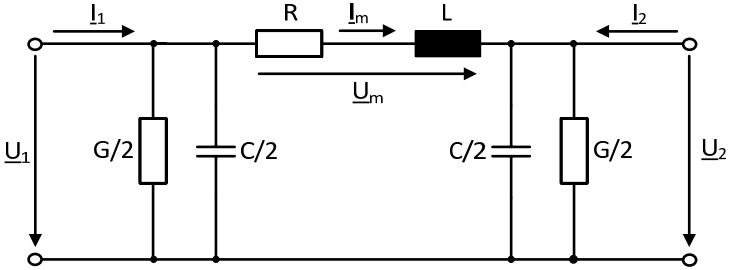

Figure 6.11: Extended π- equivalent circuit of a transmission line with lumped parameters

Using the electric circuit theory the current and the voltage values through the lumped parameters are defined.

$$\underline{I}_m = \underline{I}_1 - \underline{U}_m \cdot \left(j\omega\frac{C}{2} + \frac{G}{2}\right) \tag{6.3}$$

$$\underline{U}_m = \underline{I}_m \cdot (R + j\omega L) = \left[\underline{I}_1 - \underline{U}_1 \cdot \left(j\omega\frac{C}{2} + \frac{G}{2}\right)\right] \cdot (R + j\omega L) =$$
$$\underline{I}_1 \cdot (R + j\omega L) - \underline{U}_1 \cdot \left(j\omega\frac{CR}{2} + \frac{RG}{2} - \omega^2\frac{LC}{2} + j\omega\frac{LG}{2}\right) = \tag{6.4}$$
$$\underline{I}_1 \cdot (R + j\omega L) - \underline{U}_1 \cdot \left[\frac{1}{2}\left(RG - \omega^2 LC + j\omega(CR + LG)\right)\right]$$

The voltage at the sink terminal is calculated as

$$\underline{U}_2 = \underline{U}_1 - \underline{U}_m \tag{6.5}$$

With account of (6.4) the equation (6.5) can be rewritten as

$$\underline{U}_2 = \\ = \underline{U}_1 \left[1 + \frac{1}{2}\left(RG - \omega^2 LC + j\omega(CR + LG)\right)\right] - \underline{I}_1 \qquad (6.6)$$

Following simplifications are introduced for (6.6)

$$\underline{Z} = R + j\omega L \qquad (6.6.1)$$

and

$$\underline{K} = \left[1 + \frac{1}{2}\left(RG - \omega^2 LC + j\omega(CR + LG)\right)\right] \qquad (6.6.2)$$

Both constants depend on the line parameters. Therefore the following resulting expression of the voltage at the sink terminal in (6.7) is individual for each single transmission line in the power system.

$$\underline{U}_2 = \underline{U}_1 \cdot \underline{K} - \underline{I}_1 \cdot \underline{Z} \qquad (6.7)$$

Outgoing from the figure 6.11 the current at the sink of the transmission line is defined as

$$\underline{I}_2 = \underline{U}_2 \cdot \left(\frac{G}{2} + j\omega\frac{C}{2}\right) - \underline{I}_m \qquad (6.8)$$

The current $\underline{I}_m$ is replaced in (6.8) by its following expression

$$\underline{I}_m = \frac{\underline{U}_1 - \underline{U}_2}{\underline{Z}} \qquad (6.8.1)$$

And the equation (6.8) is changed into

$$\underline{I}_2 = -\frac{\underline{U}_1 - \underline{U}_2}{\underline{Z}} + \underline{U}_2 \cdot \left(\frac{G}{2} + j\omega\frac{C}{2}\right) \\ = \underline{U}_2 \cdot \left(\frac{1}{\underline{Z}} + \frac{G}{2} + j\omega\frac{C}{2}\right) - \frac{\underline{U}_1}{\underline{Z}} \qquad (6.9)$$

A part of (6.9) is summarized into the following constant

$$\underline{D} = \frac{1}{\underline{Z}} + \frac{G}{2} + j\omega\frac{C}{2} \tag{6.9.1}$$

The resulting expression of the current at the line sink terminal is then given by

$$\underline{I_2} = \underline{U_2} \cdot \underline{D} - \frac{\underline{U_1}}{\underline{Z}} \tag{6.10}$$

Although the expression in (6.10) is already suitable for further consideration, it can be rewritten with the consideration of (6.7).

$$\underline{I_2} = \left(\underline{U_1} \cdot \underline{K} - \underline{I_1} \cdot \underline{Z}\right) \cdot \underline{D} - \frac{\underline{U_1}}{\underline{Z}} \tag{6.11}$$

For the calculation here above the active power source was chosen as reference. The power sink can equivalently be chosen as the reference by changing the indices in the respective equations.
It means that the reference of the basic calculation con be freely chosen, the only condition in that the complex current and voltage values must be known or measured at that point.
Outgoing from the calculated voltage $\underline{U_2}$ and $\underline{I_2}$ the complex apparent power at the line sink terminal can be calculated.

$$\underline{S_2} = \underline{U_2} \cdot \underline{I_2^*} \tag{6.12}$$

The exponential form of the current conjugate in (6.12) is represented by

$$\underline{I_2^*} = \underline{U_2^*} \cdot \underline{D^*} - \frac{U_1}{Z} \cdot e^{j(\varphi_Z - \varphi_{U_1})} \tag{6.13}$$

This leads to

$\underline{S_2} = \underline{U_2} \cdot \left(\underline{U_2^*} \cdot \underline{D^*} - \frac{U_1}{Z} \cdot e^{j(\varphi_Z - \varphi_{U_1})}\right)$, which is further developed to

$$\underline{S_2} = \underline{U_2^2} \cdot \mathrm{D} \cdot \mathrm{e}^{\mathrm{j}(-\varphi_\mathrm{D})} - \frac{\mathrm{U_1 U_2}}{\mathrm{Z}} \cdot e^{j(\varphi_Z + \varphi_{U_2} - \varphi_{U_1})} \tag{6.14}$$

The real part of the calculated complex apparent power represents the active power transferred to the transmission line sink terminal. This is found as:

$$P_2 = \underline{U_2^2} \cdot \mathrm{D} \cdot \cos(-\varphi_\mathrm{D}) - \frac{\mathrm{U_1 U_2}}{\mathrm{Z}} \cdot \cos\left(\varphi_Z + \varphi_{\mathrm{U_2}} - \varphi_{U_1}\right) \qquad (6.15)$$

The visualization of the stability status is made on the base of a PU-curve. The consideration of the reactive power is foregone. If needed, it can be found as the imaginary part of the complex apparent power.
The equation (3.17) comprises the difference between the source and the sink voltage angles. This difference can be expressed as:

$$\Delta\varphi = \varphi_{\mathrm{U_2}} - \varphi_{U_1} \qquad (6.16)$$

Using the known property of the cosine function: $\cos(-\varphi_D) = \cos(\varphi_D)$ and taking equation (6.16) in account, the equation (6.15) of the transferred active power can be rewritten into:

$$P_2 = \underline{U_2^2} \cdot \mathrm{D} \cdot \cos(\varphi_\mathrm{D}) - \frac{\mathrm{U_1 U_2}}{\mathrm{Z}} \cdot \cos(\varphi_Z + \Delta\varphi) \qquad (6.17)$$

6.4.3 Validation of the developed equations

A routine for the calculation of the transferred active power using equation (6.17) is included in AHT-Vstab. AHT-Vstab permits the visualization of the equations developed in this thesis. Although the calculations take place offline, real field PMU data measured on DK-VEST and transmission lines parameter data taken from the system model in PowerFactory® serve as input for the calculations and the tests of the applicability and robustness of the developed monitoring method. As field PMU data are not available for real voltage instability cases in DK-VEST, the instability tests realised in this work used only simulated phasors data from PowerFactory as input.

6.4.3.1 Comparison with field PMU data

The results of a calculation of the transferred active power on the transmission line between TJE5 and ASR5 in DK-VEST monitored by the PMU 2 (see figure 6.2) using AHT-Vstab, are compared with the active power values obtained by the online tool for PMU data presentation (ENDK Tool) used by Energinet.dk. The resulting active power curves are presented in the figure 6.12 for the 13th of January 2007 from 13:00 pm until 13:06 pm.

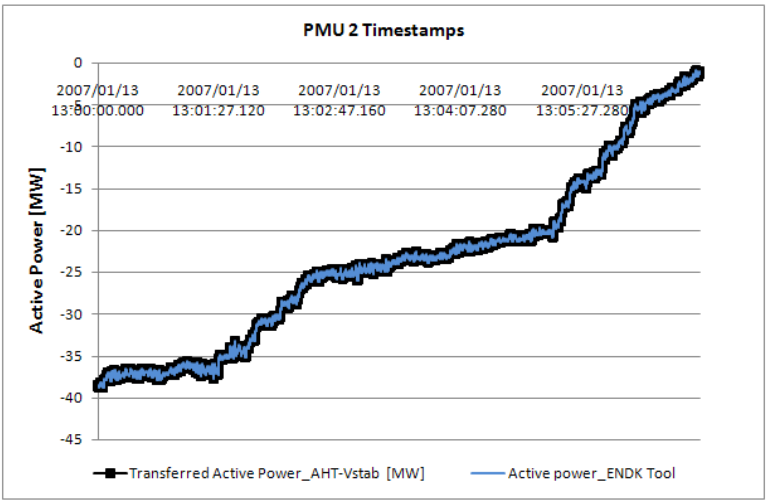

Figure 6.12: Comparison of the calculated active power by AHT-Vstab and ENDK Tool using PMU data from TJE5 measured on 13th , January 2007 from 13:00 pm until 13:06 pm.

The negative sign of the active power shows that the energy in flowing in the direction opposite to the positive measuring direction of the PMU 2, i.e.: from ASR5 to TJE5.

The curves in figure 6.12 are almost equal to each other; a difference is hardly discernable so that a curve representing the differences between each point of the active power curves is represented in figure 6.13 for more clarity.

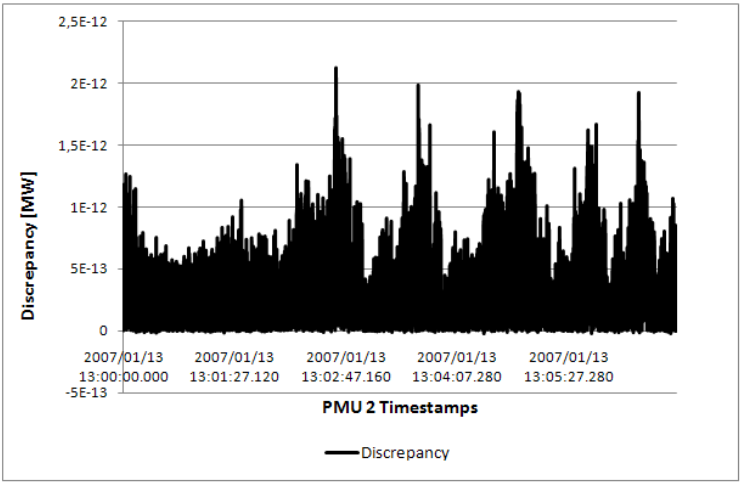

Figure 6.13: Differences between the calculated active power by AHT-Vstab and ENDK Tool using PMU data from TJE5 measured on 13th of January 2007 from 13:00 pm until 13:06 pm.

The differences which occurred can be due to software specific features. These differences are nevertheless almost equal to "0" for the entire time span chosen. The validity of the equation (6.17) is thus proven.

6.4.3.2 Comparison with simulated PMU data

In the previous section the positioning of the PMU 2 in DK-VEST and the active power flow direction shows that the PMU is placed at the line sink terminal. The problem of the determination of the power flow direction and of the terminal phasors values used for the calculations is treated in a further paragraph of this work. In forefront is can be said that the current and voltage phasors directly measured by the PMU 2 are used for the calculation of the active power with AHT-Vstab in figure 6.12.

On the other hand the development of the equation 6.17 is made with the assumption that the phasors data are known or measured only at one line terminal (with the index 1) and then calculated for the other side (with the index 2). This theory is consolidated in this section and the validity of the equations (6.7) and (6.11) respectively used for the voltage and the current phasors calculation is verified additionally to the verification of the active power formula. The verification takes place as the comparison of some with AHT-Vstab calculated and with Powerfactory® simulated time characteristics.

For this purpose a generator outage event was simulated on DK-Vest. The resulting simulated phasors characteristics were then further compared with the calculated curves. The latest are the results of a calculation in AHT-Vstab, based on the developed formulas and using the simulated phasor data sets from PowerFactory® as input.

The generator NVJB2 is put out-of-service at 0,2 seconds and in-service again at 0,6 seconds of a total simulation time of 2 seconds.

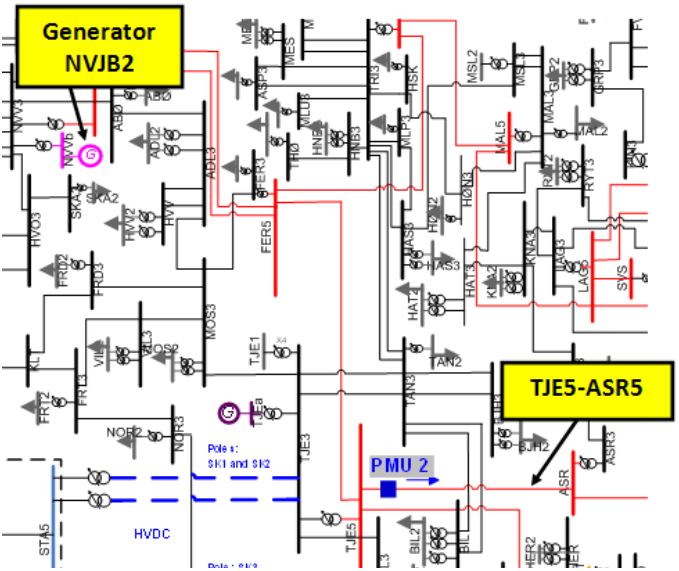

Figure 6.14: Abridgement of the single line representation of DK-VEST with the considered generator

The time characteristics (magnitudes and phase angles) obtained for the line between TJE5 and ASR5 (see figure 6.14) with ASR5 defined as the sink terminal are illustrated. Whereby calculated and simulated phasors characteristics are separately represented. Simulated characteristics are directly outputted by PowerFactory® for ASR5 whereas calculated characteristics are the results of the phasor calculations for ASR5 on the base of the formulas developed above, by using the phasors values outputted by PowerFactory for TJE5.

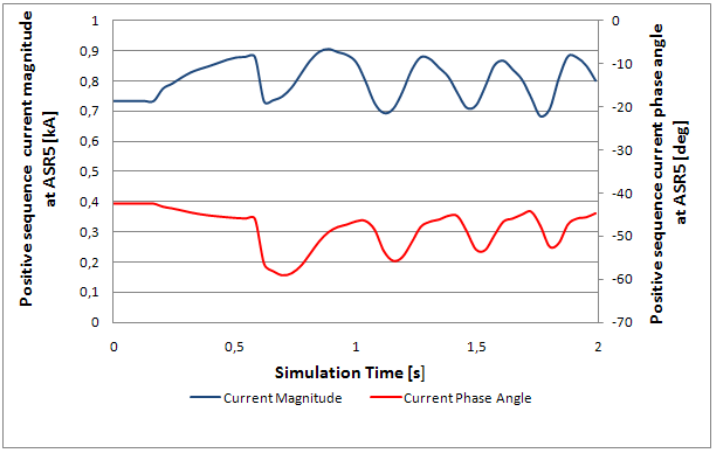

Figure 6.15: Simulated complex current at ASR5 by the outage of NVJB2

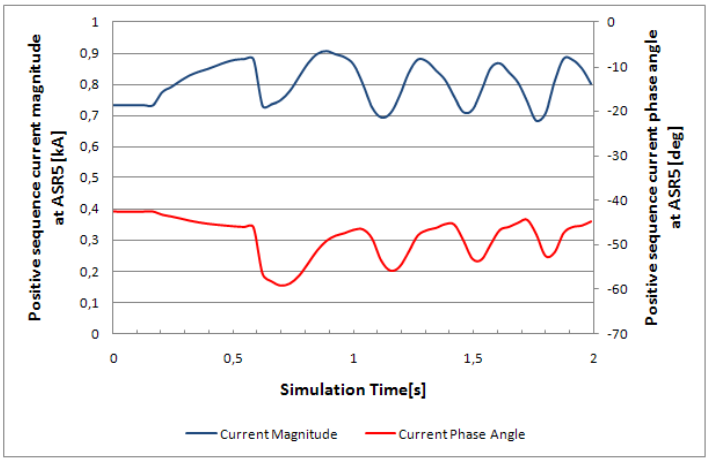

Figure 6.16: Calculated complex current at ASR5 by the outage of NVJB2

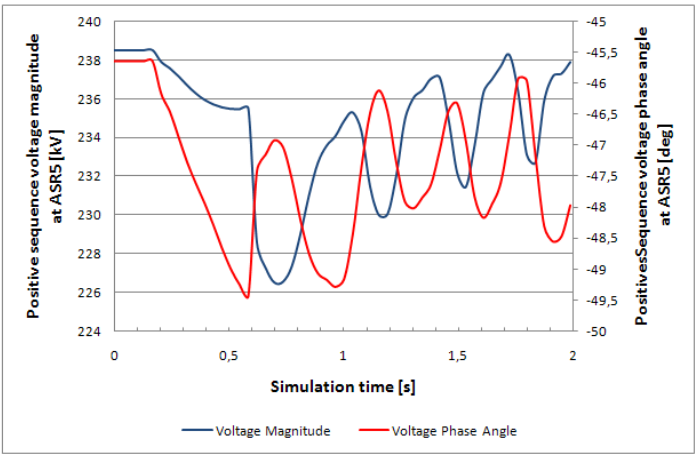

Figure 6.17: Simulated complex voltage at ASR5 by the outage of NVJB2

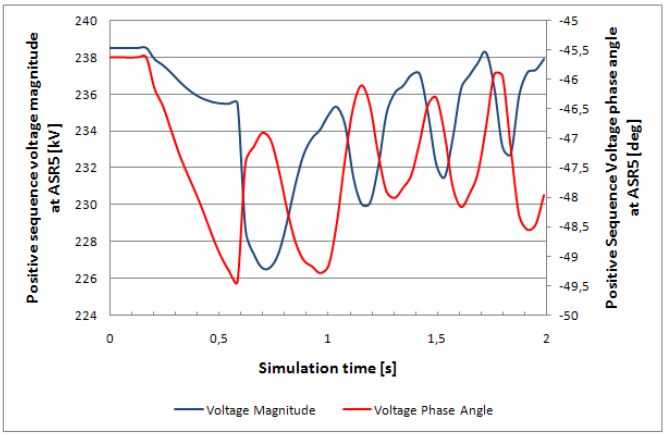

Figure 6.18: Calculated complex voltage at ASR5 by the outage of NVJB2

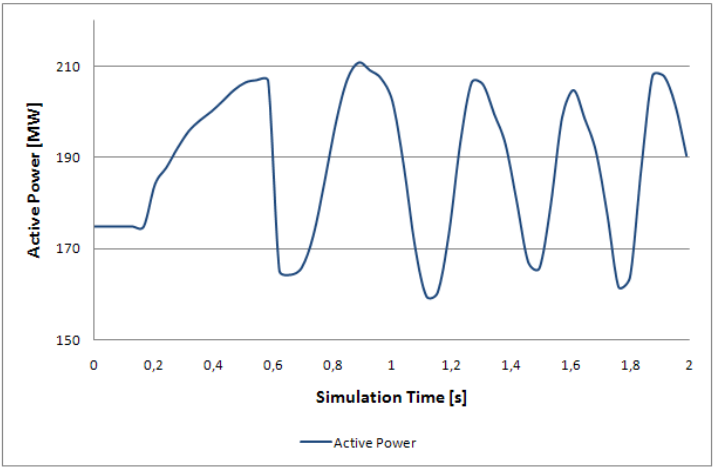

Figure 6.19: Simulated active power at ASR5 by the outage of NVJB2

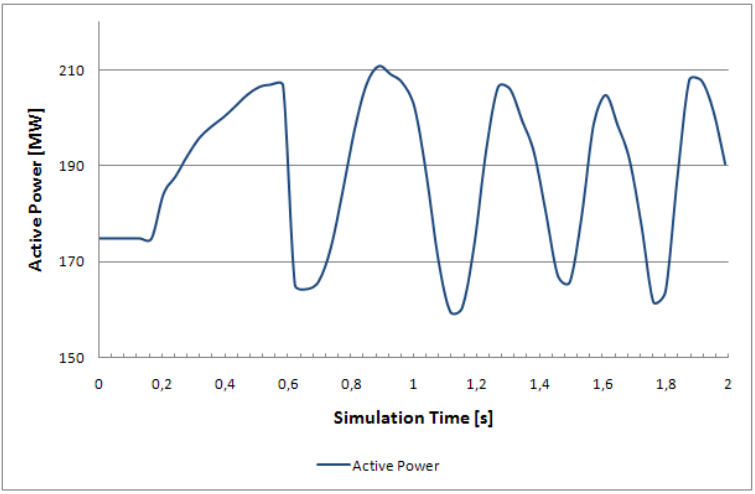

Figure 6.20: Simulated active power at ASR5 the outage of NVJB2

Also in this case the calculation of the discrepancy between the simulated and the calculated characteristics of the active power shows the differences between each point of the curves.

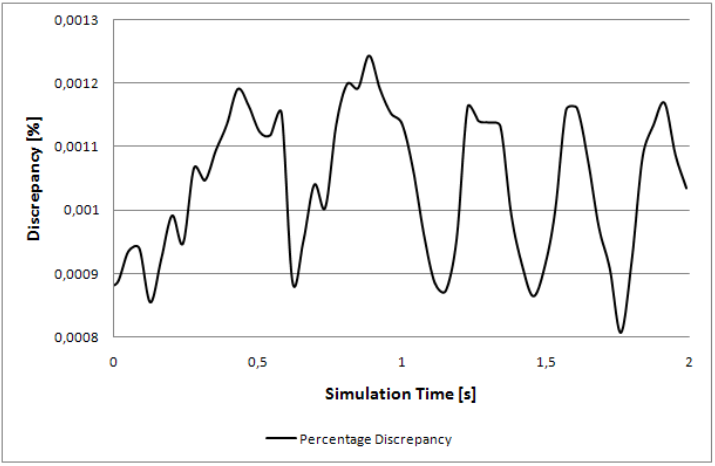

Figure 6.21: Differences between the simulated and the calculated active power at ASR5 by the outage of NVJB2

The concordance between the simulated and the calculated active power is proven by the negligible discrepancy obtained between the simulated and the calculated active powers by a simulated generator outage on DK-VEST. The differences observed can also in this case result from the specific features of the calculation tools used. Taking in account that, the results provided by the power systems calculation tools (e.g.: PowerFactory) are nowadays considered as trustful and are generally well accepted in the field of power systems analysis, the minimal differences in figure 6.21 demonstrate the validity of the developed equations.

6.5 Mathematical characterisation of the electric power transfer on a transmission path

6.5.1 Transmission line operating characteristic

Further in this work the source and sink terminal will be respectively termed as usually in the specialised literature as: the ***sending end*** (index s) and the ***receiving end*** (index R). The sending end is the terminal where the active power flows into a given line and the receiving end the bus where the active goes out of the line. The receiving end is usually named the load bus. This is right in the sense that virtually considered, the power is generated at the line considered sending end, transported by the transmission line and finally drawn at the line receiving end towards the consumer(s) or load(s).

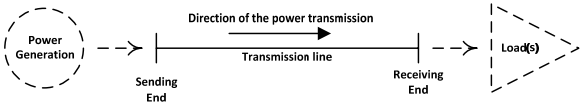

Figure 6.22: Schema of the power transmission

According to the changes in the energy flow direction on one line during the grid operation, the denomination of a given line terminals are interchangeable. Considering the one line representation of a given power system the connection of two transmission line in series (i.e.: TJE5-ASR5 and ASR5-REV5 in figure 6.2) does not automatically means that the receiving end of the first line is the sending end of the next. This is particularly true for meshed power systems. The direction of the energy flow on each line in such power systems must be separately defined for each system operating instant.

As stated earlier the loads are the driving factor of voltage instability. Based on this assumption, the method developed in this thesis concentrates on the assessment of the voltage stability situation on the load side of each power line of the transmission system as induced by the real time power transfer circumstances. The recognition of the energy flow direction is therefore primordial in this work and will be discussed in a further paragraph.

The influence of the load situation on the power transfer can be well represented by the power angle at the receiving end. This angle describes the relation of the active power to the reactive power at this node of the grid at each instant. The power angle (load angle in this thesis) is defined by the imaginary part of the introduced apparent load impedance $\underline{Z}_v$ connected at the line receiving end. This approach is also used in [29], [97], and [145]. The index "v" is used to point out the virtuality of this element.

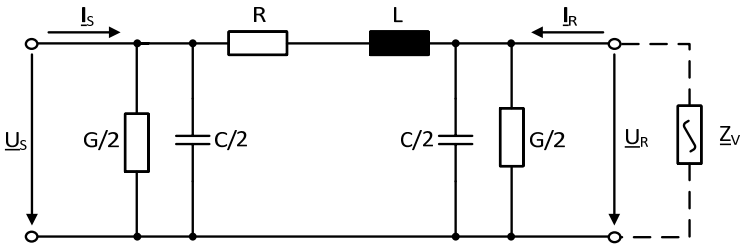

Figure 6.23: π- equivalent circuit of a transmission line with lumped parameters with connected load impedance

As a complex value the load impedance is written as

$$\underline{Z}_v = Z_v \cdot e^{j\varphi_{Z_v}} \tag{6.18}$$

Whereby the magnitude Z_v is considered as a variable parameter and the argument φ_{Z_v} is presumed to be a constant parameter.
In the next step the dependency of the complex voltage at the receiving end to the load impedance is described.

$$\underline{U}_R = \underline{U}_S \cdot \frac{\dfrac{1}{\dfrac{1}{\underline{Z}_v} + j\dfrac{\omega C}{2} + \dfrac{G}{2}}}{R + j\omega L + \dfrac{1}{\dfrac{1}{\underline{Z}_v} + j\dfrac{\omega C}{2} + \dfrac{G}{2}}} =$$

$$= \underline{U}_S \cdot \frac{\underline{Z}_v}{\underline{Z}_v\left[1 + \frac{RG}{2} + j\omega\left(\frac{RC}{2} + \frac{LG}{2}\right) - \omega^2\frac{LC}{2}\right] + R + j\omega L} \tag{6.19}$$

Considering equation (6.6.2), the equation (6.19) is simplified to

$$\underline{U}_R = \underline{U}_S \cdot \frac{\underline{Z}_v}{\underline{Z}_v[K] + R + j\omega L} \tag{6.19.1}$$

The resulting magnitude of the voltage at the line receiving end is calculated as

$$U_R = \frac{Z_v U_S}{\sqrt{\left(Z_v \cdot K \cdot cos\left(\varphi_{Z_v} + \varphi_K\right) + R\right)^2 + \left(Z_v \cdot K \cdot sin\left(\varphi_{Z_v} + \varphi_K\right) + \omega L\right)^2}} \tag{6.20}$$

The definition of the active power is made again through the definition of the apparent power at the receiving end

$$\underline{S}_R = \underline{U}_R \cdot \underline{I}_R^*.$$

The current at the receiving end is calculated as

$$\underline{I}_R = -\frac{\underline{U}_R}{\underline{Z}_v} \tag{6.21}$$

Its insertion in the expression of the apparent power one yields

$$\underline{S}_R = -\frac{U_R^2}{Z_v} \cdot e^{j\varphi_{Z_v}} = \frac{U_R^2}{Z_v} \cdot e^{j\varphi_{Z_v}} \cdot e^{j\pi} = \frac{U_R^2}{Z_v} \cdot e^{j(\varphi_{Z_v} + \pi)} \tag{6.22}$$

Putting equation (6.20) in (6.22) leads to the expression of the apparent power as a function of the load impedance.

$$\underline{S_R} = \\ = \frac{Z_v U_S^2}{\left(Z_v \cdot K \cdot cos\left(\varphi_{Z_v} + \varphi_K\right) + R\right)^2 + \left(Z_v \cdot K \cdot sin\left(\varphi_{Z_v} + \varphi_K\right) + \omega L\right)^2} e^{j\left(\varphi_{Z_v} + \pi\right)} \tag{6.23}$$

The real part of (6.26) is the active power flow at the receiving end, expressed as a function of the load impedance.

$$P_R = \frac{Z_v U_S^2}{\left(Z_v \cdot K \cdot cos\left(\varphi_{Z_v} + \varphi_K\right) + R\right)^2 + \left(Z_v \cdot K \cdot sin\left(\varphi_{Z_v} + \varphi_K\right) + \omega L\right)^2} \cdot \\ \cdot \ cos\left(\varphi_{Z_v} + \pi\right) \tag{6.24}$$

Taking the property $cos\left(\varphi_{Z_v} + \pi\right) = -cos\left(\varphi_{Z_v}\right)$ the equation (6.24) is transformed into

$$P_R = -\frac{Z_v U_S^2}{\left(Z_v \cdot K \cdot cos\left(\varphi_{Z_v} + \varphi_K\right) + R\right)^2 + \left(Z_v \cdot K \cdot sin\left(\varphi_{Z_v} + \varphi_K\right) + \omega L\right)^2} cos\left(\varphi_{Z_v}\right) \tag{6.25}$$

The equation (6.20) is equivalent to

$$\sqrt{\left(Z_v \cdot K \cdot cos\left(\varphi_{Z_v} + \varphi_K\right) + R\right)^2 + \left(Z_v \cdot K \cdot sin\left(\varphi_{Z_v} + \varphi_K\right) + \omega L\right)^2} \\ = \frac{Z_v U_S}{U_R} \tag{6.26}$$

Squaring both sides of (6.26) gives

$$\left(Z_v \cdot K \cdot cos\left(\varphi_{Z_v} + \varphi_K\right) + R\right)^2 + \left(Z_v \cdot K \cdot sin\left(\varphi_{Z_v} + \varphi_K\right) + \omega L\right)^2 \\ = \frac{Z_v^2 U_S^2}{U_R^2} \tag{6.26.1}$$

The denominator of (6.26) is then replaced by (6.26.1)

$$P_R = -\frac{U_S^2 Z_v cos(\varphi_{Z_v})}{\frac{Z_v^2 U_S^2}{U_R^2}} = -\frac{U_R^2\, cos(\varphi_{Z_v})}{Z_v} \tag{6.27}$$

Equation (6.27) is then solved for Z_v

$$Z_v = -\frac{U_R^2\, cos(\varphi_{Z_v})}{P_R} \tag{6.28}$$

The value of the load impedance magnitude in (6.28) is then reintroduced in (6.25) to give

$$P_R = \frac{U_S^2\left[\frac{U_R^2 cos(\varphi_{Z_v})}{P_R}\right]\cdot cos(\varphi_{Z_v})}{\left[-\frac{U_R^2 cos(\varphi_{Z_v})}{P_R}K\cdot cos(\varphi_{Z_v}+\varphi_K)+R\right]^2+\left[-\frac{U_R^2 cos(\varphi_{Z_v})}{P_R}K\cdot sin(\varphi_{Z_v}+\varphi_K)+\omega L\right]^2} =$$
$$\frac{\left[\frac{U_R^2 U_S^2 cos^2(\varphi_{Z_v})}{P_R}\right]}{\frac{U_R^4 cos^2(\varphi_{Z_v})K^2\cdot cos^2(\varphi_{Z_v}+\varphi_K)}{P_R^2}-\frac{2U_R^2 KR\cdot cos(\varphi_{Z_v})}{P_R}+R^2+\frac{U_R^4 cos^2(\varphi_{Z_v})K^2\cdot sin^2(\varphi_{Z_v}+\varphi_K)}{P_R^2}-\frac{2U_R^2 K\omega L\cdot sin(\varphi_{Z_v})}{P_R}+(\omega L)^2} =$$
$$\frac{\left[\frac{U_R^2 U_S^2 cos^2(\varphi_{Z_v})}{P_R}\right]}{\frac{U_R^4 cos^2(\varphi_{Z_v})K^2}{P_R^2}[cos^2(\varphi_{Z_v}+\varphi_K)+sin^2(\varphi_{Z_v}+\varphi_K)]+[R^2+(\omega L)^2]-\frac{2U_R^2\cdot cos(\varphi_{Z_v})K}{P_R}[R\cdot cos(\varphi_{Z_v}+\varphi_K)+\omega L\cdot sin(\varphi_{Z_v}+\varphi_K)]} \tag{6.29}$$

The property $\left[cos^2(\varphi_{Z_v}+\varphi_K)+sin^2(\varphi_{Z_v}+\varphi_K)\right]=1$ and the assumption $[R^2+(\omega L)^2]=Z^2$ lead to

$$P_R = \frac{U_R^2 U_S^2 cos^2(\varphi_{Z_v})}{\frac{U_R^4 cos^2(\varphi_{Z_v})K^2}{P_R}+P_R Z^2-2U_R^2\cdot cos(\varphi_{Z_v})K\cdot\left[Rcos(\varphi_{Z_v}+\varphi_K)+\omega Lsin(\varphi_{Z_v}+\varphi_K)\right]} \tag{6.30}$$

The equation (6.30) is resolved to

$$U_R^4 cos^2(\varphi_{Z_v})K^2+P_R^2 Z^2-2U_R^2 P_R\cdot\ cos(\varphi_{Z_v})\cdot\left[Rcos(\varphi_{Z_v}+\varphi_K)+\omega Lsin(\varphi_{Z_v}+\varphi_K)\right]=$$
$$U_R^2 U_S^2 cos^2(\varphi_{Z_v}) \tag{6.31}$$

Equation (6.31) can further be transformed to

$$U_R^4 cos^2(\varphi_{Z_v})K^2 + U_R^2\left[-2P_R \cdot cos(\varphi_{Z_v})K\left[Rcos(\varphi_{Z_v}+\varphi_K)+\omega Lsin(\varphi_{Z_v}+\varphi_K)\right]-U_S^2 cos^2(\varphi_{Z_v})\right]+P_R^2Z^2=0$$

This is equivalent to:

$$U_R^4 + U_R^2\left[-\frac{2P_R}{cos(\varphi_{Z_v})K}\cdot\left[Rcos(\varphi_{Z_v}+\varphi_K)+\omega Lsin(\varphi_{Z_v}+\varphi_K)\right]-\frac{U_S^2}{K^2}\right]+\frac{P_R^2Z^2}{cos^2(\varphi_{Z_v})K^2}=0 \quad (6.32)$$

Substituting $B = U_R^2$ in equation in (6.32) one gets

$$B^2 + B\left[-\frac{2P_R}{cos(\varphi_{Z_v})K}\cdot\left[Rcos(\varphi_{Z_v}+\varphi_K)+\omega Lsin(\varphi_{Z_v}+\varphi_K)\right]-\frac{U_S^2}{K^2}\right]+\frac{P_R^2Z^2}{cos^2(\varphi_{Z_v})K^2}=0 \quad (6.33)$$

The solutions of (6.33) are

$$B_{1,2}=\frac{P_R}{cos(\varphi_{Z_v})K}\left[Rcos(\varphi_{Z_v}+\varphi_K)+\omega Lsin(\varphi_{Z_v}+\varphi_K)\right]+\frac{U_S^2}{K^2}\pm \pm\sqrt{\left[\frac{P_R}{cos(\varphi_{Z_v})K}\cdot\left[Rcos(\varphi_{Z_v}+\varphi_K)+\omega L\cdot sin(\varphi_{Z_v}+\varphi_K)\right]+\frac{U_S^2}{2K^2}\right]^2-\frac{P_R^2Z^2}{cos^2(\varphi_{Z_v})K^2}} \quad (6.34)$$

After re-substitution the solutions for the voltage at the receiving end U_R are found. Mathematically seen U_R is an absolute value. For this reason only the positive solution is taken in account.

$$U_R=\sqrt{\frac{P_R}{cos(\varphi_{Z_v})K}\cdot\left[Rcos(\varphi_{Z_v}+\varphi_K)+\omega L\cdot sin(\varphi_{Z_v}+\varphi_K)\right]+\frac{U_S^2}{2K^2}\cdots \cdots\pm\sqrt{\left[\frac{P_R}{cos(\varphi_{Z_v})K}\cdot\left[Rcos(\varphi_{Z_v}+\varphi_K)+\omega L\cdot sin(\varphi_{Z_v}+\varphi_K)\right]+\frac{U_S^2}{2K^2}\right]^2-\frac{P_R^2Z^2}{cos^2(\varphi_{Z_v})K^2}}} \quad (6.35)$$

The equation (6.35) is the operating characteristic of a transmission line. It represents the system operating states at its receiving end. It describes accurately the interdependency between the terminal voltage and the active power at each measured instant. It is also a function of the transmission line parameters and of the load impedance angle.

6.5.2 Load impedance angle

The Load impedance angle φ_{Z_v} is included in the equation (6.35) as an unknown variable. In the following a formula for its calculation is given. This is done on the base of the following equivalent circuit.

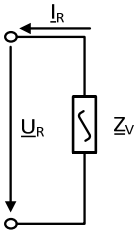

Figure 6.24: Load Impedance

For this configuration

$$\underline{I}_R \cdot \underline{Z}_v = -\underline{U}_R \tag{6.36}$$

Resolved for $\underline{Z}_v$, equation (6.36) becomes

$$\underline{Z}_v = -\frac{\underline{U}_R}{\underline{I}_R} \tag{6.37}$$

The representation in polar form is

$$\underline{Z}_v = Z_v \cdot e^{j\varphi_{Z_v}} = -\frac{U_R}{I_R} \cdot e^{j\left(\varphi_{U_R} - \varphi_{I_R}\right)} = \frac{U_R}{I_R} \cdot e^{j\left(\varphi_{U_R} - \varphi_{I_R} + \pi\right)} \tag{6.38}$$

After a coefficients comparison the load impedance is defined as:

$$\varphi_{Z_v} = \varphi_{U_R} - \varphi_{I_R} + \pi \tag{6.39}$$

6.6 Transmission line transfer capacity

6.6.1 Transmission line operating characteristic curve

A graphical representation of the mathematical results from the previous paragraph is proposed. For this purpose following line and constant parameters values are freely chosen:

Table 6.1: Parameters values for the theoretical illustration of power line operating characteristic curve

U_S	K	φ_k	ω	R	X	φ_{Z_v}
230 kV	1	0	$2\pi \cdot 50\ s^{-1}$	$1.86\ \Omega$	22.93Ω	$\in \{-50:5:50\}\ deg$

The load impedance angle φ_{Z_v} varies from -50° to 50° with a step interval of 5°. In reality the limits for this angle are respectively -90° and 90°. A positive load impedance angle indicates an inductive loading at the line terminal considered.

The operating curves resulting from the equation (6.35) using the data from the table 6.1 are shown in the next figure 6.25.

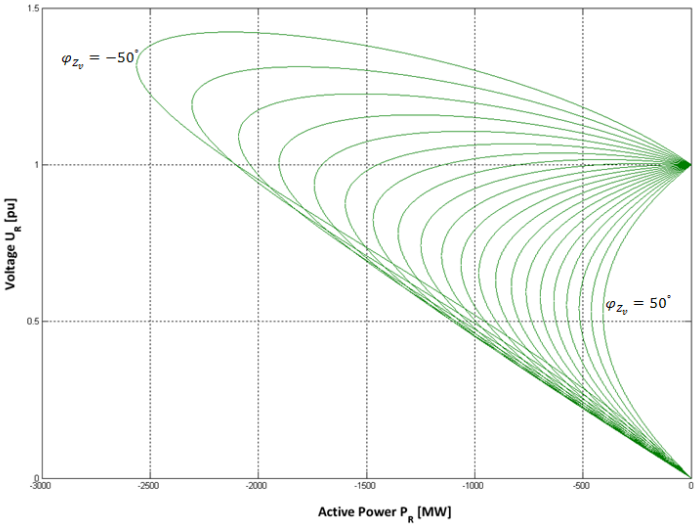

Figure 6.25: Transmission line operating characteristic curves for different values of the load angle

The line operation characteristics obtained are PU-curves represented for the line receiving end. The theoretical description is similar as made for the PU-curves obtained in subparagraph 3.2.5.1 of this work. Also for the curves resulting from equation (6.35), a stable region (upper branch) is separated from an unstable region (lower branch) by the vertex point of the parabola. The behavior of the curvatures changes badly each after the vertex point. This point is then the critical point from which the line transfer stability is jeopardized. This issue is discussed in 3.2.5.1 with more details. Thereby a particular accent is done on the concrete manifestation of this kind of instability on the electrical power transfer mode. An ascertainment is that, the shape of the line operating curves in figure 6.25 and hence the respective vertex values are influenced by the value of the apparent load impedance. The vertex reduces as the load impedance angle increases.

6.6.2 Transmission line maximal loading

At the vertex point both half-functions of equation (6.35) have one and the same solution. For a given load impedance angle, the coordinates of this point thus correspond to a unique point. In regard to the stability of the transfer mode these coordinates can be termed as: (P_{Rmax}, U_{Rmin}) for the maximum transferable active power by a corresponding minimal acceptable voltage value, for a stable transmission of the electric energy.

Outgoing from the assumed mathematical condition for the existence of a unique solution by a quadratic equation, the ansatz chosen to calculate the vertex coordinates is the nullification of the internal square-root term of (6.38).

$$\sqrt{\left[\frac{P_{Rmax}}{cos(\varphi_{Z_v})K}\cdot\left[Rcos(\varphi_{Z_v}+\varphi_K)+\omega L\cdot sin(\varphi_{Z_v}+\varphi_K)\right]+\frac{U_S^2}{2K^2}\right]^2-\frac{P_{Rmax}^2Z^2}{cos^2(\varphi_{Z_v})K^2}}=0 \tag{6.40}$$

Further mathematical steps lead to

$$\left[\frac{P_{Rmax}}{cos(\varphi_{Z_v})K}\cdot\left[Rcos(\varphi_{Z_v}+\varphi_K)+\omega L\cdot sin(\varphi_{Z_v}+\varphi_K)\right]+\frac{U_S^2}{2K^2}\right]^2-\frac{P_{Rmax}^2Z^2}{cos^2(\varphi_{Z_v})K^2}=0 \tag{6.40.1}$$

$$\left[\frac{P_{Rmax}}{cos(\varphi_{Z_v})K}\cdot\left[Rcos(\varphi_{Z_v}+\varphi_K)+\omega L\cdot sin(\varphi_{Z_v}+\varphi_K)\right]+\frac{U_S^2}{2K^2}\right]^2=\frac{P_{Rmax}^2Z^2}{cos^2(\varphi_{Z_v})K^2} \tag{6.40.2}$$

Considering $\left[cos(\varphi_{Z_v}+\pi)\right]^2=\left[-cos(\varphi_{Z_v})\right]^2=\left[cos(\varphi_{Z_v})\right]^2$, the equation (6.40.2) is reduced to:

$$\frac{P_{Rmax}}{cos(\varphi_{Z_v})K}\cdot\left[Rcos(\varphi_{Z_v}+\varphi_K)+\omega L\cdot sin(\varphi_{Z_v}+\varphi_K)\right]+\frac{U_S^2}{2K^2}=\frac{P_{Rmax}\cdot Z}{cos(\varphi_{Z_v})K} \tag{6.40.3}$$

The resolution of (6.40.3) in regard to P_{Rmax} gives

$$P_{Rmax} \cdot \left[R cos\left(\varphi_{Z_v} + \varphi_K\right) + \omega L \cdot sin\left(\varphi_{Z_v} + \varphi_K\right)\right] + \frac{U_S^2 \cdot cos\left(\varphi_{Z_v}\right)}{2K} = -P_{Rmax} \cdot Z \tag{6.40.4}$$

$$P_{Rmax} \cdot \left[R cos\left(\varphi_{Z_v} + \varphi_K\right) + \omega L \cdot sin\left(\varphi_{Z_v} + \varphi_K\right) + Z\right] = \frac{U_S^2 \cdot cos\left(\varphi_{Z_v}\right)}{2K} \tag{6.40.5}$$

And finally

$$P_{Rmax} = -\frac{U_S^2 \cdot cos\left(\varphi_{Z_v}\right)}{2K \cdot \left[R cos\left(\varphi_{Z_v} + \varphi_K\right) + \omega L \cdot sin\left(\varphi_{Z_v} + \varphi_K\right) + Z\right]} \tag{6.41}$$

The voltage corresponding to the maximal transferable active power is then easily calculated considering the internal square-root term in (6.35) as equal to zero.

$$U_{Rmin} = \sqrt{\frac{P_R}{cos\left(\varphi_{Z_v}\right)K} \cdot \left[R cos\left(\varphi_{Z_v} + \varphi_K\right) + \omega L \cdot sin\left(\varphi_{Z_v} + \varphi_K\right)\right] + \frac{U_S^2}{2K^2}} \tag{6.42}$$

6.7 Tests of the detection of the transfer instability

The validity of the developed formulas for the maximal stable power transfer on a transmission line is demonstrated by the simulation of this type of instability on the two test systems. The instability direction chosen is the increase of the line loading. The test methodology is the following:

- Connection of an apparent load to one end of a given line in the digital grid model
- Dynamic simulation with automatic definition of a sequence of grid events. These events are constituted by the step increase of the active power of the apparent load. The variation of the load active power directly yields a variation in the line loading. The power flow direction is through the point of connection of the apparent load clearly defined
- Storage of the simulated voltage and current phasors at the line sending end
- Calculation of: the voltage and current phasors, the "actual" transferred power and the maximal stable transferable power at the line receiving end.

6.7.1 Simulation of the transfer instability in a two-bus test system

A case of transmission line (over)loading is simulated on the following two-bus test system. A model of this simple system is implemented in PowerFactory® for this purpose. This simple model has the principal advantage to exclude the influences of a bulk power system.

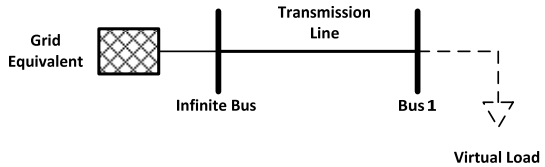

Figure 6.26: two-bus test system

Following line parameters are used:

Table 6.2: Data of the transmission line in the two bus system

$R'\ [\frac{\Omega}{km}]$	G'	$X'\ [\frac{\Omega}{km}]$	$C'\ [\frac{\mu F}{km}]$	$\ell\ [km]$
0.0269	0	0.3318	0.011	69.11

The line loading is achieved through the connection of a virtual load at bus 1 and its further increase at about 30 MW each 10 seconds from a start load value of 300 MW. The receiving end is at bus 1. During the simulation the positive-sequence phasors data are collected at the sending end (infinite bus). These are then combined to the relevant transmission line data for the calculation of the transferred active power (P_R) and of the line maximal loading (P_{Rmax}) at the receiving end (Bus1) using the equations (6.17) and (6.41). For the first equation the indices "1" and "2" are replaced by "R" and "S".

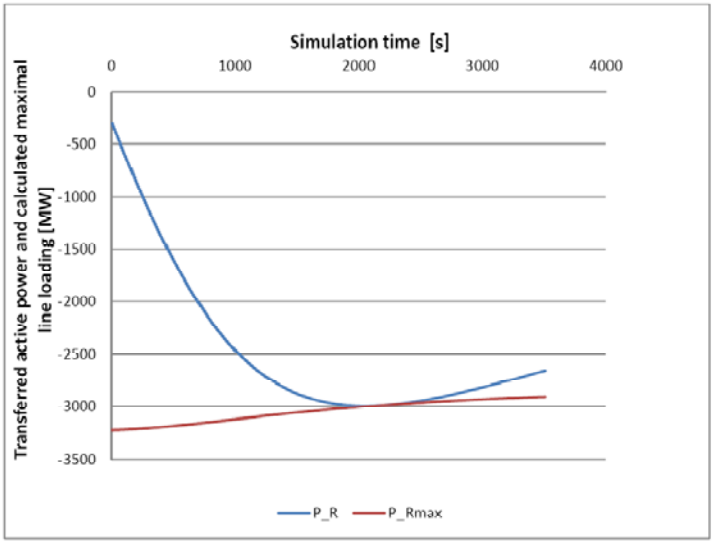

Figure 6.27: Illustration of the Occurrence of the transfer instability in the two-bus system

The constant increase in the line loading leads to an intersection zone between the curves of P_R and P_{Rmax} in figure 6.27. At these points their respective values are equal for the prevailing system and load states. After the intersection zone, a further increase in the load produces the opposite effect as before it. The transferred active power is reduced. In regard to the figure 6.25, the side of the curve P_R situated left to the intersection zone corresponds to the upper branch of the transmission line PU-curve. Accordingly the side right to the intersection zone described operation states located on the lower branch of the PU-curve.

6.7.1.1 Visualization

The visualization of the impending transfer instability is possible with the representation of the resulting PU-curves for each simulated data set. The PU-curves give only information on the value of the maximal loading found at their extreme point. As explained in chapter 3, the placement of the actual transfer point on this curve permits the easy calculation of the transfer stability margin (TSM) as the difference between the calculated values of the actual active power transferred and of the active power at the vertex (see equation: 3.11).

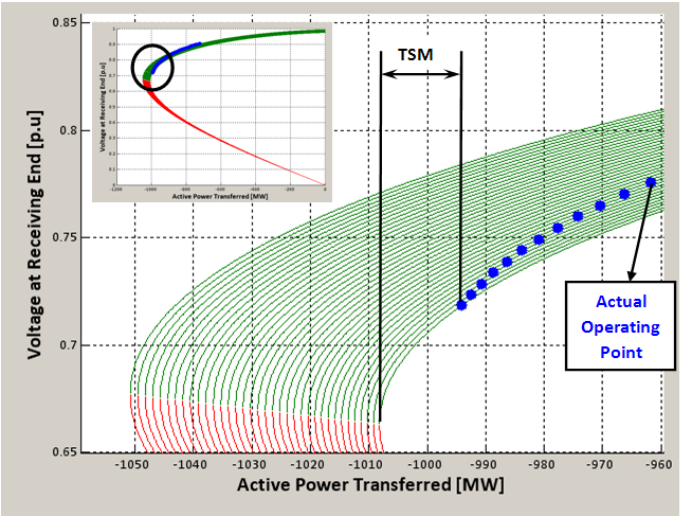

Figure 6.28: Visualization of the impending transfer instability in the two-bus system (succession of PU curves), realized with AHT-Vstab.

The figure 6.28 shows a snapshot of the evolution of the transfer stability status during the simulation on the two bus system. The voltage profile is firstly neglected for the voltage stability analysis. For each phasor set outputted by PowerFactory® at the infinite bus, a PU-curve is drawn for the receiving end in the positive direction of the power flow. Several PU-Curves are "retained" in the plotting region; they each represent the operating (transfer) characteristic at different simulation instants. The value of the actual active power transferred at the corresponding instant are automatically calculated and placed on the PU-curves as the actual operating point. The fact that the actual operating points are always exactly on their corresponding PU-curve indicates once more the exactitude of the calculations. The stable operating region is coloured in green whereas the unstable region is red. The TSM is shown for one operating instant. For a stable power transfer on a transmission line the following expression must be always true:

$$P_{Rmax} \leq P_R \leq 0 \qquad (6.43)$$

6.7.1.2 Impedances behaviour

The condition of occurrence of the transfer instability is suggested in paragraph 3.2.5 based on [29] as the equality of the magnitudes of the load impedance and of the transmission impedance. This assumption is verified equalizing the developed expressions of P_R and P_{Rmax}.

The following expressions are then reconsidered

$$P_{Rmax} = -\frac{U_S^2 \cdot cos(\varphi_{Z_v})}{2K \cdot \left[Rcos(\varphi_{Z_v} + \varphi_K) + \omega L \cdot sin(\varphi_{Z_v} + \varphi_K) + Z\right]} \tag{6.41}$$

and

$$P_R = -\frac{Z_v U_S^2}{\left(Z_v \cdot K \cdot cos(\varphi_{Z_v} + \varphi_K) + R\right)^2 + \left(Z_v \cdot K \cdot sin(\varphi_{Z_v} + \varphi_K) + \omega L\right)^2} \cdot cos(\varphi_{Z_v}) \tag{6.25}$$

$$P_{Rmax} = P_R \implies$$

$$\frac{1}{2K \cdot \left[Rcos(\varphi_{Z_v} + \varphi_K) + \omega L \cdot sin(\varphi_{Z_v} + \varphi_K) + Z\right]} =$$

$$= \frac{Z_v}{\left(Z_v \cdot K \cdot cos(\varphi_{Z_v} + \varphi_K) + R\right)^2 + \left(Z_v \cdot K \cdot sin(\varphi_{Z_v} + \varphi_K) + \omega L\right)^2}$$

After some mathematical steps the right side of the equality can be simplified to:

$$\frac{Z_v}{{Z_v}^2 K^2 + Z^2 + 2 \cdot K \cdot Z_v\left[R \cdot cos(\varphi_{Z_v} + \varphi_K) + \omega L \cdot sin(\varphi_{Z_v} + \varphi_K)\right]} =$$

$$\frac{1}{Z_v K^2 + \frac{Z^2}{{Z_v}^2} + 2 \cdot K \cdot \left[R \cdot cos(\varphi_{Z_v} + \varphi_K) + \omega L \cdot sin(\varphi_{Z_v} + \varphi_K)\right]}$$

This leads to the following new equality

$$2K \cdot \left[Rcos(\varphi_{Z_v} + \varphi_K) + \omega L \cdot sin(\varphi_{Z_v} + \varphi_K) + Z\right] =$$

$$= Z_v K^2 + \frac{Z^2}{{Z_v}^2} + 2 \cdot K \cdot \left[R \cdot cos(\varphi_{Z_v} + \varphi_K) + \omega L \cdot sin(\varphi_{Z_v} + \varphi_K)\right]$$

This is also simplified into

$Z_v K^2 + \frac{Z^2}{{Z_v}^2} - 2KZ = 0$ equivalent to the quadratic equation ${Z_v}^2 - \frac{2Z}{K} Z_v + \frac{Z^2}{K^2} = 0$

The solutions of this quadratic equation are

$$Z_{v\,1,2} = \frac{Z}{K} \pm \sqrt{\frac{Z^2}{K^2} - \frac{Z^2}{K^2}} = \frac{Z}{K}.$$

For a constant power angle, the equality $P_{Rmax} = P_R$ is reached when the load impedance becomes equal in magnitude to the transmission line impedance divided by the coefficient K. The next figure 6.29 illustrated these relationships for the instability simulation in the two bus system.

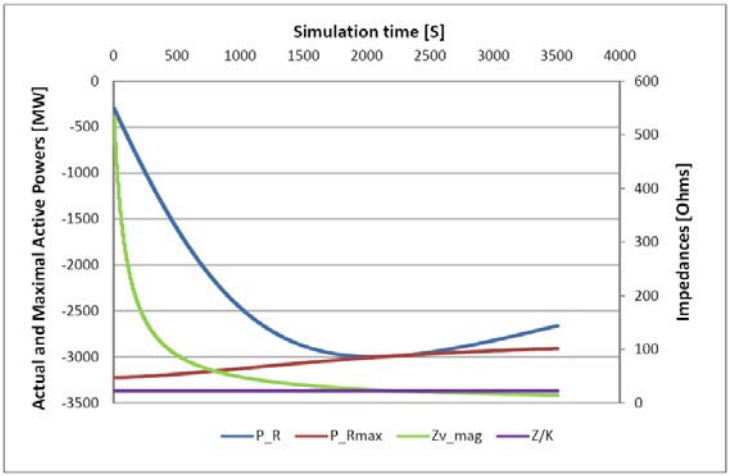

Figure 6.29: Comparison of the curves for active power and the system impedances by the simulation of the transfer instability on the two-bus system

According to the observed behaviour of the impedances, a transfer stability index is defined as

$$Z_v << \frac{Z}{K} \tag{6.44}$$

6.7.2 Simulation of the transfer instability in DK-VEST

Two simulations of the occurrence of the transfer instability are made for the line KAS5-REV5 (see Figure 6.2) in DK-VEST. The receiving end is defined at REV5. In the first simulation all equipment in the simulation model are in service (base case). For the second simulation the line between KAS5-LAG5 is set out of service. A step increase of an apparent load connected at REV5 in a 500 MW step size, beginning from 500 MW permits to achieve the loading of the line KAS5-REV5. The parameters of the line KAS5-REV5 are given in the table 6.3.

Table 6.3: Parameters data of the line KAS5-REV5 in DK-VEST

R $[\frac{\Omega}{km}]$	G'	$X\ [\frac{\Omega}{km}]$	$C'\ [\frac{\mu F}{km}]$	$\ell\ [km]$
1.47	0	18.068	0.01091	54.26

Similarly as for the two-bus system, the positive-sequence phasors data are collected at the sending end (KAS5). These are then combined to the transmission line data for the calculation of the transferred active power (P_R) and of the line maximal loading (P_{Rmax}) at REV5. The obtained time characteristics for P_R and P_{Rmax} are compared in the next figures.

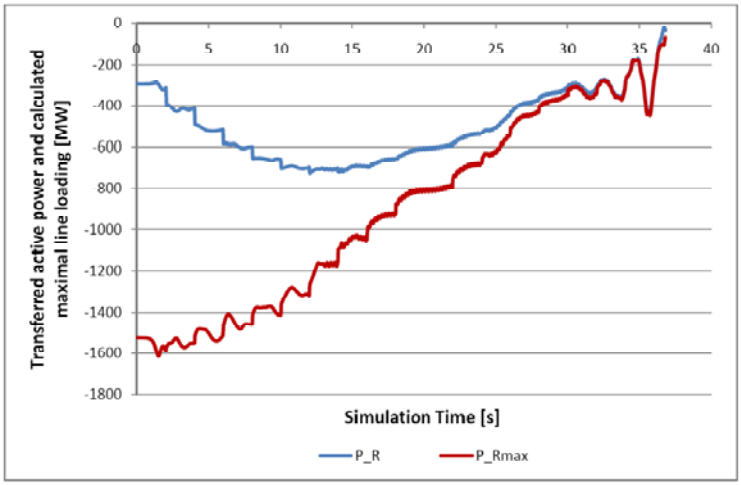

Figure 6.30: Illustration of the occurrence of the transfer instability on the line KAS5-REV5 in DK-VEST (base case)

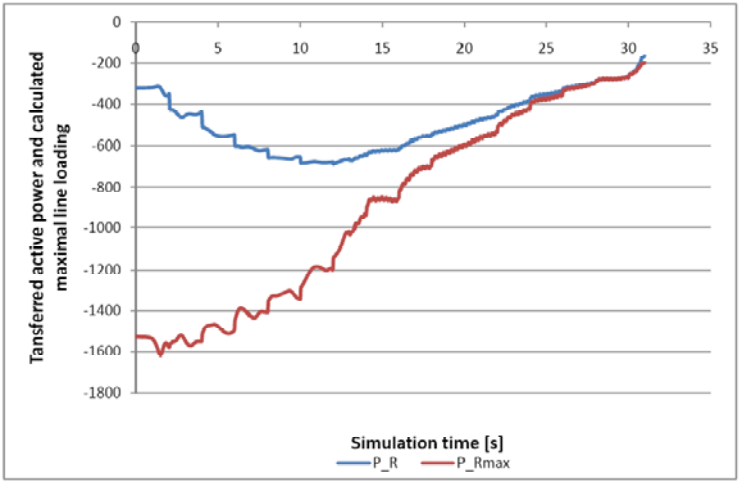

Figure 6.31: Illustration of the occurrence of the transfer instability on the line KAS5-REV5 in DK-VEST (Outage of KAS5-LAG5)

A comparison with the system impedances is also made for these cases

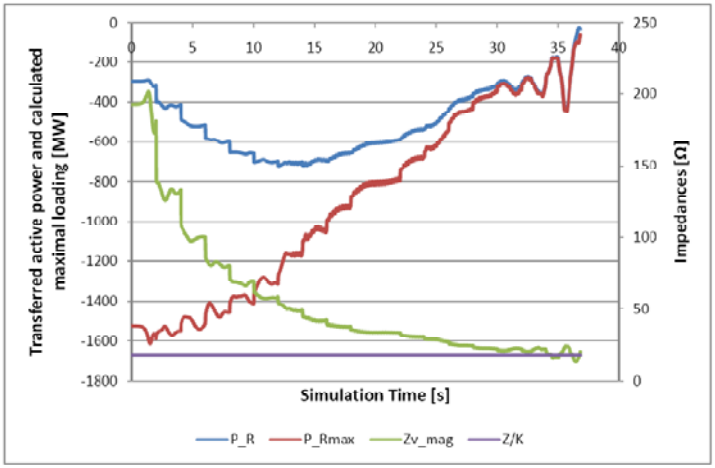

Figure 6.32: Comparison of the curves for active power and the system impedances by the simulation of the transfer instability on the line KAS5-REV5 in DK-VEST (base case)

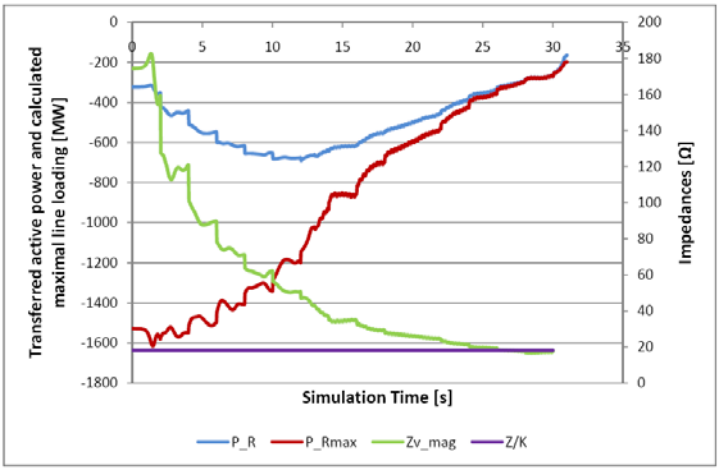

Figure 6.33: Comparison of the curves for active power and the system impedances by the simulation of the transfer instability on the line KAS5-REV5 in DK-VEST (Outage of KAS5-LAG5)

The test in a large system also shows a coincidence between P_R and P_{Rmax}. The calculation method permits also the finding of the transfer instability in large and meshed power systems. However the coincidence of the curves of P_R and P_{Rmax} presented in figures 30 and 31 is delayed and do not takes place at the exact point where the stability occurred. Previous investigations showed that the values of P_R are exactly defined by the developed formulas in all cases. The deviance result from some operational or practical inaccuracies in the calculation of P_{Rmax}, although this is mathematically correct. Reasons to this can be: the propagation of some rounding errors from the tools used for simulation and calculation, a certain influence of the rest of the system on the transmission line considered or the continuous changes in the voltage at the sending end. The last assumption is probably a decisive factor in the definition of the exact values of P_{Rmax}. This is demonstrated by the illustration of the voltages curves at both line terminals for the simulations on the two-bus system and on DK-VEST respectively.

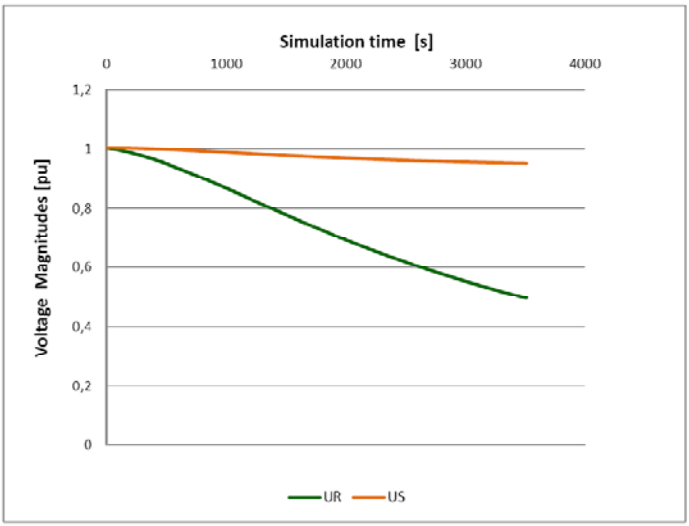

Figure 6.34: Voltage Magnitudes at the infinite bus (US) and at bus 1 (UR) during the simulation of the transfer instability on the two bus system

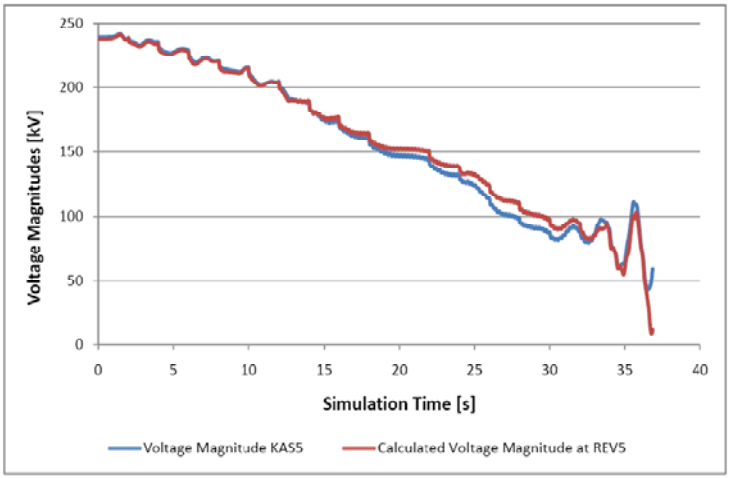

Figure 6.35: Voltage Magnitudes at KAS5 (sending End) and at REV5 during the simulation of the transfer instability on DK-VEST (base case)

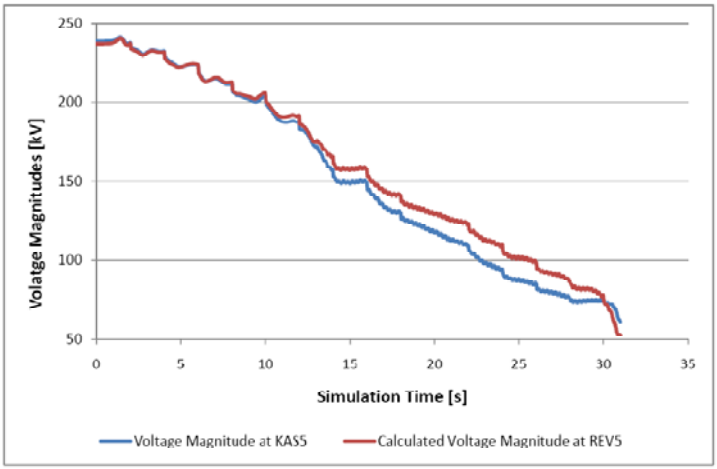

Figure 6.36: Voltage Magnitudes at KAS5 (sending End) and at REV5 during the simulation of the transfer instability on DK-VEST (Outage of KAS5-LAG5)

In the case of the two bus system the strong grid equivalent maintains the voltage at the infinite almost constant. In both simulations cases in DK-VEST the voltage at KAS5 sinks along with the voltage at REV5. This behaviour is particular to highly meshed power systems.
Much work must be done to study the systems influences on the lines terminals during its operation in order to optimize the practical calculation of P_{Rmax}. The goal of such a study could be the definition of a corrector factor taking these influences in account to be added to calculated values of P_{Rmax}.

6.8 PU-characteristic and voltage profile stability

Another definition of the voltage stability in this thesis concerns the ability of a power system to maintain acceptable voltages at all buses in the system all the time. The voltage magnitudes or profile limits were defined in chapter 3 for the framework of this thesis to 1.1 pu and 0.9 pu. These limits are practically definable by the system operator for each system node according to the stability or security requirements. Beyond the defined stability limits, the further system operation is unacceptable.
Considering the limits defined in this thesis and looking at the voltage levels at the line receiving end, particularly for the simulations in DK-VEST it is observed that the voltage profile instability take place before the transfer instability. As stated in chapter 3, a practical voltage stability monitoring considers both stability issues together. This is possible by combining the PU-curve with the defined actual power transfer with a voltage profile stability band.

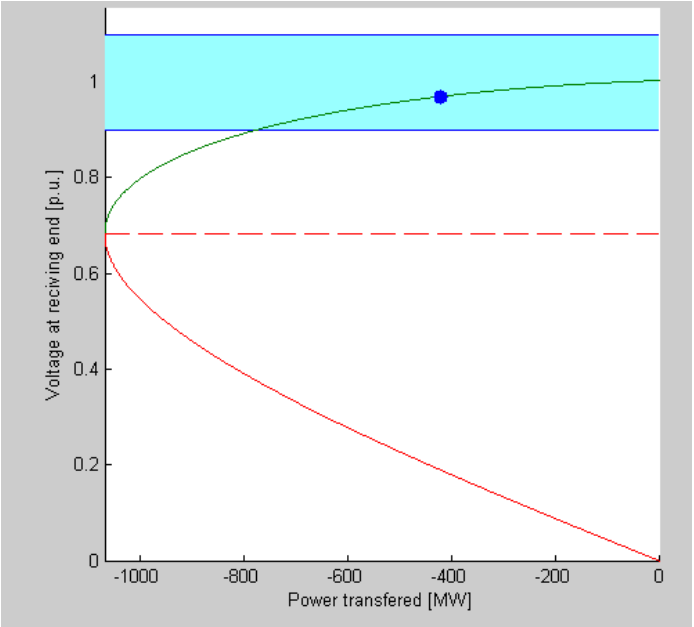

Figure 6.37: Illustration of the combination of the PU-curve with the voltage stability band (snapshot from AHT-Vstab)

The boundaries of the voltage profile stability are within the shaded area in figure 6.37. The operating point showed is stable for both stability criteria.

6.8.1 Voltage profile margin calculation

As explained in chapter 3 the first intersection (P_{limit}) of the PU curve with the voltage profile stability band is considered for the determination of the voltage profile margin. This intersection can theoretically take place on the stable or on the unstable branch of the PU curve. Particularly with regard to the practical calculation of the voltage profile margin[61], it should be carefully defined which options are possible for the margin calculation. Essential criteria for the consideration of an option are its practical as well as its

[61] e.g. with a tool for stability analysis

theoretical feasibility. The figures 6.38 and 6.39 illustrated two examples of the voltage profile margin calculation.

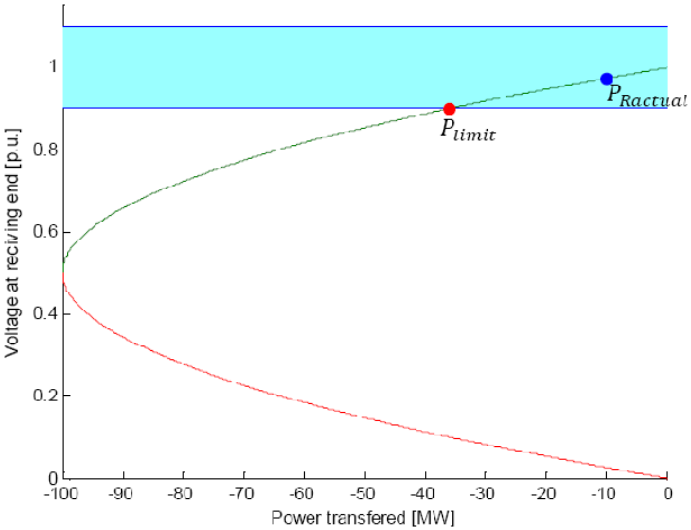

Figure 6.38: Case 1 of the voltage profile margin calculation

For this first case for example the voltage profile margin is calculated as

$$Voltage\ Profile\ Margin = P_{Ractual} - P_{limit} \tag{6.45}$$

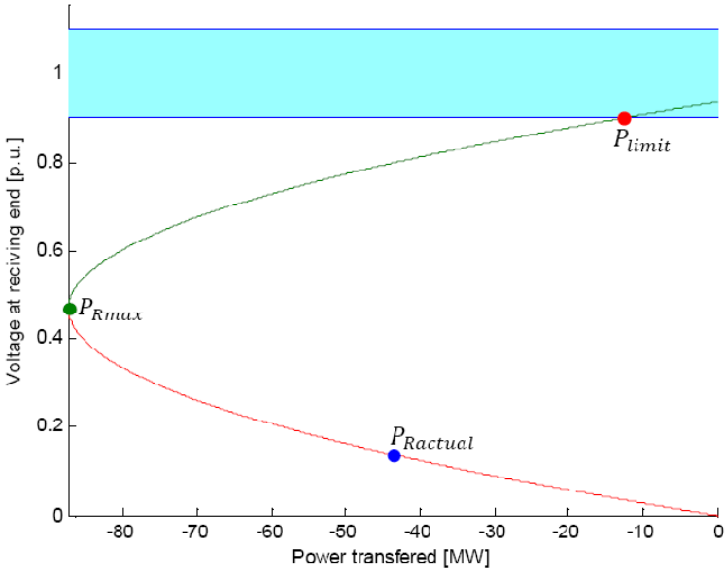

Figure 6.39: Case 2 of the voltage profile margin calculation

For the case 2 the voltage profile margin is calculated as

$$Voltage\ Profile\ Margin = (P_{Rmax} - P_{Ractual}) + (P_{Rmax} - P_{limit}) \quad (6.46)$$

6.9 PMU location and recognition of the power flow direction

Independently of the PMU location, the sign of the calculated active power is an exclusive sufficient criterion for the determination of the status of the line terminals. The stability calculations are always made for the line receiving end in this method. The denomination of the line ends are changing with the inversion of the power flow on the monitored line, the recognition of the direction of the power flow is particularly important for the monitoring method presented here. This takes place in the following steps:

- A PMU is placed at any boundary substation of the transmission line to be monitored.
- Using the data collected at the PMU location the value of the active power at the other end of the monitored line is calculated.
- According to the sign of the active power obtained, the direction of the power transfer is recognized and the line ends are accordingly denominated.

The principle of the denomination of the lines terminals is illustrated by the following simple example:

1 If $P_R > 0$

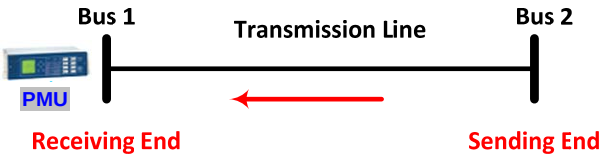

Figure 6.40: Definition of the flow direction

The power flow direction symbolized by the red arrow is from bus 2 towards bus 1.

2 If $P_R < 0$

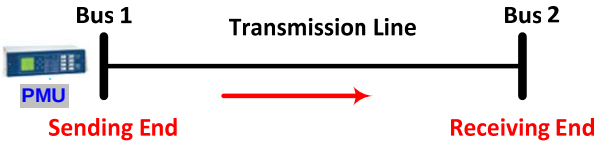

Figure 6.41: Definition of the flow direction

The power flow direction is in this case from bus 1 towards bus 2.

6.10 AHT-Vstab: A tool for voltage stability analysis

A visualization tool called AHT-Vstab, for the voltage stability analysis by the monitoring principles described above was developed in the framework of this thesis. As stated earlier the program has been developed using Matlab® Programming language. For a full functionality of the tool it is advisable to use the Matlab version 7.5 (R2007b). Rather than giving the detailed software specifications and directions of use of the tool, this paragraph just presents an overview of its general functionality. The actions supported by the actual version of AHT-Vstab are summarized in the flow chart in figure 6.42.

From a start-up window it is possible to choose the monitoring object. This could be a unique transmission device (power line) or a transmission zone (see next paragraph for more details). The next action is the selection of the device data. These are *.dat* files[62] line data comprising:

- the line connecting buses,
- the line positive Sequence Impedance magnitude,
- the line positive Sequence Impedance angle,
- the line per length capacitance,
- the line length

Other line parameters are not included because their values for the lines considered for the tests of the method are equal to zero. But other information can be included in the files if needed.

[62] The DAT file extension refers to a data file created by an application or the operating system. This type of file can contain virtually anything, such as: Application help text, or a software configuration options. DAT files are application-specific. Normally only the application that created a specific DAT file can read the DAT file, unless the information on how to read such file. [http://malektips.com/file_extensions_0027.html]

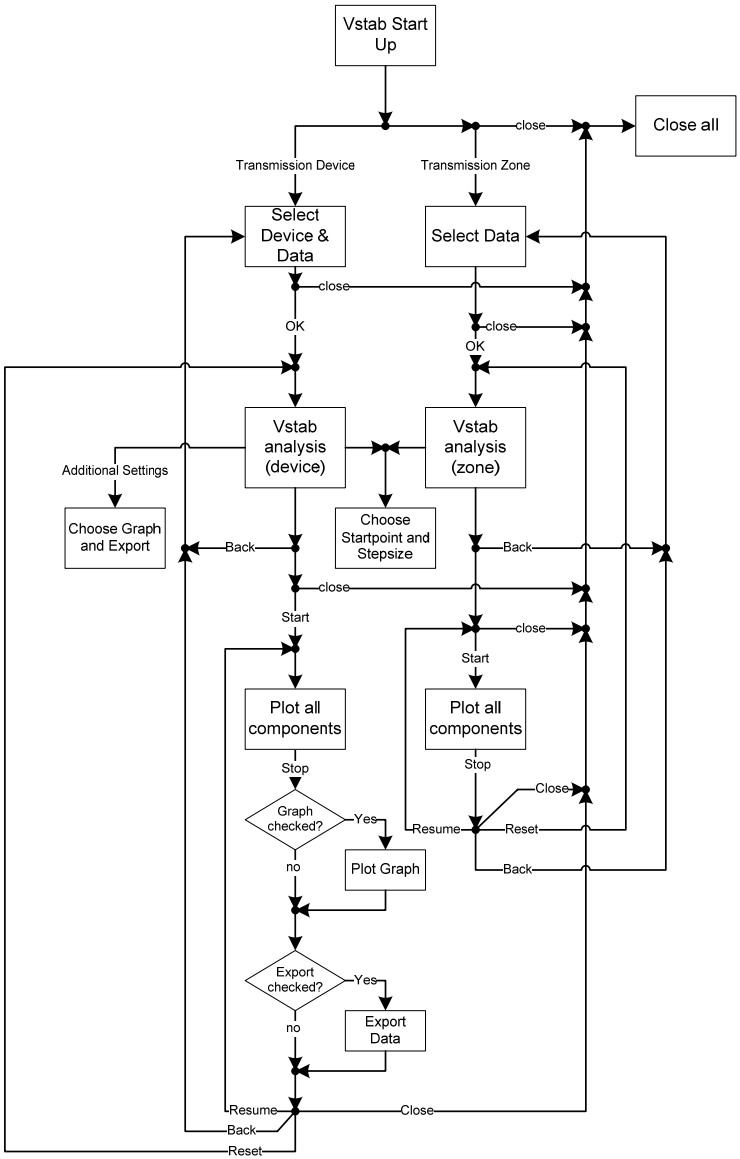

Figure 6.42: Flow chart of the AHT-Vstab functionality

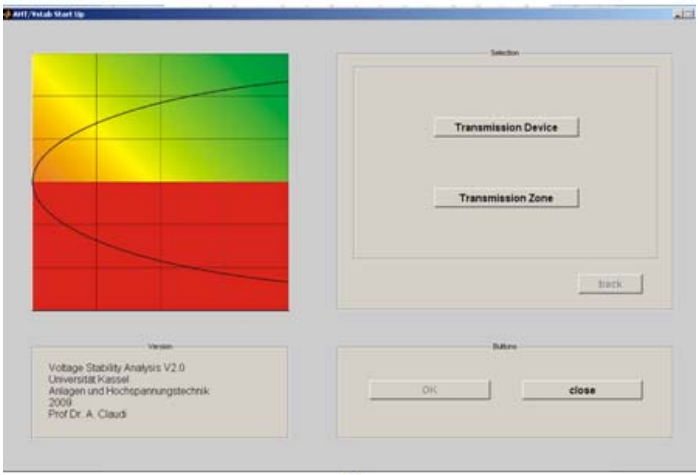

A)

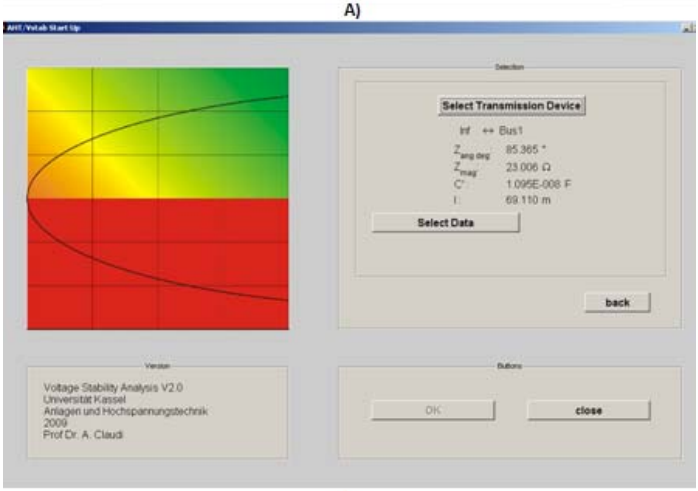

B)

Figure 6.43: AHT-Vstab Front page (A) and device selection (B) on the example of the line on the two bus test system

The device selection is followed by the phasor data selection. The program gives the possibilities of a voltage stability analysis using simulated phasor data saved as an *.xls* file or field phasor data saved in a *.csv* file.

The phasor data selection is made a predefined order which must be respected by the data saving: *PMU timestamps or simulation time-current magnitude-current phase angle-voltage magnitude-voltage phase angle*. In case of a *.csv* file usually containing more parameters, only these five parameters are picked out for further considerations. The user gets information on the data selected and can thus verified the rightness of its choice, which can be corrected if required.

By the right choice, the analysis window is opened pushing the "OK" button. This window is configured differently for stability analysis of a transmission device and for the analysis of a transmission zone. The next figure 6.44 shows a picture of the analysis window for a transmission device. A picture of this window for a transmission zone is presented in the next paragraph.

Figure 6.44: Snapshot of the AHT-Vstab analysis window on the example of the stability analysis for the two bus test system

The direction of the power is automatically recognized on the monitored line, the PU-curve is drawn for each time stamp data set and the position actual operating point is defined.

All the stability margins are calculated and the smaller margin to be considered in practical operation is shaded. The margin calculation is only made if possible or necessary. For example, the overvoltage margin calculation is only possible by an intersection of the PV curve with the upper voltage profile limit. If no intersection takes place an "EEE" message is displayed.

Further features are layed under the "additional settings" button. These include: different plotting functions activated by choosing the option "Graph" and an export function creating an *.xls* file with the calculated data values of the chosen variables. In both cases the plot or the export can be made at each instant and for the past time span when pushing the button "Stop". Multiple choices are possible for the export. The "step size" permits the variation of the interval of the timestamps considered.

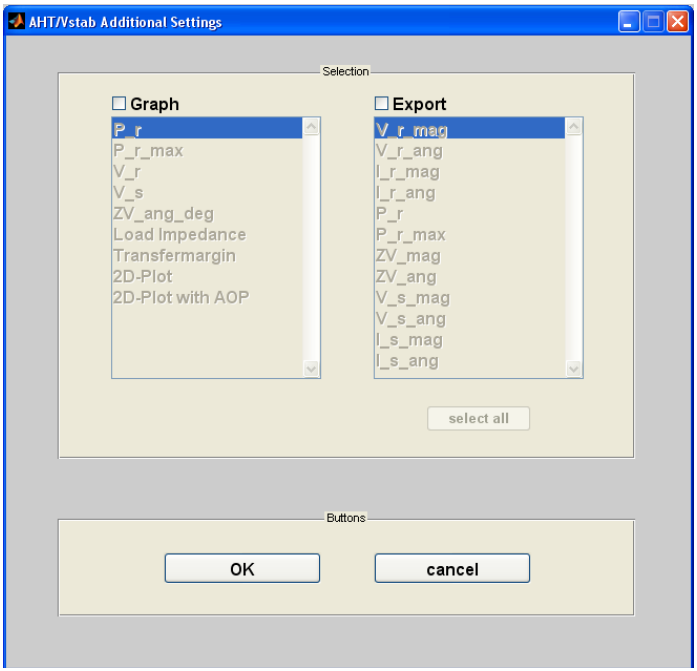

Figure 6.45: AHT-Vstab additional settings

6.11 Monitoring of transmission zones

Even if it is assumed that a PMU considered as a usual measuring item presents some advantages to the more commonly used RTU, the principal benefit of the PMU technique is the possibility of synchronization of the field measurements from different remote measuring locations and their further comparison. This property is used in this work to assess the stability status of a group of transmission lines belonging to the zone of observation of a set of PMUs. This means that, a set of transmission lines observable from of a set of defined PMU locations belong to the same transmission zone. The monitoring method developed within this work assesses the voltage stability status of each transmission line within a zone individually. In this context, the observability of a transmission line through a PMU let supposed that the PMU can directly measure the current flowing through the line and the voltage at one end of the line, or these phasors values can be indirectly calculated using the measurements done at a remote PMU location. The simultaneity of the synchrophasors measurements thus allows the surveillance of the stability status of large transmission zones with a reduced number of PMUs.

6.11.1 Application on the DK-VEST transmission grid structure

The PMUs already placed on the DK-VEST transmission grid on figure 6.2 each monitors only one transmission line. It means that PMU1 placed in KAS5 measures the voltage phasors at this substation and only the current phasors on the line between KAS5 and REV5. PMU2 measures the voltage phasors at TJE5 and the current flow on the line between TJE5 and ASR5. The transmission zones are further distinguished on this base and according to the requirements of the monitoring method proposed.

6.11.1.1 Transmission zone 1

This zone is composed of the following transmission lines

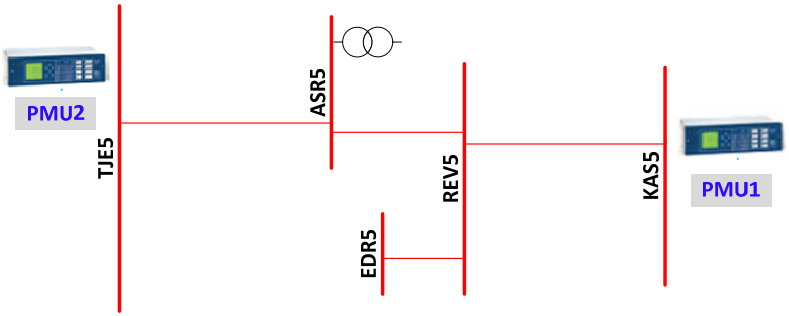

Figure 6.46: Topology of the transmission zone 1

Consequently the stability of the transfer on all the transmission lines belonging to the zone 1 is monitored using the data from the PMUs 1 and 2. Furthermore the unknown terminal voltage profiles are calculated from the measured phasor data. A representation of the zone structure as the interconnection of the π- equivalent circuits of the respective transmission lines alleviates the calculation of the unknown voltage and current phasors. Such an equivalent structure for the transmission zone 1 is represented in figure 6.47.
The phasors $\underline{U}_1$ and $\underline{I}_1$ are measured by the PMU 2 at TJE5. The PMU 1 at KAS5 measures the phasors $\underline{U}_4$ and $\underline{I}_6$. The rest of the voltage and current phasors on the equivalent representation on the transmission zone 1 are calculated in dependency of these known values.

$$\underline{U}_2 = \underline{U}_1 \cdot \underline{K}_1 - \underline{I}_1 \cdot \underline{Z}_1 \tag{6.47}$$

$$\underline{I}_2 = \left[\underline{U}_1 \cdot \underline{K}_1 - \underline{I}_1 \cdot \underline{Z}_1\right] \cdot \underline{D}_1 - \frac{\underline{U}_1}{\underline{Z}_1} \tag{6.48}$$

$$\underline{U}_3 = \underline{U}_4 \cdot \underline{K}_3 - \underline{I}_6 \cdot \underline{Z}_3 \tag{6.49}$$

$$\underline{I}_5 = \left[\underline{U}_4 \cdot \underline{K}_3 - \underline{I}_6 \cdot \underline{Z}_3\right] \cdot \underline{D}_3 - \frac{\underline{U}_4}{\underline{Z}_3} \tag{6.50}$$

Due to the transformer connected at ASR5, the complex current $\underline{I_3}$must be defined as followed:

$$\underline{U_3} = \underline{U_2} \cdot \underline{K_2} - \underline{I_3} \cdot \underline{Z_2} \tag{6.51}$$

$$\underline{I_3} = \left(\underline{U_2} \cdot \underline{K_2} - \underline{U_3}\right) \cdot \frac{1}{\underline{Z_2}} \tag{6.52}$$

$$\underline{I_4} = \left(\underline{U_3} \cdot \underline{K_2} - \underline{U_2}\right) \cdot \frac{1}{\underline{Z_2}} \tag{6.53}$$

$$\underline{I_7} = -\underline{I_4} - \underline{I_5} \tag{6.54}$$

$$\underline{U_6} = \underline{U_3} = \underline{U_4} \cdot \underline{K_3} - \underline{I_6} \cdot \underline{Z_3} \tag{6.55}$$

$$\underline{U_7} = \underline{U_6} \cdot \underline{K_4} - \underline{I_7} \cdot \underline{Z_4} \tag{6.56}$$

$$\underline{I_8} = \left[\underline{U_6} \cdot \underline{K_4} - \underline{I_7} \cdot \underline{Z_4}\right] \cdot \underline{D_4} - \frac{\underline{U_6}}{\underline{Z_4}} \tag{6.57}$$

The formulas (6.6.1), (6.6.2) and (6.9.1) representing the transmission line parameters are generalized as:

$$\underline{Z_n} = \underline{R_n} + j\omega\underline{L_n}$$

$$\underline{K_n} = \left[1 + \frac{1}{2}\left(R_n G_n - \omega^2 L_n C_n + j\omega(C_n R_n + L_n G_n)\right)\right]$$

$$\underline{D_n} = \frac{1}{Z_n} + \frac{G_n}{2} + j\omega\frac{C_n}{2}$$

Where, n means each transmission line in the transmission zone.

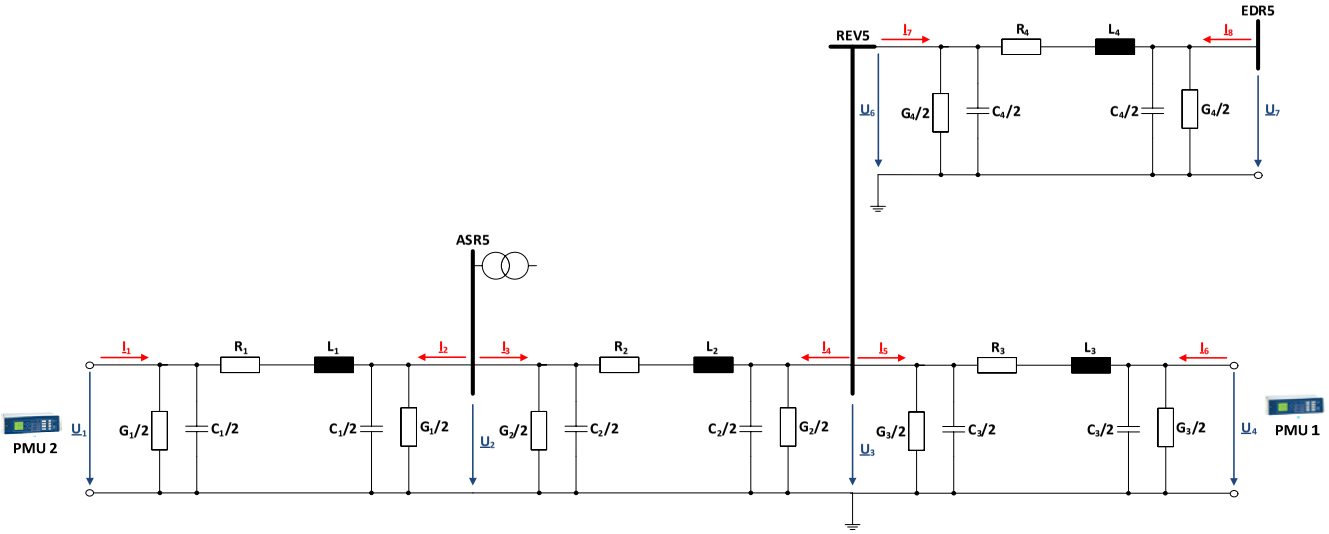

Figure 6.47: Equivalent Structure of the transmission zone 1

Validity of the current equation at ASR5

For the verification of the formula used for the current calculation at the bus ASR5, the line between ASR5 and REV5 is considered.

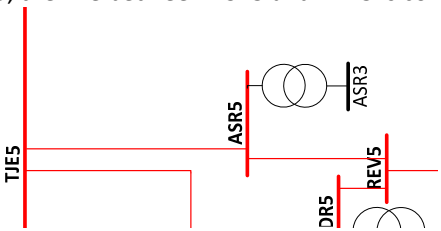

Figure 6.48: Abridgement of figure 6.2

A fictive load is connected to ASR5. Different values of the active power for this load are given and for each new value a load flow is calculated. Table 6.4 shows the resulting simulated complex voltage values at ASR5, the simulated complex voltage and current values at REV5 as well as the calculated current values at REV5.

The current at REV5 is calculated using the equation (compare with 6.56):

$$\underline{I}_{REV5} = \frac{\underline{U}_{REV5} \cdot \underline{K} - \underline{U}_{ASR5}}{\underline{Z}}$$

With $\underline{K} \approx 1$ and $Z = 16{,}52\Omega \cdot e^{j(85{,}34°)}$

Table 6.4: Results of the calculations for the verification of the current equations

active power	**8000 MW**	**6000 MW**	**4000 MW**	**2000 MW**	**1000 MW**	**500 MW**
U_{ASR5}	78,34 kV	111,04 kV	158,4 kV	211,74 kV	231,74 kV	238,05 kV
$\boldsymbol{\varphi_{UASR5}}$	-107,47°	-102,81°	-91,33°	-65,92°	-47,13°	-36,65°
U_{REV5}	131,67 kV	149,87 kV	181,02 kV	219,81 kV	234,58 kV	239,01 kV
$\boldsymbol{\varphi_{UREV5}}$	-58,44°	-64,98°	-66,55°	-54,07°	-41,3°	-33,74°
I_{REV5} (calc.)	6,04kA	5,57kA	4,61kA	2,74kA	1,45kA	0,74kA
$\boldsymbol{\varphi_{IREV5}}$ (calc.)	-107,14°	-102,56°	-91,1°	-65,32°	-46,41°	-34,95°
I_{REV5} (simul.)	6,03kA	5,58kA	4,6kA	2,74kA	1,44kA	0,74kA
$\boldsymbol{\varphi_{IREV5}}$ (simul.)	-107,34°	-102,62°	-90,99°	-65,17°	-45,57°	-33,5°
Discre-pancy between: I_{REV5} (simul.) and I_{REV5} (calc.)	**0,2%**	**0,2%**	**0,2%**	**0%**	**0,7%**	**0%**

The validity of the equation used is confirmed by the negligible percent discrepancy.

6.11.1.2 Transmission zone 2

Outgoing from the initial placement of the PMU3 in VHA5 in DK-VEST, a second transmission zone can be defined.

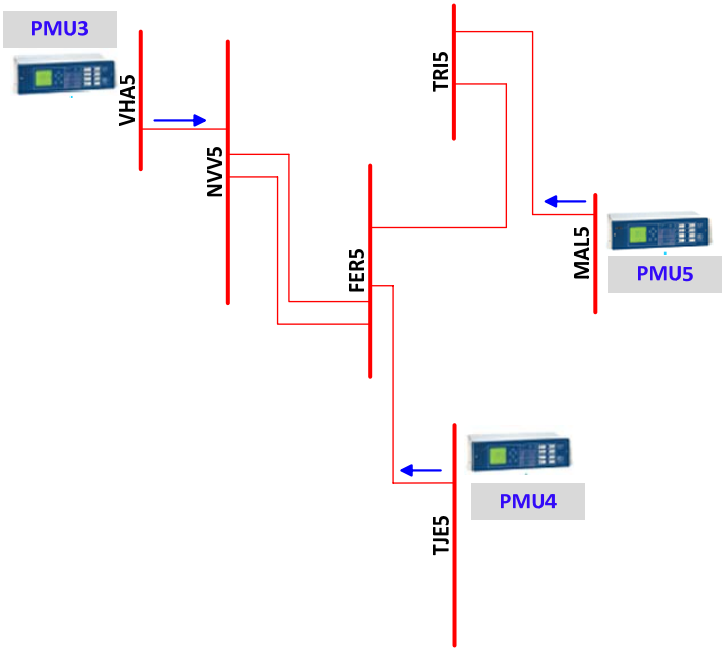

Figure 6.49: Topology of the transmission zone 2

Additionally to the PMU2 belonging to the zone 1, a further PMU4 is placed in TJE5 for the measurement of the current phasors on the line between TJE5 and FER5. The PMU set is completed by the PMU5 placed in MAL5 for a complete observation of the transmission zone 2. The π-equivalent of the topology structure (see appendix F) is used for the calculation of the unknown phasors.

The phasors directly measured by the PMUs in this case are: $\underline{U}_1$, $\underline{I}_1$, $\underline{U}_4$, $\underline{I}_8$, $\underline{U}_6$,and $\underline{I}_{12}$.

$$\underline{U}_2 = \underline{U}_1 \cdot \underline{K}_1 - \underline{I}_1 \cdot \underline{Z}_1 \tag{6.58}$$

$$\underline{I}_2 = \left[\underline{U}_1 \cdot \underline{K}_1 - \underline{I}_1 \cdot \underline{Z}_1\right] \cdot \underline{D}_1 - \frac{\underline{U}_1}{\underline{Z}_1} \tag{6.59}$$

$$\underline{U}_3 = \underline{U}_4 \cdot \underline{K}_4 - \underline{I}_8 \cdot \underline{Z}_4 \tag{6.60}$$

$$\underline{I}_7 = \left[\underline{U}_4 \cdot \underline{K}_4 - \underline{I}_8 \cdot \underline{Z}_4\right] \cdot \underline{D}_4 - \frac{\underline{U}_4}{\underline{Z}_4} \tag{6.61}$$

The currents $\underline{I}_3$, $\underline{I}_5$, $\underline{I}_4$, and $\underline{I}_6$ can now be calculated using the equations (6.58) and (6.60).

$$\underline{I}_3 = \underline{U}_3 \cdot \underline{D}_2 - \frac{\underline{U}_2}{\underline{Z}_2} \tag{6.62}$$

$$\underline{I}_5 = \underline{U}_3 \cdot \underline{D}_3 - \frac{\underline{U}_2}{\underline{Z}_3} \tag{6.63}$$

$$\underline{I}_4 = \underline{U}_2 \cdot \underline{D}_2 - \frac{\underline{U}_3}{\underline{Z}_2} \tag{6.64}$$

$$\underline{I}_6 = \underline{U}_2 \cdot \underline{D}_3 - \frac{\underline{U}_3}{\underline{Z}_3} \tag{6.65}$$

$\underline{I}_{11}$ and $\underline{U}_5$ are defined using $\underline{I}_{12}$and $\underline{U}_6$

$$\underline{U}_5 = \underline{U}_6 \cdot \underline{K}_6 - \underline{I}_{12} \cdot \underline{Z}_6 \tag{6.66}$$

$$\underline{I}_{11} = \left[\underline{U}_6 \cdot \underline{K}_6 - \underline{I}_{12} \cdot \underline{Z}_6\right] \cdot \underline{D}_6 - \frac{\underline{U}_6}{\underline{Z}_6} \tag{6.67}$$

Using

$$\underline{I}_{10} = -\underline{I}_{11} \tag{6.68}$$

one obtains,

$$\underline{I}_9 = \left[\underline{U}_5 \cdot \underline{K}_5 - \underline{I}_{10} \cdot \underline{Z}_5\right] \cdot \underline{D}_5 - \frac{\underline{U}_5}{\underline{Z}_5} \tag{6.69}$$

6.11.1.3 Transmission zone 3

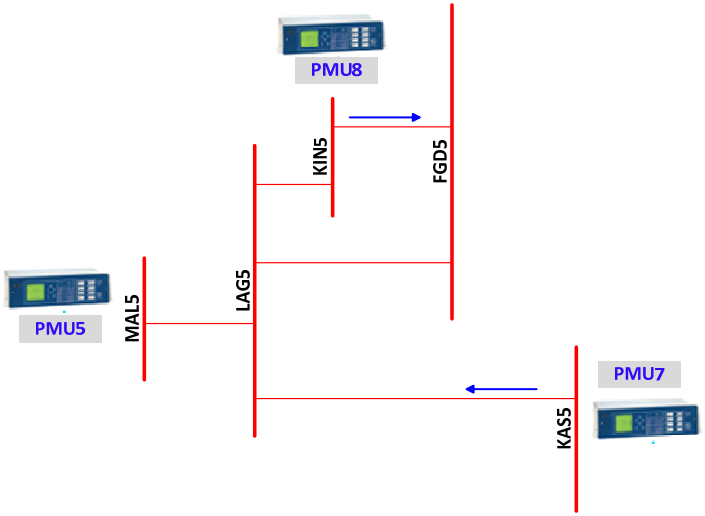

Figure 6.50: Topology of the transmission zone 3

The π-equivalent of the topology structure of the transmission zone 3 is showed in appendix F. The primarily assigned to the transmission zone 2 PMU5 is also used in the zone 3 "only" for the measurement of the voltage phasors at MAL5 ($\underline{U}_1$). The PMUs 7 and 8 measure the complex phasors: $\underline{U}_3$, $\underline{I}_4$, $\underline{U}_5$,and $\underline{I}_9$. The unknown phasors are calculated through the following formulas:

$$\underline{U}_2 = \underline{U}_3 \cdot \underline{K}_2 - \underline{I}_4 \cdot \underline{Z}_2 \tag{6.70}$$

$$\underline{I}_3 = \left[\underline{U}_3 \cdot \underline{K}_2 - \underline{I}_4 \cdot \underline{Z}_2\right] \cdot \underline{D}_2 - \frac{\underline{U}_3}{\underline{Z}_2} \tag{6.71}$$

$$\underline{I}_2 = \underline{U}_2 \cdot \underline{D}_1 - \frac{\underline{U}_1}{\underline{Z}_1} \tag{6.72}$$

$$\underline{I}_1 = \underline{U}_1 \cdot \underline{D}_1 - \frac{\underline{U}_2}{\underline{Z}_1} \tag{6.73}$$

$$\underline{U}_4 = \underline{U}_5 \cdot \underline{K}_5 - \underline{I}_9 \cdot \underline{Z}_5 \tag{6.74}$$

$$\underline{I}_{10} = \left[\underline{U}_5 \cdot \underline{K}_5 - \underline{I}_9 \cdot \underline{Z}_5\right] \cdot \underline{D}_5 - \frac{\underline{U}_5}{\underline{Z}_5} \tag{6.75}$$

$$\underline{I}_8 = \underline{U}_5 \cdot \underline{D}_4 - \frac{\underline{U}_2}{\underline{Z}_4} \tag{6.76}$$

$$\underline{I}_7 = \underline{U}_2 \cdot \underline{D}_4 - \frac{\underline{U}_5}{\underline{Z}_4} \tag{6.77}$$

$$\underline{I}_6 = \underline{U}_4 \cdot \underline{D}_3 - \frac{\underline{U}_2}{\underline{Z}_3} \tag{6.78}$$

$$\underline{I}_5 = \underline{U}_2 \cdot \underline{D}_3 - \frac{\underline{U}_4}{\underline{Z}_3} \tag{6.79}$$

The transmission lines which are not included in the transmission zones must be individually monitored by separate PMUs. The recognition of the flow direction on each transmission line takes place as described in paragraph 6.9.

6.12 Resulting PMUs positioning in DK-VEST

Outgoing from the calculations and based on the stability monitoring principles described in this chapter the resulting PMUs positioning for the voltage stability monitoring of the total transmission system of DK-VEST is showed on figure 6.51.

Eleven PMUs would be needed to carry out the stability monitoring method presented. The number of PMUs can be theoretically reduced by defining additional measurement channels for given PMUs. As an example the number of PMUs to be installed at TJE5 can be sunk from three to one by defining more channels for the measurement of the current phasors on the lines TJE5-FER5 and TJE5-IDU5 on PMU 2. Thereby the structure of the transmission zones and the resulting equations for the calculation of the eventually unknowns variables could change; But the monitoring principle itself stays unmodified. After this reduction, 8 PMUs would remain for the total observability of the 400 kV level of DK-VEST. This is equivalent to the PMUs number found by the Jansson's OPP method in chapter 5 for this structure. However this positioning is only theoretical, and due to the physical situation in the substations it is not always realizable. The positioning solution presented in figure 6.51 fits the needs of the monitoring method developed in this thesis.

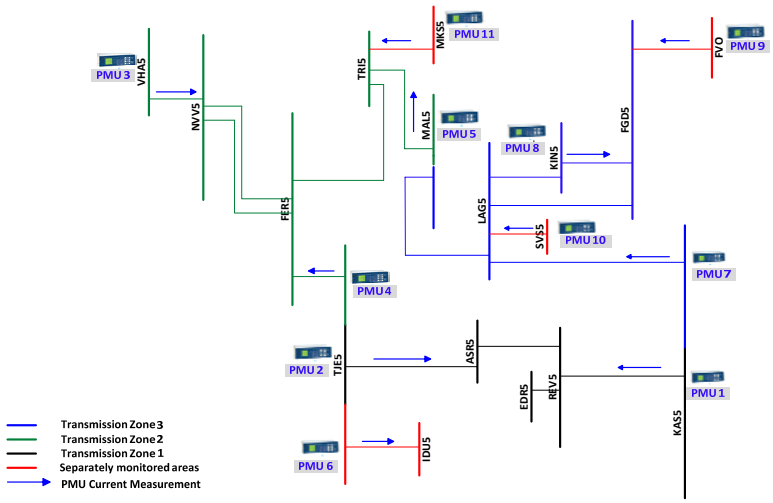

Figure 6.51: Resulting PMUs placement for the 400 kV level in DK-VEST

6.13 Visualization of the voltage stability state in a transmission zone

The formulas developed in paragraph 6.11 can be implemented in a visualization tool for the analysis of the voltage stability situation in a transmission zone. The equations for the defined transmission zone 1 are exemplarily implemented in AHT-Vstab for this purpose. Real PMU data measured at the substations TJE5 and KAS5 are used as input for the calculations of the stability margins for the entire transmission zone 1 in accordance to the regnant positive energy flow on each individual line. If any of these measurements is missing, the implemented monitoring algorithm cannot provide the results. Therefore, all measurements units must be available all the time for the stability assessment in a transmission zone. Even by the availability of the required PMUs, some interruptions can still happen during the measurements or the data transfer to the PDC.

The algorithm implemented in AHT-Vstab includes an important function verifying the concordance of the timestamps of the chosen PMU data at both locations at each calculated instant. If these timestamps are different the analysis makes no sense and an error message is given out.

Figure 6.52 exemplarily presents a picture of the complete voltage stability situation calculated for the 13th of January, 2007 at 13:00:00:01.480 pm.

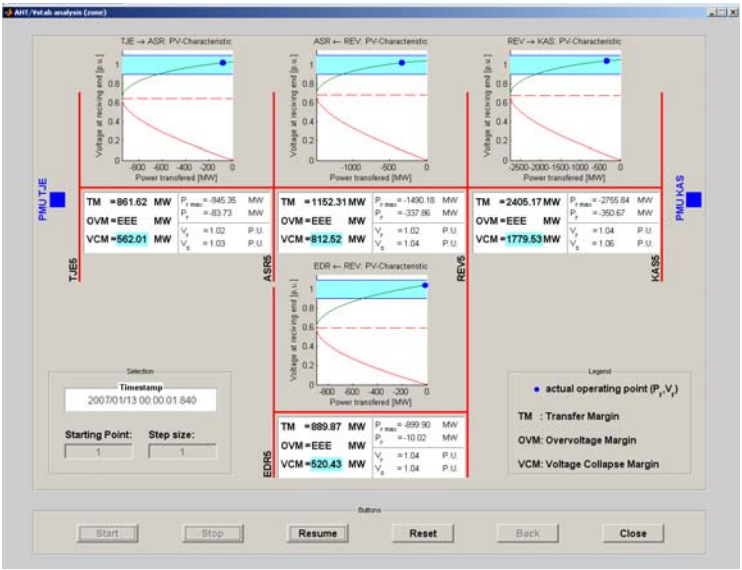

Figure 6.52: Snapshot of the AHT-Vstab analysis window on the example of the voltage stability analysis of the defined transmission zone 1 in DK-VEST, on the 13th January, 2007 at 13:00:00:01.480

The complete voltage stability situation is analyzed for each line in the transmission zone 1. The directions of the power flow are determined and the voltage stability margins are calculated for each line. The margins are directly quantified in megawatts and the computation burden is very low[63]. Altogether, the method is relatively precise and is well adapted for online voltage stability monitoring purposes.

[63] A computer with the following characteristics: Intel® Core™ 2 Duo /T7100/1,8 GHz CPU/ 3 GB RAM needs 0,1139 seconds to evaluate the complete voltage stability situation of the transmission zone 1. This computational time is the average time calculated by consideration of 2121 successive data sets from the PMUs at KAS5 and TJE5 respectively.

7 Conclusion and outlook

7.1 Conclusion

During the recent years the economic and technical framework under which the electricity sector operates is subjected to fundamental transformations. Electric utilities that were used to operate under monopoly conditions for decades have to adapt to a competitive environment today. The impact of the distributed generation connected at all voltage levels must be taken in account. On the other hand, the need for more electric power constantly increases worldwide and the power grid companies aim to maximize their profit by making optimal use of the networks. Another important factor is the increased public and political focus on environmental issues, making electric grids expansion plans more difficult. As a logical result the power systems are operated much closer to their technical and stability limits. Furthermore, the growing number of market activities, especially of wheeling contracts, results in new system's states, which the operators have to cover. The operation near the stability limit requires an extensive knowledge about the system's state to ensure the compliance of its stability limits. The yearly augmentation of the number of power outages shows that the power systems became more vulnerable to instabilities and that the systems operators need better monitoring tools and methods compatible to the actual operating conditions. For more efficiency these methods must be usable in real time.

The advent of the Phasor Measurement Units (PMU's), capable to track system's transients and to furnish the synchronized measurements of the phasors of relevant system's state variables from dispersed locations is becoming a mayor tendency in the monitoring of power systems. The PMUs collect an enormous amount of data that arrives at control centres through powerful communication systems. The PMUs data can be used for online purposes and strategies to validate and utilize this data are needed.

This thesis focuses on the development of a PMU data based method for the monitoring of voltage stability -which has been recognized as the principal cause of several power outages the last years- in power systems. For given time synchronized phasors measurements of power system variables, the voltage stability principally defined by the notions the maximum deliverable active power and the resulting level of the voltage profile at the line receiving end, is monitored at each operation instant captured by the PMUs. An emphasis is laid on the simultaneous monitoring of both notions for a complete assessment of the system voltage stability as influenced by the active power transfer on a transmission line. The assessment of the stability is done using an accurate PU-characteristic. The point of maximum possible power transfer is found in dependency of a defined load angle. This load angle exactly represents the loading situation at the line receiving end at each operation instant as measured by the PMUs.

The condition of the occurrence of the transfer instability is defined through the system and the load impedances, whereby a transfer stability index is defined. The PU-curve is combined to a voltage profile stability band, comprising the permissible voltage levels for equipment safety for the consideration of both stability notions at once. The coeval consideration of the two voltage stability issues permits the calculation of the minimal stability margin according to the predefined stability conditions. The method can be applied for the monitoring of individual transmission lines as well as for the monitoring of several transmission lines within a defined transmission zone. In the case of the monitoring of a unique transmission line, only one PMU is needed. This PMU can be placed at any end of the line to be monitored. The actual direction of the flow is recognized through an exact calculation of the amount of active power presently transferred. The monitoring of a large transmission zone is possible with a minimal number of PMUs. In this case the measured phasors are used for the calculation of the unknown phasors needed for the monitoring of the not directly observed transmission lines.

Although the principles of the method are general its application is individual to a given grid topology.
The proposed method has been tested on a two-bus system and on a large power system represented by the western Danish power grid. The tests have shown the good precision of the method to visualize the transfer status on the transmission lines and to recognize impending voltage instability. The low computational burden makes this method adequate for online monitoring purposes.

7.2 Outlook

The tests conducted on DK-VEST have shown a certain delay in the finding of the starting point of the line transfer instability. In the cases studied the point of the maximal deliverable power was found beyond the allowable voltage profile boundaries, so that in practical case, the voltage profile stability margin should have been decisive. Nevertheless, much work must be done to find out the reasons of the discrepancies in the calculation. A presumption is that, additional influences factors on the transfer on each transmission line must be considered. For the particular case of DK-VEST, a statistical study of the individual impact of the wind power production, of the CHP's production or the individual loads on each line for example could probably bring more clarity in this problem. As stated in chapter 6 the goal of such a study must be focused on the definition of a correction factor for the formulas developed for the maximal deliverable power.
To reduce the chance of voltage collapse a certain amount of stability margin needs to be maintained for the power system to withstand possible contingencies. Therefore the upgrading of the method for the voltage security monitoring of power systems can also be considered for future work. A good solution is to combine the stability analysis with a contingency screening tool to evaluate the stability margins of the system by occurrence of N-1 situations, N-2 situations, different types of short-circuits and/or other predefined contingencies or instability scenarios.

The method developed in this thesis considered only the voltage regulation and the system stability by the assessment of the power transmission capability of power lines based on the voltage stability criterion. Another determinant factor is the line thermal limit. Investigation of ways to associate the proposed method with practical sag-tension calculations will improve the power system stability assessment.

Appendix A Yearly reported power systems outages worldwide

Table A.1: listing of some yearly reported power systems outages

Date	Location	Causes and additive information
November 9, 1965	USA	Caused by a human error, i.e. incorrectly set of a protective relay on one of the transmission lines between the Niagara generating station and Southern Ontario days before the blackout. Around 25 million people and 207000 km² were left without electricity for up to 12 hours
October 13, 1974	Canada	Caused by a season blizzard. More than a million customers were affected for up to one week
July 13,1977	USA (New York City)	Caused by sequences of lightning strikes leading to loss of transmission lines and further inappropriate reactions of the system operator.
December 19, 1978	France	3.6 million people left without power. 29GW of load interrupted
December 27, 1983	Sweden	Caused by a storm which destroyed equipment connecting the power lines in Enköping and a voltage collapse.
15 October to 16 October,1987	England	Caused by a great storm which brought some power lines down
March 13, 1989	Canada	Caused by a geomagnetic storm leading to a power failure in the Quebec power system. 6 million people without power for 9 or more hours.
July 7, 1991	North-America (USA, Canada)	Caused by a powerful wind storm which affected a large portion of central North America cutting power to about 1 million customers.
October 4, 1995	Eastern and Southern North America	Caused by the Hurricane Opal. Almost 2 million customers were left without power

July 2, 1996	USA	Cascading system failures lead to electricity interruption service to millions of Customers
August 10, 1996	Mexico	Caused by high heat and high electricity demand leading to the failure of a major transmission line failure. 4 million people were left without electricity.
November 19, 1996	USA	Caused by a severe ice storm leading to power outages lasting up to two weeks
August 3, 1996	Malaysia	
January, 1998	north-eastern North America (particularly Quebec)	Caused by a great ice storm which destroyed many transmission towers leaving over 3.5 million customers in total without power.
February 20 to March 27, the 1998	New-Zealand	A line failure leads to a chain reaction leading to the failure of three other lines. The entire Auckland Central Business District was left without power for several weeks.
May 31, 1998	Central North America	Caused by a powerful wind storm which knocked out power to nearly 2 million customers
December 8, 1998	USA	A still after maintenance grounded substation was put in service and drew so much energy from the transmission lines so that 25 other substations automatically shut down. Over 350000 customers were left without power for 8 hours. Economic costs were estimated in tens of millions of dollars

March 11, 1999	Brazil	Initiated by a phase-to-ground fault at a 440 kV bus, which caused the opening of five incoming 440 kV lines, The power system survived the first event, but then collapsed because of a shortcoming of backup relaying. 25 GW of load was lost.
July 5, 1999	Canada	
July 29, 1999	Taiwan	A Derecho[64] cut power to over 600000 homes A transmission tower collapses due to a landslide. Around 8.46 million electricity consumers were disconnected
May 9, 2000	Portugal	the electrocution of an unfortunate stork left the entire southern half of Portugal, including Lisbon, without power for a few hours
June 2000 to June 2001	USA	During this period, the Western U.S. Energy Crisis was characterized by several shortage in energy and therefore power failures.
July 22, 2003	USA	A sever wind storm left over 300000 electricity customers in Memphis without power
August 14, 2003	USA, Canada	Some causes are: the high demand, line faults, out-dated protection and control systems. The result is the loss of 51 GW; 50 million people were affected
August 23, 2003	Finland	power was lost for up to an hour in Helsinki affecting half a million people

[64] Derecho: Widespread and long-lived, violent convectively induced straight-line windstorm that is associated with a fast-moving band of severe thunderstorms usually taking the form of a bow echo [60]

August 28, 2003	England	Caused by the fitting of a wrongly rated part in a backup system - similar to fitting a 1 ampere fuse instead of a 5 ampere fuse and a transformer fault
September2, 2003	Malaysia	A Power failure affected 5 of the 13 states of the country, for 5 hours, this blackout costs industries 13.8 million $
September 19, 2003	USA, Canada	Hurricane Isabel cuts electricity to 4.3 million people
September 23, 2003	Denmark, Sweden	Some causes are: the Outage of a generator block in a power plant, a two-phase short-circuit on a 400 kV bus. 3.8 million people were affected
September 28, 2003	Italy	Caused by a high power import, a short circuit event due to a power line tree contact and high load tripping. The electricity service to 50 million people was interrupted for 15 hours and the frequency in the UCTE grid increased by 0.25 Hz.
July 12, 2004	Greece	Power failure caused by the high demand during a heat wave. That led to a cascading failure causing the collapse of the entire Southern Power System, affecting several million people in Athens and Southern Greece.
September 2, 2004	Germany, Luxembourg	A fault on a 220 kV power line and a protection malfunction on other line cause a blackout in Trier (Germany) and Luxembourg.
September 4, 2004	USA	Hurricane Frances left 5 million people in Florida without power

September 15,2004	Puerto-Rico	Hurricane Jeanne constrains the authorities to shut down the power supply
November 28, 2004	Spain	A line fault causes a blackout in Costa del sol. 34000 people are affected
2005	Malaysia	Due to a fault of a main cable transmission line many states had no electricity
January 8,2005	Sweden	The storm Erwin left 341000 homes without electricity
March 2005	France	EDF cannot produce enough power by the exceptional cold weather. Its 208000 customers in Corsica suffer a 30 minutes power outage every 3 hours
May 25, 2005	Russia	The explosion of a 110 kV current transformer and circuit breaker leaded to the shutdown of a 110 and a 500 kV bus, and a fault at a 220 kV Bus. 5 million people are without electricity for 24 hours.
June 16, 2005	Puerto-Rico	Two-thirds of the country lost power due to 250 kV line damage for almost a day.
August 18, 2005	Indonesia	A transmission line between West Java, failed at 10:23 am local time; this led to a cascading failure that shut down two units of a power plant in East Java and six units of the power plant in West Java. A supply shortfall of 2700 MWh occurred and almost 100 million of people were affected

August 22, 2005	Iraq	The sabotage of a feeder line caused a cascading effect shutting multiple power plants down
August 26, 2005	USA	Almost 1.3 million people are left without power by the Hurricane Katrina
August 29,2005	USA	Hurricanes Katrina and Rita
September 12, 2005	USA	The mistaken sectioning of several cables causes a blackout which affects millions in California.
October 24, 2005	USA	Hurricane Wilma caused loss of power for 3.2 million customers in South Florida and Southwest Florida, with hundreds of thousands of customers still powerless a week later, and full restoration not complete until November 11
November 25, 2005	Germany	Ice formation on transmission lines in Münster brought transmission tower to fall down
December 15, 2005	USA	Wintry weather knocked out power to 700000 customers
December 22, 2005	Japan	A line outage knocked out power to 650000 customers.
June 12, 2006	New Zealand	The cause of the blackout was determined to be a grounding cable falling across a 110kV transmission line at a sub-station. This was caused by the failure of a corroded shackle, as the result of unusually high winds. 230000 suffers a 8 hour long power outage
July 17, 2006	Canada	nearly half a million customers in Ontario and Quebec were affected after derechos and other isolated severe thunderstorms

July 18, 2006	USA	365000 people are left without electricity due to violent storms
July 19	USA	at least 486000 customers lost power in the greater St. Louis, Missouri, area due to winds and thunderstorms that rolled through the area
July 22, 2006	England	Due to a heat wave and the higher energy demand (air conditioning) parts of London lost power.
July 25, 2006	Czech Republic	Also here a heat wave lead to system overloading
August 1, 2006	Canada	146,000, of households were left without electricity for a whole day, and some for up to a whole week due to intense thunderstorms that rolled through southern Quebec including the Greater Montreal Area. Over 450,000 customers in total were affected
August 2, 2006	Canada	Thunderstorms left nearly a quarter million customers in Eastern Ontario without power.
August 14, 2006	Japan	The extension arm of a ship crane touched a 235 power lines. 1.39 million households in Tokyo were left without power.
September 12, 2006	England	
October 12, 2006	USA, Canada	Accumulation of snow on power lines after snow storm.
October 15, 2006	USA	An 6.5 magnitude earthquake occurred in the US state of Hawaii at about 7:07 am causing a power outage to most of the state

October 24, 2006	Peru	An aerostatic balloon accidentally crashed against transmission towers causing a short circuit which affected nearly 13 districts in the capital. The power was restored that same night
November 4, 2006	Germany	Switching off a 380 kV power line in Germany and false assessment of the resulting load flow lead to the splitting of the UCTE grid in 3 grid islands. In parts of Germany, France, Italy, Belgium, Spain and Portugal over five million people were left without power after a big cascading breakdown.
November 15, 2006	Canada	A massive wind storm struck Vancouver, causing over 200,000 homes to lose power, in some cases for over a week
November 30, 2006	USA	As a result of a winter storm, about 500000 people in St. Louis, lost power due to outages which lasted from 1 day to 2 weeks
December 1, 2006	Canada	In parts of Ontario, tens of thousands of people lost power due to a severe winter storm
December 1, 2006	USA	A fire at the long Island electricity dpt. causes blackouts.
December 15, 2006	USA	The Hanukkah Eve Wind Storm of 2006 caused a power failure throughout the Seattle area, causing 1 million people to lose power.
From January 12 to 24, 2007	USA	Almost 1 million customers from Texas to Atlantic Canada lost power due to a series of winter ice storms
January 16, 2007	Australia	Bushfires cut electricity supply to 200000 in Victoria

April 19, 2007	Costa Rica	National blackout. 4.328.000 people affected
April 26, 2007	Colombia	An undetermined technical failure in Bogota causes a nation-wide blackout
June 8, 2007	Australia	A power failure occurred in Sidney affecting mainly the Northern Beaches for around 1 day
June 27, 2007	USA	A power failure occurred in New York City. About 136,700 customers were without power during the height of the outage
July 23, 2007	Spain	Due to a massive electrical substation cascading failure, the city of Barcelona suffered a near-total blackout. Several areas remained without electricity for more than 78 hours.
July 25,2007	Europe	On, a blackout occurred in the Republic of Macedonia, Albania, Greece, parts of South Serbia, Montenegro and parts of Greece were affected. The main cause of this is believed to be as result of 2007 European heat wave. Power was restored by the following day.
October 10, 2007	England	A blackout occurred around the area of Oxted in Surrey, England at about 19:00 local time (18:00 GMT) and lasted for a total of up to 20 minutes, having been restored for about 2 seconds before a second blackout occurred
December 2, 2007	Canada	A winter storm damaged transmission systems, resulting in a blackout over much of Eastern Newfoundland & Labrador affecting close to 100000 customers.

December 8, 2007	USA	A series of ice events cut power to over 1 million homes and businesses across the Great Plains of the United States from Oklahoma to Nebraska.
December 28, 2007	USA	a blackout occurred which affected 21,000 residents along the Florida Keys
January 4, 2008	USA	a winter rainstorm hit northern California causing 1.6 million Electric customers to lose power
January 9, 2008	Canada	a powerful windstorm hit Quebec leaving over 100000 Hydro-Québec customers without power for over 3 hours
January 22, 2008	England	Blackout in Manchester
January 22, 2008	USA	Partial Blackout in San-Francisco
January 6, 2008	China	Heavy snowstorms in China knocked down transmission lines.
January 28,2008	Canada	a severe ice storm caused electricity failure throughout Prince Edward Island.
January 29, 2009	USA	Strong wind gusts in excess of caused around 70000 people to lose power in Dallas County. In Southern Denton County, many customers also lost power. In Lewisville, around 2,000 people lost power. In Flower Mound, there were many dropouts. However, they only lasted from 10 seconds to 1 minute
February 11, 2008	Canada	Southern Calgary lost power due to ice buildup on power lines, overloading transformers.

February 20, 2008	Indonesia	Electricity deficit due to the stop of coal supply
February 26, 2008	USA	a failed switch and fire at an electrical substation outside Miami triggered widespread blackouts in parts of Florida affecting four million people
April 2, 2008	Australia	around 420,000 households were left without power in Melbourne, and other parts of Victoria after the state was hit by winds of up to 130 km/h
April 8, 2008	Poland	The fall of wet, heavy snow, stuck to the power cables and caused them to break. One of the major power line pillars broke in the aftermath as well. around 400,000 persons were left without power in the city of Szczecin and its surroundings for 18 days
June 24, 2008	England	a faulty underground wire caused a power failure in Maidstone Town Centre and surrounding areas for numerous hours.
September 13, 2008	USA	Hurricane Ike caused approximately 7.5 million to lose power in the United States from Texas to New York
October 12, 2008	Canada	At 5:40pm power went out for all BC Hydro customers on the South of Vancouver Island in British Columbia, Canada. Around 200000 people were left in the dark. The problem appeared to be caused by a transmission line.
November 4, 2008	France	Due to a severe storm the only 400 kV power line between Avignon and Nice were damaged. 1.5 million customers were without power for almost 5 hours

December 11, 2008	USA	Rare winter snowfall on Southern Louisiana caused 10,000 power outages, due to the accumulation of snow on transmission lines
December 26, 2008	USA	80% of power was lost for 12 hours in Hawaii at about 6:45 pm, suspected to be due to a thunderstorm with lightning striking transmission lines
December 28,2008	Canada	A power outage left 7500 customers in Kanata North without power for hours
January 15, 2009	Canada	The primary distributor of electric power in the Greater Toronto Area. shut down a transformer station after water flooding at a control centre. It initially affected 22000 homes and businesses
January 23, 2009	France	a severe windstorm knocked out power to 1.2 million customers in parts of France.
January 27, 2009	USA	an ice storm hit Kentucky knocking out power to about 769,000
January 27,2009	Australia	From 27 to 31 January, hundreds of thousands of homes in Victoria including Melbourne suffered various power failures as a result of a record heat wave
February 3, 2009	New Zealand	power to a large portion of Auckland, New Zealand was cut following failure of a substation transformer

Sources:

[60]
http://www.countrymanelectric.com/Generators/ElectricalOutages/ListingofMajorPowerOutages/tabid/128/Default.aspx
http://www.securite-electrique-paca.fr/rubrique5.html

Appendix B Data listing of the six-bus test system

Grid: Six-Buses System											
Equipment: Stations											
Name	Short-name	No.of Phases	Busbar	Type	Section	Un [kV]	Ithlim [kA]	Iplim [kA]			
Bus 3		3									
			Bus 3		0	150.00					

Grid: Six-Buses System											
Equipment: Lines											
Name	From Busbar	To Busbar	Type	Cross-Sec. [mm*2]	Num-ber	R [Ohm/km]	X [Ohm/km]	B [uS/km]	Distance [km]	In [kA]	Der. factor
CCT1	Infinite Bus	Bus 1	Line_400 k	0.00	1	0.0271	0.3329	3.4290	65.000	1.600	1.00
CCT2	Infinite Bus	Bus 1	Line_400 k	0.00	1	0.0271	0.3329	3.4290	65.000	1.600	1.00
CCT3	Bus 3/Bus 3	Bus 4	Line_165 k	0.00	1	0.0429	0.3667	3.0950	30.000	1.380	1.00

Grid: Six-Buses System									
Equipment: Loads									
Name	Busbar	Out of Service	Type	S P Q	P Q cosphi	Voltage [p.u.]	System Type	No of Phases	Conn.
Load	Bus 5	No	lodtyp_pq	50.00 MW	0.90	1.00	AC	3	D

Grid: Six-Buses System
Equipment: Shunts

Name	Busbar	Out of Service	Shunt-Type	Un [kV]	Vector Group	Capacitor
Shunt/Filte	Bus 5	No	C	60.00	Y	0.85 Mvar

Grid: Six-Buses System
Equipment: Synchronous Machines

Name	Busbar	Type	Num-ber	Sn [MVA]	Un [kV]	cos phi	xd" [p.u.]	xd"sat. [p.u.]	R2 [p.u.]	x2 [p.u.]	R0 [p.u.]	x0 [p.u.]	Re [Ohm]	xe [Ohm]
G1	Bus 2	Gen 2220MV	2	2220.00	24.00	1.00	0.23	0.20	0.000	0.200	0.000	0.100	0.000	0.000

Grid: Six-Buses System
Equipment: Terminals

Name	Inside Line	Type	Un [kV]	System Type	No. of Phases	Ithlim [kA]	Iplim [kA]
Bus 1			400.00	AC	3		
Bus 2			24.00	AC	3		
Bus 4			150.00	AC	3		
Bus 5			60.00	AC	3		
Infinite Bus			400.00	AC	3		

Grid: Six-Buses System												
Equipment: 2-Winding Transformers												
Name	From Busbar	To Busbar	Type	Num-ber	Sn [MVA]	HV-Side [kV]	LV-Side [kV]	Uk [%]	Pcu [kW]	Io [%]	Voltage/Tap [%]	[deg]
Trafo 1	Bus 1	Bus 2	Trf 400kV/	1	2220.000	400.00	24.00	15.00	0.00	0.000	0.00	0.0
Trafo 2	Bus 1	Bus 3/Bus 3	Trf 400kV/	1	2220.000	400.00	150.00	15.00	0.00	0.000	0.00	0.0
Trafo 3	Bus 4	Bus 5	Trf 150/60	1	125.000	165.00	67.00	12.31	437.50	0.130	1.50	0.0

Grid: Six-Buses System						
Equipment: External Grids						
Name	Busbar	Sk" [MVA]	Bus Type	R/X	Z2/Z1	Z0/Z1
External Grid	Infinite Bus	10000.00	PQ	0.10	1.00	1.00

Appendix C IEEE 14-Bus test system

The figure 5.8 in Chapter 5 depicts the IEEE-14 bus system, which is a benchmark for power system analysis. The complete system data [118] is as follows:

Table C.1: Exciter Data

Exciter no.	1	2	3	4	5
K_A	200	20	20	20	20
T_A	0.02	0.02	0.02	0.02	0.02
T_B	0.00	0.00	0.00	0.00	0.00
T_c	0.00	0.00	0.00	0.00	0.00
V_{Rmax}	7.32	4.38	4.38	6.81	6.81
V_{Rmin}	0.00	0.00	0.00	1.395	1.395
K_E	1.00	1.00	1.00	1.00	1.00
T_E	0.19	1.98	1.98	0.70	0.70
K_F	0.0012	0.001	0.001	0.001	0.001
T_F	1.0	1.0	1.0	1.0	1.0

Table C.2: Generator Data

Generator bus no.	1	2	3	4	5
MVA	615	60	60	25	25
x_l (p.u.)	0.2396	0.00	0.00	0.134	0.134
r_a (p.u.)	0.00	0.0031	0.0031	0.0014	0.0041
x_d (p.u.)	0.8979	1.05	1.05	1.25	1.25
x'_d (p.u.)	0.2995	0.1850	0.1850	0.232	0.232
x''_d (p.u.)	0.23	0.13	0.13	0.12	0.12
T'_{do}	7.4	6.1	6.1	4.75	4.75
T''_{do}	0.03	0.04	0.04	0.06	0.06
x_q (p.u.)	0.646	0.98	0.98	1.22	1.22
x'_q (p.u.)	0.646	0.36	0.36	0.715	0.715
x''_q (p.u.)	0.4	0.13	0.13	0.12	0.12
T'_{qo}	0.00	0.3	0.3	1.5	1.5
T''_{qo}	0.033	0.099	0.099	0.21	0.21
H	5.148	6.54	6.54	5.06	5.06
D	2	2	2	2	2

Table C.3: Bus Data

Bus No.	P Generated (p.u.)	Q Generated (p.u.)	P Load (p.u.)	Q Load (p.u.)	Bus Type*	Q Generated max.(p.u.)	Q Generated min.(p.u.)
1	2.32	0.00	0.00	0.00	2	10.0	-10.0
2	0.4	-0.424	0.2170	0.1270	1	0.5	-0.4
3	0.00	0.00	0.9420	0.1900	2	0.4	0.00
4	0.00	0.00	0.4780	0.00	3	0.00	0.00
5	0.00	0.00	0.0760	0.0160	3	0.00	0.00
6	0.00	0.00	0.1120	0.0750	2	0.24	-0.06
7	0.00	0.00	0.00	0.00	3	0.00	0.00
8	0.00	0.00	0.00	0.00	2	0.24	-0.06
9	0.00	0.00	0.2950	0.1660	3	0.00	0.00
10	0.00	0.00	0.0900	0.0580	3	0.00	0.00
11	0.00	0.00	0.0350	0.0180	3	0.00	0.00
12	0.00	0.00	0.0610	0.0160	3	0.00	0.00
13	0.00	0.00	0.1350	0.0580	3	0.00	0.00
14	0.00	0.00	0.1490	0.0500	3	0.00	0.00

*Bus Type: (1) swing bus, (2) generator bus (PV bus), and (3) load bus (PQ bus)

Table C.4: Line Data

From Bus	To Bus	Resistance (p.u.)	Reactance (p.u)	Line charging (p.u.)	tap ratio
1	2	0.01938	0.05917	0.0528	1
1	5	0.05403	0.22304	0.0492	1
2	3	0.04699	0.19797	0.0438	1
2	4	0.05811	0.17632	0.0374	1
2	5	0.05695	0.17388	0.034	1
3	4	0.06701	0.17103	0.0346	1
4	5	0.01335	0.04211	0.0128	1
4	7	0.00	0.20912	0.00	0.978
4	9	0.00	0.55618	0.00	0.969
5	6	0.00	0.25202	0.00	0.932
6	11	0.09498	0.1989	0.00	1
6	12	0.12291	0.25581	0.00	1
6	13	0.06615	0.13027	0.00	1
7	8	0.00	0.17615	0.00	1
7	9	0.00	0.11001	0.00	1
9	10	0.03181	0.08450	0.00	1
9	14	0.12711	0.27038	0.00	1
10	11	0.08205	0.19207	0.00	1
12	13	0.22092	0.19988	0.00	1
13	14	0.17093	0.34802	0.00	1

Appendix D OPP calculation data for the IEEE-57 bus system

Table D.1: IEEE 57 Bus-test system in PSADD Format

Bus		Line			Load		Xformer				Machine			Shunt	
Nr	*Name*	Nr	*FromBus*	*ToBus*	Nr	*BusRef*	Nr	*PrimBus*	*SecBus*	*Type*	Nr	*BusRef*	*Type*	Nr	*BusRef*
1	Bus01	1	1	15	1	1	1	4	18	FIXED	1	2	Gen	1	
2	Bus02	2	1	2	2	2	2	7	29	FIXED	2	3	Gen	2	
3	Bus03	3	2	3	3	3	3	20	21	FIXED	3	6	Gen	3	
4	Bus04	4	3	4	4	5	4	15	45	FIXED	4	8	Gen	4	
5	Bus05	5	3	15	5	6	5	14	46	FIXED	5	9	Gen	5	
6	Bus06	6	4	5	6	8	6	26	24	FIXED	6	12	Gen	6	
7	Bus07	7	5	6	7	10	7	24	25	FIXED	7	1	Gen	7	
8	Bus08	8	6	7	8	12	8	32	34	FIXED	8			8	
9	Bus09	9	6	8	9	14	9	11	43	FIXED	9			9	
10	Bus10	10	7	8	10	16	10	41	43	FIXED	10			10	
11	Bus11	11	8	9	11	17	11	11	41	FIXED	11			11	
12	Bus12	12	29	52	12	18	12	40	56	FIXED	12			12	
13	Bus13	13	29	28	13	19	13	39	57	FIXED	13			13	
14	Bus14	14	28	27	14	20	14	13	49	FIXED	14			14	
15	Bus15	15	27	26	15	23	15	10	61	FIXED	15			15	
16	Bus16	16	52	53	16	25	16	9	55	FIXED	16			16	
17	Bus17	17	53	54	17	27	17				17			17	
18	Bus18	18	54	55	18	28	18				18			18	
19	Bus19	19	9	12	19	29	19				19			19	
20	Bus20	20	9	10	20	30	20				20			20	
21	Bus21	21	9	13	21	31	21				21			21	
22	Bus22	22	9	11	22	32	22				22			22	
23	Bus23	23	11	13	23	33	23				23			23	
24	Bus24	24	18	19	24	35	24				24			24	
25	Bus25	25	19	20	25	38	25				25			25	
26	Bus26	26	21	22	26	41	26				26			26	
27	Bus27	27	22	38	27	42	27				27			27	
28	Bus28	28	22	23	28	43	28				28			28	
29	Bus29	29	23	24	29	44	29				29			29	
30	Bus30	30	25	30	30	47	30				30			30	
31	Bus31	31	30	31	31	49	31				31			31	
32	Bus32	32	31	32	32	50	32				32			32	
33	Bus33	33	32	33	33	51	33				33			33	
34	Bus34	34	34	35	34	52	34				34			34	
35	Bus35	35	35	36	35	53	35				35			35	
36	Bus36	36	36	37	36	54	36				36			36	
37	Bus37	37	36	40	37	55	37				37			37	
38	Bus38	38	37	39	38	56	38				38			38	
39	Bus39	39	37	38	39	57	39				39			39	
40	Bus40	40	38	44	40		40				40			40	
41	Bus41	41	38	49	41		41				41			41	
42	Bus42	42	48	49	42		42				42			42	
43	Bus43	43	38	48	43		43				43			43	
44	Bus44	44	44	45	44		44				44			44	
45	Bus45	45	14	15	45		45				45			45	
46	Bus46	46	13	15	46		46				46			46	
47	Bus47	47	14	13	47		47				47			47	
48	Bus48	48	46	47	48		48				48			48	
49	Bus49	49	47	48	49		49				49			49	
50	Bus50	50	49	50	50		50				50			50	
51	Bus51	51	50	51	51		51				51			51	
52	Bus52	52	56	57	52		52				52			52	
53	Bus53	53	42	56	53		53				53			53	
54	Bus54	54	41	56	54		54				54			54	
55	Bus55	55	41	42	55		55				55			55	
56	Bus56	56	10	12	56		56				56			56	
57	Bus57	57	12	13	57		57				57			57	
58		58	12	16	58		58				58			58	
59		59	1	16	59		59				59			59	
60		60	1	17	60		60				60			60	
61		61	17	12	61		61				61			61	

Table D.2: Results of the OPP calculation for the IEEE 57 test –system under full observability constraint using the Jansson's method

Number	DeviceRef	Location	PMU_Number	Type	Assign Device
1	1	1	1	VM	BS
2	1	1	1	VA	BS
3	2	1	1	AM	LN
4	2	1	1	AA	LN
5	59	1	1	AM	LN
6	59	1	1	AA	LN
7	60	1	1	AM	LN
8	60	1	1	AA	LN
9	4	4	2	VM	BS
10	4	4	2	VA	BS
11	6	4	2	AM	LN
12	6	4	2	AA	LN
13	1	4	2	AM	TR
14	1	4	2	AA	TR
15	9	9	3	VM	BS
16	9	9	3	VA	BS
17	11	9	3	AM	LN
18	11	9	3	AA	LN
19	19	9	3	AM	LN
20	19	9	3	AA	LN
21	20	9	3	AM	LN
22	20	9	3	AA	LN
23	21	9	4	AM	LN
24	21	9	4	AA	LN
25	22	9	4	AM	LN
26	22	9	4	AA	LN
27	16	9	4	AM	TR
28	16	9	4	AA	TR
29	20	20	5	VM	BS
30	20	20	5	VA	BS
31	25	20	5	AM	LN
32	25	20	5	AA	LN
33	3	20	5	AM	TR
34	3	20	5	AA	TR
35	25	25	6	VM	BS
36	25	25	6	VA	BS
37	30	25	6	AM	LN
38	30	25	6	AA	LN
39	7	25	6	AM	TR
40	7	25	6	AA	TR
41	29	29	7	VM	BS
42	29	29	7	VA	BS
43	12	29	7	AM	LN
44	12	29	7	AA	LN
45	13	29	7	AM	LN
46	13	29	7	AA	LN
47	2	29	7	AM	TR
48	2	29	7	AA	TR
49	32	32	8	VM	BS
50	32	32	8	VA	BS
51	32	32	8	AM	LN
52	32	32	8	AA	LN
53	33	32	8	AM	LN
54	33	32	8	AA	LN
55	8	32	8	AM	TR
56	8	32	8	AA	TR
57	47	47	9	VM	BS
58	47	47	9	VA	BS
59	48	47	9	AM	LN
60	48	47	9	AA	LN
61	49	47	9	AM	LN
62	49	47	9	AA	LN
63	50	50	10	VM	BS
64	50	50	10	VA	BS
65	50	50	10	AM	LN
66	50	50	10	AA	LN
67	51	50	10	AM	LN
68	51	50	10	AA	LN
69	53	53	11	VM	BS
70	53	53	11	VA	BS
71	17	53	11	AM	LN
72	17	53	11	AA	LN
73	56	56	12	VM	BS
74	56	56	12	VA	BS
75	53	56	12	AM	LN
76	53	56	12	AA	LN
77	54	56	12	AM	LN
78	54	56	12	AA	LN
79	12	56	12	AM	TR
80	12	56	12	AA	TR

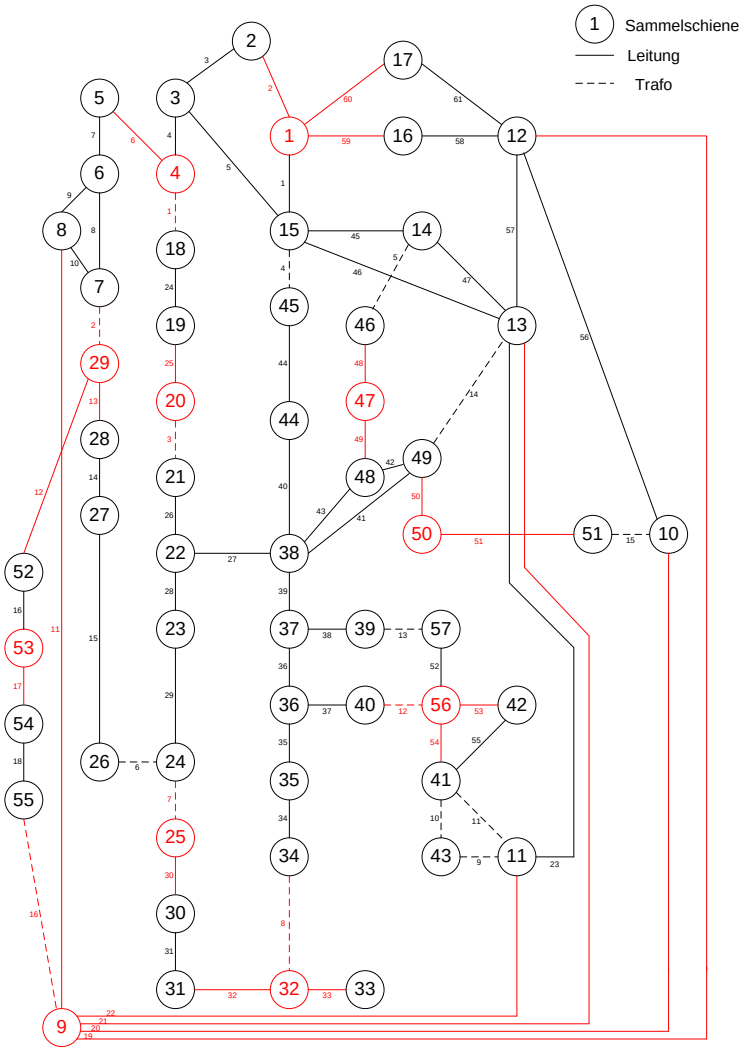

Figure D.1: Graph representation of the OPP calculation for the IEEE 57 bus test-system according to Jansson's method

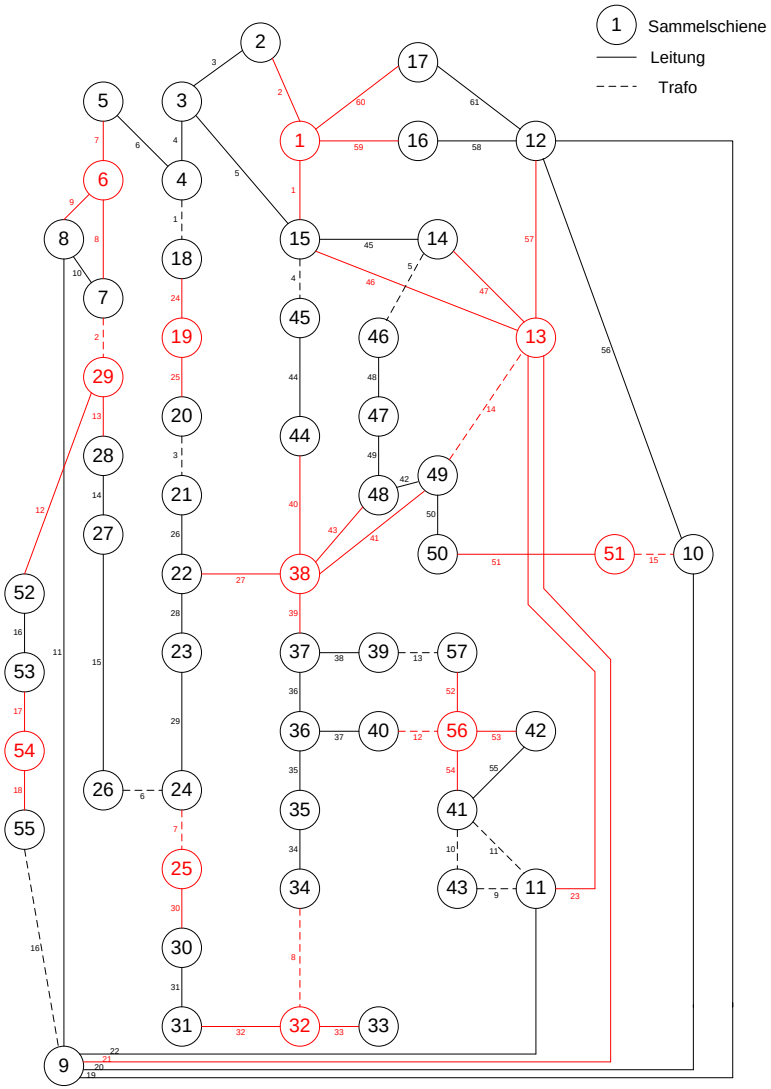

Figure D.2: Graph representation of the extended Altman's OPP calculation for the IEEE 57 bus test-system

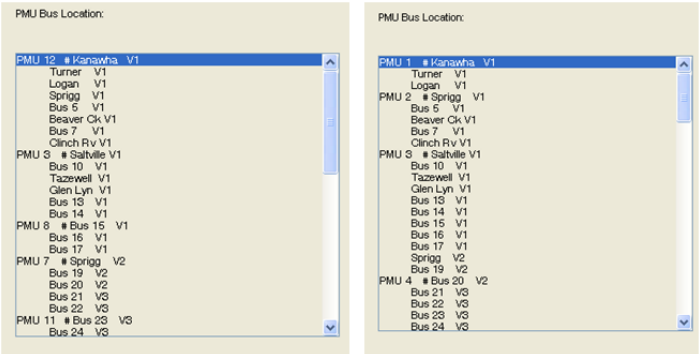

A) B)

Figure D.3: Screenshot abridgments of PSAT OPP calculation result using the bisecting search method (A) and the Recursive N algorithm (B) for the IEEE 57-bus test system.

Appendix E PSADD structure and OPP calculation for DK-Vest

The Institute of Electrical and Electronics Engineers (IEEE) has recommended a guideline called Power System Applications Data Dictionary (PSADD), to provide a standard for exchange of information about electrical transmission networks. This section is only intended to give a brief overview of the parts needed to solve the OPP problem. PSADD organizes the information in the notion of objects. Each object has a number of attributes that specifies the object.
One example is the object line. It contains the attributes: Number, FromBusRef and ToBusRef (this is just some of the attributes the object line contains). These three values describe where the line is located in the network, and correspond to one edge in the graph description of the network. The objects of interest for OPP analysis are the following structures:

- Bus
- Line
- Xformer (transformer)
- Machine
- Load
- Shunt
- Analog.

The objects are stored as structures in Matlab and stored on file in .mat format. Bus, Line and Xformer store data about the objects with the same names, while Machine, Load and Shunt store information about diverse objects in the network. These last three structures are only used to identify the non zero-injection nodes that exist in the transmission network.
Analog is used to store measurement points and the values measured at these points.

Table E.1: DK-VEST: 400 kV+1 in PSADD Format

Bus		Line			Load		Xformer				Machine			Shunt	
Nr	*Name*	Nr	*FromBus*	*ToBus*	Nr	*BusRef*	Nr	*PrimBus*	*SecBus*	*Type*	Nr	*BusRef*	*Type*	Nr	*BusRef*
1	Germany	1	1	2	1	3	1	3	2	FIXED	1	16	Gen	1	
2	AUD5	2	1	2	2	5	2	4	5	FIXED	2	22	Gen	2	
3	AUD8	3	2	4	3		3	4	5	FIXED	3	28	Gen	3	
4	KAS5	4	2	4	4		4	6	8	FIXED	4	40	Gen	4	
5	KAS3	5	4	7	5		5	9	10	FIXED	5	42	Gen	5	
6	EDR3	6	4	13	6		6	11	12	FIXED	6	35	Gen	6	
7	REV5	7	7	8	7		7	37	38	FIXED	7	34	Gen	7	
8	EDR5	8	7	11	8		8	37	38	FIXED	8	1	Gen	8	
9	IDU3	9	11	37	9		9	37	39	FIXED	9	43	Gen	9	
10	IDU5	10	10	37	10		10	39	40	FIXED	10	44	Gen	10	
11	ASR5	11	37	29	11		11	41	42	FIXED	11			11	
12	ASR3	12	21	20	12		12	37	41	FIXED	12			12	
13	LAG5	13	20	13	13		13	39	41	FIXED	13			13	
14	LAG3	14	20	17	14		14	39	41	FIXED	14			14	
15	SVS5	15	17	13	15		15	33	34	FIXED	15			15	
16	SVSa	16	13	24	16		16	31	33	FIXED	16			16	
17	KIN5	17	24	25	17		17	31	35	FIXED	17			17	
18	KIN3	18	25	29	18		18	32	36	FIXED	18			18	
19	FGD3	19	25	27	19		19	32	36	FIXED	19			19	
20	FGD5	20	29	31	20		20	29	30	FIXED	20			20	
21	FVO5	21	29	31	21		21	25	26	FIXED	21			21	
22	FVOa	22	31	32	22		22	27	28	FIXED	22			22	
23	MAL3	23	32	44	23		23	23	24	FIXED	23			23	
24	MAL5	24	41	43	24		24	13	14	FIXED	24			24	
25	TRI5	25	13	15	25		25	17	18	FIXED	25			25	
26	TRI3	26			26		26	19	20	FIXED	26			26	
27	MKS5	27			27		27	19	20	FIXED	27			27	
28	MKSb	28			28		28	21	22	FIXED	28			28	
29	FER5	29			29		29	15	16	FIXED	29			29	
30	FER3	30			30		30				30			30	
31	NVV5	31			31		31				31			31	
32	VHA5	32			32		32				32			32	
33	NVV3	33			33		33				33			33	
34	NVVb	34			34		34				34			34	
35	NVVa	35			35		35				35			35	
36	VHA2	36			36		36				36			36	
37	TJE5	37			37		37				37			37	
38	TJE2	38			38		38				38			38	
39	TJE3	39			39		39				39			39	
40	TJEa	40			40		40				40			40	
41	STA5	41			41		41				41			41	
42	RN1a	42			42		42				42			42	
43	Norway	43			43		43				43			43	
44	Sweden	44			44		44				44			44	

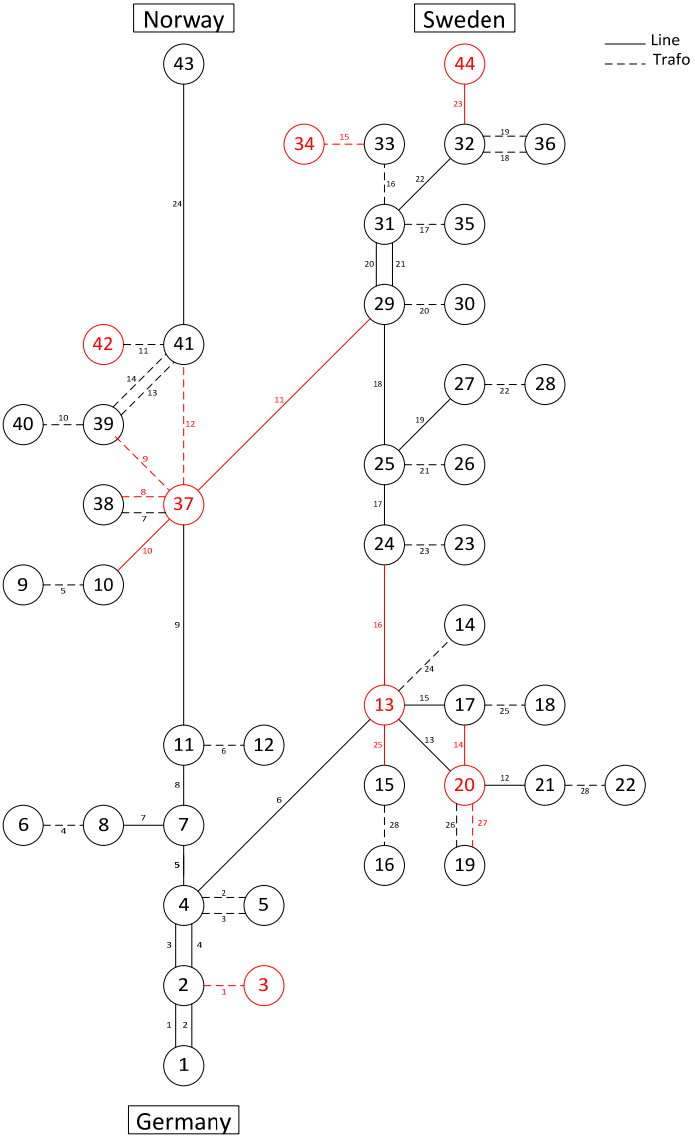

Figure E.1: Graph representation of 400 kV+1, in red are the monitoring objects as found through the OPP calculation by Jansson (compare with table results in 5.5.6.2)

DK-VEST

Table E.2: DK-VEST in PSADD Format

Bus		Line			Load		Xformer				Machine			Shunt	
Nr	*Name*	Nr	*FromBus*	*ToBus*	Nr	*BusRef*	Nr	*PrimBus*	*SecBus*	*Type*	Nr	*BusRef*	*Type*	Nr	*BusRef*
1	ABS2	**1**	2	50	**1**	1	**1**	2	1	VOLT	**1**	1	Gen	**1**	
2	ABS3	**2**	2	236	**2**	3	**2**	4	3	VOLT	**2**	3	Gen	**2**	
3	ADL2	**3**	2	244	**3**	6	**3**	4	3	VOLT	**3**	6	Gen	**3**	
4	ADL3	**4**	4	5	**4**	12	**4**	7	6	VOLT	**4**	13	Gen	**4**	
5	ADX3	**5**	4	278	**5**	13	**5**	9	8	FIXED	**5**	15	Gen	**5**	
6	AND2	**6**	5	36	**6**	15	**6**	10	12	FIXED	**6**	17	Gen	**6**	
7	AND3	**7**	5	77	**7**	17	**7**	10	12	FIXED	**7**	19	Gen	**7**	
8	ASR3	**8**	5	77	**8**	19	**8**	11	12	FIXED	**8**	21	Gen	**8**	
9	ASR5	**9**	5	123	**9**	21	**9**	13	208	FIXED	**9**	23	Gen	**9**	
10	AUD4	**10**	7	18	**10**	23	**10**	13	209	FIXED	**10**	25	Gen	**10**	
11	AUD5	**11**	7	108	**11**	29	**11**	14	13	VOLT	**11**	26	Gen	**11**	
12	AUD8	**12**	8	248	**12**	33	**12**	14	13	VOLT	**12**	29	Gen	**12**	
13	BBR2	**13**	9	211	**13**	35	**13**	15	176	FIXED	**13**	228	Gen	**13**	
14	BBR3	**14**	9	254	**14**	40	**14**	16	15	VOLT	**14**	33	Gen	**14**	
15	BDK2	**15**	10	43	**15**	44	**15**	16	15	VOLT	**15**	273	Gen	**15**	
16	BDK3	**16**	10	43	**16**	45	**16**	18	17	VOLT	**16**	35	Gen	**16**	
17	BDR2	**17**	10	61	**17**	47	**17**	18	17	VOLT	**17**	40	Gen	**17**	
18	BDR3	**18**	10	61	**18**	49	**18**	20	19	VOLT	**18**	45	Gen	**18**	
19	BED2	**19**	10	89	**19**	54	**19**	20	19	VOLT	**19**	47	Gen	**19**	
20	BED3	**20**	10	89	**20**	56	**20**	21	193	FIXED	**20**	49	Gen	**20**	
21	BIL2	**21**	11	88	**21**	59	**21**	21	194	FIXED	**21**	53	Gen	**21**	
22	BIL3	**22**	11	88	**22**	64	**22**	21	195	FIXED	**22**	52	Gen	**22**	
23	BJH2	**23**	11	276	**23**	66	**23**	21	196	FIXED	**23**	54	Gen	**23**	
24	BJH3	**24**	11	276	**24**	68	**24**	22	21	VOLT	**24**	56	Gen	**24**	
25	BROa	**25**	12	44	**25**	72	**25**	22	21	VOLT	**25**	59	Gen	**25**	
26	BRUa	**26**	14	86	**26**	74	**26**	22	21	VOLT	**26**	64	Gen	**26**	
27	DOL4	**27**	14	105	**27**	76	**27**	23	200	FIXED	**27**	66	Gen	**27**	
28	DOL5	**28**	16	129	**28**	78	**28**	23	201	FIXED	**28**	68	Gen	**28**	
29	DYB2	**29**	16	131	**29**	80	**29**	23	202	FIXED	**29**	72	Gen	**29**	
30	DYB3	**30**	18	98	**30**	83	**30**	24	23	VOLT	**30**	74	Gen	**30**	
31	EDR3	**31**	20	127	**31**	86	**31**	24	23	VOLT	**31**	76	Gen	**31**	
32	EDR5	**32**	20	233	**32**	89	**32**	28	27	FIXED	**32**	78	Gen	**32**	
33	EST2	**33**	22	233	**33**	93	**33**	29	204	FIXED	**33**	80	Gen	**33**	
34	EST3	**34**	22	246	**34**	96	**34**	29	205	FIXED	**34**	83	Gen	**34**	
35	FER2	**35**	22	246	**35**	102	**35**	30	29	VOLT	**35**	90	Gen	**35**	
36	FER3	**36**	24	246	**36**	104	**36**	32	31	FIXED	**36**	96	Gen	**36**	
37	FER5	**37**	24	246	**37**	107	**37**	34	33	VOLT	**37**	102	Gen	**37**	
38	FGA1	**38**	27	61	**38**	109	**38**	36	35	VOLT	**38**	104	Gen	**38**	
39	FGB1	**39**	27	61	**39**	112	**39**	37	36	FIXED	**39**	107	Gen	**39**	
40	FGD2	**40**	28	63	**40**	118	**40**	40	137	FIXED	**40**	109	Gen	**40**	
41	FGD3	**41**	28	63	**41**	120	**41**	40	138	FIXED	**41**	112	Gen	**41**	
42	FGD5	**42**	28	260	**42**	122	**42**	40	139	FIXED	**42**	118	Gen	**42**	
43	FLE4	**43**	28	276	**43**	126	**43**	40	181	FIXED	**43**	120	Gen	**43**	
44	FLE8	**44**	28	276	**44**	128	**44**	40	182	FIXED	**44**	122	Gen	**44**	
45	FRD2	**45**	30	221	**45**	135	**45**	41	38	FIXED	**45**	134	Gen	**45**	
46	FRD3	**46**	30	266	**46**	212	**46**	41	39	FIXED	**46**	133	Gen	**46**	
47	FRT2	**47**	31	69	**47**	218	**47**	41	40	VOLT	**47**	126	Gen	**47**	
48	FRT3	**48**	31	105	**48**	220	**48**	42	41	FIXED	**48**	128	Gen	**48**	
49	FVO2	**49**	31	105	**49**	222	**49**	42	41	FIXED	**49**	137	Gen	**49**	
50	FVO3	**50**	32	211	**50**	224	**50**	43	44	FIXED	**50**	138	Gen	**50**	
51	FVO5	**51**	34	105	**51**	225	**51**	43	44	FIXED	**51**	139	Gen	**51**	
52	FVOa	**52**	36	123	**52**	229	**52**	43	44	FIXED	**52**	140	Gen	**52**	
53	FVOb	**53**	36	250	**53**	232	**53**	46	45	VOLT	**53**	141	Gen	**53**	
54	GRP2	**54**	37	132	**54**	234	**54**	48	47	VOLT	**54**	142	Gen	**54**	
55	GRP3	**55**	37	132	**55**	243	**55**	49	163	FIXED	**55**	143	Gen	**55**	
56	HAS2	**56**	37	254	**56**	245	**56**	49	164	FIXED	**56**	144	Gen	**56**	
57	HAS3	**57**	37	257	**57**	247	**57**	49	166	FIXED	**57**	145	Gen	**57**	
58	HAT1	**58**	41	50	**58**	249	**58**	49	167	FIXED	**58**	146	Gen	**58**	
59	HAT2	**59**	41	136	**59**	258	**59**	50	49	VOLT	**59**	147	Gen	**59**	
60	HAT3	**60**	41	236	**60**	269	**60**	50	49	VOLT	**60**	148	Gen	**60**	
61	HBN4	**61**	42	51	**61**	271	**61**	50	49	VOLT	**61**	149	Gen	**61**	
62	HBN5	**62**	42	92	**62**	277	**62**	50	53	FIXED	**62**	150	Gen	**62**	
63	HBO5	**63**	42	99	**63**	279	**63**	51	52	FIXED	**63**	151	Gen	**63**	
64	HER2	**64**	43	87	**64**		**64**	55	54	VOLT	**64**	152	Gen	**64**	
65	HER3	**65**	43	227	**65**		**65**	55	54	VOLT	**65**	153	Gen	**65**	
66	HNB2	**66**	46	75	**66**		**66**	57	56	VOLT	**66**	154	Gen	**66**	
67	HNB3	**67**	46	95	**67**		**67**	57	56	VOLT	**67**	155	Gen	**67**	

Bus		Line			Load		Xformer				Machine			Shunt	
Nr	*Name*	Nr	*FromBus*	*ToBus*	Nr	*BusRef*	Nr	*PrimBus*	*SecBus*	*Type*	Nr	*BusRef*	*Type*	Nr	*BusRef*
68	HOD2	**68**	46	123	**68**		**68**	59	174	FIXED	**68**	156	Gen	**68**	
69	HOD3	**69**	48	95	**69**		**69**	59	175	FIXED	**69**	157	Gen	**69**	
70	HRA3	**70**	48	127	**70**		**70**	60	58	FIXED	**70**	158	Gen	**70**	
71	HRA7	**71**	48	272	**71**		**71**	60	59	VOLT	**71**	159	Gen	**71**	
72	HSK2	**72**	50	55	**72**		**72**	60	59	VOLT	**72**	160	Gen	**72**	
73	HSK3	**73**	50	136	**73**		**73**	62	61	FIXED	**73**	161	Gen	**73**	
74	HVO2	**74**	55	91	**74**		**74**	64	274	FIXED	**74**	162	Gen	**74**	
75	HVO3	**75**	57	110	**75**		**75**	65	64	VOLT	**75**	163	Gen	**75**	
76	HVV2	**76**	57	119	**76**		**76**	65	64	VOLT	**76**	165	Gen	**76**	
77	HVV3	**77**	57	256	**77**		**77**	66	165	FIXED	**77**	166	Gen	**77**	
78	HØN2	**78**	60	97	**78**		**78**	67	66	VOLT	**78**	167	Gen	**78**	
79	HØN3	**79**	60	110	**79**		**79**	67	66	VOLT	**79**	168	Gen	**79**	
80	IDU2	**80**	61	275	**80**		**80**	68	140	FIXED	**80**	171	Gen	**80**	
81	IDU3	**81**	61	275	**81**		**81**	68	141	FIXED	**81**	169	Gen	**81**	
82	IDU5	**82**	62	63	**82**		**82**	68	142	FIXED	**82**	172	Gen	**82**	
83	KAE2	**83**	62	63	**83**		**83**	68	143	FIXED	**83**	173	Gen	**83**	
84	KAE3	**84**	62	276	**84**		**84**	68	144	FIXED	**84**	174	Gen	**84**	
85	KAS1	**85**	62	276	**85**		**85**	68	149	FIXED	**85**	175	Gen	**85**	
86	KAS3	**86**	63	260	**86**		**86**	68	150	FIXED	**86**	176	Gen	**86**	
87	KAS4	**87**	65	223	**87**		**87**	68	151	FIXED	**87**	181	Gen	**87**	
88	KAS5	**88**	65	233	**88**		**88**	68	152	FIXED	**88**	182	Gen	**88**	
89	KIE4	**89**	67	250	**89**		**89**	69	68	VOLT	**89**	187	Gen	**89**	
90	KIEa	**90**	67	256	**90**		**90**	70	71	FIXED	**90**	183	Gen	**90**	
91	KIN3	**91**	70	84	**91**		**91**	73	72	VOLT	**91**	184	Gen	**91**	
92	KIN5	**92**	73	79	**92**		**92**	75	74	VOLT	**92**	185	Gen	**92**	
93	KLF2	**93**	73	256	**93**		**93**	77	76	VOLT	**93**	186	Gen	**93**	
94	KLF3	**94**	75	129	**94**		**94**	77	76	VOLT	**94**	188	Gen	**94**	
95	KLT3	**95**	75	131	**95**		**95**	79	78	VOLT	**95**	189	Gen	**95**	
96	KNA2	**96**	75	131	**96**		**96**	80	173	FIXED	**96**	190	Gen	**96**	
97	KNA3	**97**	75	230	**97**		**97**	81	80	VOLT	**97**	191	Gen	**97**	
98	LAG3	**98**	79	110	**98**		**98**	81	80	VOLT	**98**	192	Gen	**98**	
99	LAG5	**99**	81	233	**99**		**99**	82	81	FIXED	**99**	193	Gen	**99**	
100	LDO3	**100**	81	270	**100**		**100**	83	169	FIXED	**100**	194	Gen	**100**	
101	LDO5	**101**	82	254	**101**		**101**	83	170	FIXED	**101**	195	Gen	**101**	
102	LOL2	**102**	84	105	**102**		**102**	83	171	FIXED	**102**	196	Gen	**102**	
103	LOL3	**103**	84	105	**103**		**103**	84	83	VOLT	**103**	197	Gen	**103**	
104	LYK2	**104**	84	235	**104**		**104**	84	83	VOLT	**104**	198	Gen	**104**	
105	LYK3	**105**	86	108	**105**		**105**	86	85	FIXED	**105**	199	Gen	**105**	
106	MAG1	**106**	86	213	**106**		**106**	86	85	FIXED	**106**	200	Gen	**106**	
107	MAG2	**107**	86	226	**107**		**107**	87	86	FIXED	**107**	201	Gen	**107**	
108	MAG3	**108**	86	226	**108**		**108**	88	86	FIXED	**108**	202	Gen	**108**	
109	MAL2	**109**	88	99	**109**		**109**	88	86	FIXED	**109**	203	Gen	**109**	
110	MAL3	**110**	88	211	**110**		**110**	89	90	FIXED	**110**	204	Gen	**110**	
111	MAL5	**111**	92	99	**111**		**111**	92	91	FIXED	**111**	205	Gen	**111**	
112	MES2	**112**	94	95	**112**		**112**	94	93	VOLT	**112**	206	Gen	**112**	
113	MES3	**113**	97	98	**113**		**113**	97	96	VOLT	**113**	207	Gen	**113**	
114	MKS3	**114**	97	248	**114**		**114**	97	96	VOLT	**114**	208	Gen	**114**	
115	MKS5	**115**	98	219	**115**		**115**	101	281	FIXED	**115**	209	Gen	**115**	
116	MKSa	**116**	98	238	**116**		**116**	101	281	FIXED	**116**	210	Gen	**116**	
117	MKSb	**117**	99	111	**117**		**117**	267	281	FIXED	**117**	214	Gen	**117**	
118	MLP2	**118**	99	239	**118**		**118**	267	281	FIXED	**118**	215	Gen	**118**	
119	MLP3	**119**	103	253	**119**		**119**	100	282	FIXED	**119**	216	Gen	**119**	
120	MLU2	**120**	105	213	**120**		**120**	100	282	FIXED	**120**	212	Gen	**120**	
121	MLU3	**121**	105	223	**121**		**121**	267	282	FIXED	**121**	218	Gen	**121**	
122	MOS2	**122**	110	125	**122**		**122**	267	282	FIXED	**122**	220	Gen	**122**	
123	MOS3	**123**	111	257	**123**		**123**	99	98	FIXED	**123**	224	Gen	**123**	
124	MSL2	**124**	113	256	**124**		**124**	100	215	FIXED	**124**	225	Gen	**124**	
125	MSL3	**125**	113	280	**125**		**125**	101	216	FIXED	**125**	240	Gen	**125**	
126	NOR2	**126**	114	256	**126**		**126**	102	210	FIXED	**126**	116	Gen	**126**	
127	NOR3	**127**	114	256	**127**		**127**	103	102	VOLT	**127**	117	Gen	**127**	
128	NSP2	**128**	114	256	**128**		**128**	103	102	VOLT	**128**	232	Gen	**128**	
129	NSP3	**129**	115	257	**129**		**129**	105	104	VOLT	**129**	234	Gen	**129**	
130	NVT3	**130**	119	256	**130**		**130**	105	104	VOLT	**130**	243	Gen	**130**	
131	NVV3	**131**	121	256	**131**		**131**	105	273	FIXED	**131**	245	Gen	**131**	
132	NVV5	**132**	123	253	**132**		**132**	108	106	FIXED	**132**	247	Gen	**132**	
133	NVVa	**133**	123	272	**133**		**133**	108	106	FIXED	**133**	249	Gen	**133**	
134	NVVb	**134**	130	131	**134**		**134**	108	107	VOLT	**134**	255	Gen	**134**	
135	OSØ2	**135**	130	266	**135**		**135**	108	107	VOLT	**135**	258	Gen	**135**	
136	OSØ3	**136**	130	278	**136**		**136**	110	109	VOLT	**136**	261	Gen	**136**	

Bus		Line			Load		Xformer				Machine			Shunt	
Nr	*Name*	Nr	*FromBus*	*ToBus*	Nr	*BusRef*	Nr	*PrimBus*	*SecBus*	*Type*	Nr	*BusRef*	*Type*	Nr	*BusRef*
137	QB1a	**137**	131	221	**137**		**137**	111	110	FIXED	**137**	268	Gen	**137**	
138	QB2a	**138**	131	266	**138**		**138**	113	112	VOLT	**138**	269	Gen	**138**	
139	QB3a	**139**	132	267	**139**		**139**	113	112	VOLT	**139**	271	Gen	**139**	
140	QBDa	**140**	219	238	**140**		**140**	114	116	FIXED	**140**	274	Gen	**140**	
141	QBDb	**141**	226	244	**141**		**141**	115	117	FIXED	**141**	277	Gen	**141**	
142	QBDc	**142**	226	259	**142**		**142**	119	118	VOLT	**142**	1	Gen	**142**	
143	QBDd	**143**	226	263	**143**		**143**	120	188	FIXED	**143**	3	Gen	**143**	
144	QBDe	**144**	235	270	**144**		**144**	121	120	VOLT	**144**	6	Gen	**144**	
145	QBJa	**145**	238	259	**145**		**145**	123	122	VOLT	**145**	13	Gen	**145**	
146	QBJb	**146**	246	253	**146**		**146**	123	122	VOLT	**146**	15	Gen	**146**	
147	QBJc	**147**	246	253	**147**		**147**	125	124	VOLT	**147**	17	Gen	**147**	
148	QBJd	**148**	246	256	**148**		**148**	127	126	VOLT	**148**	19	Gen	**148**	
149	QBMa	**149**	246	256	**149**		**149**	128	153	FIXED	**149**	21	Gen	**149**	
150	QBMb	**150**	256	280	**150**		**150**	128	154	FIXED	**150**	23	Gen	**150**	
151	QBMc	**151**			**151**		**151**	128	155	FIXED	**151**	29	Gen	**151**	
152	QBMd	**152**			**152**		**152**	128	156	FIXED	**152**	35	Gen	**152**	
153	QBSa	**153**			**153**		**153**	128	157	FIXED	**153**	40	Mot	**153**	
154	QBSb	**154**			**154**		**154**	128	158	FIXED	**154**	45	Gen	**154**	
155	QBSc	**155**			**155**		**155**	128	159	FIXED	**155**	47	Gen	**155**	
156	QBSd	**156**			**156**		**156**	129	128	VOLT	**156**	49	Gen	**156**	
157	QBSe	**157**			**157**		**157**	129	128	VOLT	**157**	54	Gen	**157**	
158	QBSf	**158**			**158**		**158**	131	134	FIXED	**158**	56	Gen	**158**	
159	QBSg	**159**			**159**		**159**	132	131	FIXED	**159**	59	Gen	**159**	
160	QCNa	**160**			**160**		**160**	132	133	FIXED	**160**	64	Gen	**160**	
161	QCNb	**161**			**161**		**161**	136	135	VOLT	**161**	66	Gen	**161**	
162	QCNc	**162**			**162**		**162**	212	183	FIXED	**162**	68	Gen	**162**	
163	QDPa	**163**			**163**		**163**	212	184	FIXED	**163**	71	Gen	**163**	
164	QDPb	**164**			**164**		**164**	212	185	FIXED	**164**	74	Gen	**164**	
165	QDSa	**165**			**165**		**165**	212	186	FIXED	**165**	78	Gen	**165**	
166	QF1a	**166**			**166**		**166**	212	187	FIXED	**166**	80	Gen	**166**	
167	QF3a	**167**			**167**		**167**	213	212	VOLT	**167**	83	Gen	**167**	
168	QFRa	**168**			**168**		**168**	218	177	FIXED	**168**	93	Gen	**168**	
169	QGDa	**169**			**169**		**169**	218	178	FIXED	**169**	96	Gen	**169**	
170	QGDb	**170**			**170**		**170**	218	179	FIXED	**170**	102	Gen	**170**	
171	QGDc	**171**			**171**		**171**	218	180	FIXED	**171**	104	Gen	**171**	
172	QGRa	**172**			**172**		**172**	218	203	FIXED	**172**	107	Gen	**172**	
173	QHLa	**173**			**173**		**173**	219	217	FIXED	**173**	109	Gen	**173**	
174	QHOa	**174**			**174**		**174**	219	217	FIXED	**174**	112	Gen	**174**	
175	QHOb	**175**			**175**		**175**	219	218	VOLT	**175**	118	Gen	**175**	
176	QHØa	**176**			**176**		**176**	219	218	VOLT	**176**	120	Gen	**176**	
177	QKEa	**177**			**177**		**177**	220	168	FIXED	**177**	122	Gen	**177**	
178	QKEb	**178**			**178**		**178**	220	197	FIXED	**178**	126	Gen	**178**	
179	QKEc	**179**			**179**		**179**	220	198	FIXED	**179**	128	Gen	**179**	
180	QKEd	**180**			**180**		**180**	220	199	FIXED	**180**	131	Gen	**180**	
181	QKKa	**181**			**181**		**181**	221	220	VOLT	**181**	212	Gen	**181**	
182	QKKb	**182**			**182**		**182**	221	220	VOLT	**182**	218	Gen	**182**	
183	QRBa	**183**			**183**		**183**	223	222	FIXED	**183**	220	Gen	**183**	
184	QRBb	**184**			**184**		**184**	223	222	FIXED	**184**	222	Gen	**184**	
185	QRBc	**185**			**185**		**185**	224	189	FIXED	**185**	224	Gen	**185**	
186	QRBd	**186**			**186**		**186**	224	190	FIXED	**186**	225	Gen	**186**	
187	QRBe	**187**			**187**		**187**	224	191	FIXED	**187**	232	Gen	**187**	
188	QRVa	**188**			**188**		**188**	224	192	FIXED	**188**	234	Gen	**188**	
189	QS1a	**189**			**189**		**189**	226	225	VOLT	**189**	243	Gen	**189**	
190	QS1b	**190**			**190**		**190**	226	225	VOLT	**190**	245	Gen	**190**	
191	QS1c	**191**			**191**		**191**	226	228	FIXED	**191**	247	Gen	**191**	
192	QS1d	**192**			**192**		**192**	227	226	FIXED	**192**	249	Gen	**192**	
193	QSEa	**193**			**193**		**193**	231	283	FIXED	**193**	258	Gen	**193**	
194	QSEb	**194**			**194**		**194**	231	283	FIXED	**194**	269	Gen	**194**	
195	QSEc	**195**			**195**		**195**	253	283	FIXED	**195**	271	Gen	**195**	
196	QSEd	**196**			**196**		**196**	253	283	FIXED	**196**	279	Gen	**196**	
197	QSGa	**197**			**197**		**197**	231	284	FIXED	**197**			**197**	
198	QSGb	**198**			**198**		**198**	231	284	FIXED	**198**			**198**	
199	QSGc	**199**			**199**		**199**	254	284	FIXED	**199**			**199**	
200	QSIa	**200**			**200**		**200**	254	284	FIXED	**200**			**200**	
201	QSIb	**201**			**201**		**201**	230	229	VOLT	**201**			**201**	
202	QSIc	**202**			**202**		**202**	231	214	FIXED	**202**			**202**	
203	QSLa	**203**			**203**		**203**	232	160	FIXED	**203**			**203**	
204	QSÆa	**204**			**204**		**204**	232	161	FIXED	**204**			**204**	
205	QSÆb	**205**			**205**		**205**	232	162	FIXED	**205**			**205**	

Bus		Line			Load		Xformer				Machine			Shunt	
Nr	*Name*	Nr	*FromBus*	*ToBus*	Nr	*BusRef*	Nr	*PrimBus*	*SecBus*	*Type*	Nr	*BusRef*	*Type*	Nr	*BusRef*
206	QSØa	**206**			**206**		**206**	233	232	VOLT	**206**			**206**	
207	QSØb	**207**			**207**		**207**	233	232	VOLT	**207**			**207**	
208	QTØa	**208**			**208**		**208**	235	234	VOLT	**208**			**208**	
209	QTØb	**209**			**209**		**209**	236	224	VOLT	**209**			**209**	
210	QVIa	**210**			**210**		**210**	236	224	VOLT	**210**			**210**	
211	REV5	**211**			**211**		**211**	238	237	FIXED	**211**			**211**	
212	RIB2	**212**			**212**		**212**	238	241	FIXED	**212**			**212**	
213	RIB3	**213**			**213**		**213**	239	240	FIXED	**213**			**213**	
214	RN1a	**214**			**214**		**214**	243	206	FIXED	**214**			**214**	
215	RS1a	**215**			**215**		**215**	243	207	FIXED	**215**			**215**	
216	RS2a	**216**			**216**		**216**	244	242	FIXED	**216**			**216**	
217	RYT1	**217**			**217**		**217**	244	243	VOLT	**217**			**217**	
218	RYT2	**218**			**218**		**218**	244	243	VOLT	**218**			**218**	
219	RYT3	**219**			**219**		**219**	245	145	FIXED	**219**			**219**	
220	SBA2	**220**			**220**		**220**	245	146	FIXED	**220**			**220**	
221	SBA3	**221**			**221**		**221**	245	147	FIXED	**221**			**221**	
222	SFE1	**222**			**222**		**222**	245	148	FIXED	**222**			**222**	
223	SFE3	**223**			**223**		**223**	246	245	VOLT	**223**			**223**	
224	SFV2	**224**			**224**		**224**	248	247	VOLT	**224**			**224**	
225	SHE2	**225**			**225**		**225**	250	249	VOLT	**225**			**225**	
226	SHE3	**226**			**226**		**226**	253	251	FIXED	**226**			**226**	
227	SHE4	**227**			**227**		**227**	253	251	FIXED	**227**			**227**	
228	SHEa	**228**			**228**		**228**	253	251	FIXED	**228**			**228**	
229	SKA2	**229**			**229**		**229**	253	251	FIXED	**229**			**229**	
230	SKA3	**230**			**230**		**230**	253	255	FIXED	**230**			**230**	
231	STA5	**231**			**231**		**231**	254	252	VOLT	**231**			**231**	
232	STR2	**232**			**232**		**232**	254	252	VOLT	**232**			**232**	
233	STR3	**233**			**233**		**233**	254	253	FIXED	**233**			**233**	
234	STS2	**234**			**234**		**234**	257	256	FIXED	**234**			**234**	
235	STS3	**235**			**235**		**235**	259	258	FIXED	**235**			**235**	
236	SVB3	**236**			**236**		**236**	260	261	FIXED	**236**			**236**	
237	SVS1	**237**			**237**		**237**	263	262	VOLT	**237**			**237**	
238	SVS3	**238**			**238**		**238**	266	264	FIXED	**238**			**238**	
239	SVS5	**239**			**239**		**239**	266	264	FIXED	**239**			**239**	
240	SVSa	**240**			**240**		**240**	266	268	FIXED	**240**			**240**	
241	SVSb	**241**			**241**		**241**	267	265	FIXED	**241**			**241**	
242	SØN1	**242**			**242**		**242**	267	265	FIXED	**242**			**242**	
243	SØN2	**243**			**243**		**243**	270	269	VOLT	**243**			**243**	
244	SØN3	**244**			**244**		**244**	270	269	VOLT	**244**			**244**	
245	TAN2	**245**			**245**		**245**	272	271	VOLT	**245**			**245**	
246	TAN3	**246**			**246**		**246**	272	271	VOLT	**246**			**246**	
247	THY2	**247**			**247**		**247**	276	25	FIXED	**247**			**247**	
248	THY3	**248**			**248**		**248**	276	26	FIXED	**248**			**248**	
249	THØ2	**249**			**249**		**249**	276	275	FIXED	**249**			**249**	
250	THØ3	**250**			**250**		**250**	278	277	VOLT	**250**			**250**	
251	TJE1	**251**			**251**		**251**	278	277	VOLT	**251**			**251**	
252	TJE2	**252**			**252**		**252**	279	172	FIXED	**252**			**252**	
253	TJE3	**253**			**253**		**253**	280	279	VOLT	**253**			**253**	
254	TJE5	**254**			**254**		**254**				**254**			**254**	
255	TJEa	**255**			**255**		**255**				**255**			**255**	
256	TRI3	**256**			**256**		**256**				**256**			**256**	
257	TRI5	**257**			**257**		**257**				**257**			**257**	
258	TYS1	**258**			**258**		**258**				**258**			**258**	
259	TYS3	**259**			**259**		**259**				**259**			**259**	
260	UCP5	**260**			**260**		**260**				**260**			**260**	
261	UCTa	**261**			**261**		**261**				**261**			**261**	
262	UWN2	**262**			**262**		**262**				**262**			**262**	
263	UWN3	**263**			**263**		**263**				**263**			**263**	
264	VHA1	**264**			**264**		**264**				**264**			**264**	
265	VHA2	**265**			**265**		**265**				**265**			**265**	
266	VHA3	**266**			**266**		**266**				**266**			**266**	
267	VHA5	**267**			**267**		**267**				**267**			**267**	
268	VHAa	**268**			**268**		**268**				**268**			**268**	
269	VID2	**269**			**269**		**269**				**269**			**269**	
270	VID3	**270**			**270**		**270**				**270**			**270**	
271	VIL2	**271**			**271**		**271**				**271**			**271**	
272	VIL3	**272**			**272**		**272**				**272**			**272**	
273	VKEa	**273**			**273**		**273**				**273**			**273**	
274	VKHa	**274**			**274**		**274**				**274**			**274**	

Bus		Line			Load		Xformer				Machine			Shunt	
Nr	*Name*	Nr	*FromBus*	*ToBus*	Nr	*BusRef*	Nr	*PrimBus*	*SecBus*	*Type*	Nr	*BusRef*	*Type*	Nr	*BusRef*
275	WIL4	**275**			**275**		**275**				**275**			**275**	
276	WIL5	**276**			**276**		**276**				**276**			**276**	
277	ÅBØ2	**277**			**277**		**277**				**277**			**277**	
278	ÅBØ3	**278**			**278**		**278**				**278**			**278**	
279	ÅSP2	**279**			**279**		**279**				**279**			**279**	
280	ÅSP3	**280**			**280**		**280**				**280**			**280**	
281	KS1A	**281**			**281**		**281**				**281**			**281**	
282	KS2	**282**			**282**		**282**				**282**			**282**	
283	SK12	**283**			**283**		**283**				**283**			**283**	
284	SK3	**284**			**284**		**284**				**284**			**284**	

Appendix F Equivalent structure of the transmission zones 2 and 3

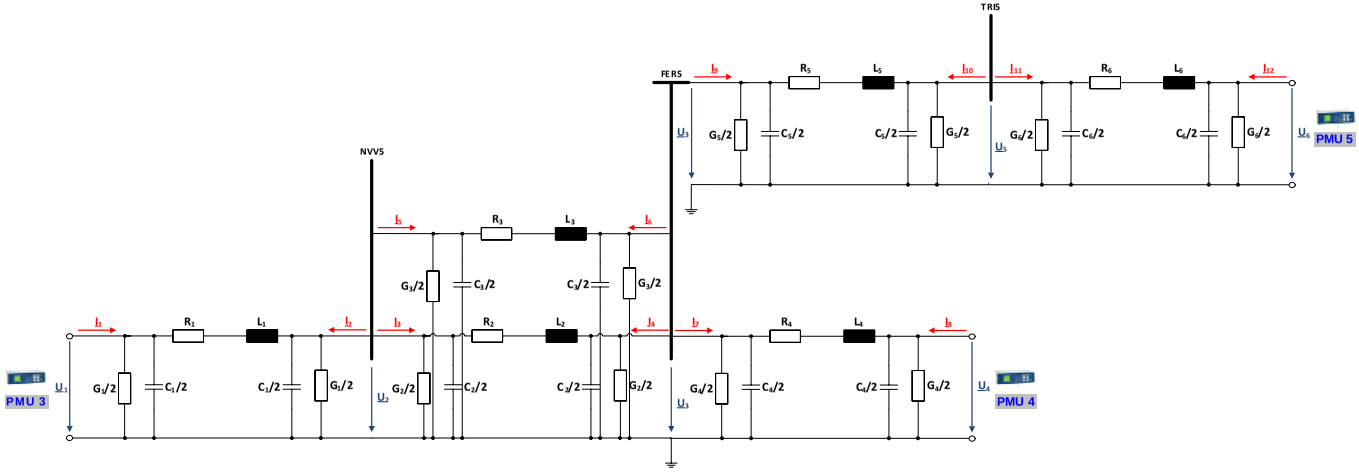

Figure F.1: Equivalent Structure of the transmission zone 2

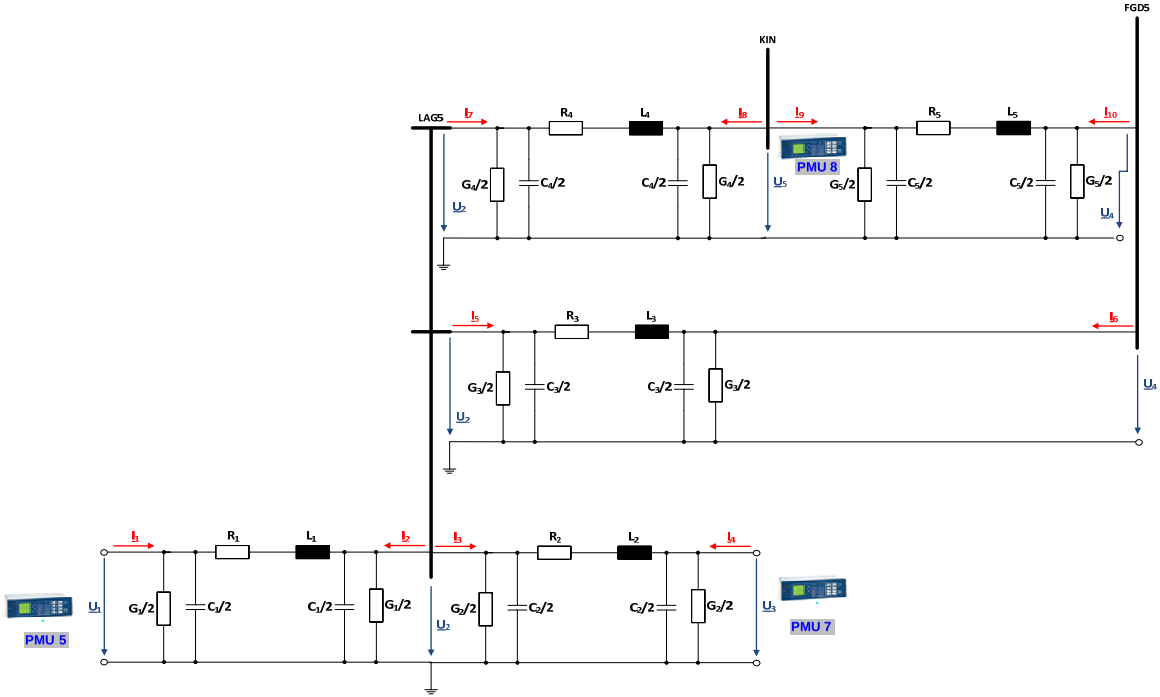

Figure F.2: Equivalent Structure of the transmission zone 3

Bibliographies

[1] Royal Belgian Academy Council of Applied Science: "Evolution of the European electric power system: new challenges for the research" (Évolution du système électrique européen Nouveaux défis pour la recherché); Comité de l'Académie pour les Applications de la Science Académie royale des Sciences, des Lettres et des Beaux Arts, Belgium, July 2006. (*in French*)

[2] P. Kundur, J. Paserba, V. Ajjarapu, G. Andersson, A. Bose, C. Canizares, N. Hatziargyriou, D. Hill, A. Stankovic, C. Taylor, T. Van Cutsem, and V. Vittal: "Definition and classification of power system stability", IEEE Trans. on Power Systems, 19:1387-1401, 2004.

[3] C.S. Indulkar, B. Viswanathan, S.S. Venkata: Maximun: "Power Trasnfer Limited by Voltage Stability in Series and Shunt Compensated Shemes for AC Transmissions Systems"; IEEE Transactions on Power Delivery, Vol. 4, No. 2, April 1989

[4] Lorrin Philipson H., Lee Willis: "Understanding Electric Utilities and De-Regulation" Second Edition, ISBN: 0824727738, 2005

[5] Jochen Markard, Bernhard Truffer, Dieter Rothenberger, Dieter Imboden: "Market Liberalization Changes in the Selection Environment of the Electricity Sector and its Consequences on Product Innovation", http://www.druid.dk/uploads/tx_picturedb/ds2001-237.pdf

[6] Torsten Lund: "Analysis of distribution systems with a high penetration of distributed generation", PhD. Thesis presented at the DTU, Denmark, 2007.

[7] Joseph Euzebe Tate, Thomas J. Overbye: "Line Outage Detection Using Phasor Angle Measurements", IEEE Transactions on Power Systems, Nov. 2007.

[8] US-Canada Power System Outage Task Force: “Final Report on the August 14, 2003 Blackout in the United States and Canada”, pp. 104-107, Apr.2004

[9] IEEE Standard for SCADA and Automation Systems, IEEE Std C37.1™-2007

[10] Walter Sattinger, Rudolf Baumann and Philippe Rothermann: “A New Dimension in Grid Monitoring”, February 1, 2007, http://tdworld.com/overhead_transmission/power_new_dimension_grid/

[11] William T. Shaw: “Cybersecurity for Scada Systems” PennWells Books, ISBN: 978-1-59370-068-3

[12] IEEE/CIGRE Joint Task Force on Stability Terms and Definitions: “Definition and Classification of Power System Stability”, IEEE TRANSACTIONS ON POWER SYSTEMS, VOL. 19. N^{O} 2, MAY 2004

[13] Gerrit Jan Schaeffer, Peter Vaessen: “Future Power System Transition – step into the light” IEEE International Conference on Future Power Systems, 2005.

[14] Carsten Leder: “Visualisation concepts for the process control in electric transmission systems” (Visualisierungskonzepte für die Prozesslenkung elektrischer Energieübertragungssysteme), PhD. Thesis, University of Dortmund, 2002 (*in German*)

[15] Jie Bao: “Short-term Load Forecasting based on neural network and Moving Average” http://www.public.iastate.edu/~baojie/pub/2002-05-08_stlf.pdf

[16] Georges G., Francisco D. Galiana: “Short-term Load Forecasting” Proccedings of the IEEE, Vol. 75, N^{O}. 12, December 1987

[17] Yassine HAMMOUCHE, Mohamed Tarek KHADIR: “A model for the Algerian electric load prediction using the method of Box Jenkins” (Un modèle de prédiction pour la charge électrique journalière Algérienne en utilisant la méthode Box-Jenkins), http://www.labged.net/khadir_tarek/index.php?rubrique=mapage32 (*in French*)

[18] Ian Dobson et al.:"Complex Systems Analysis of Series of Blackouts: Cascading Failure, Criticality, and Self-organization", Bulk Power System Dynamics and Control - VI, August 22-27, 2004 Cortina d'Ampezzo, Italy

[19] NERC (North American Electric Reliability Council), 1996 system disturbances, (Available from NERC, Princeton Forrestal Village, 116-390 Village Boulevard, Princeton, New Jersey 08540-5731), 2002.

[20] NERC (North American Electric Reliability Council), Operating Limit Definitions and Reporting, 2004

[21] Voropai N.I. and Efimov D.N.: "Analysis of blackout development mechanisms in electric power systems", IEEE PES, 2008

[22] Hua Li et al., "An On-Line Tool for Voltage Stability Assessment and Control of Large Scale Power Systems", IEEE Power System Dynamics and Control - VI, August 22-27, 2004

[23] Kundur Prabha: "Power System Stability and Control" The EPRI Power System Engineering Series ISBN: 007035958X

[24] Leonard L. Grigsby: "Power System Stability and Control". CRC Press, 2007 ISBN-13: 9780849392917

[25] CIGRE WG C4.6.01: "Review of On-line Dynamic Security Assessment Tools & Techniques", Draft 3, 2006

[26] D. Tziouvaras and D. Hou: "Out-of-Step Protection Fundamentals and Advancements", Proc. 30th Annual Western Protective Relay Conference, Spokane, WA, October 21–23, 2003.

[27] Teeuwsen S.: "Oscillatory Stability Assessment of Power Systems Using Computational Intelligence", Dissertation, University of Duisburg-Essen, Germany 2005.

[28] Bogdan Lucus et al., "Load-Frequency Control UCTE Operation Handbook", 2005

[29] Thierry Van Cutsem, Costas Vournas:, "Voltage Stability of Electric Power Systems", Kluwer Academic Publishers 1998.

[30] H. Wayne Beaty, "Handbook of Electric Power Calculations", 3rd Edition McGraw Hill

[31] IEEE PSSS Special Publication, “Voltage Stability Assessment; Concepts, Practices and Tools”, 2002, ISBN 0780378695

[32] C. W. Taylor, “Power System Voltage Stability”, EPRI Power System Engineering Series, McGraw Hill, 1994.

[33] Costas D. Vournas and Emmanuel G. Potamianakis, “Investigation of Short-term Voltage Stability Problems and Countermeasures”, IEEE PES, Power Systems Conference and Exposition, 2004; page(s): 385- 391 vol.1 ISBN: 0-7803-8718-X

[34] Mariesa L. Crow and Bernard C, Lesieutre, “Voltage Collapse: An engineering challenge”, IEEE Potentials, 1994

[35] LIMING LU, “Immediate Change in Stability and Voltage Collapse when power systems limits are encountered”, Master Thesis, at the University of Madison, 1991

[36] Rowena Ball: Control, Stability, and Bifurcations of Complex Dynamical Systems, Australian National University, 2003

[37] Ajjarapu, V. and Lee, B., “Bifurcation Theory and its Application to Nonlinear Dynamical Phenomena in an Electrical Power System”, IEEE Transaction on Power Systems, Vol. 7, No. 1, pp. 424-431, February 1992.

[38] Ahmad M. Harb, “Application of Bifurcation Theory to Subsynchronous Resonance in Power Systems”, PhD. Thesis at the Virginia Polytechnic Institute and State University, 1996

[39] Joe H. Chow et al., “Systems and Control Theory for Power systems”, Springer Verlag 1995 ISBN-13-9780387944388

[40] Inés Romero Navarro, “Dynamic load Models for power systems; Estimation of time-varying parameters during normal operation” Licentiate PhD. Thesis at the Department of Industrial Electrical Engineering and Automation Lund University Sweden, 2002

[41] IEEE Task Force on Load Representation for Dynamic Performance, “Load representation for dynamic performance analysis”, IEEE Transactions on Power Systems, Vol.8, No.2, pp. 472-482, May 1993.

[42] DIgSILENT Technical Documentation: General Load Model, Build 220 30.03.2007

[43] ML Coker, H Kgasoane: “Load Modeling”, IEEE AFRICON Volume 2, Page(s):663-668 vol.2, 1999 10.1109/AFRCON.1999.821844

[44] Van Cutsem T., “Power systems I” (Systèmes électrique de puissance I), Lecture notes University of Liège, Belgium, Department of Electrical Engineering and Computer Sciences, 2005 (*in French*)

[45] IEEE Task Force, “Load Presentation for Dynamic Performance Studies”, IEEE Transaction on Power Systems, Vol. 8, No. 2, pp. 472-482, May 1993.

[46] W. Xu and Y. Mansour, “Voltage stability analysis using generic dynamic load models”, IEEE Transactions on Power Systems, Vol. 9, No. 1, pp. 479-493, February, 1994.

[47] D. Karlsson, D. J. Hill, “Modelling and Identification of Non-linear Dynamic Loads in 1994.

[48] F T Dai et al., “The influence of voltage variations on estimated load parameters”, IEE Conference Publication N°. 482, CIRED. 16th International Conference and Exhibition, 2001 Volume 2, on page(s): 6 pp.

[49] North American Electric Reliability Council Report, “Survey of the Voltage Collapse Phenomenon optimized”, published by North American Electric Reliability Council, 1991.

[50] Gustafsson, M.N. Kratnz N.U., Daalder J.E., “Voltage stability: significance of load characteristics and current limiters”, IEE Proceedings Generation, Transmission and Distribution, May 1997 Volume: 144, page(s): 257-262

[51] John Winders, “Power Transformers: Principles and Applications”, CRC Press; 1 edition 12 April 2002, ISBN-10: 0824707664

[52] Liu, Chen-Ching and Khôi Tien Vu, “Analysis of mechanisms of voltage instability in electric power systems”, Systems Control Theory for Power Systems, volume 64 of IMA Volumes in Mathematics and Its Applications, pp. 235-258, Springer Verlag, New York, 1995

[53] H. Ohtsuki, A. Yokoyama, and Y. Sekine, “Reverse action of on-load tap changer: its association with voltage collapse”. IEEE Transactions on Power Systems, 6:300-306, 1991

[54] IEEE Task force on Excitation limiters, “Recommended models for overexcitation limiting devices”, IEEE transactions on Energy Conversion, 1996

[55] Oswald, B., „Grid calculations: Calculations of static and quasistic operational states in electric power systems“, (Netzberechnung: Berechnung stationärer und quasistationärer Betriebszustände in Elektroenergieversorgungsnetzen), Berlin, Offenbach: VDE Verlag, 1992 (*in German*)

[56] G. H aleksandrov, “Transmission of Electrical Energy” (Передача Электрической Энергии), St. Petersburg Polytechnical University, 2007 (*in Russian*)

[57] Mats Larsson, “Coordinated Voltage Control in Electric Power Systems”, Doctoral Dissertation, Department of Industrial Electrical Engineering and Automation Lund Institute of Technology Lund University; Sweden 2000

[58] Prof. B. R. Oswald, “University of Hannover, Institute for Power Systems and High Voltage engineering”, Notes to lecture: Electrical power transmission; Transmission Overhead lines, 2005 (*in German*)

[59] D. J. Hill and I. M. Y. Mareels: Stability Theory for Differential/Algebraic Systems with Application to Power Systems, IEEE Trans. Circuits and Systems, vol. 37, no. 11, pp. 1416-1423, Nov. 1990.

[60] http://en.wikipedia.org

[61] Jean-Olivier Irisson: “Bifurcations Analysis” (l’analyse des bifurcations), Lectures notes, Ecole Pratique des Hautes Études,: Perpignan France, (*in French*).

[62] Castro Abad José Angel and Phulpin Yannick, “local estimation of voltage stability” (Estimation locale de la stabilité de tension), Engineering Sciences/Electric power Supélec, France 2007 (*in French*).

[63] A. A. P. Lerm, C. A. Cañizares, F. A. B. Lemos, and A. S. e Silva, “Multi-parameter Bifurcation Analysis of Power Systems”, Proceedings of the North American Power Symposium (NAPS), Cleveland, Ohio, pp. 76-82, Oct. 1998.

[64] Saffet Ayasun, Chika O. Nwankpa, Harry G. Kwatny, “Computation of Singular and Singularity Induced

Bifurcation Points of Differential-Algebraic Power System Model", IEEE Transactions on circuits and systems Vol. 51, N°. 8, August 2004.

[65] William D. Rosehart, "Stability analysis of detailed power systems", Master Thesis, presented at University of Waterloo, Ontario, 1997.

[66] Seydel, Rüdiger U., "Practical Bifurcation and Stability Analysis: From Equilibrium to Chaos", Springer, Berlin, ISBN 978-0-387-94316-9

[67] Hassan Ghasemi, "On-line Monitoring and Oscillatory Stability Margin Prediction in Power Systems Based on System Identification", PhD. thesis presented to the University of Waterloo, Ontario, Canada, 2006

[68] Hansjörg Kielhöfer, Bifurcation Theory: An Introduction with Applications to PDEs, Springer, Berlin, ISBN 978-0-387-40401-1

[69] Antonio Carlos Zambroni de Souza, "New technique to efficiently determine proximity to static voltage collapse", PhD Thesis presented to the University of Waterloo, Ontario, Canada, 1996

[70] Claudio A. Cañizares, "Conditions for Saddle-Node Bifurcations in AC/DC Power Systems", International Journal of Electrical Power & Energy Systems, vol. 17, no. 1, 1995, pp.61-68.

[71] Van Cutsem, Thierry, "Voltage Instability: Phenomena, Countermeasures and Analysis Methods", Proceedings of the IEEE, Volume 88, 208-227, 2000.

[72] Venkataramana Ajjarapu, Colin Christy, "The continuation power flow: a tool for steady voltage stability analysis" IEEE Transactions on Power Systems, Vol. 7, n°. 1. February 1992

[73] Claudio A. Cañizares, Antonio Z. de Souza, Victor H. Quintana, "Improving continuation methods for tracing bifurcations diagrams in power systems" Proc. Bulk Power System Voltage phenomena, III Seminar, Davos, Switzerland August 1994, PP 349-358.

[74] F. Alvarado and T.H Jung: "Direct detection of voltage collapse conditions" in [75] PP 5.23-5.38

[75] L.H Fink, editor Bulk Power System Voltage Phenomena III-Voltage Stability and Security, Davos, Switzerland August 1994

[76] C. A. Cañizares, F. L. Alvarado, C. L. DeMarco, I. Dobson and W. F. Long, "Point of Collapse methods applied to AC/DC Power Systems", IEEE Transactions on Power Systems Vol. 7,673-683, 1992

[77] William W. Price *et. Al.*: "Large Scale System Testing of a power system dynamic equivalencing program", IEEE Transactions on Power Systems, Vol. 13, No. 3, August 1998

[78] Wang, L. Klein, M. Yirga, S. Kundur, P., "Dynamic reduction of large power systems for stability studies" IEEE Transactions on Power Systems Vol: 12, PP 889-895,May 1997

[79] G. Jang, B. Lee, S.-H Kwon. H.-J. Kim, Y.-B. Yoon, J.-B Choo: "Development of KEPCO equivalent systems for the KEPCO enhanced power simulator" Electrical Power and Energy Systems Vol. 23, PP 577-583, 2001, ELSEVIER

[80] T. L. Baldwin, L. Mili, A. G. Phadke: „Dynamic Ward Equivalents fro transient Stability Analysis",
IEEE Transactions on Power Systems, Vol. 9, No. 1 February 1994

[81] Oscar Clovis YUCRA LINO: „Development of intelligent, robust, and non-linear Models in Dynamic Equivalencing for Interconnected Power Systems" PhD Thesis, University of Paderborn, 2006

[82] G. J. Berg, A. Ghafurian, "Representation of coherency-based equivalents in transient stability studies", Electric Power Systems, Research, Vol. 6, pp. 235-241, 1983.

[83] R. J. Galarza, J. H. Chow, W. W. Price, A. W. Hargrave, P. M. Hirsch, "Aggregation of exciter models for constructing power system dynamic equivalents", IEEE Transaction on Power Systems, Vol. 13, No. 3, pp. 782-788, August 1998

[84] W. F. Tinney, J. M. Bright, "Adaptive reductions for power flow equivalents", IEEE Transactions Vol. PWRS-2, pp. 351-360, May, 1987.

[85] M. M. Begovic and A. G. Phadke, “Voltage Stability Assessment through Measurement of a Reduced State Vector,” IEEE Transactions on Power Systems, Vol. 5, No. 1, Feb. 1990, pp. 198-203

[86] J. Tong and K. Tomsovic, “Estimating the Active Power Transfer Margin for Transient Voltage Stability” Proceedings of the 5th International Conference on Power Systems Operations and Planning, Abuja, Nigeria, Dec. 2002, pp. 244-248.

[87] A.A. El-Keib and X. Ma, “Application of Artificial Neural Networks in Voltage Stability Assessment”, IEEE Trans. Power System, Vol. 10, No.4, Nov. 1995, pp. 1890-1896

[88] Hamada, M.M. Wahab, M.A.A. Hemdan; N.G.A. Al-Minia, “Artificial Neural Network Modeling Technique for Voltage Stability Assessment of Radial Distribution Systems” Universities Power Engineering Conference, 2006. UPEC '06. Proceedings of the 41st International Publication Date: 6-8 Sept. 2006 Volume: 3, PP: 1011-1015

[89] F.A.El-Sheikhi, Y.M.Saad, S.O.Osman, K.M.El Arroudi,"Voltage stability assessment using modal analysis of power systems including flexible AC transmission system (FACTS)", Power Systems Engineering Conference, 7-9 May, 2003, pp. 105-108

[90] Gao, B., Kundur, P., Morisson, G.K, "Voltage Stability Evaluation Using Modal analysis", IEEE Transactions on Power Systems, vol.7, no. 4, pp. 1423-1543, November 1992

[91] Chandrabhan Sharma and Marcus G. Ganness, “Determination of the Applicability of using Modal Analysis for the Prediction of Voltage Stability”, IEEE/PES, Transmission and Distribution Conference and Exposition, 2008.

[92] Claudia Reis, F.P. Maciel Barbosa “A Comparison of Voltage Stability Indices” IEEE MELECON May 16-19, 2006.

[93] P.Kessel, H.Glavitsch “Estimating the Voltage Stability of a Power System” IEEE, Transactions on Power Delivery, Vol.PWRD-1, N3, July 1986

[94] Huang, G. M. and Nair, "Detection of dynamic voltage collapse", Power System Engineering Research Centre; www.pserc.wisc.edu/ecow/get/publicatio/ 2002public/dynamic_summer.pdf

[95] Nizam, M., Mohamed, A. Hussain, "A. Dynamic Voltage Collapse Prediction on a Practical Power System Using Power Transfer Stability Index" The 5th Student Conference on Research and Development–SCOReD 2007

[96] Julian, D.E. ,Schulz, R.P., Vu, K.T., Quaintance, W.H, Bhatt, N.B., Novosel, D., "Quantifying proximity to voltage collapse using the Voltage Instability Predictor (VIP)" IEEE Power Engineering Society Summer Meeting, 2000, On page(s): 931-936 vol. 2

[97] Leif Warland, "A Voltage Instability Predictor Using Local Area Measurements VIP++", PhD Thesis presented at the Norwegian University of Science and Technology, 2002

[98] Bergovic M., Milosevic B., Novosel D., "A Novel Method for Voltage Instability Protection", Proceeding of the 35th Hawaii International Conference on System Science. 2002 (HICSS'02).

[99] M.Moghavvemi, F.M.Omar "Technique for Contingency Monitoring and Voltage Collapse Prediction" IEEE Proceeding on Generation, Transmission and Distribution, Vol. 145, N6, pp. 634-640 November 1998

[100] Michael Hurtgen, Petr Zajac, Pavel Praks, Jean-Claude Maun, "Comparison of measurement placement algorithms for state estimation based on theoretic and eigenvector centrality procedures", Power Systems Computation Conference 2008, PSCC08.

[101] Cristina Olaru, Pierre Geurts, Louis Wehenkel: "Data mining tools and applications in power system engineering" Department of Electrical Engineering, University of Liege, Belgium, www.montefiore.ulg.ac.be/services/stochastic/pubs/1999/ OGW99/

[102] Ming-Syan Chen *et.al* "Data Mining, "An Overview from Database Perspective", IEEE Transactions on Knowledge and Data Engineering, 8(6):866-883, December 1996.

[103] Usama Fayyad, Gregory Piatetsky-Shapiro, and Padhraic Smyth, “From Data Mining to Knowledge Discovery in Databases” www.daedalus.es/fileadmin/daedalus/doc/MineriaDeDatos/fayyad96.pdf

[104] Post F. H., Hin A. J. S., “Advances in Scientific Visualization“, Springer Verlag ISBN 35405203-0

[105] James S. Thorp, “Digital Relaying” in [24]

[106] A.G. Phadke and J. S. Thorp, “History and Applications of phasor Measurements” Power Systems Conference and Exposition, Oct. 29–Nov. 1 2006, pp. 331-335

[107] A.G. Phadke and J. S. Thorp, “Synchronized Phasor Measurements and their applications, Springer, ISBN: 978-0-387-76535-8, 2008

[108] Adamiak M., Premerlani W., Kasztenny B., “Synchrophasors: Definition, Measurement, and Application” Proceedings of the 59th Annual Georgia Tech Protective Relaying, Atlanta, GA, April 27-29, 2005

[109] “IEEE Standard Common Format for Transient Data Exchange (COMTRADE) for Power Systems” IEEE Std C37.111-1999 (Revision of IEEE Std C37.111-1991)

[110] “IEEE Standard for Synchrophasors for Power Systems”, IEEE Std C37.118™-2005 (Revision of IEEE Std 1344™-1995)

[111] Radio Subcommittee of IEEE Power System Communications Committee, “Analog/digital microwave considerations for electric/gas utilities”, IEEE Transactions on Power Delivery, vol. 8, pp. 798-815, July 1993

[112] D. Radford, “Spread spectrum data leap through ac wiring”, IEEE Spectrum, pp. 48-53, November 1996

[113] Vahid Madani, Alfredo Vaccaro, Domenico Villacci and Roger L. King, “Satellite Based Communication Network for Large Scale Power System Applications”, iREP Symposium- Bulk Power System Dynamics and Control - VII, Revitalizing Operational Reliability August 19-24, 2007, Charleston, SC, USA.

[114] Naduvathuparambil, B.Valenti, and M.C. Feliachi, A., "Communication delays in wide area measurement systems", IEEE Proceedings of the Thirty-Fourth South-eastern Symposium on System Theory, 2002.

[115] Phasor Advanced FAQ, www.phasortdms.com/phaserconcepts/phasor_adv_faq.html

[116] Baldwin, T. L.; Mili, L.; Boisen, Jr. M. B.; Adapa, R., "Power System Observability with Minimal Phasor Measurement Placement" IEEE Transactions on Power Systems, Vol. 8, No. 2, May 1993 Page(s): 707 -715

[117] Jansson, Patrick, "Optimal Placement of Phasor Measurement Units in Power Systems with Redundancy and Detection of Topology as Constraints" Master Thesis, Swiss Federal Institute of Technology Zurich, 2002

[118] Sameh Kamel Mena Kodsi, Claudio Cañizares, "Modelling and Simulation of 14 Bus System with FACTS Controllers" www.power.uwaterloo.ca/~claudio/papers/IEEEBenchmarkTFreport.pdf

[119] Alvarado, F. L "Solving Power Flow Problems with a Matlab Implementation of the Power System Applications Data Dictionary" Systems Sciences, 1999. HICSS-32. Proceedings of the 32nd Annual Hawaii International Conference on System Sciences, 1999 Page(s): 7 pp.

[120] Clemens Heppner „Tabu Search: Overview/introduction in an modern metaheuristic" (Übersicht/Einführung in eine moderne MetaHeuristik) www.informatik.uni-hamburg.de/WSV/teaching/sonstiges/EwA-Folien/Heppner-_Paper.pdf (*in german*)

[121] Glover Fred and Laguna Manuel, "Tabu Search", Boston: Kluwer Academic Publishers, 1997; ISBN 0-7923-8187-4

[122] Altman, James Ross, "A Practical Comprehensive Approach to PMU Placement for Full Observability. Blacksburg", Master Thesis presented at the Virginia Polytechnic Institute and State University, 2007

[123] Working Group on a Common Format for the Exchange of Solved Load Flow Data, "Common Data Format for the Exchange of Solved Load Flow Data",IEEE Transactions on Power Apparatus and Systems_, Vol. PAS-92, No. 6, November/December 1973, pp. 1916-1925.

[124] Thomas H. Cormen, Charles E. Leiserson, Ronald L. Rivest, "Introduction to Algorithms", 2nd Edition, Cambridge, MA, MIT Press, 2001

[125] Abur, Ali and Xu, Bei, "Observability Analysis and Measurement Placement for Systems with PMUs" IEEE PSCE 2004

[126] Federico Milano, "Power System Analysis Toolbox Quick Reference Manual for PSAT version 2.1.2", June 26, 2008 http://www.power.uwaterloo.ca/~fmilano/archive/psat-2.1.2-ref.pdf

[127] Federico Milano, "Power System Analysis Toolbox Documentation for PSAT" version 2.0.0 β, March 8, 2007

[128] Denegri, D. B.; Invernizzi, M. und Milano F., "A Security Oriented Approach to PMU Positioning for Advanced Monitoring of a Transmission Grid" Proc. Of PowerCon 2002; Kunming, China

[129] Reynaldo F. Nuqui, Argun G. Phadke, "Phasor Measurement Unit Placement Techniques for Complete and Incomplete Observability", IEEE Transactions on Power Delivery, Vol. 20, No. 4, October 2005, pp. 2381-2388.

[130] Reynaldo Francisco Nuqui, "State Estimation and Voltage Security Monitoring Using Synchronized Phasor Measurements" Ph.D. dissertation, Virginia Polytechnic Institute & State University, Blacksburg, VA, USA, 2001.

[131] Vladislav Akhmatov et. Al.: "Integration of Offshore Wind Power into the western Danish Power system", Offshore Wind International Conference and Exhibition, Copenhagen 2005

[132] Peter B. Eriksen, Antje G. Orths and Vladislav Akhmatov "Integrating Dispersed Generation into the Danish Power System – Present Situation and Future Prospects", IEEE Power Engineering Society General Meeting, 2006.

[133] M. Hajian, A. M. Ranjbar, T. Amraee, and A. R. Shirani, “Optimal Placement of Phasor Measurement Units: Particle Swarm Optimization Approach”, 3rd IEEE Conference on Industrial Electronics and Applications, 2008. ICIEA 2008.

[134] Peng Chunhua, Xu Xuesong “A hybrid algorithm based on immune BPSO and N-1 principle for PMU multi-objective optimization placement” IEEE Third International Conference on Electric Utility Deregulation and Restructuring and Power Technologies, 2008. DRPT 2008.

[135] Ranjana Sodhi, S.C.Srivastava, “Optimal PMU Placement to Ensure Observability of Power System”, Fifteenth National Power Systems Conference (NPSC), IIT Bombay, December 2008, http://www.ee.iitb.ac.in/~npsc2008/NPSC_CD/Data/Poster/p2.pdf

[136] Li Shengfang, Fan Chunju, Yu Weiyong, Cai Huarong, and K.K. Li “A new phase measurement unit (PMU) based fault location algorithm for double circuit lines”, 8th IEE International Conference on Developments in Power System Protection (CP500), p. 188 -191

[137] Ann Helen Berkestedt, “Phasor Measurement based Out-Of-Step Detection” Master Thesis presented at CHALMERS UNIVERSITY OF TECHNOLOGY Göteborg, Sweden.

[138] K. Ketabi, A.M. Ranjbar, “New Approach to Standing Phase Angle Reduction for Power System Restoration” IEEE Electric Power Engineering, PowerTech Budapest, 1999.

[139] O. Samuelson, H. Jóhannsdóttir, N. Gustavsson, T. Hrafnsson, D.Novosel, and D.Karlsson, “Power System Damping in Iceland based on Phasor Measurements”, CRIS, Beijing, China, Sep. 20002

[140] IEEE Std 738-2006 “IEEE Standard for calculating the current-temperature of Bare Overhead conductors”.

[141] B. Milosevic and M. Begovic, “Voltage-Stability Protection and Control Using a Wide-Area Network of Phasor Measurements”, IEEE Trans. Power Systems, vol. 18, No.1, pp 121-127, Feb. 2003

[142] A. Leirbukt et al, “Voltage Monitoring and Control for Enhanced Utilization of Power Grids”, IEEE Power Systems Conference and Exposition, vol.1, pp 342- 347, 2004.

[143] Yanfeng Gong and Noel Schulz, Armando Guzmán “Synchrophasor-Based Real-Time Voltage Stability Index” Proceedings of the Western Protective Relaying Conference, Spokane, WA, October, 2005.

[144] Benjamin Genêt and Jean-Claude Maun, “Voltage Stability Monitoring Using Wide Area Measurement Systems” in Proceedings of the Power Tech Conference, Lausanne, Switzerland, July 1-5 (2007)

[145] Mats Larsson Christian Rehtanz Joachim Bertsch, “Real Time Voltage Stability Assessment of transmissisn corridors”, www.dii.unisi.it/cohes/cc/publications/2003/iifacpps2003.pdf

[146] I. C. Decker, et al., “Phasor Measurement Development and Applications in Brazil,” presented in First International Conference in Electrical Engineering. Coimbra, Portugal, 2005.

[147] John J. Crainger, William D. Stevenson Jr.: Power System Analysis. McGraw Hill Inc. 1994

[148] Gerhard Herold: Basics of the electrical power transmission, B.G Teubner Stuttgart 1997 (*in German*)

[149] Charles Proteus Steinmetz “Complex Quantities and their use in Electrical Engineering” Proceedings of the International Electrical Congress, Chicago, IL; AIEE Proceedings, 1893; pp 33-74